

**REMOVAL OF HEAVY METALS FROM WATER USING
CARBON NANOTUBES FUNCTIONALIZED WITH DEEP
EUTECTIC SOLVENTS**

MOHAMED KHALID MOHAMED SAIED

**FACULTY OF ENGINEERING
UNIVERSITY OF MALAYA
KUALA LUMPUR**

2017

**REMOVAL OF HEAVY METALS FROM WATER
USING CARBON NANOTUBES FUNCTIONALIZED
WITH DEEP EUTECTIC SOLVENTS**

MOHAMED KHALID MOHAMED SAIED

**THESIS SUBMITTED IN FULFILMENT OF THE
REQUIREMENTS FOR THE DEGREE OF DOCTOR OF
PHILOSOPHY**

**FACULTY OF ENGINEERING
UNIVERSITY OF MALAYA
KUALA LUMPUR**

2017

UNIVERSITY OF MALAYA
ORIGINAL LITERARY WORK DECLARATION

Name of Candidate: Mohamed Khalid Mohamed Saied

Matric No: KHA130129

Name of Degree: Doctor of philosophy

Title of Project Paper/Research Report/Dissertation/Thesis (“this Work”):
**REMOVAL OF HEAVY METALS FROM WATER USING CARBON
NANOTUBES FUNCTIONALIZED WITH DEEP EUTECTIC SOLVENTS**

Field of Study: Environmental Engineering (Civil Engineering)

I do solemnly and sincerely declare that:

- (1) I am the sole author/writer of this Work;
- (2) This Work is original;
- (3) Any use of any work in which copyright exists was done by way of fair dealing and for permitted purposes and any excerpt or extract from, or reference to or reproduction of any copyright work has been disclosed expressly and sufficiently and the title of the Work and its authorship have been acknowledged in this Work;
- (4) I do not have any actual knowledge nor do I ought reasonably to know that the making of this work constitutes an infringement of any copyright work;
- (5) I hereby assign all and every rights in the copyright to this Work to the University of Malaya (“UM”), who henceforth shall be owner of the copyright in this Work and that any reproduction or use in any form or by any means whatsoever is prohibited without the written consent of UM having been first had and obtained;
- (6) I am fully aware that if in the course of making this Work I have infringed any copyright whether intentionally or otherwise, I may be subject to legal action or any other action as may be determined by UM.

Candidate’s Signature

Date:

Subscribed and solemnly declared before,

Witness’s Signature

Date:

Name:

Designation

ABSTRACT

Heavy metal pollution in water and wastewater is the cause of major environmental and industrial concern. Carbon nanotubes (CNTs) have proved to be sophisticated adsorbents to remove heavy metals, but require functionalization with non-environmental friendly acids and chemicals through complicated processes. Herein, we present the use of a novel functionalization agent for CNTs, namely deep eutectic solvents (DESs) or, in other words, analogous ionic liquids. Because of their capability as novel solvents in chemistry, DESs were recently involved in a variety of applications. The DESs were prepared using different molar ratios of hydrogen bond donors (HBDs) to salts. The characteristic physical properties of the DESs, specifically freezing point, density, viscosity, electrical conductivity and surface tension, were investigated with respect to temperature. In addition, the functional groups associated with the syntheses of DESs were analyzed utilizing FTIR spectroscopy. Subsequently, the selected DESs were used as functionalization agents with pristine CNTs to form novel adsorbents for the removal of lead ions (Pb^{2+}), arsenic ions (As^{3+}), and mercury ions (Hg^{2+}) from water. Furthermore, the DESs were applied to pre-oxidized CNTs with KMnO_4 , and pre-acidified CNTs, with HNO_3 and H_2SO_4 , respectively. The adsorbents were characterized using Raman, FTIR, XRD, FESEM, EDX, BET surface area, TGA, TEM, and Zeta potential. A screening process was conducted for each heavy metal to select the best adsorbent, with highest removal, of a particular DES-CNTs combination. Response surface methodology was used to optimize the removal conditions for each adsorbent. Isotherm and kinetics studies were performed for each selected adsorbent. The optimization study showed that the optimum conditions for Pb^{2+} removal were pH 5 with adsorbent dosage of 5 mg and a contact time of 15 min. The maximum adsorption capacity (q_{max}) of the selected adsorbent (KTEG-CNTs) for Pb^{2+} was 288.4 mg/g and the experimental data fitted well to both Langmuir and Freundlich isotherms models. The removal of Hg^{2+} was successful with

two adsorbents specifically, KA-CNTs and KT-CNTs. First, the experimental q_{max} was 186.97 mg/g using the phosphonium based DES-functionalized CNTs and the Freundlich isotherm model. The optimum removal conditions were pH 5.5, a contact time 28 min, and an adsorbent dosage of 5 mg. Secondly, by using an ammonium based DES as functionalization agent, Langmuir and Freundlich isotherms models described the absorption of Hg^{2+} with acceptable accuracy and the q_{max} was 177.76 mg/g. The optimum removal conditions were pH 6.4, an adsorbent dosage of 6.0 mg, and a contact time of 45 min. Adsorption of As^{3+} was achieved using three CNTs-DES combinations selected based on the previously described screening study. When using an ammonium based DES to functionalize CNTs, the q_{max} was 17 mg/g. Meanwhile, with phosphonium based DESs the q_{max} reached 23.4 mg/g. The optimum removal conditions for As^{3+} adsorbents were found to be at a contact time of 55 min, an adsorbent dosage of 20 mg, and pH of 6.0 and 3.0. The adsorption kinetics rates for all adsorbents were described well by a pseudo-second-order kinetics model and the Langmuir isotherm model described the adsorption isotherm.

ABSTRAK

Pencemaran logam berat dalam air dan sisa kumbahan mengundang suatu kebingungan yang besar kepada industri dan alam sekitar. Nano-tiub karbon (CNTs) telah terbukti sebagai satu adsorben yang canggih untuk menyingkirkan logam berat, tetapi ia perlu berfungsi bersama asid dan bahan kimia yang berbahaya serta melalui proses yang rumit. Oleh itu, di sini kami menunjukkan penggunaan ejen kefungsiian yang baharu untuk CNTs iaitu pelarut eutektik (DESs), atau dikenali juga sebagai analog kepada cecair berion (IL). Disebabkan keupayaannya sebagai pelarut kimia yang baharu, DESs telah digunakan dalam pelbagai aplikasi. DESs ini telah disediakan dengan menggunakan nisbah Penderma Ikatan Hidrogen (HBD) kepada garam yang berbeza. Sifat-sifat fizikal DESs ini terhadap suhu juga telah disiasat iaitu titik beku, ketumpatan, kelikatan, kekonduksian elektrik dan ketegangan permukaan. Di samping itu, kumpulan berfungsi yang terlibat dalam sintesis DESs ini juga telah dianalisis menggunakan spektroskopi FTIR. Kemudian, DESs yang terpilih telah digunakan sebagai ejen kefungsiian terhadap CNTs untuk membentuk adsorben-adsorben baharu bagi penyingkiran ion plumbum (Pb^{2+}), ion arsenik (As^{3+}) dan ion merkuri (Hg^{2+}) dari air. DESs telah digunakan sebagai ejen kefungsiian untuk memantapkan CNTs. Selain itu, ia juga telah digunakan terhadap CNTs pra-teroksida dengan $KMnO_4$, dan CNTs pra-berasid sebanyak sekali dengan HNO_3 dan sekali lagi dengan H_2SO_4 . Adsorben-adsorben ini telah dikenalpasti menggunakan Raman, FTIR, XRD, FESEM, EDX, luas permukaan BET, TGA, TEM dan potensi Zeta. Proses saringan bagi setiap logam berat telah dijalankan untuk memilih adsorben yang terbaik dengan penyingkiran tertinggi, berdasarkan kombinasi DES-CNTs yang tertentu. Metod permukaan respon (RSM) telah digunakan untuk mengoptimumkan keadaan penyingkiran bagi setiap adsorben. Kajian isoterma dan kinetik telah dilakukan ke atas setiap adsorben yang terpilih. Hasil pengoptimuman menunjukkan bahawa kondisi yang optimum untuk penyingkiran Pb^{2+} ialah pada pH 5 dengan dos adsorben sebanyak 5 mg

dan masa sentuhan selama 15 menit. Kapasiti maksimum bagi adsorben yang dipilih untuk penjerapan Pb^{2+} didapati sebanyak 288.4 mg/g dan data eksperimen didapati sangat bertepatan dengan model isoterma Langmuir dan Freundlich. Penyingkiran Hg^{2+} pula berjaya melalui dua jenis adsorben. Yang pertama, dengan menggunakan CNTs berfungikan DES jenis fosfonium, eksperimen dan model isoterma Freundlich menunjukkan nilai q_{max} sebanyak 186.97 mg/g. Keadaan penyingkiran yang optimum ialah pada pH 5.5, masa sentuhan selama 28 menit dan dos adsorben sebanyak 5 mg. Yang kedua, dengan menggunakan DES jenis ammonium sebagai ejen kefungisan, model isoterma Langmuir dan Freundlich menunjukkan penjerapan Hg^{2+} yang baik, serta q_{max} sebanyak 177.76 mg/g. Keadaan penyingkirannya yang optimum pula adalah pada pH 6.4, dos adsorben sebanyak 6 mg dan masa sentuhan selama 45 menit. Penjerapan As^{3+} telah berjaya dicapai dengan menggunakan tiga kombinasi DESs-CNTs yang dipilih berdasarkan proses saringan. Apabila DES jenis ammonium digunakan untuk memfungikan CNTs, q_{max} adalah sebanyak 17 mg/g, manakala DES jenis fosfonium pula menunjukkan q_{max} sebanyak 23.4 mg/g. Keadaan penyingkiran yang optimum untuk adsorben As^{2+} adalah pada masa sentuhan selama 55 menit, dos adsorben sebanyak 20 mg, serta pada pH 6.0 dan 3.0. Kinetik penjerapan untuk semua adsorben ini juga telah dibuktikan dengan baik melalui model isoterma pseudo-second-order dan Langmuir.

ACKNOWLEDGEMENTS

In the name of Allah, the Most Gracious and the Most Merciful

All the praise and absolute thankfulness are to Almighty Allah for providing me with this opportunity and for granting me the patience and the capability to complete this work successfully.

I would like to express my sincere appreciation and gratitude to my supervisors Prof. Dr. Mohd Ali Hashim, Dr. Mohammed Abdulhakim AlSaadi and Asco. Prof. Dr. Shatirah Akib for their endless support and guidance, and mostly for their patience and encouragement through the period of this study. I would like to express my sincere appreciation to my supervisor Dr. Mohammed Abdulhakim AlSaadi for all the knowledge I have gained from him. Furthermore, I would like to thank him for his advice in terms of academics and in life as well. Finally, I would like to say to my mentor in life Dr. Mohammed Abdulhakim AlSaadi, thank you for everything, may Allah the Almighty gives me the ability to be like you.

I would like to present my appreciation to my brother Omar Khalid for his help and patience through all the stages of this study.

Finally, to Hj. Khalid Mohamed Saied AlOmar and Hj. Bushrah Abdulwahab AlTimemi, may parents who without them my life has no existence and no meaning, I would like to present my deepest sincere thanks and warmest gratitude. My sisters and their families are also deserved my gratitude and kind thanks for their support.

TABLE OF CONTENTS

Abstract	iii
Abstrak	v
Acknowledgements	vii
Table of Contents	viii
List of Figures	xvi
List of Tables.....	xxii
List of Appendices	xxv
CHAPTER 1: INTRODUCTION.....	1
1.1 Overview.....	1
1.2 Problem statement	3
1.3 Objectives of study	5
1.4 Research methodology.....	6
1.5 Outlines of thesis	8
CHAPTER 2: LITERATURE REVIEW.....	12
2.1 Introduction.....	12
2.2 Heavy metals in water: impact and remediation.....	12
2.2.1 Lead	13
2.2.2 Arsenic.....	13
2.2.3 Mercury	13
2.2.4 Water remediation techniques to treat heavy metals.....	14
2.2.5 Adsorption technique for the removal of heavy metals.....	15
2.3 Removal of heavy metals by functionalized carbon nanotubes.....	16
2.3.1 Functionalization of CNTs	19

2.3.1.1	Adsorption of Lead (Pb) ions by functionalized CNTs.....	22
2.3.1.2	Adsorption of Mercury (Hg) ions by functionalized CNTs	30
2.3.1.3	Adsorption of Arsenic (As) ions by functionalized CNTs	33
2.4	Deep eutectic solvents (DESs) and its applications.....	35
2.4.1	DES preparation	37
2.4.2	Physical properties	38
2.4.2.1	Freezing point of DESs	38
2.4.2.2	Density of DESs	39
2.4.2.3	Viscosity of DESs	39
2.4.2.4	Electrical conductivity of DESs	40
2.4.2.5	Surface tension of DESs.....	40
2.4.3	DES application.....	44
2.4.4	DESs and Nanotechnology.....	45
2.5	Summary.....	53

CHAPTER 3: GLYCEROL-BASED DEEP EUTECTIC SOLVENTS:

PHYSICAL PROPERTIES	54	
3.1	Introduction.....	54
3.2	Materials and experimental methodology	56
3.2.1	Chemicals	56
3.2.2	Synthesis and characterization of DESs.....	56
3.3	Results and discussion	58
3.3.1	Freezing point.....	58
3.3.2	Density.....	59
3.3.3	viscosity.....	62
3.3.4	Electrical Conductivity.....	64

3.3.5	Surface Tension	66
3.3.6	FTIR	67
3.4	summary	69

CHAPTER 4: STUDY OF PHYSICAL PROPERTIES OF NOVEL BENZYL TRIMETHYL AMMONIUM CHLORIDE-BASED DEEP EUTECTIC SOLVENTS

	SOLVENTS	70
4.1	Introduction.....	70
4.2	Experimental.....	72
4.2.1	chemicals	72
4.2.2	Synthesis of Benzyl trimethyl ammonium chloride-based DESs	72
4.2.3	Physical properties measurement	74
4.3	Results and discussion	75
4.3.1	Freezing point.....	75
4.3.2	Density.....	76
4.3.3	Viscosity.....	78
4.3.4	Conductivity	82
4.3.5	Surface tension	85
4.3.6	FTIR	87
4.4	Summary.....	90

CHAPTER 5: LEAD REMOVAL FROM WATER BY CHOLINE CHLORIDE BASED DEEP EUTECTIC SOLVENTS FUNCTIONALIZED CARBON NANOTUBES

	NANOTUBES	93
5.1	Introduction.....	93
5.2	Experiment.....	96

5.2.1	Chemicals and materials.....	96
5.2.2	Synthesis of DES.....	96
5.2.3	Oxidation and acidification of MWCNT.....	96
5.2.4	Functionalization by DES	97
5.2.5	Characterization of functionalized CNT	97
5.2.6	Adsorption experiments	98
5.2.7	Screening of different adsorbents.....	98
5.2.8	Optimization of Pb (II) removal.....	99
5.2.9	Adsorption isotherm and kinetics.....	99
5.3	Results and discussion	101
5.3.1	Characterization of DES-functionalized CNT.....	102
5.3.1.1	Raman spectroscopy.....	102
5.3.1.2	Surface chemistry analysis (FTIR).....	104
5.3.1.3	XRD analysis.....	105
5.3.1.4	FESEM and EDX	107
5.3.1.5	Zeta potential.....	108
5.3.1.6	Thermogravimetric analyses (TGA)	109
5.3.1.7	BET surface area	111
5.3.2	Optimization study	112
5.3.2.1	Effects of Optimization Variables on Adsorption of Pb(II)	112
5.3.3	Kinetics study	118
5.3.4	120	
5.3.5	Isotherm study	120
5.4	Summary.....	124

CHAPTER 6: FUNCTIONALIZATION OF CNTS SURFACE WITH PHOSPHONUM BASED DEEP EUTECTIC SOLVENTS FOR ARSENIC REMOVAL FROM WATER	125
6.1 Introduction.....	125
6.2 Experimental methodology.....	127
6.2.1 Chemicals and materials.....	127
6.2.2 Synthesis of DESs	127
6.2.3 Oxidation and acidification of MWCNTs.....	128
6.2.4 Functionalization by DES	128
6.2.5 Characterization of functionalized CNTs.....	128
6.2.6 Adsorption experiments	130
6.3 Result and Discussion.....	130
6.3.1 Characterization of DES-functionalized CNTs.....	131
6.3.1.1 Raman spectroscopy.....	131
6.3.1.2 Surface chemistry analysis (FTIR).....	133
6.3.1.3 XRD analysis.....	134
6.3.1.4 EDX analysis and FESEM	135
6.3.1.5 BET surface area	136
6.3.1.6 Thermogravimetric analyses (TGA)	137
6.3.1.7 Zeta potential.....	138
6.3.2 Optimization study	139
6.3.3 Kinetics study	146
6.3.4 Adsorption mechanism.....	147
6.3.5 Isotherm study	149
6.4 Summary.....	153

**CHAPTER 7: N,N-DIETHYLETHANOLAMMONIUM CHLORIDE BASED
DES-FUNCTIONALIZED CARBON NANOTUBES FOR ARSENIC
REMOVAL FROM AQUEOUS SOLUTION..... 154**

7.1	Introduction.....	154
7.2	Materials and methods.....	156
7.2.1	Chemicals and materials.....	156
7.2.2	Synthesis of DES.....	156
7.2.3	Oxidation and acidification of MWCNTs.....	156
7.2.4	Characterization of functionalized CNTs.....	157
7.2.5	Adsorption studies.....	157
7.3	Results and discussion.....	158
7.3.1	Characterization of the adsorbent.....	158
7.3.1.1	Raman spectroscopy.....	159
7.3.1.2	XRD analysis.....	160
7.3.1.3	FTIR analysis.....	160
7.3.1.4	FESEM and EDX.....	161
7.3.1.5	BET surface area.....	163
7.3.2	Optimization studies.....	163
7.3.3	Kinetics study.....	168
7.3.4	Isotherm study.....	169
7.4	Summary.....	172

**CHAPTER 8: ALLYL TRIPHENYL PHOSPHONIUM BROMIDE BASED
DES-FUNCTIONALIZED CARBON NANOTUBES FOR THE REMOVAL
OF MERCURY FROM WATER..... 173**

8.1	Introduction.....	173
-----	-------------------	-----

8.2	Experiment.....	175
8.2.1	Chemicals and materials.....	175
8.2.2	Functionalization of CNTs	175
8.2.3	Characterization of functionalized CNTs.....	175
8.2.4	Adsorption experiments	176
8.3	Result and discussion.....	176
8.3.1	Characterization of DES-functionalized CNTs.....	177
8.3.2	Leaching study	183
8.3.3	Optimization.....	184
8.3.4	Kinetics and Isotherm studies.....	187
8.3.5	Desorption and regeneration	191
8.4	Summary.....	192

**CHAPTER 9: NOVEL DEEP EUTECTIC SOLVENT-FUNCTIONALIZED
CARBON NANOTUBES ADSORBENT FOR MERCURY REMOVAL FROM
WATER 193**

9.1	Introduction.....	193
9.2	Experiments and Methods	195
9.2.1	Chemicals and materials.....	195
9.2.2	Functionalization of CNTs	196
9.2.3	Characterization of functionalized CNTs.....	196
9.2.4	Adsorption experiments	197
9.3	Results and discussion	199
9.4	Summary.....	216

CHAPTER 10: CONCLUSION AND RECOMMENDATIONS 217

10.1 Conclusion.....	217
10.2 Recommendations.....	221
REFERENCES	223
LIST OF PUBLICATIONS AND PAPERS PRESENTED	253
APPENDICES	255

University of Malaya

LIST OF FIGURES

Figure 1.1: The sequences of the research methodology.	7
Figure 1.2: Work flow of the thesis from the articles to the objectives	8
Figure 2.1: The structure of single and multi-walled carbon nanotubes(N. M. Mubarak, Sahu, Abdullah, & Jayakumar, 2014).....	17
Figure 2.2: Patterns of CNT twist. (a) Zigzag Single-Walled Nanotube. Note the zigzag pattern around circumference and $m = 0$. (b) Armchair Single-Walled Nanotube. Note the chair-like pattern around circumference and $n = m$ (c) Chiral Single-Walled Nanotube. Note	18
Figure 2.3: Alumina coated MWCNTs structure (V. K. Gupta et al., 2011).....	23
Figure 2.4: Functionalization of MWCNTs by amino groups and the abbreviations (G. Vuković et al., 2009; G. D. Vuković et al., 2010)	26
Figure 2.5: ChCl:U eutectic mixture.....	36
Figure 2.6: DESs starting materials (salts and HBDs) (Francisco, van den Bruinhorst, & Kroon, 2013).....	37
Figure 2.7: ILs and DESs in nanotechnology related publication (Abo Hamed et al. 2015)	46
Figure 2.8: SEM images of immobilized microalgae cells on the surface of hairmicrofibers without treatment with the IL composite (a) and (b); hair microfiber after treatment with the IL composite, (c) and (d); hair microfibers after IL composite and liqu.....	47
Figure 2.9: DES encapsulated SWCNT (S. Chen et al., 2009).....	48
Figure 3.1: Chemical structure of the six salts and the HBD.....	57
Figure 3.2: Variations of densities with temperature	60
Figure 3.3: Variations of viscosity with temperature.....	63
Figure 3.4: Variations of conductivities with temperature	65
Figure 3.5: Variations of surface tension with temperature.....	67
Figure 3.6: FTIR spectrum for the six selected DESs and the HBD.....	69

Figure 4.1: Molecular structure of BTAC and the four HBDs	73
Figure 4.2: Variations of densities with temperature for glycols DESs systems.....	77
Figure 4.3: Variation of densities with temperature for the Gly based DESs with different molar ration	78
Figure 4.4: Variations of viscosity with temperature for glycols DESs systems.....	80
Figure 4.5: Variation of viscosity with temperature for the Gly based DESs with different molar ration	81
Figure 4.6: Variations of conductivities with temperature for glycols DESs systems ...	83
Figure 4.7: Variation of conductivity with temperature for the Gly based DESs with different molar ration	84
Figure 4.8: Variations of surface tension with temperature for glycols DESs systems..	85
Figure 4.9: Variation of Surface tension with temperature for the Gly based DESs with different molar ration	86
Figure 4.10: FTIR spectrum of EG, BTAC and DES23	88
Figure 4.11: FTIR spectrum of DEG, BTAC and DES13	88
Figure 4.12: FTIR spectrum of TEG, BTAC, and DES13.....	89
Figure 4.13: FTIR spectrum for Gly DESs system with different molar ratio, Gly and BTAC salt	89
Figure 5.1: Screening study for the best Pb(II) absorber	102
Figure 5.2: Raman spectroscopy of P-CNTs, K-CNTs and KTEG-CNTs for a) D band and G band, and b) D` band shift	104
Figure 5.3: FTIR spectrum for P-CNTs, K-CNTs and KTEG-CNTs, a) from 400 to 2000 cm^{-1} , and b) from 2000 to 4000 cm^{-1} , waver number.....	106
Figure 5.4: X-ray diffraction patterns for P-CNTs, K-CNTs and KTEG-CNTs	107
Figure 5.5: FESEM images for a) P-CNTs, b) K-CNTs and c) KTEG-CNTs.....	108
Figure 5.6: TGA curves for P-CNTs, K-CNTs, KTEG-CNTs and KTEG-CNTs-Pb ..	111
Figure 5.7: Theoretical Vs Experimental values for a) removal (%) of Pb(II) and b) uptake capacity of KTEG-CNTs.....	115

Figure 5.8: Surface response representation of, a) Pb(II) removal (%) interaction with pH and contact time and b) uptake capacity of KTEG-CNTs interaction with pH and contact time, by fixing the adsorbent dose to the optimum	116
Figure 5.9: Surface response representation of a) Pb(II) removal (%) interaction with pH and adsorbent dosage and b) uptake capacity of KTEG-CNTs interaction with pH and adsorbent dosage, by fixing contact time to the optimum.....	117
Figure 5.10: Pseudo-first-order adsorption kinetics at different initial concentrations	119
Figure 5.11: Pseudo-second-order adsorption kinetics at different initial concentrations	119
Figure 5.12: Intraparticle diffusion adsorption kinetics at different initial concentrations	120
Figure 5.13: Langmuir isotherm model plot of Pb(II) sorption on KTEG-CNTs surface at pH 2.7.	122
Figure 5.14: Langmuir isotherm model plot of Pb(II) sorption on KTEG-CNTs surface at pH 5.	122
Figure 5.15: Freundlich isotherm model plot of Pb(II) sorption on KTEG-CNTs surface at pH 2.7.	123
Figure 5.16: Freundlich isotherm model plot of Pb(II) sorption on KTEG-CNTs surface at pH 5.	123
Figure 6.1: Functionalization process and the abbreviation of each adsorbent	129
Figure 6.2: Screening for best adsorbent of As ³⁺	130
Figure 6.3: Raman spectroscopy, a) D band and G band location and intensity, b) D' band.....	131
Figure 6.4: FTIR spectroscopy for P-CNTs, K-CNTs, KM-CNTs and KB-CNTs.....	134
Figure 6.5: XRD patterns for P-CNTs, K-CNTs, KM-CNTs and KB-CNTs.....	135
Figure 6.6: FESEM image for a) P-CNTs, b) K-CNTs, C) KM-CNTs, and d) KB-CNTs	136
Figure 6.7: TGA graph of P-CNTs, K-CNTs, KM-CNTs, KB-CNTs and (KM-CNTs-As and KB-CNTs-As) after adsorption.....	138
Figure 6.8: Theoretical vs experimental data for a) As ³⁺ removal (%) and b) uptake capacity (mg/g) on KM-CNTs adsorbent.....	141

Figure 6.9: Theoretical vs experimental data for a) As^{+3} removal (%) and b) uptake capacity (mg/g) on KB-CNTs adsorbent.....	142
Figure 6.10: Surface response representation of a) Removal (%) of As^{+3} verses contact time and pH by fixing adsorbent dosage to the optimum value and b) uptake capacity of KM-CNTs verses contact time and pH by fixing adsorbent dosage to the optimum value.....	144
Figure 6.11: Surface response representation of a) Removal (%) of As^{+3} verses contact time and pH by fixing adsorbent dosage to the optimum value and b) uptake capacity of KB-CNTs verses contact time and pH by fixing adsorbent dosage to the optimum value.....	145
Figure 6.12: Pseudo-second-order kinetic model for As^{3+} adsorption on KM-CNTs surface	148
Figure 6.13: Pseudo-second-order kinetic model for As^{3+} adsorption on KB-CNTs surface	149
Figure 6.14: Linear form of Langmuir adsorption isotherm for As^{+3} on KM-CNTs surface	151
Figure 6.15: Linear form of Langmuir adsorption isotherm for As^{+3} on KB-CNTs surface	151
Figure 6.16: Linear form of Freundlich adsorption isotherm for As^{+3} on KM-CNTs surface	152
Figure 6.17: Linear form of Freundlich adsorption isotherm for As^{+3} on KB-CNTs surface	152
Figure 7.1: Raman spectroscopy of P-CNTs, K-CNTs and KD-CNTs	160
Figure 7.2: XRD patterns of P-CNTs, K-CNTs and KKD-CNTs	161
Figure 7.3: FTIR spectrum for each adsorbent	162
Figure 7.4: FESEM images of a) P-CNTs, b) K-CNTs and c) KD-CNTs.....	162
Figure 7.5: Theoretical values vs actual values for a) removal response and b) adsorption capacity response.....	165
Figure 7.6: pH and contact time effect on the removal of As^{3+}	166
Figure 7.7: The effect of pH and contact time on the adsorption capacity of KD-CNTs at a) maximum adsorbent dosage and b) minimum adsorbent dosage.....	167

Figure 7.8: The effect of pH and adsorbent dosage on the adsorption capacity of KD-CNTs at the optimum contact time	167
Figure 7.9: Plot of pseudo-second-order kinetics model	169
Figure 7.10: Linear form of Langmuir isotherm model	171
Figure 7.11: Linear form of Freundlich isotherm model	172
Figure 8.1: Screening study for all adsorbents	177
Figure 8.2: FESEM images of a) P-CNTs, b) K-CNTs, c) KA-CNTs, and TEM images of d) P-CNTs, e) K-CNTs, f) KA-CNTs	178
Figure 8.3: TGA curves of P-CNTs, K-CNTs, KA-CNTs and KA-CNTs-HG	179
Figure 8.4: XRD spectrum of P-CNTs, K-CNTs and KA-CNTs	180
Figure 8.5: FTIR spectrum of P-CNTs, K-CNTs and KA-CNTs	181
Figure 8.6: Raman Spectrum of P-CNTs, K-CNTs and KA-CNTs	182
Figure 8.7: Leaching of Mn at different pH with respect to time	184
Figure 8.8: a) effect and interaction of pH and adsorbent dosage on the removal percentage, b) effect and interaction of pH and contact time on the removal percentage of, c) effect and interaction of pH and contact time on the adsorption capacity of KA-CNTs, and d) the effect and interaction of pH and adsorbent dosage on the adsorption capacity of KA-CNTs.....	186
Figure 8.9: Pseudo-second order adsorption kinetics	188
Figure 8.10: Linear form of Langmuir isotherm model for the Hg ²⁺ adsorption onto KA-CNTs	190
Figure 8.11: Linear form of Freundlich isotherm model for the Hg ²⁺ adsorption onto KA-CNTs	190
Figure 8.12: Desorption of Hg ²⁺ at different pH	191
Figure 9.1: Primary screening study for all adsorbents.....	200
Figure 9.2: Raman Spectrum of P-CNTs, K-CNTs and KT-CNTs	201
Figure 9.3: FTIR spectrum for P-CNTs, K-CNTs and KT-CNTs	202
Figure 9.4: XRD pattern of P-CNTs, K-CNTs, and KT-CNTs	203

Figure 9.5: FESEM images for P-CNTs, K-CNTs and KT-CNTs	204
Figure 9.6: Theoretical vs experimental data for Hg ²⁺ a) removal (%) and b) uptake capacity (mg/g) on KT-CNT adsorbent	206
Figure 9.8: Effect of pH and contact time on the removal % at the optimum adsorbent dosage.....	208
Figure 9.8: Effect of pH and contact time on the removal % at the maximum adsorbent dosage	208
Figure 9.10: Effect of pH and adsorbent dosage on the removal %	209
Figure 9.10: Effect of pH and contact time on the adsorption capacity of KT-CNTs ..	209
Figure 9.11: Effect of pH and adsorbent dosage on the adsorption capacity of KT-CNTs	210
Figure 9.12: Pseudo-second-order adsorption kinetics model	211
Figure 9.13: Langmuir adsorption isotherm model	214
Figure 9.14: Freundlich adsorption isotherm model	214
9.15 desorption study of Hg ²⁺ from KT-CNTs at different pHs	215

LIST OF TABLES

Table 2.1: Different CNTs based adsorbents for lead ions	28
Table 2.2: Different CNTs based adsorbents for mercury ions	32
Table 2.3: Different CNTs- based adsorbents for arsenic ions.....	34
Table 2.4: Physical properties of some reported DESs.....	42
Table 2.5: Nano-technology applications involving DESs	50
Table 3.1: Selected DESs, abbreviations, and molecular weights	59
Table 3.2: Density–temperature model parameters and regression coefficients.....	61
Table 3.3: Viscosity–temperature model parameters and regression coefficients.....	64
Table 3.4: Conductivity–temperature model parameters and regression coefficients. ...	66
Table 3.5: Surface tension–temperature model parameters and regression coefficients	68
Table 4.1: Selected DESs, abbreviations, and molecular weights	74
Table 4.2: Uncertainties of the measurements	75
Table 4.3: Density–temperature model parameters and regression coefficients.....	79
Table 4.4: Viscosity–temperature model parameters and regression coefficients.....	82
Table 4.5: Conductivity–temperature model parameters and regression coefficients. ...	84
Table 4.6: Surface tension–temperature model parameters and regression coefficients	87
Table 4.7: Functional groups of the novel DESs	90
Table 5.1: List of the synthesized DESs used as functionalization agents.	97
Table 5.2: Functionalized CNTs classification and abbreviation	98
Table 5.3: List of design of experiments runs and the actual values obtained from each response	100
Table 5.4: Kinetics models equations and parameters	101

Table 5.5: Raman spectroscopy bands intensities and locations.....	103
Table 5.6: Weight percentage of each material based on TGA analysis.	110
Table 5.7: BET surface area and pore volume and diameter of all adsorbents.....	111
Table 5.8: Reduced Cubic Model Analysis of variance (ANOVA) for Pb (II) removal (%) on KTEG-CNTs	113
Table 5.9: Reduced Cubic Model Analysis of variance (ANOVA) for uptake capacity of KTEG-CNTs	114
Table 5.10: Adsorption kinetics constants and correlation coefficient for each model	118
Table 5.11: Isotherm models constants and the maximum adsorption capacity.....	121
Table 6.1: List of the synthesized DESs used for functionalization.	128
Table 6.2: Intensity of Raman bands and the I_D/I_G ratios	132
Table 6.3: Comparative BET summary result for all adsorbent	137
Table 6.4: Linearized forms of kinetics models and their parameters	146
Table 6.5: Experimental values of constants of adsorption kinetics models	147
Table 6.6: Isotherm models parameters and comparison of adsorption capacity of other adsorbents	150
Table 7.1: Screening study for the removal of As^{3+}	158
Table 7.2: I_D/I_G intensity ratios of each adsorbent	159
Table 7.3: BET surface area and pore volume and diameter of all adsorbents.....	163
Table 7.4: Isotherm models parameters and comparison of adsorption capacity of other adsorbents	171
Table 8.1: Experimental values of constants of adsorption kinetics models	187
Table 8.2: Isotherm models parameters and comparison of adsorption capacity of other adsorbents	189
Table 9.1: Constraints for optimization process based on CCD for Hg^{2+} adsorption...	207
Table 9.2: Experimental values of constants of adsorption kinetics models	210

Table 9.3: Isotherm models parameters and comparison of adsorption capacity of other adsorbents213

University of Malaya

LIST OF APPENDICES

Appendix A: supplementary information of article 1	255
Appendix B: supplementary information of article 2.....	263
Appendix C: supplementary information of article 3.....	271
Appendix D: supplementary information of article 4.....	272
Appendix E: supplementary information of article 5.....	279
Appendix F: supplementary information of article 6.....	283
Appendix G: supplementary information of article 7.....	287

University of Malaya

CHAPTER 1: INTRODUCTION

1.1 Overview

Water, a vital nutrient, is the most important resource in the existence and maintenance of known life. It is a major challenge to supply pure water to all human civilization, since more than 700 million people currently face difficulty in accessing pure water sources (HWO, 2014). While the continued consumption of pure water occurs with increasing population activities, pollution is also contributing to the depletion of pure water resources. Water pollution may occur from natural sources or human industrial activities. There are different types of pollution, including organic compounds, heavy metals, oil, and radioactive metals. Therefore, the demand for new effective ways to eliminate any contaminants in water, especially harmful compounds, is crucial (Ihsanullah et al., 2016).

Heavy metals are one of the most challenging pollutants that require continues monitoring and creative solutions to be removed from contaminated water. Whatever the source of heavy metals in water, natural or from human activities, their removal or control keep attracting great concern based on environmental and economic considerations. In addition, heavy metals are destructive to human health and thus it is recommended that their existence in water be minimized. Different techniques have been developed to reduce heavy metals concentration in water supplies, such as adsorption, coagulation, precipitation, and ion exchange.

Nanotechnology has become a promising approach to revolutionize the environmental remediation techniques. Nanotechnology is distinct in a group of emerging applications because it works on a nanometer scale to produce materials, devices, and systems with new characteristics and purposes by governing the size and the shape of matters (Mansoori & Soelaiman, 2005; NSTC/NNI/NSET, August 29, 2003; Ramsden, 2009). The global interest of nanotechnology has developed huge momentum due to its potential

applications in many fields, e.g., medicine (Kiparissides & Kammona, 2015; Müller et al., 2015; Usui et al., 2008), food industry (Duncan, 2011; Shanthilal & Bhattacharya, 2014), energy (Hussein, 2015; Serrano, Rus, & García-Martínez, 2009; Zang, 2011) and pollution treatment (Brame, Li, & Alvarez, 2011; Karn, Kuiken, & Otto, 2009). This nanotechnology momentum presents the opportunities for leapfrogging scenarios in the development and alteration of conventional remediation technologies.

Carbon nanotubes (CNTs), including single-walled SWCNTs and multi-walled MWCNTs, have gained significant attention because of their mechanical, electrical, optical, physical, and chemical properties (Koziol et al., 2007). They can be considered as alternates for activated carbon as they can efficiently remove both heavy metals and organic contaminants with higher adsorption efficiency due to their binding sites, which are more available than those on activated carbon (Ji, Chen, Duan, & Zhu, 2009).

Recently, ionic liquids (ILs) have been involved in many applications due to their solvation and physicochemical properties, which has led them to be considered as designer solvents. Nevertheless, ILs have many flaws, specifically their relatively costly processes of synthesis and associated waste disposal. Lately, Abbott et al. (2003) introduced the so called deep eutectic solvents (DESs) for the development of cheaper replacement for ILs (Andrew P. Abbott, Capper, Davies, Rasheed, & Tambyrajah, 2003). DESs are an evolving class of solvents that are considered ionic liquid analogues, and sometimes as fourth generation of (ILs) (Cvjetko Bubalo, Vidović, Radojčić Redovniković, & Jokić, 2015b). Along with their mesmerizing solvation properties, they are chemically stable with suitable physical properties, including low vapor pressure and high boiling point. DESs consist of two or more compounds and the mixture of these components have a melting point lower than that of the individual compounds (Andrew P. Abbott, Boothby, Capper, Davies, & Rasheed, 2004; M. Hayyan, Mjalli, Hashim, &

AlNashef, 2010). Correspondingly, DESs have many advantages over conventional ILs, which can be summarized as simplicity of synthesis, variety of the physical properties with different molar ratios, and the reasonable price of components (M. Hayyan, M. A. Hashim, M. A. Al-Saadi, et al., 2013; M. Hayyan, M. A. Hashim, A. Hayyan, et al., 2013; M. Hayyan, Looi, Hayyan, Wong, & Hashim, 2015). Recently, ILs and DESs have been applied in many nanotechnology related fields. The first combination of nanotechnology and ionic liquids was introduced by Deshmukh et al. (2001) (Deshmukh, Rajagopal, & Srinivasan, 2001). Next, ILs and DESs were used as a media for synthesis of nanoparticles (Chakrabarti et al., 2015; F. Chen, Xie, Zhang, & Liu, 2013; Jia et al., 2015; Mohammad Karimi, Hesarak, Alizadeh, & Kazemzadeh, 2016; Xiong, Tu, Ge, Wang, & Gu, 2015; Xu et al., 2016). Moreover, DESs have been employed in many nanotechnology related fields, including as the electrolyte in a nanostructure sensor (Zheng, Ye, Yan, & Gao, 2014), the electrolyte in nanoparticle deposition (Andrew P. Abbott, El Ttaib, Frisch, McKenzie, & Ryder, 2009; Andrew P. Abbott, Ttaib, Frisch, Ryder, & Weston, 2012; C. Gu & J. Tu, 2011; X. Guo et al., 2014; Renjith, Roy, & Lakshminarayanan, 2014; Wei, Fan, Tian, et al., 2012; Wei, Fan, Wang, et al., 2012; Wei et al., 2013; You, Gu, Wang, & Tu, 2012), a dispersant (Mała, Szychaj, & Kowalczyk, 2014; Martis, Dilimon, Delhalle, & Mekhalif, 2010; Mondal, Bhatt, Sharma, Chatterjee, & Prasad, 2014), an exfoliation (Boulos et al., 2013), in a nanodroplet embedded in a microstructure (C.-D. Gu & J.-P. Tu, 2011), in nano-confinement (S. Chen et al., 2009), and in nanocatalytic assembly (J. Lu, Li, Ma, Mo, & Zhang, 2014).

1.2 Problem statement

The lack of water in many parts of the world and rampant pollution has led to the exertion of enormous pressure on resources and motivated the establishment of new techniques to provide good quality water for human life and other organisms. Due to their high toxicity, even at low concentration, removing heavy metals contamination from

water has become a great concern. Many conventional methods have been used to remove heavy metals from water, including coagulation, precipitation, ion exchange, reverse osmosis, and oxidation. However, these techniques have significant drawbacks in terms of cost effectiveness and limitations in removing different kinds of pollutants. Therefore, the need for new alternatives or modified technologies is imperative. Adsorption has been considered as one of the most effective techniques for removal of heavy metals ions since it excels at separating small amounts of pollutants from a large amount of solution. Furthermore, adsorption has advantages over other techniques due to the simplicity of operation, the wide range of available adsorbents, and the ability to remove soluble organic, inorganic and biological pollutants from water. However, adsorption also suffers from limitations, including low adsorption capacity for some adsorbents, complicated scale up for industrial production processes, and the high cost associated with relatively high adsorption capacity, such as nano-based adsorbents (Ali, 2012).

It is well known that CNTs are considered of most promising adsorbent, compared to other nano-based adsorbents. However, in the aqueous solution, the application of CNTs is significantly hindered by their poor dispersion due to the hydrophobicity of their graphitic surface and the strong intermolecular Vander Waals interaction between tubes, which can lead to the formation of loose bundles/ aggregates that reduce the effective surface area (G. D. Vuković et al., 2010). In order to overcome these drawbacks and enhance CNTs performance, CNTs can be functionalized by chemical treatment methods in which the pristine CNTs can gain functional groups on the surface after being treated with certain chemicals. CNTs functionalization is subject to the purpose of the specific application, since each functional group adds different characteristics and serves different types of applications. Thus, activation of CNTs plays a key role in improving the maximum adsorption capacity because of the modification in the surface morphology and surface functional groups (Han, Zou, Li, Li, & Shi, 2006). The need for green solvents to

functionalize CNTs is essential. Where conventional functionalization usually involves strong acids and harsh chemicals, which involve complicated processes and are environmentally harmful. Consequently, the need for new types of economical and environmentally friendly functionalization agents is crucial for the development of new applications (M. Hayyan, A. Abo-Hamad, M. AlSaadi, & M. Hashim, 2015a; Martínez et al., 2003).

Eventually, one of the greatest challenges facing humanity in this century is the conservation of water resources. Combining the sophisticated properties of CNTs and DESs as a green novel functionalization agent was the main motivation of this research. This research is an attempt to advance the DESs physicochemical properties in modifying the surface of CNTs to be utilized in the field of environmental engineering, specifically water treatment.

DESs could be a successful option to replace conventional acids and other chemicals that require a complicated process to modify the surface of CNTs. Furthermore, DESs are green, biodegradable, economical, and simple to synthesize solvents.

1.3 Objectives of study

1. To synthesis and characterize deep eutectic solvents.
2. To functionalize MWCNTs using deep eutectic solvents and comprehensively characterize them.
3. To utilize the deep eutectic solvent-functionalized MWCNTs for the removal of heavy metals contaminants from water.
4. To optimize heavy metals removal parameters (pH, contact time, adsorbent dosage, etc.) by developing empirical models.
5. To investigate adsorption isotherms and kinetics by determining their coefficients.

1.4 Research methodology

The specific research stages, which are illustrated in Figure 1.1, can be summarized as:

- Syntheses of novel DESs and studies of the stability of each DES to find the most stable molar ratio.
- Full characterization of the synthesized DESs, including freezing point, density, viscosity, conductivity, surface tension, and FTIR.
- Adopting the molar ratios of stable DESs as functionalization agents of CNTs.
- Comprehensive characterization of DES-CNT combinations, including Raman, FTIR, XRD, TEM, FESEM, EDX, BET surface area, zeta potential, and TGA.
- Utilizing the DESs-functionalized CNTs as adsorbents of toxic heavy metals, specifically lead, arsenic, and mercury.
- Developing an estimated regression model using Response Surface Methodology (RSM) to optimize the conditions of heavy metals removal from water.
- Investigate the adsorption kinetics and isotherms of the novel adsorbents.

The objectives of this thesis were published in a form of research papers. Figure 1.2 illustrate the work flow of the thesis from the articles to the objectives.

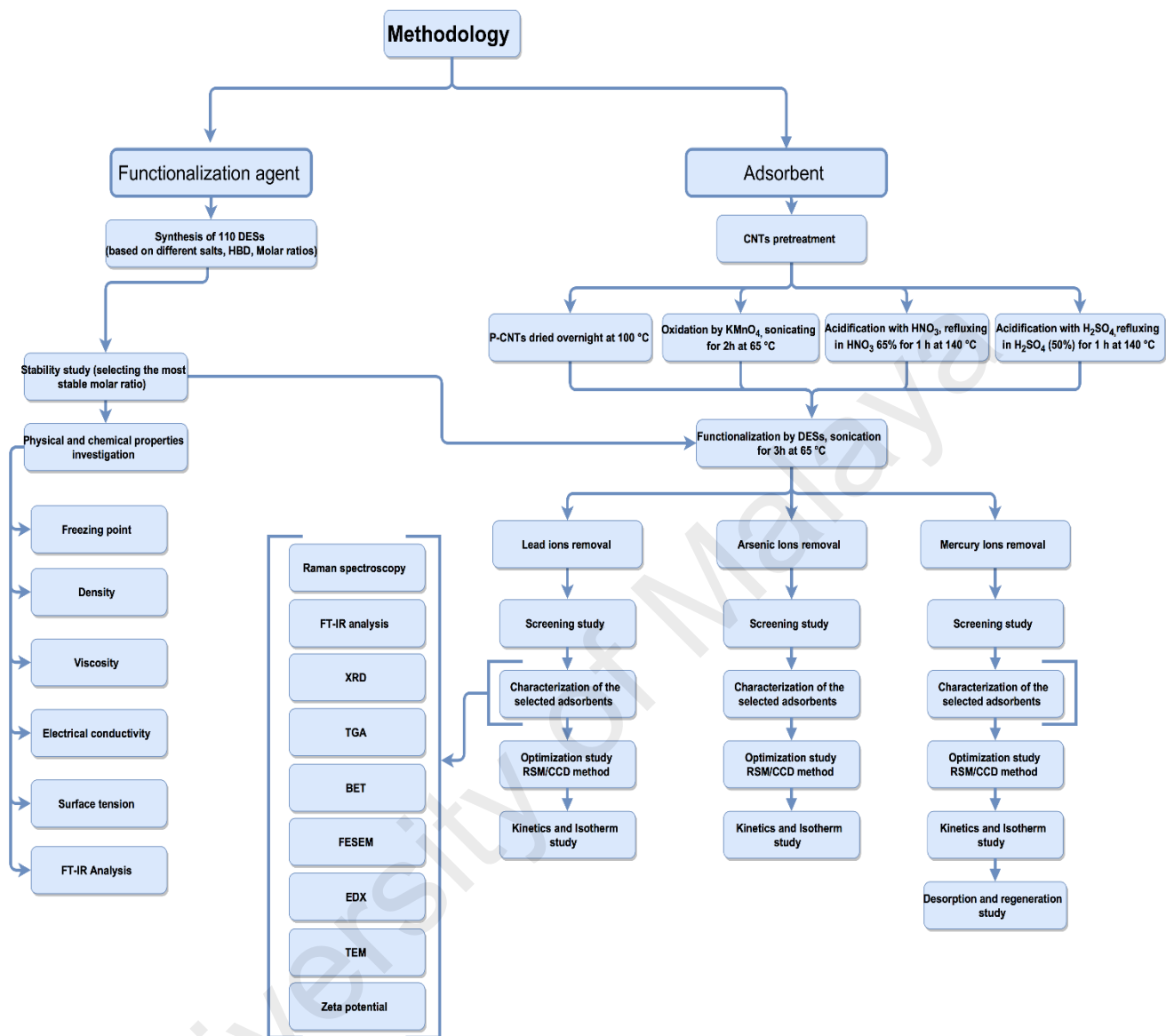


Figure 1.1: The sequences of the research methodology.

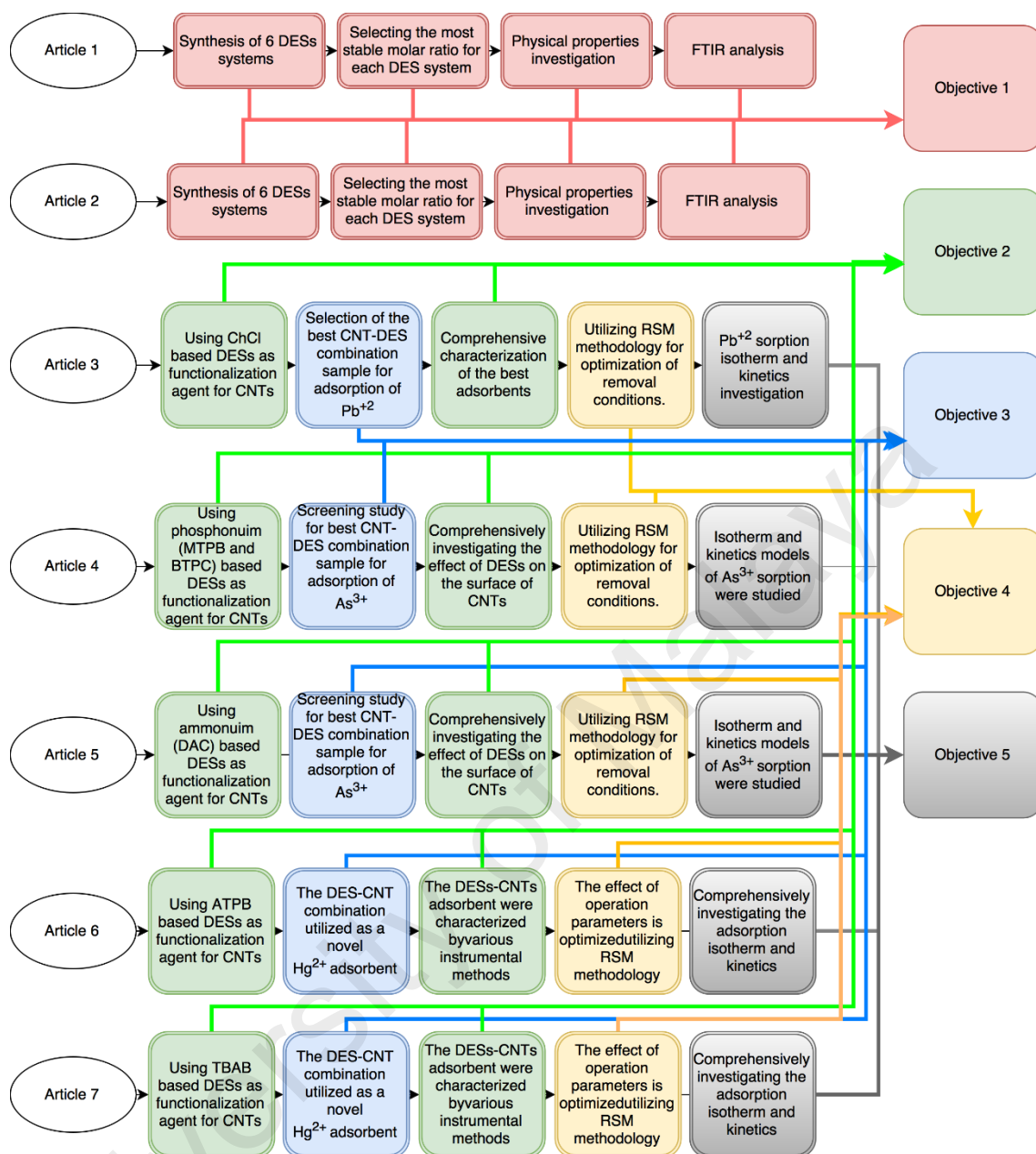


Figure 1.2: Work flow of the thesis from the articles to the objectives

1.5 Outlines of thesis

The format of this thesis followed the article style format approved by the University of Malaya. This style gives the author a flexibility to present the work in the form of various independent articles arranged in a sequence of chapters. The research objectives are comprehensively satisfied through these articles with a smoothly flowing research story. The work in this thesis has been submitted to ISI journals in the form of technical

articles. Upon the writing of this thesis, four articles have been published in Q1 ISI journals and many other articles are under review. The outline of this thesis is as follows:

Chapter 1 (Introduction): Includes a brief background on water treatment and the use of nanomaterials as adsorbents of heavy metals. The purpose of this research is mentioned, followed by the objectives of the research and finally a brief description of the methodology.

Chapter 2 (Literature Review): This chapter covers a literature survey of nanotechnology in water treatments. CNTs properties and previous works done by various researchers regarding the functionalization of CNTs surface is also covered. A comprehensive review on the functionalization of CNTs to remove Pb^{2+} , As^{3+} and Hg^{2+} from water is presented. In addition, the background, characterization, and applications of DESs are provided. Finally, this chapter includes a brief review of the involvement of DESs in nanotechnology related fields.

Chapter 3 (Article 1: Glycerol-based deep eutectic solvents: physical properties): This chapter includes the synthesis of 70 DESs based on three ammonium salts and three phosphonium salts based DESs using Gly as an HBD. Stability studies are presented in this chapter, along with a comprehensive investigation of the physical properties of these DESs. This chapter has been published in the Journal of Molecular Liquids. (AlOmar, M. K., Hayyan, M., Alsaadi, M. A., Akib, S., Hayyan, A., & Hashim, M. A. (2016). *Journal of Molecular Liquids*, 215, 98-103.

Chapter 4 (Article 2: Study of physical properties of novel benzyl trimethyl ammonium chloride-based deep eutectic solvents): This chapter presents the synthesis of BTAC based DESs with four different HBD, Gly, EG, TEG, and DEG. The physical properties of these DESs systems were investigated. In addition, the effects of molar ratio

on the physical properties were investigated. This chapter was submitted to the Journal of Physics and Chemistry of Liquids (under review).

Chapter 5 (Article 3: Lead removal from water by choline chloride based deep eutectic solvents functionalized carbon nanotubes): In this chapter, six DESs systems based on ChCl and six different HBD were synthesized to be used as functionalization agents of CNTs to create novel adsorbents of Pb^{2+} from water. This chapter was published in the Journal of Molecular Liquids. (AlOmar, M. K., Alsaadi, M. A., Hayyan, M., Akib, S., Ibrahim, R. K., & Hashim, M. A. (2016) *Journal of Molecular Liquids*, 222, 883-894.

Chapter 6 (Article 4: Functionalization of CNTs surface with phosphonium based deep eutectic solvents for arsenic removal from water): This chapter presents the use of DESs as functionalization agents of CNTs to form novel adsorbents for removal of As^{3+} from water. Two DESs systems were prepared using MTPB and BTPC as salts, in conjugation with Gly as a hydrogen bond donor. This chapter was published in the Journal of Applied Surface Science. (AlOmar, M. K., Alsaadi, M. A., Hayyan, M., Akib, S., & Hashim, M. A. (2016). *Applied Surface Science*, 389, 216-226.

Chapter 7 (Article 5: N,N-diethylethanolammonium chloride based DES-functionalized carbon nanotubes for arsenic removal from aqueous solution): In this chapter, the preparation of novel adsorbents for As^{3+} by functionalizing CNTs with DESs based on ammonium salt, i.e., DAC and Gly. This chapter was Published in the Journal of Desalination and Water Treatment (Accepted).

Chapter 8 (Article 6: Allyl triphenyl phosphonium bromide based DES-functionalized carbon nanotubes for the removal of mercury from water): This chapter introduces CNTs functionalized with DESs as novel adsorbents of Hg^{2+} from water. A phosphonium based salt, ATPB, was combined with Gly as the HBD to form a DES,

which can act as a novel functionalization agent of CNTs. This chapter was published in Chemosphere. (AlOmar, M. K., Alsaadi, M. A., Hayyan, M., Akib, S., Ibrahim, M., & Hashim, M. A. (2017). *Chemosphere*, 167, 44-52.

Chapter 9 (Article 7: Novel deep eutectic solvent-functionalized carbon nanotubes adsorbent for mercury removal from water): This chapter present a novel Hg²⁺ adsorbent that is based on CNTs functionalized by DESs. A DES formed from ammonium based salt, named TBAB, and Gly were used as functionalization agents for CNTs. This chapter was published in Journal of Colloid and Interface Science (AlOmar, M. K., Alsaadi, M. A., Jassam, T. M., Akib, S., & Ali Hashim, M. (2017). *Journal of colloid and interface science*, 497, 413-421.

Chapter 10 (Conclusion and recommendations): In this chapter, a comprehensive conclusion of the study is presented, along with recommendations for future work.

CHAPTER 2: LITERATURE REVIEW

2.1 Introduction

Water is the most important and indispensable substance on the earth for the vital bodily processes of most existing organisms. Unfortunately, through the growth of population and the needs of industrialization and civilization, the quality of available resources is deteriorating continuously and more than 700 million people cannot access to pure water sources (Ali & Gupta, 2007; HWO, 2014; Tchobanoglous & Burton, 1991). There are many different types of pollutants: organic, heavy metals, oil, radioactive nucleating metals, etc. and some of these pollutants have serious side effects on living beings. Therefore, water purification has been a focus of researchers worldwide because water availability is a major global concern which requires on going evaluation and revision to the water polices.

2.2 Heavy metals in water: impact and remediation

Toxic heavy metals refer to any relatively dense metal or metalloid that is noted for its potential toxicity (S. Srivastava & Goyal, 2010). Generally, heavy metals have a density greater of 5 g/cm^3 and an atomic weight range of 63.5 and 200.6 (Fu & Wang, 2011; N. K. Srivastava & Majumder, 2008). Heavy metal contamination is mainly caused by modern chemical industries, including metal plating facilities, fertilizer, battery manufacturing, mining, fossil fuel, paper and pesticides, tannery, metallurgical, and production of different plastics, such as polyvinyl chloride. Different kinds of hazardous heavy metals currently contaminate our water resources, including mercury, lead, chromium, zinc, nickel, and arsenic (Gong et al., 2014; C. Luo, Tian, Yang, Zhang, & Yan, 2013; Nriagu, 1988; Yamauchi & Yamamura, 1983). Owing to their high toxicity, heavy metals are considered extremely hazardous pollutants, even at very low concentration.

2.2.1 Lead

Lead (Pb) is presence in water can cause many health problems. Lead has garnered enormous concern worldwide through to its physiological effects, especially for children (Ngueta et al., 2014). Lead is a toxic element to both animals and humans and exposure to lead affects the nervous system, possibly causing brain disorders (Gad & Pham, 2014). Lead can enter into water resources through the corrosion of plumbing materials, and it can be found in water sources from the waste disposal associated with some industries (Tong, Schirnding, & Prapamontol, 2000). It has been reported that the main source of Pb in human body is drinking water (Ihsanullah et al., 2016).

2.2.2 Arsenic

One of the most toxic heavy metal is arsenic (As), which has been recognized as a deadly poison since ancient times, due to causing severe side effects and lethality. It exists in many forms with varying levels of toxicity. Relative toxicity of As species follows this trend: arsenite > arsenate > monomethyl arsenic acid (MMA) > dimethyl arsenic acid (DMA) (Duffus, 2002). Many water resources have been contaminated either naturally or through human activities (Black, 1999; Mandal & Suzuki, 2002). The maximum arsenic allowable level in drinking water is 10 µg/L, as recommended by the World Health Organization (WHO) (Smedley & Kinniburgh, 2001; B. S. Tawabini, Al-Khaldi, Khaled, & Atieh, 2011). Exposure of arsenic has been associated with many dangerous and lethal diseases, including liver, urinary tract, lung, skin, and bladder cancer (Ng, 2005; Sharma & Sohn, 2009).

2.2.3 Mercury

Mercury (Hg) is a heavy metal that exists in liquid or vapor phase at room temperature. Hg is considered to be one of the most toxic element in nature. The neurologic, gastrointestinal (GI) and renal organ systems are the most affected. Mercury can be found

in three forms: metallic element, organic salt, and inorganic salt (Goldman, Shannon, & Health, 2001). This element exists in seawater, fresh water, and in soil (*Mercury Study Report to Congress*, December 1997). In addition, Hg is a waste product of many industries, including production of chloralkali, fossil fuels, various switches, wiring devices, measuring and control devices, lighting, and dental work (A. Gupta, Vidyarthi, & Sankararamakrishnan, 2014). According to the World Health Organization (WHO), the maximum allowable concentration of Hg in water is 1µg/L. This value is due to its extremely hazardous effects, even at low concentrations (Mohan, Gupta, Srivastava, & Chander, 2001).

2.2.4 Water remediation techniques to treat heavy metals

Various conventional methods are currently being used to eliminate heavy metal ions in water, including coagulation (P. R. Kumar, Chaudhari, Khilar, & Mahajan, 2004), precipitation (Bissen & Frimmel, 2003), ion exchange (J. Kim & Benjamin, 2004), reverse osmosis (Ning, 2002), oxidation (Gihring, Druschel, McCleskey, Hamers, & Banfield, 2001), photocatalysis and flotation. However, all these techniques have limitations. For example, the hazardous waste associated with the precipitation technique needs to be treated further. The lack of availability for recyclability is considered as drawback for ion exchange remediation method, even though this method results in high removal efficiency. The cost and generation, along with the disposable of the residuals materials, are the limitations of membrane filtration technique. The coagulation and flocculation methods also suffer from the sludge volume generated and a long duration is the disadvantage of the photocatalytic technique. High selectivity is usually associated with electro dialysis, but this method also suffers from a high cost of operation and high energy consumption (Ihsanullah et al., 2016). Due to the significant drawbacks associated with the above mentioned techniques, the need for new alternatives or modified

technologies is imperative (Payne & Abdel-Fattah, 2005; Tuutijärvi, Lu, Sillanpää, & Chen, 2009). The adsorption method has been proven to be the most effective technique due to its ability to remove low concentration pollutants, the possibility of regeneration, the availability of adsorbents, and the simplicity of the process (Mobasherpour, Salahi, & Ebrahimi, 2012; G. P. Rao, Lu, & Su, 2007).

2.2.5 Adsorption technique for the removal of heavy metals

Adsorption has been proposed as a suitable water treatment technique due the ability to remove contaminants at very low concentrations, the availability of raw materials to prepare different kind of adsorption materials, and low energy consumption compared to other techniques (Ali, 2012). Adsorption defined as the attachment of soluble gas or liquid onto the surface of the adsorbent (Kaneko, 1994). Depending on the bonding types, adsorption can be classified into physisorption, where the concerned molecules, the adsorbate and adsorbent, come together through van der Waals forces, and chemisorption, where the concerned molecules are attached to the surface of the adsorbent through a strong covalent chemical bond. The criteria determining the quality of the adsorbent is the adsorption capacity, which is influenced by the surface characteristics of the adsorbent. For example, surface area, surface charge and the functional groups provide active sites with affinity toward different pollutants.

Different types of adsorbents have been reported in the field of heavy metals removal, namely activated carbon (Kadirvelu, Thamaraiselvi, & Namasivayam, 2001; Kobya, Demirbas, Senturk, & Ince, 2005; Sounthararajah, Loganathan, Kandasamy, & Vigneswaran, 2015), landfill clay (Ghorbel-Abid & Trabelsi-Ayadi, 2015), extracellular polymeric substances (J. Yang et al., 2015), fly ash (Weng & Huang, 2004), granular biomass (Hawari & Mulligan, 2006), sewage sludge ash (Pan, Lin, & Tseng, 2003), peat (Ho & McKay, 1999), peanut hulls (Brown, Atly Jefcoat, Parrish, Gill, & Graham, 2000),

manganese oxides (E.-J. Kim, Lee, Chang, & Chang, 2013), bagasse (M. Rao, Parwate, & Bhole, 2002), modified chitosan (Justi, Fávere, Laranjeira, Neves, & Peralta, 2005), and many others. However, these adsorbents have numerous drawbacks, including low removal efficiency and low adsorption capacity (Ihsanullah et al., 2016). Therefore, the need to explore new adsorbents is essential. The revolution of nanotechnology opened the door for a new era of adsorption processes. Carbon nanotubes (CNTs) have been reported to be the best nano-based adsorbent due to extraordinary physical and chemical properties. CNTs are naturally stable, but the raw-CNTs are considered to be poor adsorbents. However, by adding functional groups to the CNT surface, the adsorption efficiency, selectivity, and sensitivity toward heavy metals can be increased remarkably. The functionalization and activation of the CNTs surface is essential to create an affinity for different pollutants. Many studies have been done to improve the adsorption capacity of CNTs based adsorbents for heavy metals adsorption.

2.3 Removal of heavy metals by functionalized carbon nanotubes

Carbon nanotubes (CNTs) were first reported by Iijima (Iijima, 1991). CNTs consist of either one or more graphite sheets wrapped around itself in a cylindrical shape with a radius of less than 100 nanometer (nm) and a length up to 20 cm (H. W. Zhu et al., 2002). So called single walled carbon nanotubes (SWCNTs) are shaped from one graphene sheet. Meanwhile, the term multi walled carbon nanotubes (MWCNTs) is used for CNTs that consist of more than one graphene sheets. Figure 2.1 illustrates the differences between MWCNTs and SWCNTs. CNTs are usually classified into three different types: armchair, zigzag, and chiral nanotubes, depending on the way the graphene sheet is rolled up in the two-dimensional direction. The zigzag, which is usually defined by the pattern of hexagons as one moves circumferentially around the body of the tubule, as illustrated in Figure 2.2 a. The armchair, which is presented Figure 2.2 b, can be described as one of

the two conformers of cyclohexane, a hexagon of carbon atoms, and is defined by the shape of the hexagons as one moves around the body of the tubule. Figure 2.2 c demonstrates the third form of CNTs, which is known as the chiral form. It is believed that this type usually occurs in SWCNT. The name chiral means handedness and indicates that the tubes may twist in either direction. The geometry of the chiral SWCNTs lies between that of the armchair and zigzag SWCNTs (Baughman, Zakhidov, & de Heer, 2002).

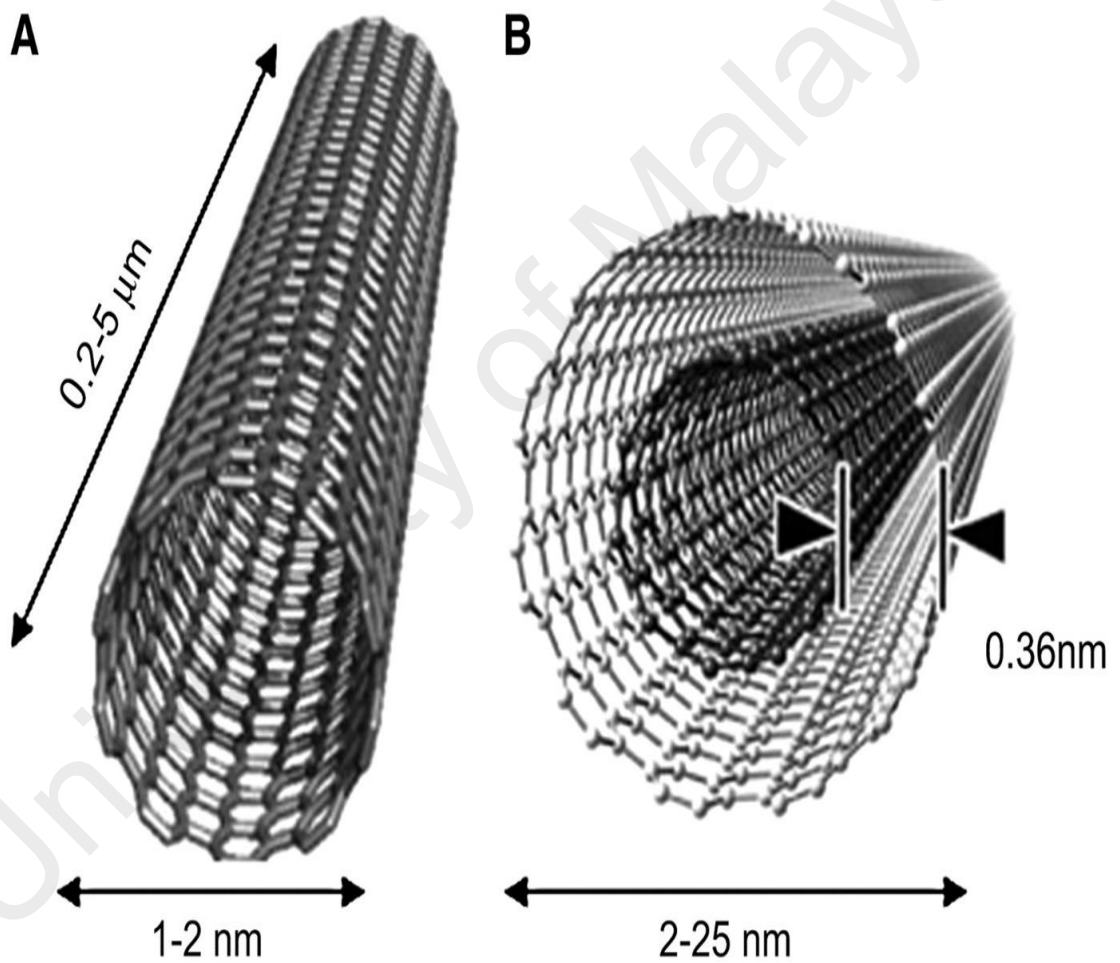


Figure 2.1: The structure of single and multi-walled carbon nanotubes(N. M. Mubarak, Sahu, Abdullah, & Jayakumar, 2014)

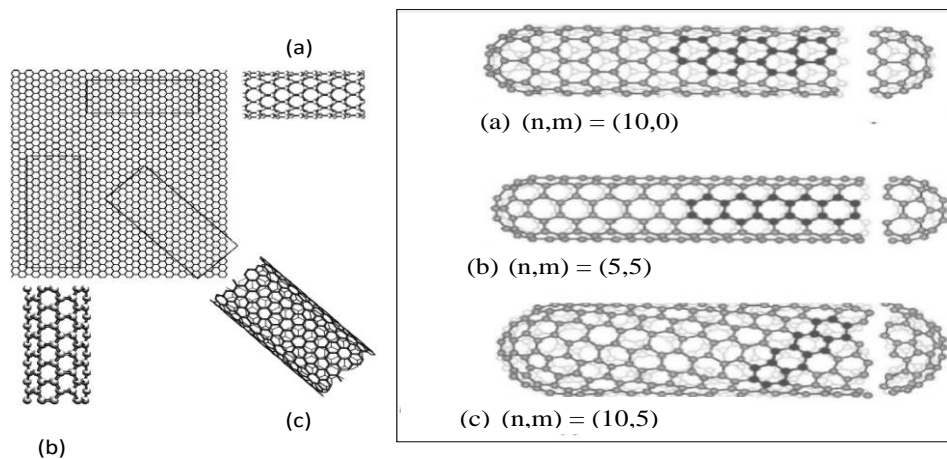


Figure 2.2: Patterns of CNT twist. (a) Zigzag Single-Walled Nanotube. Note the zigzag pattern around circumference and $m = 0$. (b) Armchair Single-Walled Nanotube. Note the chair-like pattern around circumference and $n = m$ (c) Chiral Single-Walled Nanotube. Note

MWCNTs consist of more than one graphene cylinder nested one into another. TEM analysis revealed that the spacing of inter shell can vary from 0.335 nm to 0.34 nm, augmenting the diameter of diminishing tube. Gogotsi & Corporation, 2006; and Saito et al., 1998, reported that the biggest spacing for the smallest diameter is found in the high curve, following in an unfavorable augmented force, and linked to a diminishing diameter diminished in the shells of the CNTs. A value of 0.34 nm spacing in the bulk graphite crystal is roughly that of the CNTs (Gogotsi, 2006; Saito, Dresselhaus, & Dresselhaus, 1998). However, Ru, 2000, reported that the mean value of the interlayer spacing is 0.3444 ± 0.001 nm. Meanwhile, the CNTs values are slightly larger, by few percent, than those in the bulk graphite crystal (C. Q. Ru, 2000). The distance between the two layers is $d = 3.39 \text{ \AA}$, as per the theoretical calculations, which is slightly larger than that observed for graphite. Experimentally, by using TEM images, the MWCNTs have been found to exhibit an interlayer separation of $d = 3.4 \text{ \AA}$ (Ebbesen & Ajayan, 1992).

The fascinating structure of CNTs results in magnificent physical and chemical properties. The CNTs can be considered as one of the strongest materials on earth, due to then way the carbon atoms bond in the sp_2 direction. It has been reported that CNTs have

the highest Young's modulus and a strength that is higher than steel by 10-100 times (Thostenson, Ren, & Chou, 2001; Yamabe, 1995). Popover, 2004, reported the thermal conductivity and the specific heat using phonons (Popov, 2004). The thermal conductivity of MWCNTs has been reported to be 4-300 k (Yi, Lu, Dian-lin, Pan, & Xie, 1999), while, for SWCNTs, it has been reported as 8-350 K (Hone, Whitney, Piskoti, & Zettl, 1999). In addition, CNTs have a relatively high electrical conductivity compared to other conductive materials (Collins & Avouris, 2000). The arrangement of hexagonal rings along the tubular surface affects the conductivity status of CNTs whether it is metallic or a semiconductor. In SWCNTs, the chiral vector (n, m) is responsible for the metallic or semiconducting properties, where n and m are two integers. The differences of n and m are responsible for the metallic state or semiconducting, whereby, a multiple three difference in n-m results in a metallic state of CNTs and, if it varies from three, then the CNTs would be a semiconductor. In addition, it is also the possibility to connect nanotubes with different chiralities, creating nanotube heterojunctions, which can form a variety of nanoscale molecular electronic device components (Arnold, Green, Hulvat, Stupp, & Hersam, 2006).

2.3.1 Functionalization of CNTs

Due to extraordinary physical, electrical, and chemical properties, CNTs have highly promising applications in material science, electrical engineering, environmental engineering, and medical science. Nevertheless, there are issues regarding solubility, aggregation, and difficult manipulation, which impose a significant limitation on the applications of CNTs. In addition, CNTs have no chemically active dangling bonds and the ratio of weak sites (C-C bonds involved in heterocyclic) over strong sites (C-C bonds between regular hexagons) is approaches 0 for ideally perfect tubes (Bhushan, Kasai, Nguyen, & Meyyappan, 2004). Moreover, the chemical reactivity of carbon nanotubes is proposed to mainly originate from the caps, since they contain six pentagons, with each

opposed to the tube body that supposedly contains hexagon only. However, CNTs have shown a great affinity for interaction with different compounds (Andrews, Jacques, Qian, & Rantell, 2002; Fischer, 2002; Hirsch & Vostrowsky, 2005; T. Lin, Bajpai, Ji, & Dai, 2003; X. Lu & Chen, 2005; Niyogi et al., 2002; Y.-P. Sun, Fu, Lin, & Huang, 2002; Thostenson et al., 2001). Functionalization of CNTs is a key feature, depend on their physical and chemical properties, that is directly affected by their chemical composition, particle size, and surface nature. In other word, functionalization of CNTs, through the addition of functional groups on its surface, is considered as one of the special characteristic of CNTs. Whereby, functionalization can be designed to fit certain applications. Consequently, functionalization can be split into two classes: the covalent attachment of the functional groups via chemical reaction with the skeleton of the CNT, and non-covalent functional groups which coat the walls of the CNT (Karousis, Tagmatarchis, & Tasis, 2010). Based on the first class, functionalization of CNTs results in many applications. Chen et al., (1998) reported the functionalization of SWCNTs by adding chlorine (Cl) to the sidewalls through reaction with soluble dichlorocarbene, which resulted in saturation of 2% of the carbon atoms in SWCNTs with C-Cl, which led to dramatic changes in the electronic band structure (J. Chen et al., 1998). Oxidative functionalization is the most common functionalization technique. Basically, this technique consists of acidification of CNTs by refluxing in boiling acids, including nitric acids, sulfuric acid, or a mixture of both (Esumi, Ishigami, Nakajima, Sawada, & Honda, 1996). The other type of oxidation occurs using a strong oxidant, such as KMnO_4 (Salam, 2013; R. Yu et al., 1998). Adding carboxylic groups to CNTs by oxidative procedures results in a significant number of functional groups, which can be further expanded to more application and functionalization (Hirsch & Vostrowsky, 2007). The most chemically active functional groups are carboxylic acid ($-\text{COOH}$) or hydroxyl ($-\text{OH}$) groups (P.-C. Ma, Siddiqui, Marom, & Kim, 2010). Furthermore, the attachments of such

functional groups results in changes to the hydrophobic nature of CNTs, resulting in a hydrophilic structure due to the polar groups attached to its surface that allow the CNTs to be soluble in organic solvents. Haddon et al. (1998) introduced the use of alkyl amines and less nucleophilic aniline derivatives as functionalization agents of oxidatively treated SWCNTs. The effect of octadecyl amine obtained from the acid functionality resulted in soluble SWCNTs. (J. Chen et al., 1998; Mark A. Hamon et al., 1999). CNTs have also been functionalized by silanation (P. C. Ma, Kim, & Tang, 2006), thiolation (Hirsch & Vostrowsky, 2007), polymer grafting (P. Liu, 2005; Mittal, Dhand, Rhee, Park, & Lee, 2015), esterification (M. A. Hamon, Hui, Bhowmik, Itkis, & Haddon, 2002), alkylation and arylation (Stephenson, Sadana, Higginbotham, & Tour, 2006), and biomolecules (Coleman, Khan, & Gun'ko, 2006).

Recently, ionic liquids (ILs) have gained increasing interest as green solvents due to their unique properties. ILs were also introduced as functionalization agents of nanomaterials. The first combination of nanotechnology and ionic liquids was presented by Deshmukh et al. (2001) (Deshmukh et al., 2001). Park et al. (2006) investigated the role of IL anion on MWCNT solubility in water and organic solvents through a series of anion exchanges (i.e. [Br], [BF₄], [PF₆], and [TFSI]) to functionalize acid-treated MWCNTs (MWCNTs-COOH) using ILs (Park et al., 2006). ILs have succeeded in replacing strong acids or organic solvents as functionalization reaction media. The main advantage of using ILs as functionalization agents is the non-distractive reaction, where the organic solvent strategy retains the properties of CNTs (Polo-Luque, Simonet, & Valcárcel, 2013).

Since CNTs have the tendency to accept different kinds of functional groups, CNTs have conquered almost all fields of science. Owing to their specific structure, surface area, and morphology, CNTs have been shown to be an excellent adsorbent due to the variety of

possible adsorption sites. CNTs have great potential to remove many kinds of pollutants, including dioxin (Long & Yang, 2001), nitrogen, methane (Bienfait et al., 2004), ammonia (Bauschlicher & Ricca, 2004a), hydrogen (A. C. Dillon, 1997), and ozone (Yim & Liu, 2004), from air, and cadmium (Y.-H. Li, Wang, Luan, et al., 2003), zinc (C. Lu & Chiu, 2006), lead (Y.-H. Li et al., 2002), 1,2-dichlorobenzene (Peng et al., 2003), fluoride (Y.-H. Li, Wang, Zhang, et al., 2003), and trihalomethanes (C. Lu, Chung, & Chang, 2005). Therefore, CNTs have been a subject of interest for researchers worldwide as an adsorbent, and have resulted in more publications than any other adsorbent (Ali, 2012).

2.3.1.1 Adsorption of Lead (Pb) ions by functionalized CNTs

Due to the serious effects of Pb ions in water, several techniques have been proposed to decrease aqueous Pb concentrations. Adsorption is considered to be the most effective method for removal of lead ions (H. J. Wang, Zhou, Peng, Yu, & Chen, 2007). Different types of adsorbents have been used to remove Pb(II) from water. Examples include rice husks, maize cobs, sawdust (Abdel-Ghani, Hefny, & El-Chaghaby, 2007), aquatic plant (Axtell, Sternberg, & Claussen, 2003), kaolinitic clay, giru clay (Orumwense, 1996), and granulated blast-furnace slag (Dimitrova & Mehandgiev, 1998). Furthermore, the most useable adsorbent is activated carbon, which can originate from different sources (Goel, Kadirvelu, Rajagopal, & Kumar Garg, 2005; Imamoglu & Tekir, 2008; Netzer & Hughes, 1984; Sekar, Sakthi, & Rengaraj, 2004; Tao, Zhang, Li, & Ding, 2015). Nanoparticles have been found to be effective adsorbents for many pollutants due to their unique features, including small size, catalytic potential, high reactivity, and large surface area (Ali, 2012). In the field of water treatment, carbon nanotubes (CNTs) are the most commonly used nanomaterial. Herein, the adsorption of lead by CNTs will be reviewed and discussed.

It is well known that the most conventional functionalization is oxidation with acids or by KMnO_4 . It was reported that the maximum adsorption capacity of acidified CNTs with HNO_3 reached 85 mg/g at 50 mg/L initial metal concentration in 6h, and that Pb(II) can be regenerated by reducing the pH of the solution to 2.0 (H. J. Wang et al., 2007). Tofighy et al. (2011) (Tofighy & Mohammadi, 2011) reported that the maximum adsorption capacity of HNO_3 treated CNT sheets was 101.5 mg/g for Pb(II) . Meanwhile, the attachments of MnO_2 on the MWCNTs, by mixing the CNTs with KMnO_4 at 70 °C with drop-wise addition of NaOH , increased the reaction speed to reach a maximum adsorption at 5 min contact time (Salam, 2013). Furthermore, other researchers used a redox process to coat Mn on the surface of CNTs (Richter, Berndt, Eckelt, Schneider, & Fricke, 1999). The adsorption on MnO_2/CNTs was highly pH depended and the adsorption percentage increased from 77% to 98% at a pH range between 2 and 4. Another type of efficient functionalization to reduce Pb(II) is the alumina coating of MWCNTs. The structure of this is explained in Figure 2.3 (Vinod K. Gupta, Agarwal, & Saleh, 2011).

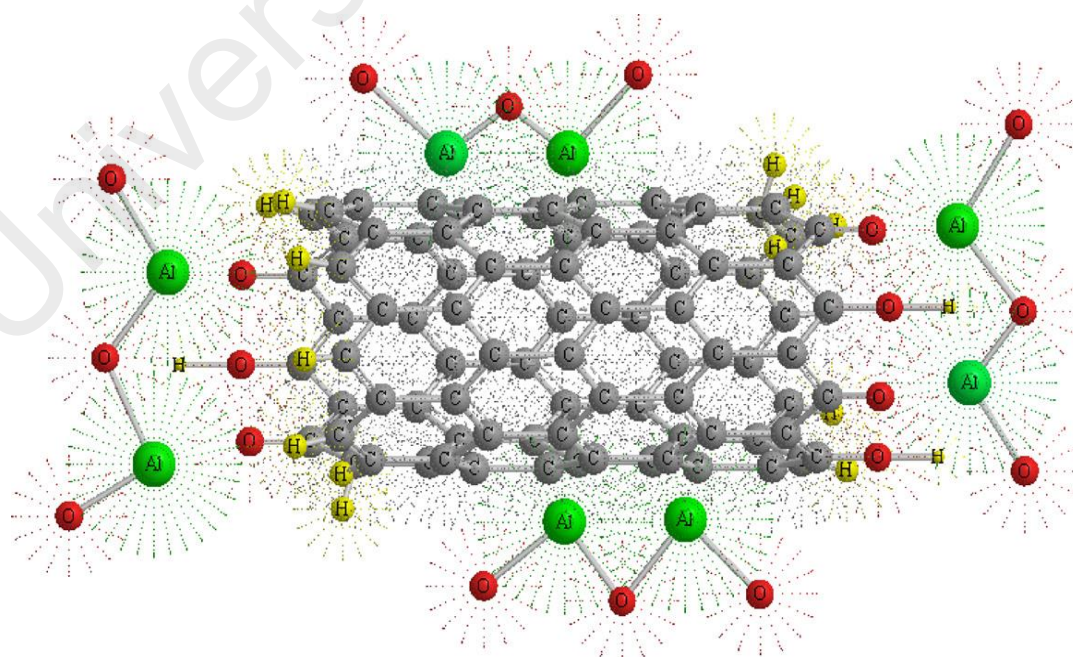


Figure 2.3: Alumina coated MWCNTs structure (V. K. Gupta et al., 2011)

Due to the strong affinity of the nitrogen in amine and imine functional groups towards metals ions, two steps of a plasma induced polymerization procedure were performed to synthesis polymerized aniline molecules (PANI) functionalized MWCNTs magnetic composite. This procedure increased the maximum adsorption capacity of Pb(II) from 13.3 mg/g on MWCNTs to 21.0 mg/g on a PANI/MWCNT composite (Shao, Chen, & Wang, 2012). Zhou et al. (2014) synthesized MWCNTs coated with magnetic amino modified CoFe_2O_4 ($\text{CoFe}_2\text{O}_4\text{-NH}_2$) nanoparticles via a simple one-pot polyol method. Then, the prepared composite was modified with chitosan (CTS), and the final product (MNP-CTS) was used as an adsorbent for tetrabromobisphenol A (TBBPA) and Pb(II). The maximum adsorption capacity of Pb(II) onto MNP-CTS reached 140.1 mg g^{-1} . As for most heavy metals adsorbents, the adsorption was highly pH dependent (Zhou et al., 2014). Likewise, the maximum adsorption capacity of Pb(II) onto titanium dioxide/MWCNTs ($\text{TiO}_2/\text{MWCNTs}$) reached 137.0 mg/g at pH 6.0 (X. Zhao, Jia, Song, Zhou, & Li, 2010).

Hamza et al. (2013) reported that the use of a sugarcane bagasse/MWCNTs composite that increased the maximum adsorption capacity to 56.6 mg/g at pH 4 with a temperature of 28 °C, and the isotherm model fit the Langmuir model. In addition, it was observed that pH had a significant effect on the removal efficiency, which increased from 23.4 % to 99.8% when the pH was increased from 1 to 4.5 (Hamza, Martincigh, Ngila, & Nyamori, 2013). Similarly, the maximum adsorption capacity of impregnated CNTs on bamboo charcoal (CNT/BC) reached 47.4 mg/g at pH 5 (Huang, Zhang, Wang, Lv, & Kang, 2012).

Lin et al. (2012) reported the uses of solid humic acid (HA) and MWCNTs (HA-MWCNTs) as adsorbents of Pb(II) ions from water. It is well known that CNTs have a weakly positive charge, however, the charge reached zero after coating with HA. Later,

by adding acidic functional groups, the surface was negatively charged, which led to an increase in the adsorption efficiency of Pb(II) ions due to increased electrostatic attraction. The Langmuir model describes the isotherm of the three adsorbents with a maximum adsorption capacity of 318 and 333 mg/g for 25% HA-CNTs and 50% HA-CNTs, respectively (D. Lin et al., 2012). Response surface methodology was utilized in order to optimize the removal conditions of Pb(II) with commercialized CNT-COOH. The maximum removal percentage reached 96.84 % at pH 5.1 and an initial Pb(II) concentration of 10 mg/l (Bingöl & Bozbaş, 2012).

The structure of CNTs and their specific surface area play an important role in the removal of heavy metals ions. It was reported that decreasing the outer diameter of CNTs results in increasing the adsorption capacity. However, by increasing the outer diameter with oxygen functional groups, by oxidizing CNTs with NaClO for example, the adsorption capacity increased. This indicates that the adsorption capacity actually depends on both oxygen groups and the specific surface area of the MWCNTs. In addition, the effects of surface oxidation were remarkably obvious with regard to adsorption capacity due to increasing negative charge, and the phonic groups play an important role in the adsorption capacity due the large affinity of phonic groups toward Pb(II) ions. Therefore, the adsorption mechanism involved both chemisorption and physisorption (F. Yu, Ma, & Wu, 2011; F. Yu, Wu, Ma, & Zhang, 2013).

Vukovic et al. (2009, 2010, and 2011) functionalized MWCNTs with amino groups via chemical modification of carboxyl groups using O-(7-azabenzotriazol-1-yl)-N,N,N',N'-tetramethyluronium hexa fluorophosphate (N-HATU) and N,N-diisopropylethylamine (DIEA) (G. Vuković et al., 2009; G. D. Vuković et al., 2010). The adsorption of Pb⁺² on o-MWCNT, e-MWCNT and d-MWCNT (Figure 2.4 a and b) was less than 25% at pH<5 and reached 75% at pH>5. The optimum pH was 6.2 for adsorption

of Pb^{2+} . However, for the adsorption capacities of t-MWCNTs, pHs between 2 and 11 only caused a 15 to 20% increase in the adsorption capacity, which indicates that the additional amino groups have a considerable influence on the adsorption capacity (G. D. Vuković et al., 2011).

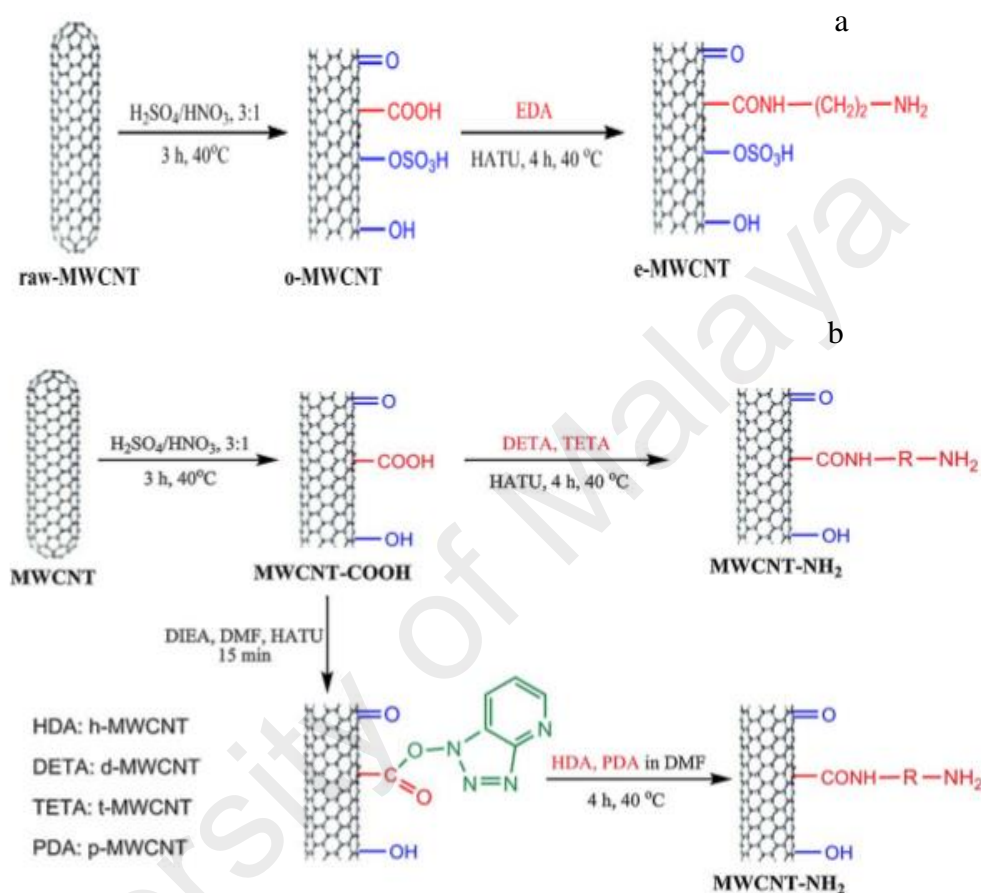


Figure 2.4: Functionalization of MWCNTs by amino groups and the abbreviations (G. Vuković et al., 2009; G. D. Vuković et al., 2010)

Kabbashi et al , 2009 reported the usage of CNTs as an adsorbent for the removal of $Pb(II)$ ions from aqueous solution. PH, agitation speed, amount of CNTs, and contact time were investigated. The $Pb(II)$ removal rate reached 96.03% at pH 5.0, 40 mg/L CNTs, 80 min contact time, and 50 r/min agitation speed(Kabbashi et al., 2009). Zhang et al. (2013) reported that the adsorption capacity of graphene–CNT aerogels was between 230-451 mg/g, and the amount of CNT and $FeSO_4$ are the most important factors for efficient removal (M. Zhang, Gao, Cao, & Yang, 2013). Another method to modify CNTs for

Pb(II) removal is the synthesized Zeolite supported carbon nanotubes (ZCNTs), which have an adsorption capacity of 55.74 mg/g. The adsorption rate on ZCNTs follows a pseudo-second-order kinetics model with a fair fit and the Langmuir model fitted the isotherm data (Venkata Ramana et al., 2012). Moreover, Tan et al. (2012) studied the effects of hyperchromic on the adsorption of Pb(II) onto carboxylic CNTs by investigating the order of the reaction for the absorbance (Tan et al., 2012).

An electrochemical adsorption technique has also been used to reduce Pb(II) concentration in water. Liu et al. (2013) used a stainless-steel net coated with SWCNT (SWCNT@SSN) as an anode and cathode. The Pb(II) ions were attracted to the cathode surface and removal reached 97.2% and 99.6% with initial concentrations of Pb(II) at 20 and 159 mg dm⁻³, respectively (Y. Liu, Yan, Yuan, Li, & Wu, 2013). Table 2.1 lists the other types of CNTs modifications for Pb(II) removal, along with the adsorption effective parameters.

Table 2.1: Different CNTs based adsorbents for lead ions

Adsorbent	Isotherm	Kinetics model	remarks	Ref.
acid-treated CS-CNTs	Langmuir	Pseudo second-order	The adsorption capacity was 158.7	(Gong et al., 2014)
HNO ₃ functionalized CNTs	Langmuir	Pseudo second-order	The adsorption capacity was 25.6	(Pyrzynska & Stafiej, 2012)
8-hydroxyquinoline/CNTs	NA	NA	The adsorption performance decreased from 93.65% to 68.6% by increasing pH from 6 to 9	(Kosa, Al-Zhrani, & Abdel Salam, 2012)
MWCNTs	NA	NA	1 mg metals ion pH 2.0, shaking for 30 min the adsorption capacity was 10.3	(Tuzen, Saygi, Usta, & Soylak, 2008)
NN-mSiO ₂ @MWCNTs	NA	NA	The optimum pH was 6.5	(W. Yang et al., 2013b)
MPTS-CNTs/Fe ₃ O ₄)	Langmuir	pseudo-first-order model	The adsorption was pH depended, the maximum adsorption capacity was 65.40 at pH 6.5	(C. Zhang, Sui, Li, Tang, & Cai, 2012)
MWCNTs-TB	NA	NA	The maximum adsorption capacity was 3.69 at pH 6.0	(Jie Zhang, 2013)
CNTs oxidized with HNO ₃	Freundlich	NA	The maximum adsorption capacity was 2.96 at pH 9.0 initial concentration 2-20 mg/l	(Stafiej & Pyrzynska, 2007)
<i>Pseudomonas aeruginosa</i> immobilized multiwalled carbon nanotubes	NA	NA	The maximum adsorption capacity was 6.07 at pH 9.0	(Tuzen et al., 2008)
Schiff base-chitosan-grafted multiwalled carbon nanotubes (S-CS-MWCNTs)	NA	NA	The optimum pH occurs at pH 7.0	(Dai et al., 2012)
Carbon nanotubes-iron oxides magnetic composites	Freundlich	NA	The maximum adsorption capacity was 0.51 at pH of 5.0 at 20 °C	(Peng, Luan, Di, Zhang, & Zhu, 2005)

Table2.1 continued: Different CNTs based adsorbents for lead ions

MWCNTs	intra-particle diffusion	pseudo-second order	Study the effect of pH, ionic strength, and ect.	(Salam, Al-Zhrani, & Kosa, 2012)
CNT oxidized with nitric acid	Langmuir and Freundlich	Various with the different initial concentration	The maximum adsorption capacity was 101.05 at pH 7.0, 25 °C	(Tofighy & Mohammadi, 2011)
Functionalized MWCNT with encapsulated Fe nanoparticles	NA	NA	The variation in metal ions concentration shows a slightly negative effect on the adsorption efficiency	(H. Wang et al., 2012)

2.3.1.2 Adsorption of Mercury (Hg) ions by functionalized CNTs

Removing Hg ions from water is crucial to maintaining drinkable water resources. With this in mind, many conventional techniques have been utilized to reduce Hg concentrations in water. Examples include solvent extraction, precipitation, ion-exchange, reverse osmosis, membrane separation, coagulation, and photoreduction (Bandaru et al., 2013). However, most of these methods require either high energy or large quantities of chemicals (F.-S. Zhang, Nriagu, & Itoh, 2005). Based on this, new techniques for Hg elimination are essential. Adsorption processes are considered the most applicable in the industrial complex and, consequently, are the most studied technique for Hg removal from water (Chandra & Kim, 2011; Chiarle, Ratto, & Rovatti, 2000).

Based on the forgoing, this section reviews the removal of mercury by adsorption techniques using CNTs based adsorbents. Amino thiol functionalized CNTs have significantly increased the adsorption capacity of CNTs toward Hg^{2+} . Examples include the synthesis of thiol-derivatized SWCNT via reacting acid-cut SWCNTs with cysteamine hydrochloride using carbodiimide coupling (SWCNT-SHs), which have a much higher adsorption capacity compared to pristine SWCNTs and fourfold that of activated carbon. The maximum adsorption capacity was 131 mg/g. The adsorption efficiency of recovered SWCNT-SH remains up to 91% after five-fold usage (Bandaru et al., 2013). Another example is the synthesis of thiol-functionalized MWCNTs/ magnetite nanocomposite via grafting mercaptopropyltriethoxysilane (MPTS) onto the surface of (CNTs/ Fe_3O_4) to create MPTS-CNTs/ Fe_3O_4 nanocomposites and remove Hg^{2+} and Pb(II). The maximum adsorption capacity reached 65.52 and 65.40 mg/g for Hg^{2+} and Pb(II), respectively, at pH 6.5. The results show that the adsorption capacity is highly pH depended, with an optimum pH at 6.5. As the pH increased, the adsorption decreased due to the competition between the metals ions and H^+ , while the H^+ ion bonds are weakened due to combination with thiol groups, or through the tendency of metals ions to hydrate

M(OH)₂ at higher pHs (C. Zhang et al., 2012). El-Sheikh et al. (2011) studies the effects of geometrical dimension with oxidized and non-oxidized MWCNTs on the adsorption efficiency of Hg(II) from water samples (El-Sheikh, Al-Degs, Al-As'ad, & Sweileh, 2011). Kinetics studies were reported by Chen et al. (2014) for conventional functionalization MWCNTs with HNO₃ and also for MWCNTs functionalized with KMnO₄/H₂SO₄. This work indicated that the experimental data fitted well with a pseudo-second order model. However, the results also revealed that the adsorption mechanism was chemisorption, according to the Elovich model. Also, using the intraparticle diffusion model, the adsorption implicated intraparticle diffusion, but not as the sole rate-controlling mechanism. In addition, the isotherm model was described well by the Langmuir equation and the adsorption capacity for the functionalized MWCNTs was higher than that of pristine MWCNTs (P. H. Chen, Hsu, Tsai, Lu, & Huang, 2014). Table 2.2 lists different CNTs based adsorbents of Hg ions.

Table 2.2: Different CNTs based adsorbents for mercury ions

Adsorbent	Adsorption capacity	Isotherm	Kinetics	Remarks	Ref.
COOH-MWCNTs	127.6	Langmuir	pseudo-second-order	Electrostatic interactions, pH of 4.3, initial concentration of 4 mg/L	(P. H. Chen et al., 2014)
Sulfur containing MWCNTs (SMWCNTs)	72.8 $\mu\text{g/g}$	Freundlich	NA	pH of 12.15, initial concentration of 100 ppb	(Pillay, Cukrowska, & Coville, 2013)
MnO ₂ -coated carbon nanotubes	58.82	Langmuir	Intraparticle diffusion	initial concentration of 10 mg/L, pH of 5–7, contact time of 80 min, t 50 °C	(Moghaddam & Pakizeh, 2015)
Functionalized (sulfur incorporated MWCNT (CNT-S))	151.51	Langmuir	Pseudo second order	The adsorption occurs due Ion exchange, pH 6, initial concentration 100–500 mg/L	(A. Gupta et al., 2014)
MWCNT	13.16	Langmuir	Pseudo second order	Initial concentration of 0.1 mg/l	(B. Tawabini, Al-Khaldi, Atieh, & Khaled, 2010)
Ox-MWCNTs impregnated Chitosan beads	183.2	Langmuir	NA	pH of 4, electrostatic adsorption	(Shawky, El-Aassar, & Abo-Zeid, 2012)

2.3.1.3 Adsorption of Arsenic (As) ions by functionalized CNTs

Arsenic (As) is considered to be one of the most difficult heavy metal in terms of removal. Hence, the CNTs based adsorbents are applied less for arsenic removal, compared to other heavy metals. Velickovic' et al. (2013) oxidized CNTs with a mix of H₂SO₄ and HNO₃ combined with sonication for 3 h at 40 °C. Later, the Oxidized MWCNTs (O-MWCNT) dispersed in EDA–ethylenediamine (EDA) in the presence of (1-[Bis(dimethylamino) methylene]-1H-1,2,3-triazolo[4,5-b] pyridinium 3-oxid hexafluorophosphate) and methanol) (N-HATU) as a coupling agent with sonication for 4h at 40°C. The adsorption was described well by the Freundlich model and the maximum adsorption capacity reached 12 mg/g for O-MWCNT (Z. S. Veličković et al., 2013). It is well known that arsenic has affinity to different metal oxides, which can be seen in the many publications for different metals based adsorbents (Andjelkovic et al., 2013; Cui, Li, Gao, & Shang, 2012; Di et al., 2006; Feng et al., 2012; Ghosh, Poinern, Issa, & Singh, 2011; K. Gupta et al., 2011; Mak, Rao, & Lo, 2009; Martinson & Reddy, 2009; Mohmood et al., 2013; Patel, Byun, & Yavuz, 2012; Ramos, Yan, Li, Koel, & Zhang, 2009; Selvakumar et al., 2011; Tresintsi et al., 2013; Tuutijärvi et al., 2009). With this in mind, Tawabini et al. (2011) used an iron oxide (Fe-MWCNT) composite to remove As³⁺. The removal reached 84.8% at pH 7-8 and the adsorption showed good agreement with the Langmuir isotherm model and the kinetics followed a pseudo-second-order rate model (B. S. Tawabini et al., 2011). Table 2.3 lists some CNTs- based adsorbents of As ions.

Table 2.3: Different CNTs- based adsorbents for arsenic ions.

As state	Adsorbent	Adsorption capacity	Isotherm	Kinetics	Remarks	Ref.
As ⁵⁺	Fe(III) oxide coated ethylene-diamine modified MWCNTs	23.47	Langmuir	pseudo-second-order	Ion exchange, pH of 4.0	(Z. Veličković et al., 2012)
As ⁵⁺	MWCNT-zirconia nanohybrid (MWCNT-ZrO ₂)	5000 µg/g	Langmuir	pseudo-second order	pH 6, Initial concentration, 100 µg/L Chemisorption/ physisorption	(Addo Ntim & Mitra, 2012)
As ⁵⁺	Iron oxide coated MWCNT	189 µg/g	Langmuir	Pseudo-second-order	Initial concentration 100 µg/L, pH 4.0	(Addo Ntim & Mitra, 2011)
As ³⁺	Iron oxide coated MWCNT	1723	Langmuir	Pseudo-second-order	The removal happened due Electrostatic interactions/complexation	(Addo Ntim & Mitra, 2011)
As ³⁺	MWCNT-zirconia nanohybrid (MWCNT-ZrO ₂)	2000	Langmuir, Freundlich	pseudo-second order	The optimum removal conditions were at pH 6, initial concentration of 100 lg/L	(Addo Ntim & Mitra, 2012)

2.4 Deep eutectic solvents (DESs) and its applications

In the last two decades, there has been increasing interest in the applications of ionic liquids (ILs), especially with respect to catalysts, electrochemistry process technology and analytics, biotechnology, and functional liquids. ILs are solvents which consist solely of ions. Mainly, the synthesis of ILs can be split into two distinct categories, those formed from eutectic mixtures of metal halides and organic salts, and those containing discrete anions (E. L. Smith, Abbott, & Ryder, 2014). Many of the possible applications of ILs are dependent on their physical and chemical properties (Q. Zhang, Zhang, & Deng, 2011). Nevertheless, ionic liquids have limitations due to their relatively high cost and the waste disposal associated with their synthesis (Phadtare & Shankarling, 2010). Consequently, many researchers in the last decades have attempted to reduce the cost of ILs. Therefore, the need for solvents with reasonable prices that are easy to synthesize, and are environmentally benign inspired Abbot et al. (2003) to present the so-called deep eutectic solvents (DESs) for the first time as a replacement or improvement of ILs (Andrew P. Abbott et al., 2003).

DESs are a developing class of solvents that are ionic liquid analogues (A. P. Abbott et al., 2001). Basically, DESs are mixtures of two or more compounds that have a melting point that is lower than that of the individual components (Andrew P. Abbott, Boothby, et al., 2004; M. Hayyan et al., 2010). Furthermore, DESs are prepared by mixing a salt and a hydrogen bond donor (HBD). DESs can be made of different types of salts (organic and inorganic) and different kinds of HBDs (Q. Zhang, De Oliveira Vigier, Royer, & Jerome, 2012). DESs can be divided into three distinct types. Class (A) DESs are composed of an ionize salt and a HBD. This class is the most heavily studied and choline chloride and urea DES are examples of this type of DESs, as shown in Figure 2.5. Class (B) DESs involve the combination of an ionize salt with a metal salt, such as choline chloride and zinc chloride (A. P. Abbott, G. Capper, D. L. Davies, & R. Rasheed, 2004).

The third class (C) are complex compared to the other classes. This class of DESs is usually represented by the combination of a carbohydrate, urea, and an ammonium salt in varying ratios. An example of this type is the choline chloride : d-fructose DES (A. Hayyan et al., 2012).

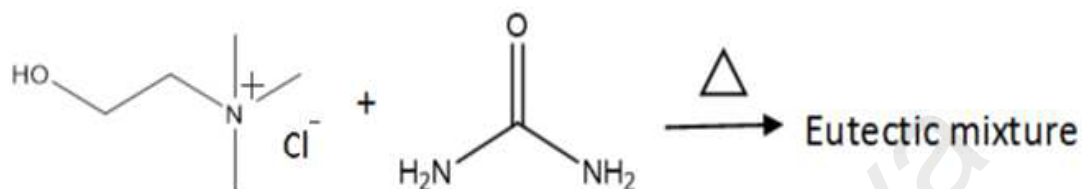


Figure 2.5: ChCl:U eutectic mixture

The physicochemical properties of DESs are much like those of conventional ILs (M. Hayyan, M. A. Hashim, M. A. Al-Saadi, et al., 2013). Generally, both DESs and ILs are similar in terms of non-flammability, non-volatility, starting materials, and high viscosity. Based on this, DESs are referred to as the fourth generation of ILs (Cvjetko Bubalo, Vidović, Radojčić Redovniković, & Jokić, 2015a). However, DESs have many advantages over conventional ILs, including simplicity of the synthesis, lower production cost, low or negligible toxicity profiles, and sustainability with respect to environmental and economic benefits (M. Hayyan, Abo-Hamad, et al., 2015a; M. Hayyan, M. A. Hashim, M. A. Al-Saadi, et al., 2013; M. Hayyan, M. A. Hashim, A. Hayyan, et al., 2013). In another words, the components of DESs can be synthesized easily, economically, conveniently and in a large scale. Furthermore, the syntheses of DES are done by simply mixing the components, which eliminates the tedious jobs of purification and waste disposal (Q. Zhang et al., 2012).

2.4.1 DES preparation

The first DESs were prepared by mixing urea and choline chloride at 80 °C until the mixture became a homogenous liquid (Andrew P. Abbott et al., 2003). Subsequently, different types of DESs were reported using different salts and HBDs. Figure 2.6 illustrates some of the starting materials reported for DESs preparation.

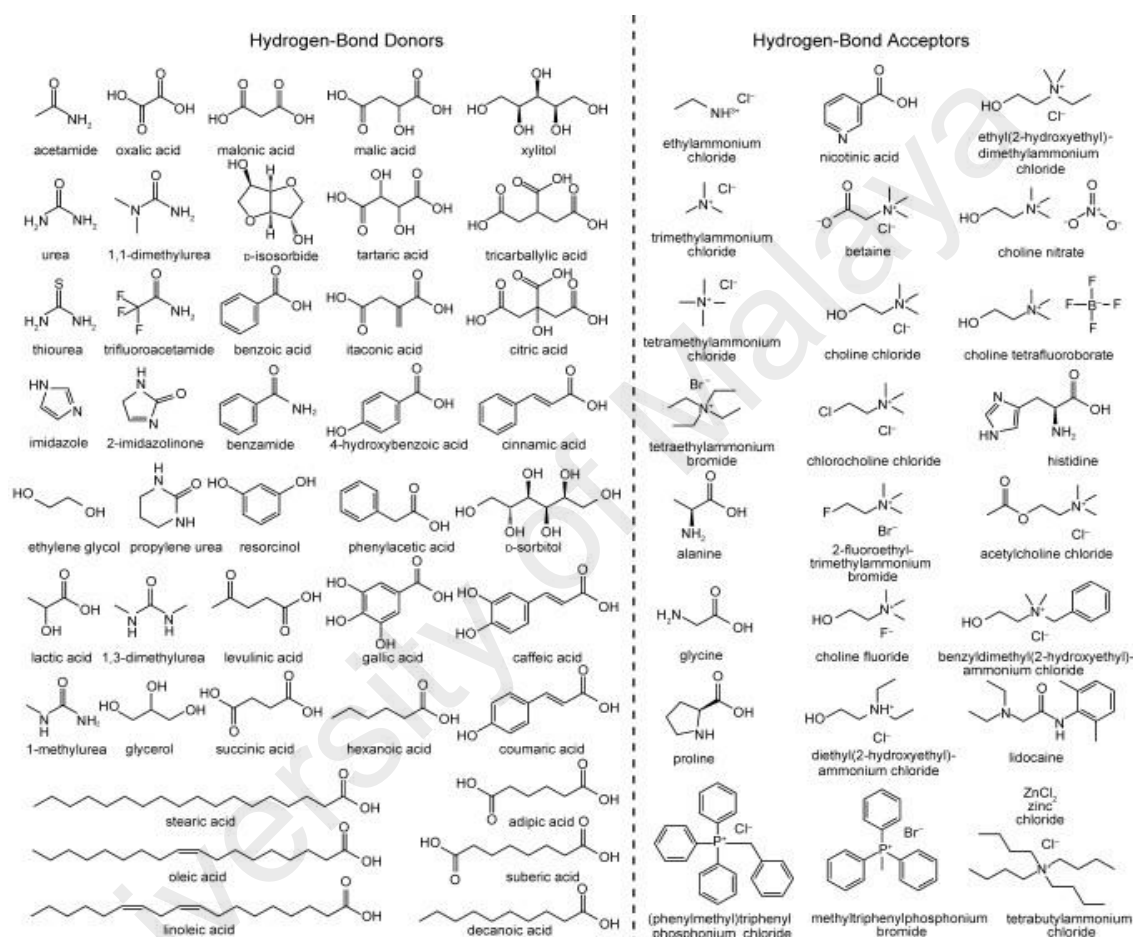


Figure 2.6: DESs starting materials (salts and HBDs) (Francisco, van den Bruinhorst, & Kroon, 2013)

Some researchers have also reported the preparation of DESs by the freeze drying method, which consists of mixing a concentrated aqueous solution of the two DESs compounds and freeze drying the mixture in order to obtain a DES mixture (Gutiérrez, Ferrer, Mateo, & del Monte, 2009). Hayyan et al. (2012 and 2013) prepared fruit sugar and glucose based DESs, respectively (A. Hayyan et al., 2012; A. Hayyan, F. S. Mjalli, et al., 2013). Meanwhile, phenol based DESs were synthesized based on phenol, o-cresol, 2,3-xyleneol, and ChCl at different molar ratios (W. Guo, Hou, Ren, Tian, & Wu, 2013).

The current literature has focused on the lowest eutectic point can be formed from mixing molar ratios. Recently, Hayyan et al. (2015) investigated the stability of the TEG based DESs by observing the mixture for eight weeks to obtain the first eutectic molar ratio without any precipitate (M. Hayyan, Aissaoui, Hashim, AlSaadi, & Hayyan, 2015).

2.4.2 Physical properties

Just like many types of ILs, DESs are considered to be designer solvents (Cvjetko Bubalo et al., 2015a; Q. Zhang et al., 2012), due to the involvements of DESs in many applications, either as a replacement of ILs or as novel solvents. Many studies have been done to investigate the physical and chemical properties of the DESs. The effects of molar ratio and temperature also attract the attention of many researchers.

2.4.2.1 Freezing point of DESs

DESs are well known for their unique properties, especially their relatively low freezing points, which gives them an advantage over other solvents. The low freezing point of a particular DES is dependent on the molar ratio and structure of the salt and the HBD (M. Hayyan et al., 2010). Abbott et al. (2003) presented the first DES, which consisted of ChCl and urea. The freezing point of this DES was investigated which reported to be lower than that of ChCl and urea. Later, many studies were conducted on different kinds of DESs. Kareem et al. (2010) introduced phosphonium based DESs by preparing different DESs based on different types of phosphonium based salts and different HBDs (Kareem, Mjalli, Hashim, & AlNashef, 2010). Subsequently, Hayyan et al. (2012) investigated the effects of molar ratio on ChCl: fruit sugar DESs (A. Hayyan et al., 2012). Later, the same team authenticated the role of molar ratio on the freezing points of glucose based DESs (A. Hayyan, F. S. Mjalli, et al., 2013). Table 2.6 lists the freezing point of representative reported DESs.

2.4.2.2 Density of DESs

Knowing the density of any novel liquid is essential in many industrial applications. Many researchers have investigated the density of different types of DES systems with respect to temperature. Hence, the density of most DESs follow the general rule of most liquids materials, i.e., the density reduction with respect to temperature takes a linear form. Increasing temperatures cause increased molecular mobility, which results in increasing the molar volume and a reduction in density (A. Hayyan et al., 2012). Abbot et al. (2007) investigated the effects of ethylene glycol, glycerol, and 1,4-butanediol weight percentage, as HBD in conjugation with ChCl. They found that the addition of 5% ChCl to 1,4-butanediol caused the resulted density to be lower, compared to other ratios and other HBDs. In addition, the density approached the density of water (Andrew P. Abbott, Harris, & Ryder, 2007b). In 2010, a group of researchers conducted an investigation into the physical properties of phosphonium based DESs and found that the densities of all DESs fitted linearly. Later, Abbott et al. (2011) also investigated the effects of salt concentration on the density of certain DESs formed from ChCl and Gly. It was observed that the density declined with increasing ChCl concentration until it reached 1.18 g/cm³ at 33% ChCl (Andrew P Abbott et al., 2011). Table 2.6 lists DESs densities of interest.

2.4.2.3 Viscosity of DESs

Basically, viscosity can be defined as the resistance of a substance to flow. It was observed that most DESs have a relatively high viscosity (>100 cp), which similar to the viscosity of ILs (Q. Zhang et al., 2012). Table 2.6 lists the viscosity of most known DESs. Strong hydrogen bonding, unsurprisingly, reduces the mobility of DES molecules, which result in the high viscosity observed for most DESs (Andrew P. Abbott, Capper, & Gray, 2006; D'Agostino, Harris, Abbott, Gladden, & Mantle, 2011; Fukaya, Iizuka, Sekikawa, & Ohno, 2007; Ru & Konig, 2012). In addition, temperature, molar ratio, the atomic

structure of the component, interaction forces including van der Waals and electrostatic forces, and void volume also have significant effects on the viscosity of DESs. Since, DESs are considered to be designer solvents, they have an advantage over other solvent in industrial applications. It has been demonstrated that by increasing the salt content in a DES, the viscosity of the DES increases. Hence, viscosity differences are caused by the ratio of the ion radius to the hole size within the liquid. To this end, according to hole theory, the viscosity of ILs and DESs is controlled by the cation size of the salt. Surprisingly, the viscosity of ChCl:glycerol DESs exhibit a different behavior where the viscosity decreases with increasing salt ratio. The reason behind this is the three OH groups in the glycerol molecule undergo extensive hydrogen bonding. The presence of the cation contributes to dissociation of the hydrogen bond between the glycerol molecules to form new weak hydrogen bonds with the cation of the salt (Andrew P Abbott et al., 2011; AlOmar, Hayyan, et al., 2016).

2.4.2.4 Electrical conductivity of DESs

Basically, electrical conductivity can be defined as the ability of a material to conducting electrical current. In other words, conductivity is the resistivity of materials to the movement of an electron in the molecular structure. It is well known that the viscosity of a liquid has a significant influence on the conductivity, due to the movements of ions in the liquids. Hence, most of DESs have low ionic conductivity and high viscosity (Q. Zhang et al., 2012). This may result from poor ion mobility caused by the large size of ions or pairings, or by agglomeration, which results in a smaller amount of available charge carriers. Table 2.6 lists the most well studied DESs conductivities.

2.4.2.5 Surface tension of DESs

The intermolecular attractive forces in the liquid result in a cohesive tension that reduces the surface area of the liquid's interface with other phases in contact with that

liquid, which is a phenomenon known as surface tension. Surface tension is defined as the energy required to increase the surface area of a liquid by an area unit. Many industries that involve various processes, such as mixing, fluid flow, and separation, require accurate quantitative values for the surface tension of material used in design and unit operations. Usually, the trend of surface tension with respect to temperature is similar to the viscosity trend, which is Arrhenius-like. However, the influence of temperature on surface tension for DESs and ILs is similar. Whereas, a linear form fitting describes the surface tension temperature relationship (Andrew P Abbott et al., 2011; Q. Zhang et al., 2012). Table 2.6 list the surface tension reported for DESs..

University of Malaysia

Table 2.4: Physical properties of some reported DESs

DES (Salt:HBD)	Molar ratio (salt:HBD)	Freezing point °C	μ (cP)	ρ (g cm⁻³)	K (mS/cm)	γ (mN/m)	Ref.
ChCl:Urea	1:2	12	750 (25 °C)	1.25	0.199 (40 C)	52	(Andrew P Abbott, Barron, Ryder, & Wilson, 2007; Andrew P. Abbott et al., 2003; Andrew P. Abbott et al., 2006; D'Agostino et al., 2011)
ChCl:EG	1:2	-66	37 (25 °C)	1.12	7.61 (20 °C)	48.91	(Andrew P. Abbott, Harris, & Ryder, 2007a; Andrew P Abbott et al., 2011; Shahbaz, Baroutian, Mjalli, Hashim, & AlNashef, 2012)
ChCl:Gly	1:2	-40	350 (25 °C)	1.15	985 (25 °C)	57.93	(Andrew P Abbott et al., 2011)
ChCl:TEG	1:3	-19	110 (80 °C)	1.13	1.41 (25 °C)	-	(M. Hayyan, Aissaoui, et al., 2015)
ChCl:TFA	1:3	Liquid	77 (40 °C)	1.342	-	35.9	(Andrew P. Abbott et al., 2006)
ChCl:D-F	2:1	10	280.6 (40 °C)	1.25	-	74	(A. Hayyan et al., 2012)
BTPC:Gly	1:5	50.36	553.7 (55 °C)	-	0.162 (55 °C)	-	(Kareem et al., 2010)
MTPB:EG	1:4	-49.34	109.8 (25 °C)	1.23	2.85 (75 °C)	-	(Kareem et al., 2010)

Table 2.4 continued: Physical properties of some reported DESs

BTPC:TEG	1:8	-19.49	116.7 (80 °C)	1.1	2.46 (80 °C)	-	(M. Hayyan, Aissaoui, et al., 2015)
ATPB:TEG	1:10	-19.52	84.6 (80 °C)	1.145	4.0 (80 °C)	-	(M. Hayyan, Aissaoui, et al., 2015)
TBAC:Gly	1:5	-42.78	1110 (25 °C)	1.143	2.2 (80 °C)	47	(Jibril, Mjalli, Naser, & Gano, 2014)
TBAC:EG	1:3	-30.88	110 (25 °C)	1.03	6.0 (80 °C)	40	(Jibril et al., 2014)
TBAC:TEG	3:1	-12.69	-	0.99	0.25 (80 °C)	40	(Jibril et al., 2014)
TPAB:EG	1:4	-23.4	55 (25 °C)	1.138	11.0 (80 °C)	47	(Jibril et al., 2014)
TPAB:TEG	1:3	-19.2	120 (25 °C)	1.148	4.0 (80 °C)	46.2	(Jibril et al., 2014)
TPAB:Gly	1:3	-16.1	900 (25 °C)	1.21	2.5 (80 °C)	53	(Jibril et al., 2014)

2.4.3 DES application

The current increase in research papers and patents concerning DESs synthesis and applications indicates the significant role of DESs as solvents of the future. Herein, a brief review is presented to specify the main applications of DESs.

DESs were first established as solvents in electrodeposition and electroplating application (Andrew P. Abbott & McKenzie, 2006). Subsequently, the development of DESs as media for electroplating with different metals has been the focus of significant and non-stoppable efforts from many researchers worldwide (E. L. Smith et al., 2014). DESs have been applied extensively in the field of biodiesel production and purification, since Hayyan et al. introduced this technique in 2010 by extracting glycerol from biodiesel (M. Hayyan et al., 2010).

Due to concerns regarding CO₂ and CH₃, which are the major greenhouse gases emitted nowadays, the separation and adsorption of these gases has gained significant interest worldwide. The ability of DESs to dissolve CO₂ is comparable to that of ILs (Q. Zhang et al., 2012). Li et al. (2008) used a ChCl and urea mixture to examine the solubility of CO₂ under different conditions, i.e., temperature, pressure and molar ratio (X. Li, Hou, Han, Wang, & Zou, 2008). Further advantages of DESs in the field of gas storage include the unique route that can be provided by DESs for the creation of porosity and coordinative unsaturated metal centers which enhance gas-storage capacity (Ferey, 2008; Jian Zhang, Wu, Chen, Feng, & Bu, 2009). Yang et al. (2013) used ChCl:glycerol to adsorb SO₂ with respect to temperature, pressure, and molar ratio (D. Yang et al., 2013). Salas et al. (2014) synthesized two DESs-based hierarchical carbon monoliths. They then studied the effects of DESs on the composition of the pore structure for carbon, which plays a significant role in the adsorption of CO₂. DES based carbon shows excellent adsorption capacity and selectivity toward CO₂ (López-Salas et al., 2014).

DESs are also of use in the enzymatic field, as shown by an emerging number of publications concerning the use of DESs in biotransformation. Gorke et al. (2008) reported, for the first time, the use of DESs in the biotransformation field by examining the catalytic activity of hydrolases in DESs (Gorke, Srienc, & Kazlauskas, 2008). In addition, reactions involving lipase-catalyzed processes have been extensively studied (Singh, Lobo, & Shankarling, 2011; Sonawane, Phadtare, Borse, Jagtap, & Shankarling, 2010; H. Zhao, Baker, & Holmes, 2011).

2.4.4 DESs and Nanotechnology

The first application of ILs in the nanotechnology field appeared in the paper published by Deshmukh et al. (2001), where room temperature IL was used as the media to synthesis Pd–biscarbene complexes and stabilize clusters of zero-valent Pd nanoparticles (Deshmukh et al., 2001). Later, many research papers and patents were published involving ILs in nanotechnology. Recently, DESs have been used as a replacement for ILs in many fields, including many nanotechnology applications. However, the number of nanotechnology related publications concerning ILs is comparable to that of DESs. Figure 2.7 illustrates the number of publication for both ILs and DESs in the fields of nanotechnology (M. Hayyan, A. Abo-Hamad, M. A. AlSaadi, & M. A. Hashim, 2015b). Herein, a brief review is presented to assess all the fields involving DESs and nanotechnology.

It is well known that a major drawback for nanomaterials is their tendency aggregate. Therefore, to reach the full potential of nanomaterials, the need for a media that guarantees a good dispersion is crucial. According to the ASTM standards, the criteria for “good stability” requires a zeta potential with an absolute value above 40 mV (Fan, Shi, Tian, Wang, & Yin, 2012). Consequently, as with ILs, DESs were used as a dispersant media for synthesis of nanoparticles. For example, Oh and Lee (2014) used

ChCl: malonic acid as the reaction media and structure directing agent for gold nanoparticle synthesis (Oh & Lee, 2014).

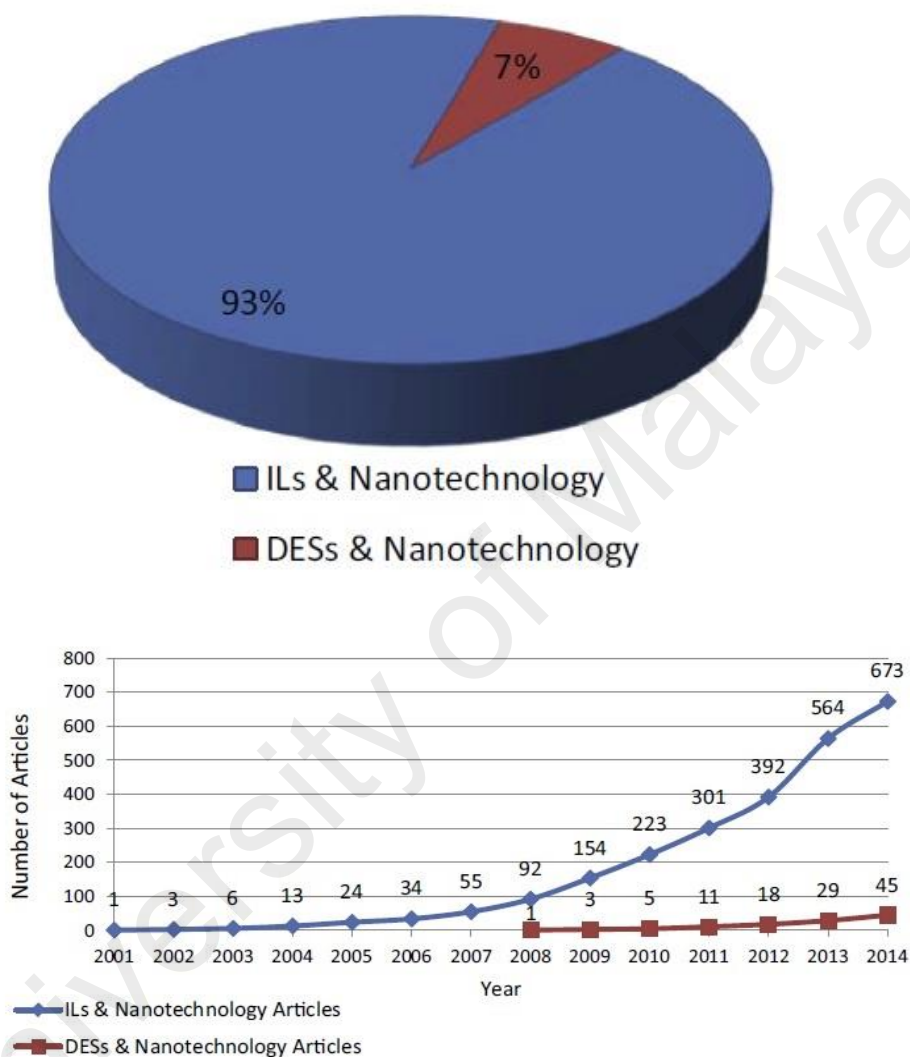


Figure 2.7: ILs and DESs in nanotechnology related publication (Abo Hamed et al. 2015)

Mota-Morales et al. (2013) used an acrylic acid: ChCl DES as the solvent in the synthesis of macroporous poly (acrylic acid)–carbon nanotube composites. The authors claimed that the use of a green DES in the synthesis process resulted in the production of a nanocomposite for biological and environmental applications (Mota-Morales et al., 2013). Meanwhile, Maęka et al. (2014) used a ChCl: tris(hydroxymethyl) propane DES as

the epoxy resin curing agent to produce GNP/DES/ epoxy resin. The presence of the DES positively affected the electrical volume resistivity of epoxy composites (Mačka et al., 2014).

The DESs have also been used as exfoliation agent for nanomaterials. Boulos et al. (2013) used ChCl: urea as an exfoliation media in the transformation of human hair into functional nanoparticles. The SEM results (Figure 2.8) revealed the cuticle cells, which were completely exfoliated from the hair after the treatment with DES (Boulos et al., 2013).

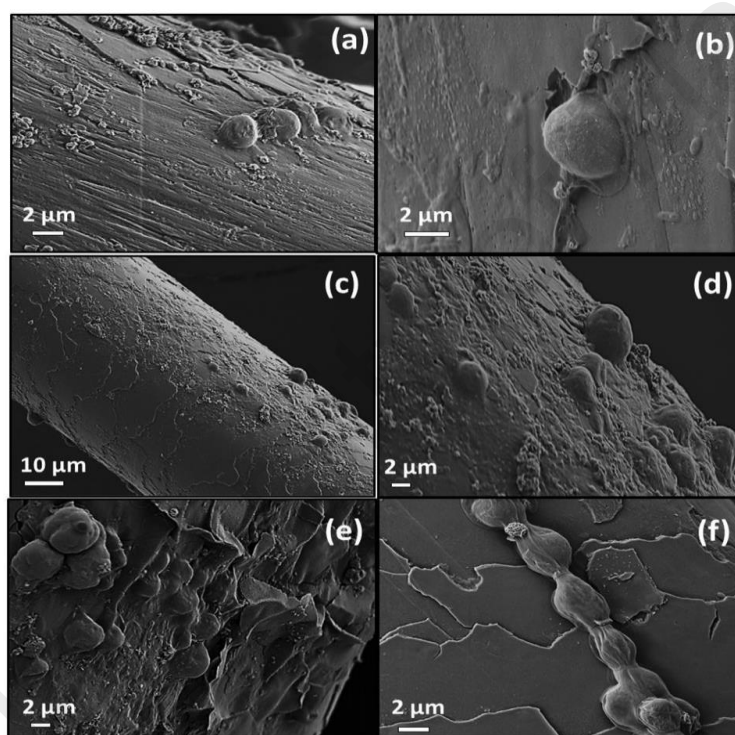


Figure 2.8: SEM images of immobilized microalgae cells on the surface of hair microfibers without treatment with the IL composite (a) and (b); hair microfiber after treatment with the IL composite, (c) and (d); hair microfibers after IL composite and liqu

In the fields of electrochemistry, the role of DESs and nanomaterials are obvious. Zheng et al. (2014) used ChCl: urea as the electrolyte for quercetin sensors. They use an MWCNT electrode, which proved to be easier and more convenient than using an ILs-CNTs composite (Zheng et al., 2014). Wei et al. (2012) used DESs with electrochemically

shaped control techniques to produce uniform Pt nanoflowers, which exhibited a higher electrocatalytic activity and stability (Wei, Fan, Wang, et al., 2012).

Chen et al. (2009) encapsulated a ChCl: ZnCl DES with a molar ratio of 1:1 in SWCNTs (Figure 2.9). This method involves thermal treatment of the SWCNTs to remove the ending cups. The resulting product was characterized using different methodologies. The morphology study showed that the DES was encapsulated in single-chain, double-helix, and zigzag tubes (S. Chen et al., 2009).

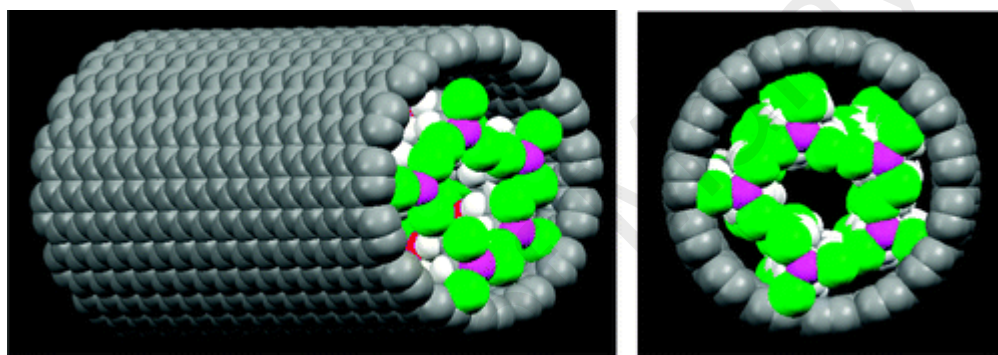


Figure 2.9: DES encapsulated SWCNT (S. Chen et al., 2009)

Gu and Tu (2011) advanced a novel method to dissolve metal complexes and enable thermochromism. Their method involved using two DESs systems, ChCl:urea and ChCl:ethylene glycol, to dissolve several transition metal chlorides. NiCl₂·6H₂O showed stable and outstanding thermochromic behavior within a temperature range starting from ambient temperature and ending at 150 °C. The authors suggested that their results have potential in terms of development of high performance thermochromic materials for the facile fabrications (C.-D. Gu & J.-P. Tu, 2011).

Finally, Hayyan et al. (2015) used DESs as a functionalization agent for graphene. Several types of DESs were used in this study to evaluate the effects of each type of DES on the graphene surface. The results demonstrate that the DESs-functionalizing graphene have great potential for use in many application due to the new functional groups

introduced to the surface of graphene (M. Hayyan, Abo-Hamad, et al., 2015b). Table 2.7 lists some of the reported applications of DESs in nanotechnology related fields.

University of Malaya

Table 2.5: Nano-technology applications involving DESs

DES		Molar ratio	Nano application	Remark	Ref.
salt	HBD				
ChCl	EG	1:2	SnO ₂ nanocrystalline	room temperature Homogeneous precipitation of SnO ₂ nanocrystalline	(GU, MAI, ZHOU, & TU, 2011)
ChCl	Urea	1:2	Spherical Fe ₃ O ₄ magnetic nanoparticles	Co-precipitation of Spherical Fe ₃ O ₄ magnetic nanoparticles using 2.164 g (8 mmol) of FeCl ₃ .6H ₂ O and 1.194 g (6 mmol) of ground FeCl ₂ .4H ₂ O were added to 15.585 g of DES, or adding 2.613 g (46.7 mmol) of KOH to the mixture	(F. Chen et al., 2013)
ChCl	Urea	1:2	Used as a dispersant of Pristine MWCNTs / oxidized MWCNTs	The dispersion of oxidized CNT was much higher than that with the pristine CNT	(Martis et al., 2010)
ChCl	Urea	1:2	Production of CuCl nanoparticles	The rule of DES was in the oxidation-reduction reaction. The reaction time was 1 h in the presence of polyvinylpyrrolidone in the DES	(Y. Huang et al., 2012)
ChCl	Gallic acid: glycerol	1:0.25:0.25	Cold gold nanoparticles coated gum Arabic	The rule of DES was Reduction of HAuCl ₄	(Shahidi et al., 2015)
ChCl	para-Toluene sulfonic acid	1:1	Hierarchical carbon-carbon nanotube composites	DES was used as catalysis, reaction media and structure director agent	(Gutiérrez et al., 2011)
ChCl	EG	1:2	codeposition of SiO ₂ nanoparticles in Ni matrix	The new composite showed excellent corrosion resistance compare to Ni coating alone	(Xu et al., 2016)
ChCl	FeCl ₃	1:2	Fe ₃ O ₄ /Fe doped graphene nanosheets	The DES play a significant rule as catalysts based on the complexation of ChoCl-FeCl ₃	(Mondal et al., 2016)

Table 2.5 continued: Nano-technology applications involving DESs

ChCl	EG	1:2	magnetic graphene oxide ($\text{Fe}_3\text{O}_4\text{-NH}_2\text{@GO}$) nanoparticles in core-shape structure	This study demonstrates the use of ($\text{Fe}_3\text{O}_4\text{-NH}_2\text{@GO}$) coated with DES for protein extraction	(Xu et al., 2016)
ChCl	Gly	1:1			
ChCl	D-glucose	2:1			
ChCl	D-sorbitol solution	1:1			
ChCl	Urea	1:2	silver nanoparticles	Synthesis of silver nanoparticles by laser ablation in DES. The rule of DES was controlling the formation of uniform nanoparticles.	(Oseguera-Galindo, Machorro-Mejia, Bogdanchikova, & Mota-Morales, 2016)
ChCl	EG	1:2	DNA-N-doped graphene hybrid	The DES was used as a dissolution media of DNA. Also it was used as a dispersion media of Fe_3O_4 .	(Bhatt, Mondal, Devkar, & Prasad, 2016)
ChCl	Urea	1:2	Copper-zinc-tin chalcogenide (CZTS) nanoparticles	The DES was used as green solvent, thiourea as sulfur source and metal chloride reagents.	(M. Karimi, Eshraghi, & Jahangir, 2016)
ChCl	succinic acid	1:1	TiO_2 Nanobamboos	The high conductivity and viscosity might be the main reason for the self-organization of NBs	(C.-Y. Chen et al., 2015)
ChCl	EG	1:2	Ni matrix coatings micro or nano-sized SiC particles	The DES was used as electrolyte. The Ni-SiC composite coatings exhibits very good water resistance.	(R. Li, Chu, & Liang, 2015)

Table 2.5 continued: Nano-technology applications involving DESs

ChCl	Urea	1:2	Nanoporous copper films	An in situ electrochemical process involving alloying/dealloying of Cu–Zn surface alloys from DES containing ZnO at elevated temperatures from 353 to 393 K	(Q. B. Zhang, Abbott, & Yang, 2015)
ChCl	gallic acid/Gly	1 : 0.25 : 0.25	Ultra-thin and large gold nanosheets	The DES was used as directing and reduction agent. Along with the Arabic gum which acted as stabilizer and shape-controlling agent	(Tohidi, Mahyari, & Safavi, 2015)

2.5 Summary

A detail overview was presented in this section that covered the historical background, properties, and structure of CNTs. The importance of functionalization on CNT surface was highlighted. Water pollution by heavy metals and the associated environmental challenges were discussed, along with the available technique for environmental remediation. A review was presented in this section covering the recent developments in CNTs modifications to remove different heavy metals ions, including lead, mercury, and arsenic ions. The information and techniques obtained from the published literature were the platform utilized to construct the experimental work in this thesis, such as functionalization techniques, characterization techniques, and adsorption processes.

The second section contains a detailed review covering the historical background of DESs. The physical and chemical properties of DESs are reviewed as well. In addition, the applications of DESs in different fields of science is discussed. Finally, the involvement of DESs in the nanotechnology applications is critically discussed. The construction of the experimental work, including synthesis of DESs and an investigation of the physical properties of DESs in the present research, was motivated by knowledge obtained from the literature review in this section. Furthermore, the use of DESs as functionalization agents for CNTs to be used as heavy metals adsorbents was proposed in the light of the collected knowledge presented in this section.

CHAPTER 3: GLYCEROL-BASED DEEP EUTECTIC SOLVENTS: PHYSICAL PROPERTIES

3.1 Introduction

In the last two decades, there has been increasing interest in the applications of ionic liquids (ILs), especially with respect to catalysts, electrochemistry process technology and analytics, biotechnology, and functional liquids. ILs are solvents which consist solely of ions. Mainly, the synthesis of ILs can be split into two distinct categories, those formed from eutectic mixtures of metal halides and organic salts, and those containing discrete anions (E. L. Smith et al., 2014). Due to the increasing need for organic solvents and the high cost of ILs (Q. Zhang et al., 2012), researchers recently have focused on ionic liquids analogues, i.e., deep eutectic solvents (DESs), which were introduced by Abbot et al. in 2003 (Andrew P. Abbott et al., 2003). Basically, DESs are mixtures of two or more compounds, and the mixtures have a melting point that is lower than that of the individual compounds (Andrew P. Abbott, Boothby, et al., 2004; M. Hayyan et al., 2010). Furthermore, DESs are prepared by mixing a salt and a hydrogen bond donor (HBD), hence, the hydrogen bonds with the anion of the salt. DESs can be made from different kinds of salts (organic and inorganic) and different kinds of HBDs (Q. Zhang et al., 2012). The physicochemical properties of DESs are much like those of conventional ILs (M. Hayyan, M. A. Hashim, M. A. Al-Saadi, et al., 2013). However, DESs have many advantages over conventional ILs, including the simplicity of the synthesis, lower production cost, low or negligible toxicity profiles, and sustainability with respect to environmental and economic benefits (M. Hayyan, M. A. Hashim, M. A. Al-Saadi, et al., 2013; M. Hayyan, M. A. Hashim, A. Hayyan, et al., 2013; M. Hayyan, Looi, et al., 2015).

Recently, DESs have been reported in many applications, one of which was the use of ChCl-based DESs as functional additives for starch-based plastics (Leroy et al., 2012). Also, they have been used as catalysts for the production of biodiesel fuel from low grade

palm oil (A. Hayyan, Ali Hashim, Mjalli, Hayyan, & AlNashef, 2013; A. Hayyan, Hashim, Hayyan, Mjalli, & AlNashef, 2014), as an electrolyte in electrochemical processes such as, deposition of specific metals in the electroplating and electroless plating of metals (Andrew P. Abbott, Capper, McKenzie, & Ryder, 2007; Andrew P. Abbott et al., 2008), and as viable co-solvents for enzyme-catalyzed epoxide hydrolysis (Lindberg, de la Fuente Revenga, & Widersten, 2010).

Glycerol is a conventional solvent that is defined simply as a polyol (sugar alcohol), and it is used extensively in many industrial applications, especially in the food and pharmaceutical industries. However, there is a limited use of glycerol in organic transformations due to its low solubility in organic compounds and the intrinsic reactivity of the polyol backbone which leads to the side products formation (Hamel et al., 2014). Therefore, to overcome these disadvantages, researchers have been working to enhance the physicochemical properties of glycerol by different methods (Hamel et al., 2014; Smarrito-Menozzi, Matthey-Doret, Devaud-Goumoens, & Viton, 2013). One of these methods is preparing of DESs containing glycerol as HBD.

In the current work, six DES systems were prepared based on glycerol as a HBD and six different salts, i.e., methyl triphenyl phosphonium bromide (MTPB); benzyl triphenyl phosphonium chloride (BTPB); allyl triphenyl phosphonium bromide (ATPB); choline chloride (ChCl); N, N-diethyl ethanol ammonium chloride (DAC); and tetra-n-butyl ammonium bromide (TBAB). The physical properties of these DESs were investigated, including freezing point, density, viscosity, conductivity, and surface tension. Furthermore, the functional groups of these new DESs were analyzed using FTIR.

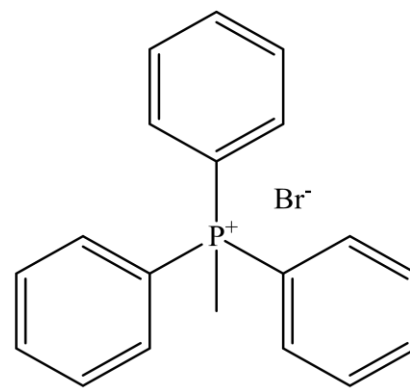
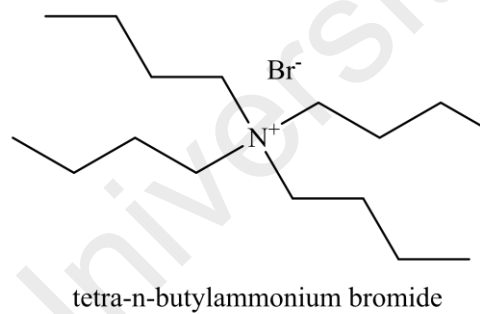
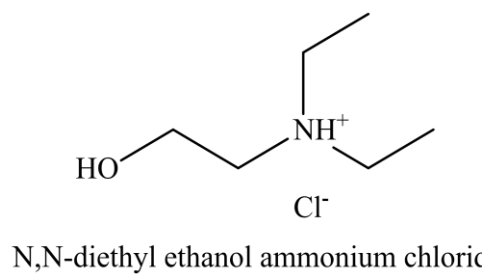
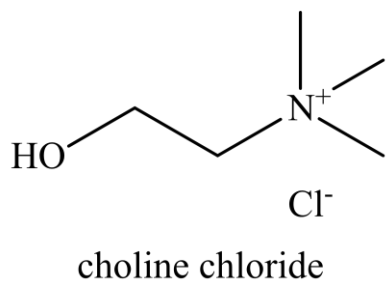
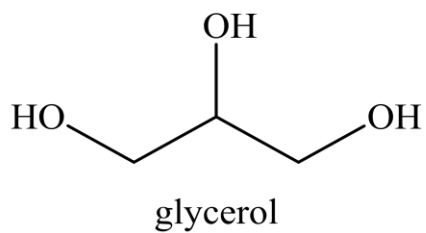
3.2 Materials and experimental methodology

3.2.1 Chemicals

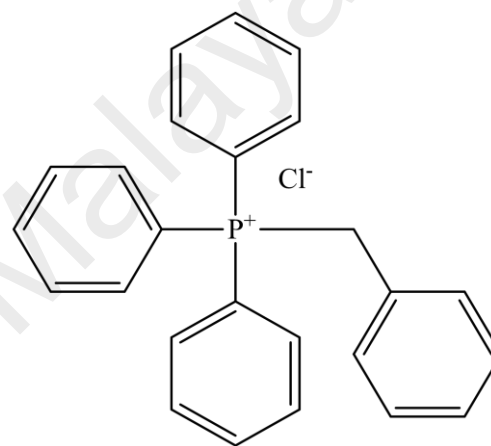
All chemicals with purity >99%, except for ChCl, were supplied by Merck, Germany. ChCl was supplied by Sigma-Aldrich. Table 1A (Appendix A) shows the salts, HBD, abbreviations, molar ratios, symbols, and phases of the synthesized DESs. Figure 3.1 show the molecular structure of the six salts and the HBD.

3.2.2 Synthesis and characterization of DESs

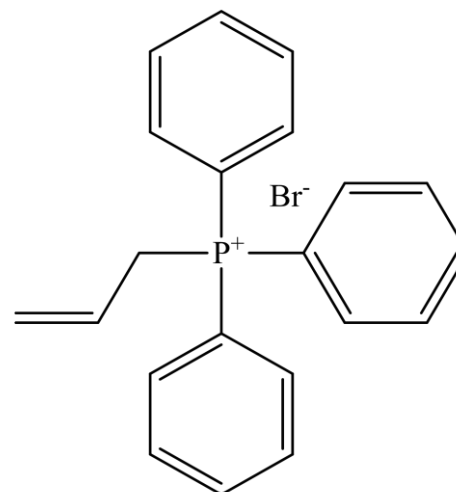
In this study, DESs were synthesized with different ratios of salt and HBD. Table 1A (Appendix A) and Figures 1A, 2A, 3A, 4A, 5A and 6A shows the 70 DESs that are synthesized. Different phases appeared during and after preparing the DESs, such as solid, semi-solid, crystal, and liquid. Only six of the DESs that were synthesized were selected. All chemicals were dried overnight in a vacuum oven and placed in moisture controlled area. Each salt was mixed with HBD using magnetic stirring. The mixtures of the salts and HBD were shaken at 400 RPM and 353 K until a homogeneous mixture without any precipitate was obtained. The DESs were synthesized under atmospheric pressure in a glove box. Differential Scanning Calorimetry (DSC) METTLER TOLEDO[®] was used to measure the freezing points of the DESs. A rotational viscometer (Anton Paar[®] Rheolab QC) was used to measure the viscosity in the temperature range of 298.15-353 K, and the variation of temperature was controlled by water circulator. The densities of the DESs and glycerol were determined using a densitometer DM 40 METTLER TOLEDO[®]. The surface tension of samples was determined by utilizing an automatic tensiometer (Krüss[®] K10ST classification B with the Du Noüy ring method) in the temperature range of 298.15-348.15 K, with the temperature being controlled by using a water circulator. The conductivity was measured by an Eutech Cyberscan Con 11 hand-held meter. A Spectrum 400 FT-IR Spectrometer was used to analyze the functional groups of the DESs at room temperature.



methyl triphenyl phosphonium bromide



benzyl triphenyl phosphonium chloride



allyl triphenyl phosphonium bromid

Figure 3.1: Chemical structure of the six salts and the HBD

Different molar ratios were used to prepare 70 DESs based on MTPB:Gly DAC:Gly, ChCl:Gly, ATPB:Gly, BTPC:Gly, and TABB:Gly. Molar ratios of 1:1-1:10 were prepared for each DES system except for ATPB:Gly and BTPC:Gly, which required the synthesis of molar ratios in the ranges of 1:1-1:14 and 1:1-1:16, respectively, in order to get a stable liquid state of DES at room temperature. Many phases were observed, such as solid, semi-solid, crystal, and liquid phases. Table 1A indicates the phases of the DESs and the associated abbreviations. Note that some of the DESs were in the liquid phase, which was stable at room temperature; however, after a few days, some precipitates formed in the DESs even though that they were kept in a well-controlled environment. It should be noted, the mixing time of DES₃, DES₂₆, and DES₄₀ was around 3 h, while the mixing time of DES₄₂, DES₅₂, and DES₆₄ was around 30 min.

3.3 Results and discussion

To obtain stable DESs at room temperature in the liquid phase and without any precipitate, the DESs were observed for 60 days, and, after that, the first molar ratio that led to a homogeneous liquid DES at room temperature was adopted. The DESs of the adopted molar ratio were subjected to examine the physical properties. Table 3.1 shows the selected DESs.

3.3.1 Freezing point

The low freezing point of the DESs depended on the molar ratio and structure of the salt and the HBD (M. Hayyan et al., 2010). The freezing points of the selected DESs were in the range of 251.16 to 239.68 K for DES₂₆ and DES₄₂, respectively. It was found that the freezing point of DES₄₂ was in a fair agreement with that of a similar DES reported by previous studies (Andrew P Abbott et al., 2011; Shahbaz et al., 2012).

Table 3.1: Selected DESs, abbreviations, and molecular weights

DES		Salt		HBD		Molar ratio	
Abb. ^a	M _{DES} ^b	Abb. ^a	M _S ^c	Abb. ^a	M _H ^d	Salt	HBD
DES ₃	158.37	MTPB	357.224	Gly	92.09	1	3
DES ₂₆	109.55	BTPC	388.869	Gly	92.09	1	16
DES ₄₀	111.50	ATBP	383.261	Gly	92.09	1	14
DES ₄₂	107.93	ChCl	139.624	Gly	92.09	1	2
DES ₅₂	112.61	DAC	153.65	Gly	92.09	1	2
DES ₆₄	138.14	TABB	322.368	Gly	92.09	1	4

^a Abbreviation, ^b M_{DES} molecular weight of DES calculated using Eq. (3.2), ^c molecular weight of salt, ^d molecular weight of HBD.

The freezing points of DES₃, DES₄₀, DES₅₂, and DES₆₄ were 248.82, 249.39, 249.12, and 249.09 K, respectively. However, the freezing point of the Gly is 291 K (Pagliaro & Rossi, 2010), and the melting points of the six salts, i.e., MTPB, BTPC, ATPB, ChCl, DAC, and TBAB, were 507.15, 603.15, 498.15, 575.15, 409.15, and 376.15 K, respectively. Thus, the freezing points of the selected DESs were lower than that of both components, and they complied with the definition of a DES. Furthermore, the advantage of such low freezing points allows the selected DESs to be considered for possible applications in many fields, such as chemical and electrochemical reaction media and separation processes.

3.3.2 Density

Density is an important physical property due to its effect on the design and operation of processes. Thus, it is essential to identify the behavior of density with respect to temperature. In this study, the density of the DESs and HBD were measured in

temperature range of 298 -363 K. The results indicated that DES₃ had the highest density (1.2965 g cm⁻³), which reached its maximum value at 298 K. DES₆₄ had the lower density at 298 K, i.e., 1.1507 g cm⁻³, and the density of Gly was 1.2577 g cm⁻³ at 298 K. At 363 K, the densities of DES₃, DES₂₆, DES₄₀, DES₄₂, DES₅₂, DES₆₄, and pure Gly were 1.2513, 1.1968, 1.2201, 1.1548, 1.1342, 1.1067, and 1.2152 g cm⁻³, respectively. In general, density decreases as temperature increases. This is due to the increased activity and molecular mobility, which increase the molar volume of the solution, thereby reducing the density (A. Hayyan et al., 2012). Figure 3.2 shows these data graphically.

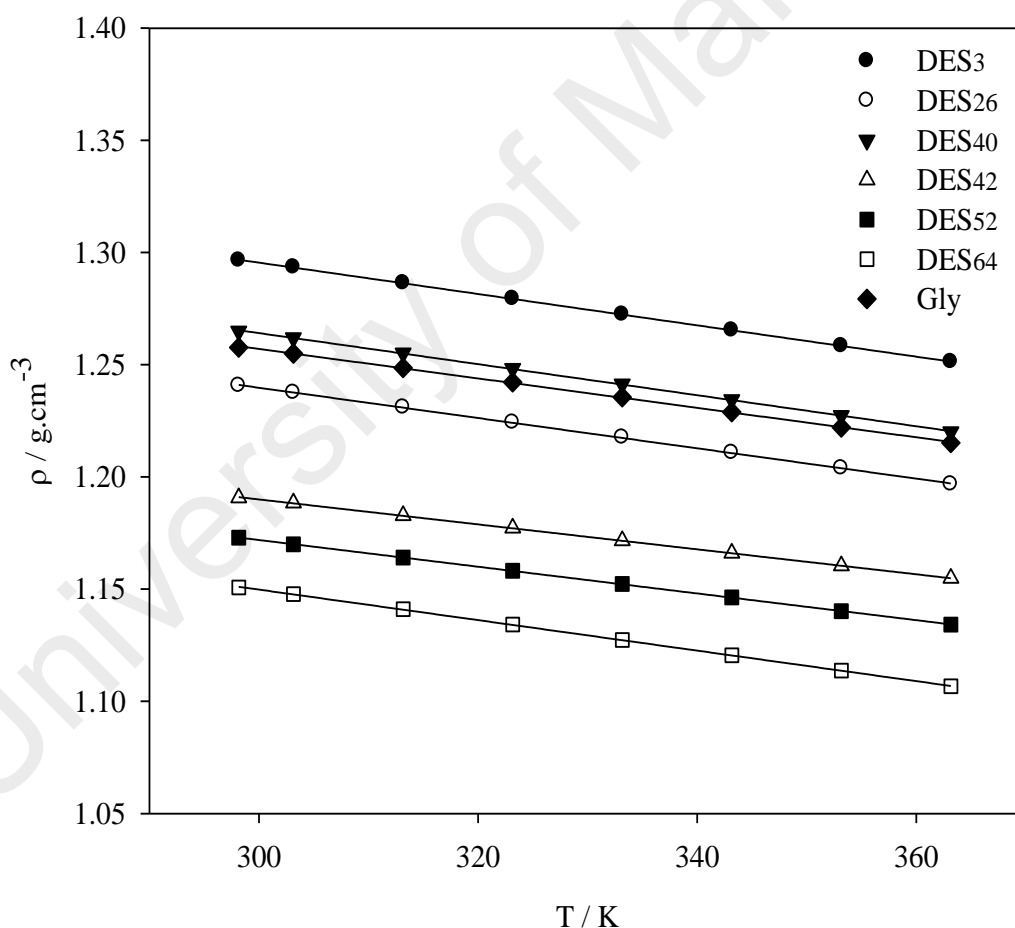


Figure 3.2: Variations of densities with temperature

The results of this work were compared to results that had been reported previously. A slight difference was found between DES₃ and MTPB:Gly reported by Kareem et al. (Kareem et al., 2010), which was 1.2899 g cm⁻³ at 298 K even though the molar ratio used

in that study was 1:1.75 and, at 358 K, the density was 1.248 g cm⁻³. Furthermore, the density of DES₃ was approximately in agreement with that of ChCl:D-glucose with a molar ratio of 1:1, as reported by Hayyan et al. (A. Hayyan, F. S. Mjalli, et al., 2013). DES₃, DES₄₂, and DES₅₂ were found to be in agreement with previously-reported values (Shahbaz et al., 2012). DES₂₆ was in agreement with 1-ethyl-3-methylimidazolium iodine (Deng et al., 2008; Sato, Masuda, & Takagi, 2004), while the density of DES₄₀ was found to be in agreement with 1-(2-methoxyethyl)-3-methylimidazolium (Branco, Rosa, Moura Ramos, & Afonso, 2002).

The experimental data of the density as a function of temperature were fit Eq. (3.1):

$$\rho = aT + b \quad (3.1)$$

where ρ is the density in g cm⁻³, T is the temperature in Kelvin, and a and b are constants that represent the molar ratio of DES to HBD. Table 3.2 provides the values of a and b. The R² was found to be more than 0.9995, which indicated that the density-temperature relationship was linear.

Table 3.2: Density–temperature model parameters and regression coefficients

DES	a	b	R ²
DES ₃	-7×10 ⁻⁴	1.5050	0.9999
DES ₂₆	-7×10 ⁻⁴	1.4423	0.9999
DES ₄₀	-7×10 ⁻⁴	1.4716	0.9998
DES ₄₂	-5×10 ⁻⁴	1.3568	0.9997
DES ₅₂	-6×10 ⁻⁴	1.3505	1.0000
DES ₆₄	-6×10 ⁻⁴	1.3537	0.9999
Gly	-7×10 ⁻⁴	1.4539	0.9995

3.3.3 viscosity

Viscosity is an important property that must be addressed, especially for equipment design and fluid flow calculations. Herein, the viscosities of the selected DESs were measured at various temperatures in the range of 298 -353 K. For a given temperature, the viscosities of the DESs were found to be in the following order: DES₃ > DES₂₆ > DES₄₀ > DES₆₄ > DES₅₂ > DES₄₂. It is well known that DESs have a high viscosity due to the presence of a massive hydrogen bond network between each component, resulting in a lower mobility of free species within the DES (Q. Zhang et al., 2012). Figure 3.3 shows the trend of the reduction of the viscosities as the temperature increased. In this study, DES₃ had the highest viscosity of 2775.9 cP at 298 K, while DES₄₂ had the lowest viscosity of 281 cP at 298 K. The results showed that the ammonium-based salt DESs have a much lower viscosities than the phosphonium-based salt DESs. Within the ammonium group, it was observed that the viscosities of the different DESs increased as their molecular weights increased. This trend was compatible with the Mark–Houwink equation (Hiemenz & Lodge, 2007), which is commonly used to describe the viscosity behavior of polymers. On the contrary, the viscosity behavior of the phosphonium-based salts DESs was independent of molecular weight, since DES₂₆ has higher viscosity than DES₄₀. Table 3.1 provides the average molecular weights that are computed according to Eq. (3.2), as reported by Yadav and Pandey (Yadav & Pandey, 2014).

$$M_{DES} = X_S \times M_S + X_H \times M_H \quad (3.2)$$

where M_{DES} is the molecular weight of DES in $\text{g}\cdot\text{mol}^{-1}$, X_S is the molar ratio of the salt, M_S is the molecular weight of the salt in $\text{g}\cdot\text{mol}^{-1}$, X_H is the molar ratio of the HBD, and M_H is the molecular weight of the HBD in $\text{g}\cdot\text{mol}^{-1}$.

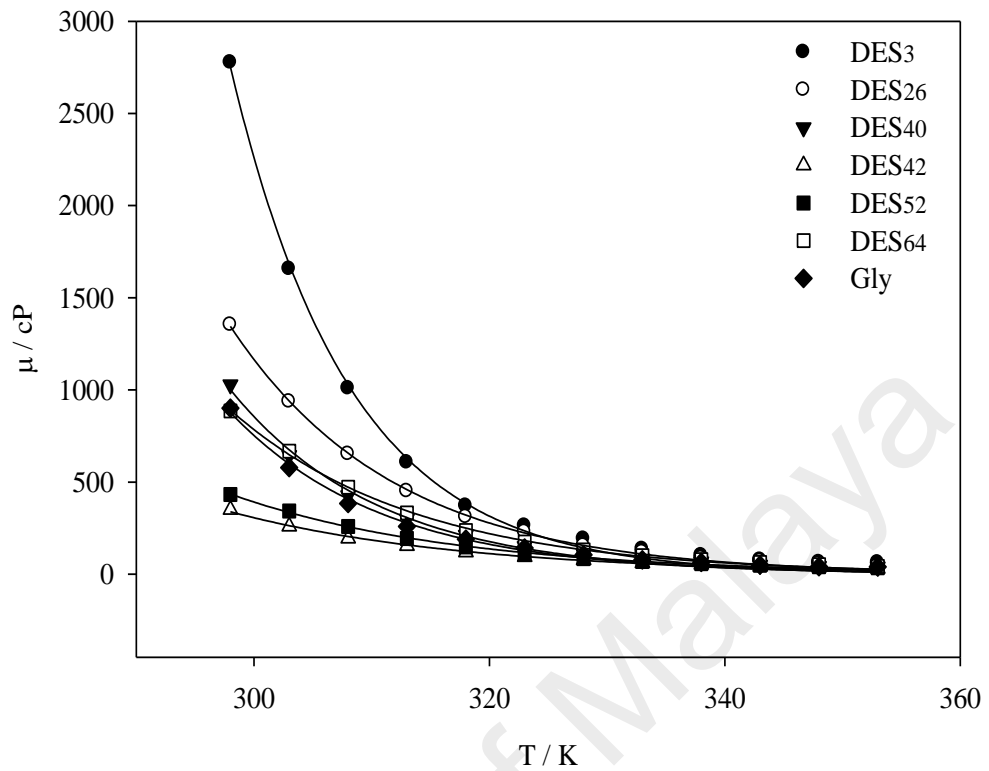


Figure 3.3: Variations of viscosity with temperature

The viscosity-temperature relationship is described well by the Arrhenius equation Eq. (3.3):

$$\mu = \mu^{\circ} e^{\frac{E_{\mu}}{RT}} \quad (3.3)$$

where μ is the dynamic viscosity, μ° is the pre-exponential constant, E_{μ} is the activation energy, R is the gas constant, and T is the temperature in Kelvin. Table 3 lists the values of viscosity and temperature. The minimum R^2 was 0.9936. Values of μ° , E_{μ} , and the regression coefficient are provided in Table 3.3.

Table 3.3: Viscosity–temperature model parameters and regression coefficients

DES	$\mu \cdot cP$	$\frac{E\mu}{R}$	R^2
DES ₃	2.59519E-08	7501.386	0.981404
DES ₂₆	2.84782E-07	6631.381	0.997152
DES ₄₀	4.926E-07	6346.973	0.989704
DES ₄₂	9.48393E-05	4468.867	0.996292
DES ₅₂	2.63693E-05	4948.304	0.995276
DES ₆₄	1.84688E-06	5953.608	0.997318
Gly	1.02289E-06	6086.643	0.98775

3.3.4 Electrical Conductivity

Electrochemical applications are major fields for DESs to have significant roles in industry, so there is a great demand for information concerning their electrical and electronic properties, including their electrical conductivity. Due to their relatively high viscosity, DESs have low conductivity. In general, the conductivity of DESs increases as temperature increases. In this study, DESs conductivity values were measured for the temperature range of 298-348 K. The results indicated that DES₄₂ had the highest conductivity among the DESs, i.e., 985 $\mu S \text{ cm}^{-1}$ at 298 K and 4880 $\mu S \text{ cm}^{-1}$ at 348 K. These values were in good agreement with those reported for the same DES by Abbot (2011) (Andrew P Abbott et al., 2011; E. L. Smith et al., 2014). The DESs conductivity followed the order of DES₄₂>DES₅₂>DES₆₄>DES₃>DES₂₆>DES₄₀. Figure 3.4 shows the trend of the conductivity increment for selected DESs with increasing temperature.

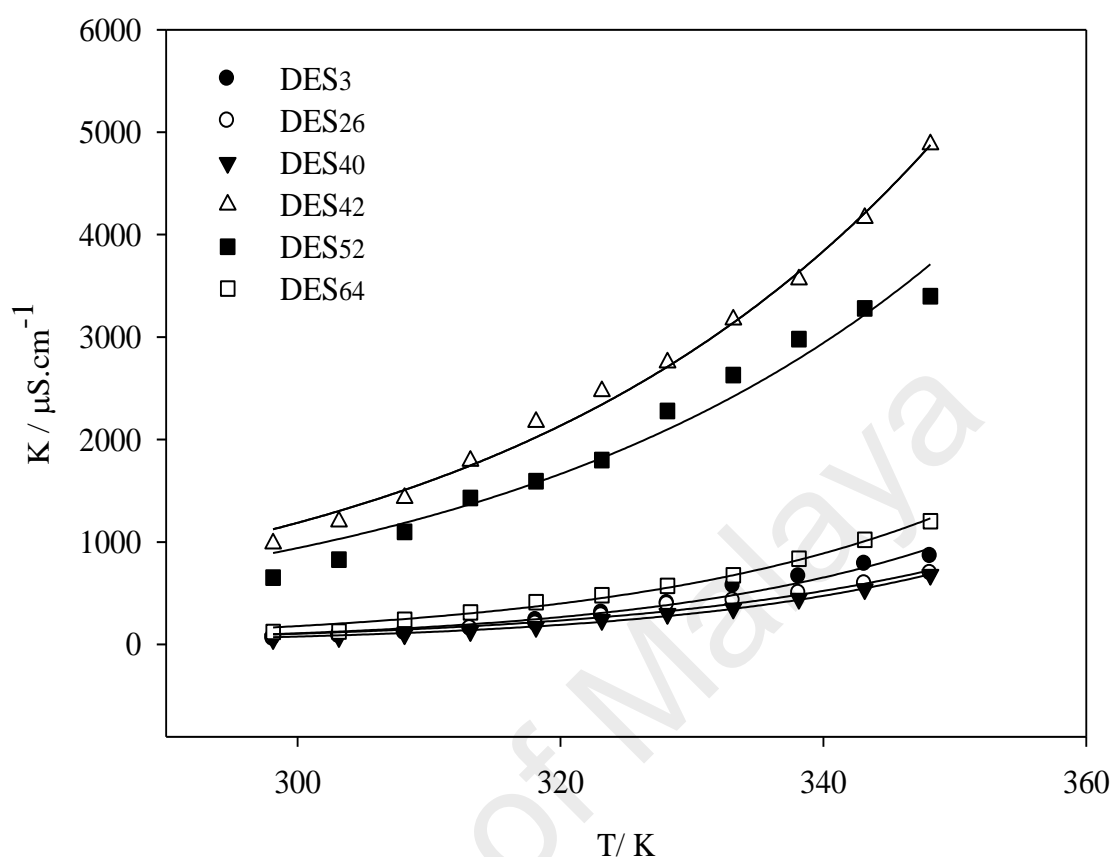


Figure 3.4: Variations of conductivities with temperature

Note that the conductivity increased significantly as viscosity decreased due to the free mobility of ionic species as the hole mobility increased (Andrew P. Abbott, Robert C. Harris, et al., 2007b; Q. Zhang et al., 2012). Thus, the results of this study show that the conductivities of the ammonium-based salt DESs were greater than those of the phosphonium-based salt DESs. The conductivity-temperature relationship is described well by the Arrhenius equation Eq. (3.4):

$$K = K^{\circ} e^{-\frac{E_k}{RT}} \quad (3.4)$$

where K is the conductivity in $\mu\text{S cm}^{-1}$, K° is a constant, E_k is the activation energy of conductivity, R is the gas constant, and T is the temperature in Kelvin. The value of R^2

was greater than 0.96 for all of the DESs. Table 3.4 provides the values of K° , E_k , and regression coefficient.

Table 3.4: Conductivity–temperature model parameters and regression coefficients.

DES	$K^\circ \mu\text{S}\cdot\text{cm}^{-1}$	$\frac{E_K}{R}$	R^2
DES ₃	3.04E+10	-5977.53	0.988243
DES ₂₆	1.35E+09	-5000.81	0.989833
DES ₄₀	2.62E+09	-5267.28	0.99708
DES ₄₂	5.3E+07	-3237.8	0.995446
DES ₅₂	8.6E+07	-3482.03	0.980527
DES ₆₄	1.3E+09	-4821.81	0.976006

3.3.5 Surface Tension

The intermolecular attractive forces in the liquid result in cohesive tension that reduces the surface area of the liquid’s interface with other phases in contact with the liquid, a phenomenon known as surface tension, which is measured as the energy required to increase the surface area of a liquid by a unit of area. Many industries that involve various processes, such as mixing, fluid flow, and separations, require accurate quantitative values of surface tension in unit design and operations. In this study, the surface tension of the six selected DESs was measured at different temperatures in the range of 298-348 K. Figure 3.5 shows the decrease in surface tension with respect to temperature increase since the salts are expected to break up the intermolecular forces of Gly such as hydrogen bonding (Andrew P Abbott et al., 2011). The results showed that

the highest surface tension was recorded for DES42 at all temperatures, and this was in accordance with the result reported by Abbott et al. (2011) (Andrew P Abbott et al., 2011).

There is a linear reduction in surface tension as temperature increases (Q. Zhang et al., 2012). The data of surface tension for the selected DESs fitted a linear model according to Eq. (3.5):

$$\gamma = a + b(T) \quad (5)$$

where γ is surface tension in mN m^{-1} , a and b are constants, and T is temperature in Kelvin. Table 3.5 shows the values of a , b and the regression coefficient.

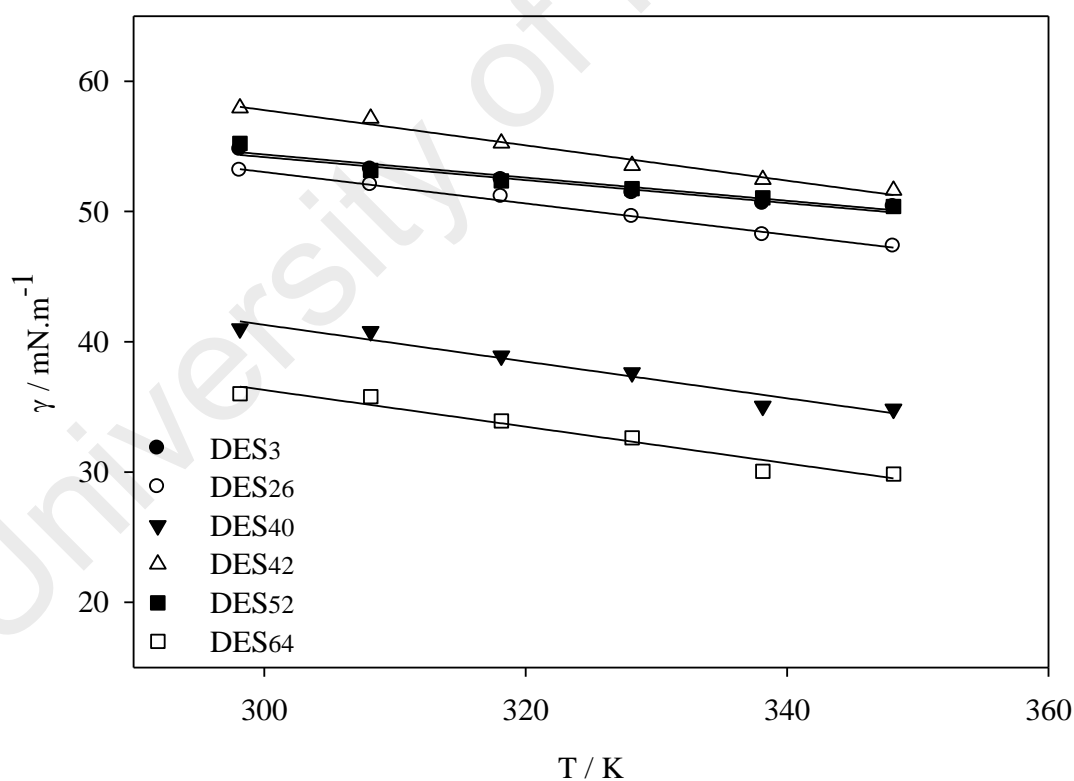


Figure 3.5: Variations of surface tension with temperature

3.3.6 FTIR

It is essential to study the functional groups that exist in new solvents, the combinations of different substances, such as DESs, and the possible changes in structure.

FTIR is usually utilized to study the interaction of different groups in order to analyze and identify the structure of a material (Yue, Jia, Yao, Sun, & Jing, 2012). In this work, FTIR analyses were performed to observe the functional groups. As indicated in Figure 3.6, the six DESs have very similar spectra because HBD is the same in each case and because of the effect of water content. The presence of water obviously is indicated by the stretching bond between 3200-3600 cm^{-1} , where the existence of the O-H functional group is usually indicated (J. Luo, Conrad, & Vankelecom, 2012; B. H. Stuart, 2005b).

Table 3.5: Surface tension–temperature model parameters and regression coefficients

DES	a	B	R ²
DES ₃	80.6763	-0.0883	0.9626
DES ₂₆	89.1717	-0.1205	0.9937
DES ₄₀	83.5773	-0.1409	0.9538
DES ₄₂	98.3885	-0.1353	0.9818
DES ₅₂	81.0207	-0.0888	0.9321
DES ₆₄	78.5773	-0.1409	0.9538

In all ammonium-based DESs, N-H stretching is also observed to be overlapped with the O-H between 3000-3400 cm^{-1} (B. H. Stuart, 2005b). The C-H stretching appeared between 2921 and 2880 cm^{-1} (J. Luo et al., 2012; Stoyanov, Kim, & Reed, 2006). Similarly, for the phosphonium-based DESs, P-H stretching might overlap with C-H vibration bond in the range of 3000-2800 cm^{-1} (B. H. Stuart, 2005b). Figure 3.6 shows that, after the formation of the DESs, there are no peaks in the region of 2800-1500 cm^{-1} . Due to the chemical structure of HBD, the absorbance spectrum showed C-H bonding in

the range of 600-1400 cm^{-1} for all of the DESs (B. H. Stuart, 2005a). The presence of Br and Cl was identified in the range of 600-400 cm^{-1} (B. C. Smith, 1998).

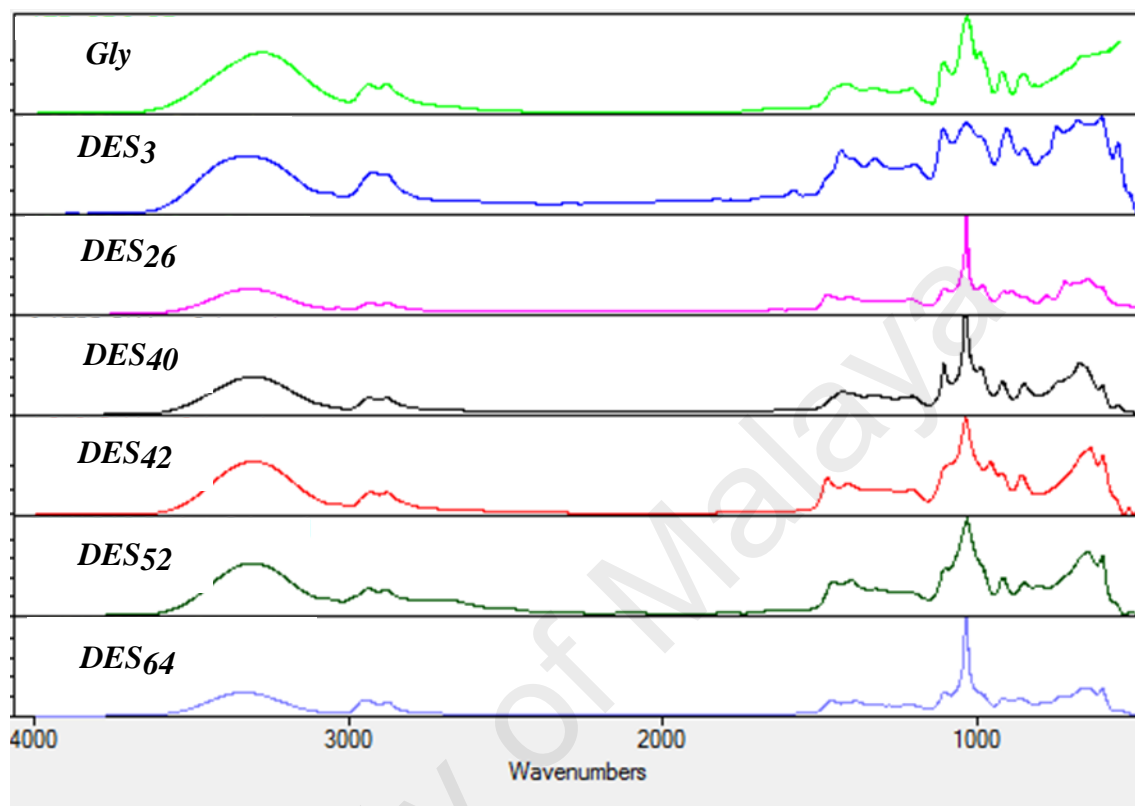


Figure 3.6: FTIR spectrum for the six selected DESs and the HBD

3.4 summary

In this study, six DES systems were synthesized using Gly as HBD and six different ammonium and phosphonium salts. The selection of DESs for further investigation was based on the best mixture stability. The physical properties of these six DESs were investigated as function of temperature, including, density, viscosity, conductivity, and surface tension. In addition, the freezing point was measured. The freezing points of the selected DESs were between 239.68 and 251.16 K. The values of surface tension were in the range of 57.9 to 36 mN m^{-1} , and these results attracted attention to the effect of different salts on the intermolecular forces in the DESs. In addition, FTIR analyses were conducted to study the functional groups of the selected DESs.

CHAPTER 4: STUDY OF PHYSICAL PROPERTIES OF NOVEL BENZYL TRIMETHYL AMMONIUM CHLORIDE-BASED DEEP EUTECTIC SOLVENTS

4.1 Introduction

In recent years, research interest has been raised in the area of ionic liquids, due to their extensive reach of possible applications depending on physical and chemical properties (Q. Zhang et al., 2011). Nevertheless, ionic liquids had limitations due to their relatively high cost and waste disposal associated with their synthesis (Phadtare & Shankarling, 2010). Consequently, many researchers in the last decades have been trying to reduce the cost of ILs. Therefore, the need for solvents with reasonable prices, easy to synthesize and environmentally benign, inspired Abbot et al. (2003) (Andrew P. Abbott et al., 2003) to present the so-called deep eutectic solvent DES for the first time as a replacement for or improvement on ILs.

DES is simply a mixture of ions and other molecules, and that makes it different from the ILs. DES is synthesized by mixing two or more components. The generation of DESs occurring due to the bonding between hydrogen and the anion of the salt contributes to having a solvent with a freezing point lower than that of each constituent. DESs share many physicochemical properties with ILs (Q. Zhang et al., 2012); additionally, they have great potential applications due to their advantages over ILs. Those advantages could be summarised in the simplicity of synthesis, the variety of the physical properties with different molar ratios and the reasonable price of its components (M. Hayyan, M. A. Hashim, M. A. Al-Saadi, et al., 2013; M. Hayyan, M. A. Hashim, A. Hayyan, et al., 2013; M. Hayyan, Looi, et al., 2015).

Recently, DESs were reported in many applications; examples of such are the uses of ChCL-based DES as a functional additive for starch-based plastics (Leroy et al., 2012),

the synthesis of zeolite analogues (Cooper et al., 2004), as catalysts for biodiesel production from industrial low-grade crude palm oil (A. Hayyan, M. Ali Hashim, et al., 2013; A. Hayyan et al., 2014), mediums for the deposition of specific metals in electro and electroless plating of metals (Andrew P. Abbott, Glen Capper, et al., 2007; Andrew P. Abbott et al., 2008). And recently, nanotechnology applications (Abo-Hamad, Hayyan, AlSaadi, & Hashim, 2015). Benzyl trimethyl ammonium chloride (BTAC) is widely used in many industrial applications such as a gelling inhibitor in polyester resins, a solvent for cellulose, a chemical intermediate, a paint dispersant, and an acrylic dyeing agent (Abdo, 2000). It is likewise applied in plant growth regulator compositions and synthetic operations. Moreover, Abbot et al. (2001) have prepared BTAC/Aluminium chloride $AlCl_3$ ionic liquid for electroplating applications (A. Abbott, Eardley, Farley, Griffith, & Pratt, 2001).

Knowing the physical properties of a solvent is essential for many applications. Subsequently, many researchers have reported physical properties investigation. Choline Chloride-based DESs have been reported by Abbot (2004) and Hou (2008) (Andrew P. Abbott, Boothby, et al., 2004; Hou et al., 2008). A phosphonium-based DES has been reported by Kareem et al. (2010) (Kareem et al., 2010). Shahbbaz et al. (2011, 2012) have used artificial intelligence for the prediction of physical properties for ammonium and phosphonium alts-based DESs (Shahbaz et al., 2012; Shahbaz, Mjalli, Hashim, & AlNashef, 2011). Hayyan et al. (2012, 2013) have investigated the physical properties of glucose and fruit sugar-based DESs (A. Hayyan et al., 2012; A. Hayyan, F. S. Mjalli, et al., 2013). Ghareh Bagh et al. (2015) have reported the electrochemical widow of Zn (II)-based deep eutectic solvents along with other physical properties (Ghareh Bagh, Shahbaz, Mjalli, Hashim, & AlNashef, 2015). Hayyan et al. (2015) reported on the physical properties of Triethylene glycol-based DESs using different phosphonium and ammonium salts (M. Hayyan, Aissaoui, et al., 2015).

Based on the foregoing, four novel DESs systems were synthesized based on Benzyl trimethyl ammonium chloride (BTAC) with four HBDs, which include ethylene glycol (EG), diethylene glycol (DEG), triethylene glycol (TEG) and glycerol (Gly). The first stable DESs of each system were chosen for the physical properties investigation, which includes freezing point, density, viscosity and surface tension. The effect of molar ratio on the Gly base DESs was also investigated. Furthermore, an FTIR analysis has been performed to investigate the function groups of these solvents.

4.2 Experimental

4.2.1 chemicals

BTAC and DEG with purity of (>97%) and (99%) respectively were supplied by Sigma-Aldrich. EG, TEG and Gly with purity (>99%) were supplied by Merck, Germany. Figure 4.1 shows the molecular structure of the salt and HBDs.

4.2.2 Synthesis of Benzyl trimethyl ammonium chloride-based DESs

In this study, DESs were synthesized in different ratios of BTAC and HBD. Table 1S (Supporting Information) shows the 40 synthesized DESs. Different phases appeared during and after preparing the DESs such as solid, semi-solid, crystal and liquid. All chemicals were dried overnight in a vacuum oven and kept in a glove box to control the moisture. The salt was mixed with each HBD using magnetic stirring. The mixtures of the salts and HBDs were mixed at 400 rpm and 353 K until the DES became a homogeneous mixture without any precipitate. The mixing time was approximately 30 minutes. Each DES system (salt-HBD) consisted of several molar ratios (1:1 to 1:10). At a high ratio of salt, precipitate appears with time and disappears with increasing HBD ratio. The chosen molar ratio among each DES system was the first molar ratio that showed the most stable and homogeneous mixture without any precipitate after eight weeks of observation. However, regarding Gly-based DESs, the first three molar ratios

were chosen to study the effect of salt to HBD molar ratio on the physical properties.

Table 4.1 listed the molar ratios and the abbreviations of the studied DESs.

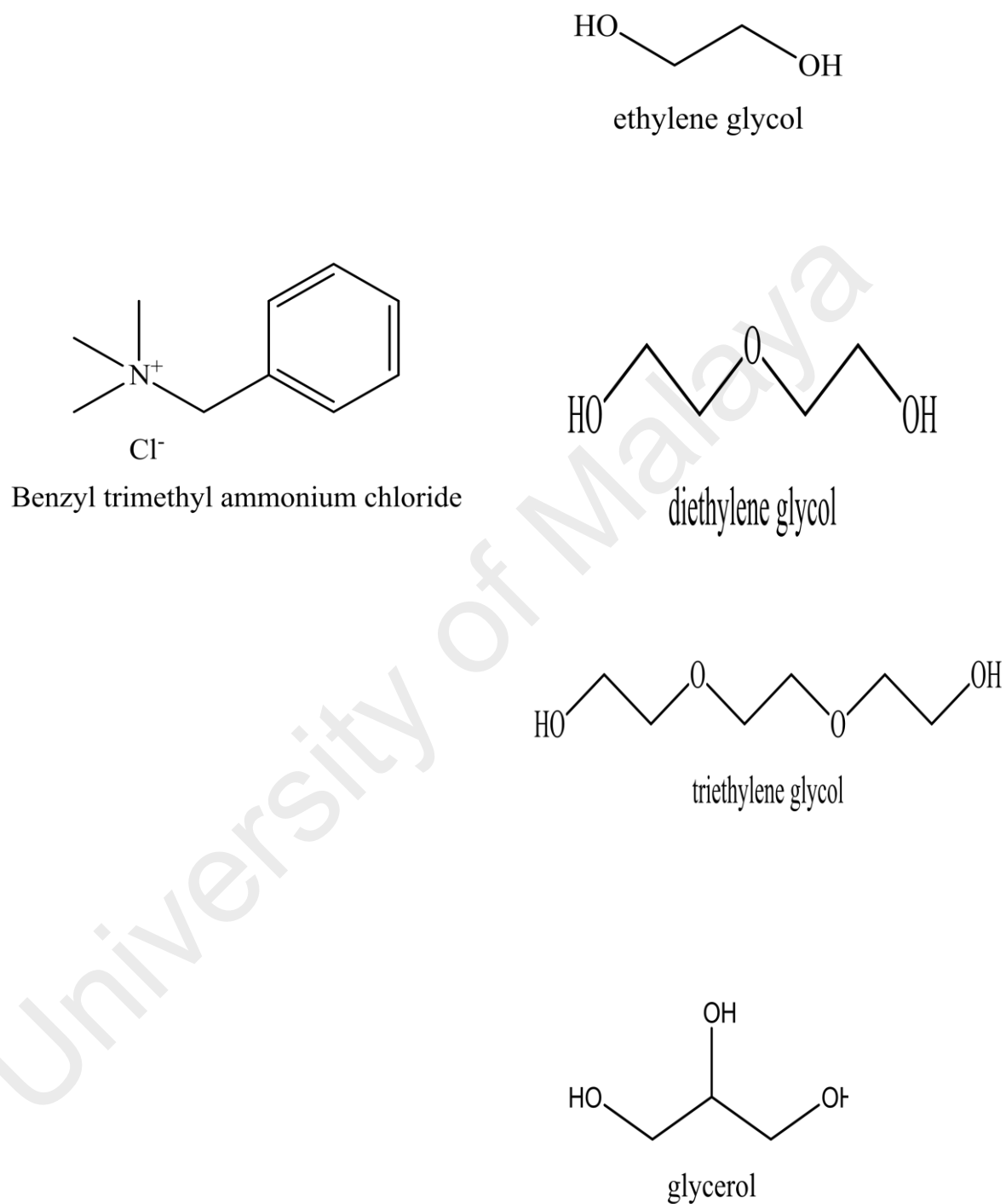


Figure 4.1: Molecular structure of BTAC and the four HBDs

Table 4.1: Selected DESs, abbreviations, and molecular weights

DES Abb. ^a	Salt Abb. ^a	M _S ^b	HBD	M _H ^c	Molar ratio		M _{DES} ^d
DES2	BTAC	185.69	EG	62.06	1	2	103.2765
DES13	BTAC	185.69	DEG	106.12	1	3	126.0135
DES23	BTAC	185.69	TEG	150.17	1	3	159.0533
DES32	BTAC	185.69	Gly	92.09	1	2	123.2938
DES33	BTAC	185.69	Gly	92.09	1	3	115.4938
DES34	BTAC	185.69	Gly	92.09	1	4	110.8138

^a Abbreviation, ^b molecular weight of the salt, ^c molecular weight of HBD ^d molecular weight of DES calculated using ($M_{DES} = X_S \times M_S + X_H \times M_H$)

4.2.3 Physical properties measurement

All samples were kept in well-sealed vials and in desiccator to avoid the humidity effect. Furthermore, fresh samples were synthesized to be used for analysis in order to avoid any structural change in the environment. Differential Scanning Calorimetry (DSC) METTLER TOLEDO[®] was used to estimate the freezing point for the selected DESs. Brookfield[®] An R/S Rheometer was used for measuring the viscosity. The fluctuation in the temperature was controlled by the external water circulator (Techne-Template TE-8A) with a temperature range of 298-353 K. Density meter (DM 40) METTLER TOLEDO[®] was used to measure the density at a temperature range of 298-363 K. Conductivity was measured by a Eutech Cyberscan[®] Con 11 hand-held meter at a temperature range of 298-348 K. Spectrum 400 FT-IR Spectrometer was used to analyse the functional groups of the DESs at room temperature. Table 4.2 listed the slandered uncertainty of each measurement.

Table 4.2: Uncertainties of the measurements

Measurement	Estimated uncertainty
Melting point	0.01 K
Density	0.0001 g·cm ⁻³
viscosity	5 % of measured value
Conductivity	5 μS·cm ⁻¹

4.3 Results and discussion

4.3.1 Freezing point

In this work, the freezing point of DES2, DES13, and DES23 is 237, 236, and 232 K respectively, while the freezing point of EG, DEG, and TEG is 260, 262, and 266 K respectively. The melting point of BTAC is 511 K. Thus, the melting points of the selected DESs were lower than that of both of the components, and they complied with the definition of a DES. The freezing point of DES23 is much like that of Choline Chloride:Glycerol reported by Hayyan et al. (2010) (M. Hayyan et al., 2010) and Abbot et al. (2011) (Andrew P Abbott et al., 2011). The melting point of DES2 is almost the same as that of Choline Chloride:Oxalic acid with a molar ratio of 1:1 as reported by Abbot et al. (2014) (Andrew P. Abbott, Boothby, et al., 2004).

The freezing points of DES23, DES33, and DES34 were 242, 239 and 225 respectively. The results indicated that the eutectic point for these three novel DESs was for DES34, which was prepared at a molar ratio of 1:4 of BTAC to Gly. Furthermore, the advantage of such low melting points allows the selected DESs to be considered for possible applications in many fields, such as chemical and electrochemical reaction media and separation processes. Figure 5B-9B (Appendix B) shows the DSC curves for DES2, DES13, DES23, DES32, DES33 and DES34 respectively.

4.3.2 Density

The density is considered to be one of the most significant physical properties due to its role in any industrial applications. The density can be reduced by increasing the temperature due to rising molecular mobility, which leads to an increase in the solution molar volume, and the density will be reduced as a result (A. Hayyan et al., 2012). Herein, the density was conducted as a function of a temperature range of 298 to 363 K. Figure 4.2 shows the density of the selected DESs, which followed the order of DES23>DES13>DES2, with 1.1183, 1.1114, and 1.1016 g cm⁻³ at 298 K respectively. Hence, the effect of the length of the carbon atom chain of the HBD is inversely proportional to the density (Yusof, Abdulmalek, Sirat, & Rahman, 2014). DES2 density is similar to that of N,N diethylenethanol ammonium chloride:EG at a molar ratio of 1:3 (Shahbaz et al., 2011), while DES23 density is much like that of Choline Chloride:EG with a molar ratio of 1:1.75 (Shahbaz et al., 2012).

Figure 4.3 shows the density of Gly- and BTAC-based DES with different molar ratios. The density is reduced by increasing the salt ratio in the mixture. The presence of three hydroxyl groups on the Gly play a part in the increased density for Gly-based DESs. That could be attributed to the shortening in intermolecular distances under the increasing intermolecular forces caused by hydroxyl groups.

It should be mentioned that the density of DES2 was less than that of EG at room temperature, and they become the same in the temperature range around 358 K. The same phenomenon was observed for DES13 and DES23; however, for those DESs the density reduction with temperature interacted with the density of each DES's HBD at around 313 K. On the contrary, the Gly reduction with temperature was comparatively in agreement with the reduction of DES23, DES33 and DES34.

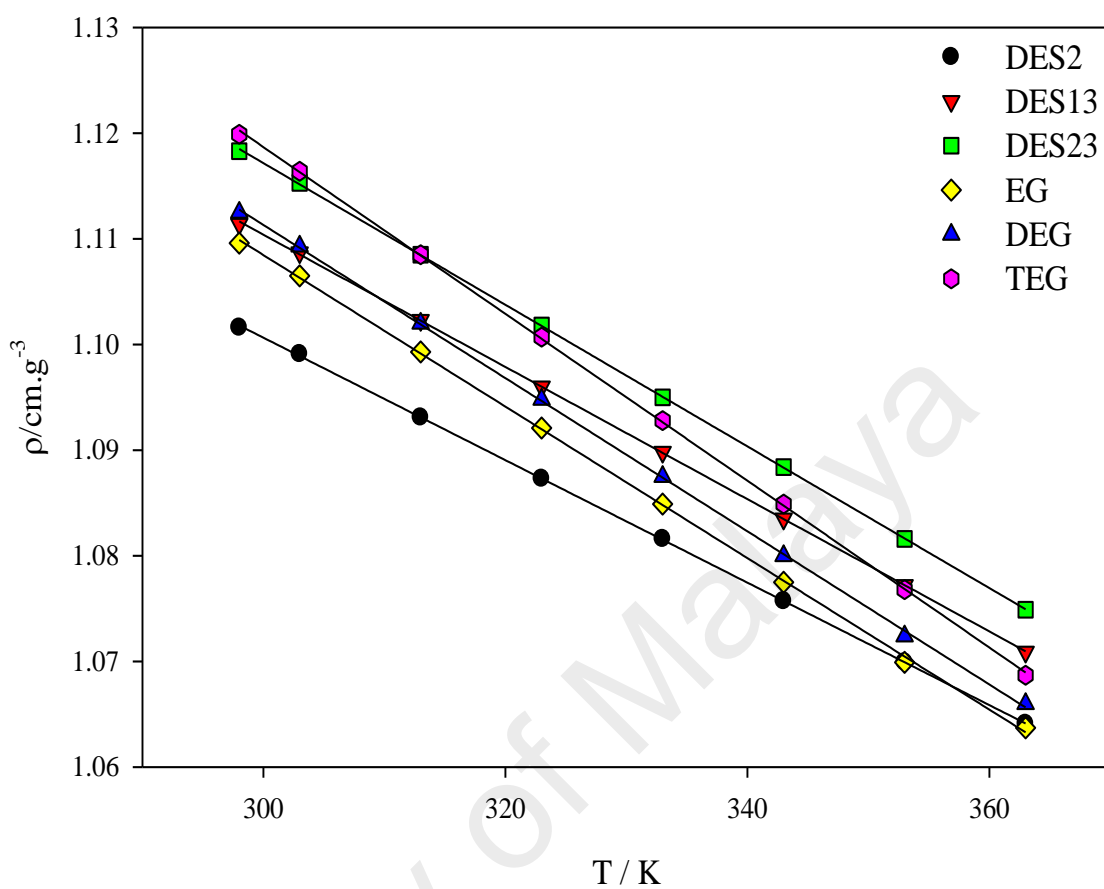


Figure 4.2: Variations of densities with temperature for glycols DESs systems

The experimental data of the density as a function of temperature fitted in Eq. 4.1:

$$\rho = a(T) + b \quad (4.1)$$

Where ρ is the density in gm.cm^{-3} , T is the temperature in Kelvin, (a and b) is constant represent the molar ratio of DES with HBD. The values of (a and b) are represented in Table 4.3. The regression coefficient was found to be more than 0.9995, which indicated the density, temperature relationship is in a linear frame.

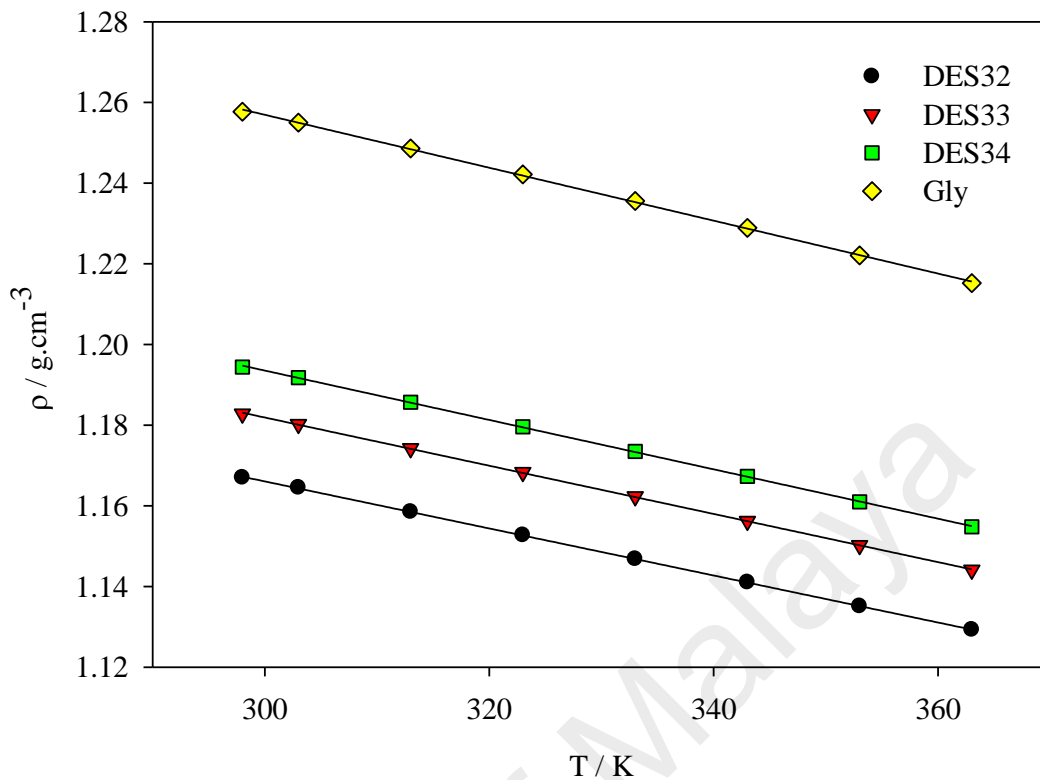


Figure 4.3: Variation of densities with temperature for the Gly based DESs with different molar ration

4.3.3 Viscosity

Knowing the viscosity is crucial for the design stages of any industrial process; it is also essential for fluid calculations and piping design. Just like most ILs, DES has a high viscosity due to the extensive hydrogen bond between each component and the large ion size, which results in a lower mobility of free species within the DES. Owing to their potential applications as green media, the development of DESs with low viscosities is highly desirable (Q. Zhang et al., 2012). Herein, the viscosity measurements were a function of a temperature range of 298-353 K. The results showed that DES2, DES13, and DES23 all have a low viscosity below 100 cP. Figure 4.4 showed the viscosity trend with temperature of the glycols-based DESs and the HBDs consisting of these DESs.

Table 4.3: Density–temperature model parameters and regression coefficients.

DES	a	b	R ²
DES2	1.2745	-6×10 ⁻⁴	0.9999
DES13	1.2982	-6×10 ⁻⁴	0.9999
DES23	1.3183	-7×10 ⁻⁴	1.0000
DES32	1.3410	-6×10 ⁻⁴	0.9999
DES33	1.3612	-6×10 ⁻⁴	0.9998
DES34	1.3772	-6×10 ⁻⁴	0.9998
EG	1.3236	-7×10 ⁻⁴	0.9997
DEG	1.3288	-7×10 ⁻⁴	0.9997
TEG	1.3555	-8×10 ⁻⁴	0.9999
Gly	1.4538	-7×10 ⁻⁴	0.9995

The viscosity of DES2, DES13 and DES23 is close to 1-Methylimidazolium bis (trifluoromethyl sulfonyl) imide IL reported by Ohno (2002) (Ohno & Yoshizawa, 2002). Besides, it was close to ChCl:1,4Butanediol DES with a molar ratio of 1:4 reported by Abbot (2007) (Andrew P. Abbott, Robert C. Harris, et al., 2007b). Furthermore, the viscosity data of these novel glycols-based DESs are close to each other. According to Abbott (2004, 2006) (A. P. Abbott, G. Capper, D. L. Davies, & R. K. Rasheed, 2004; Andrew P. Abbott et al., 2006), the viscosity differences caused by the ratio of the ion radius to the hole size within the liquid, to this end, according to hole theory, the viscosity of ILs and DESs is controlled by the cation size of the salt. Based on that, there is no significant effect of HBD on the viscosity of these systems. Similarly, the effect of molar ratio was obvious for DES32, DES33 and DES34. The viscosity decreased with the

incrimination of salt ratio in the mixture, and this behaviour was consistent with the results reported by Abbot et al. (2011) (Andrew P Abbott et al., 2011) for the choline chloride:Gly. Figure 4.5 showed the trend of viscosity for DES32, DES33, DES34 and Gly.

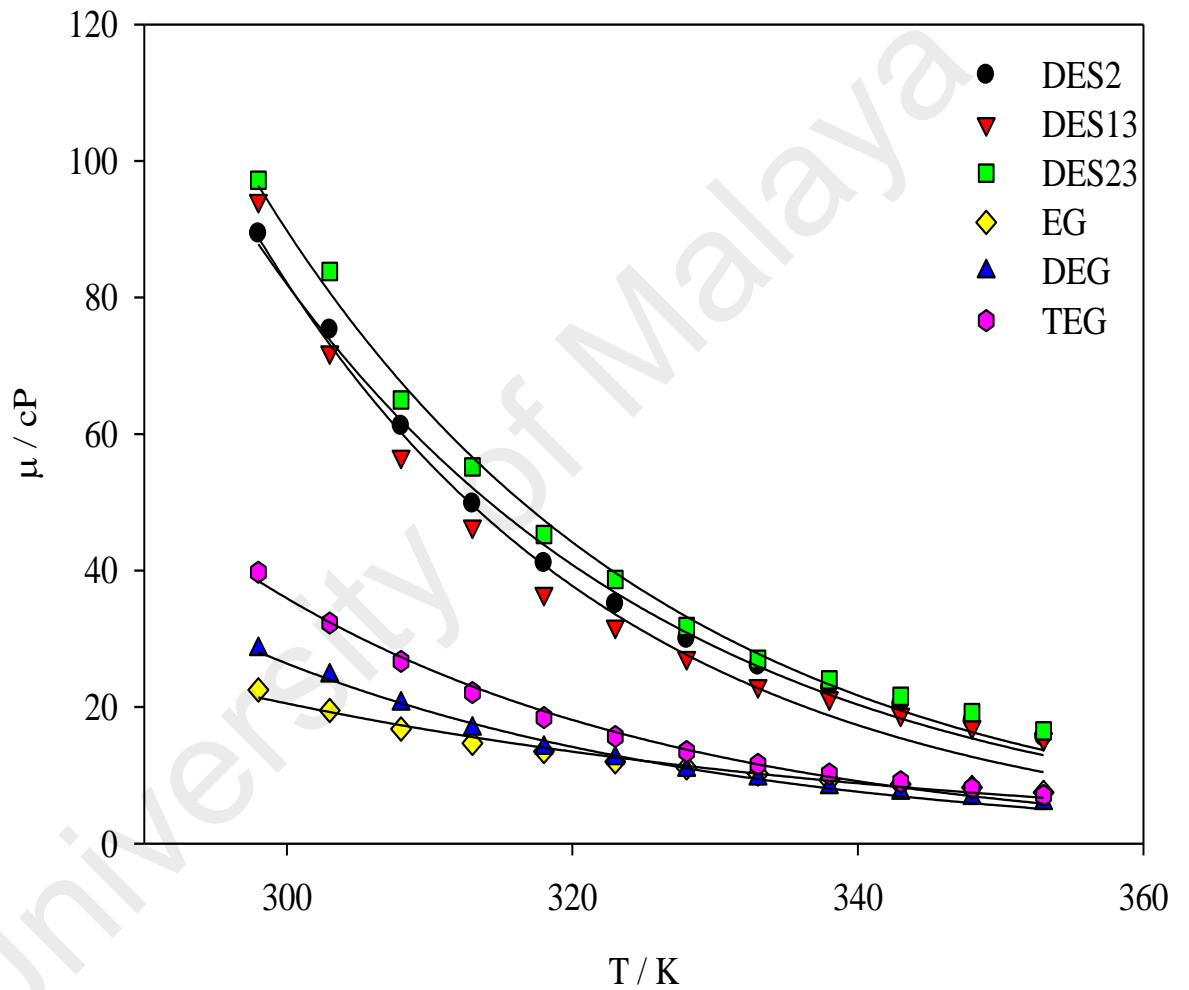


Figure 4.4: Variations of viscosity with temperature for glycols DESs systems

The viscosity-temperature relationship is described well by Arrhenius equation Eq.

4.2:

$$\mu = \mu^{\circ} e^{\frac{E_{\mu}}{RT}} \quad (4.2)$$

Where μ is the dynamic viscosity, μ° is the pre-exponential constant, E_{μ} is the activation energy, R is the gas constant, and T is the temperature in Kelvin. The minimum R^2 was 0.9936. The values of μ° , E_{μ} , and the regression coefficient can be seen in Table 4.4.

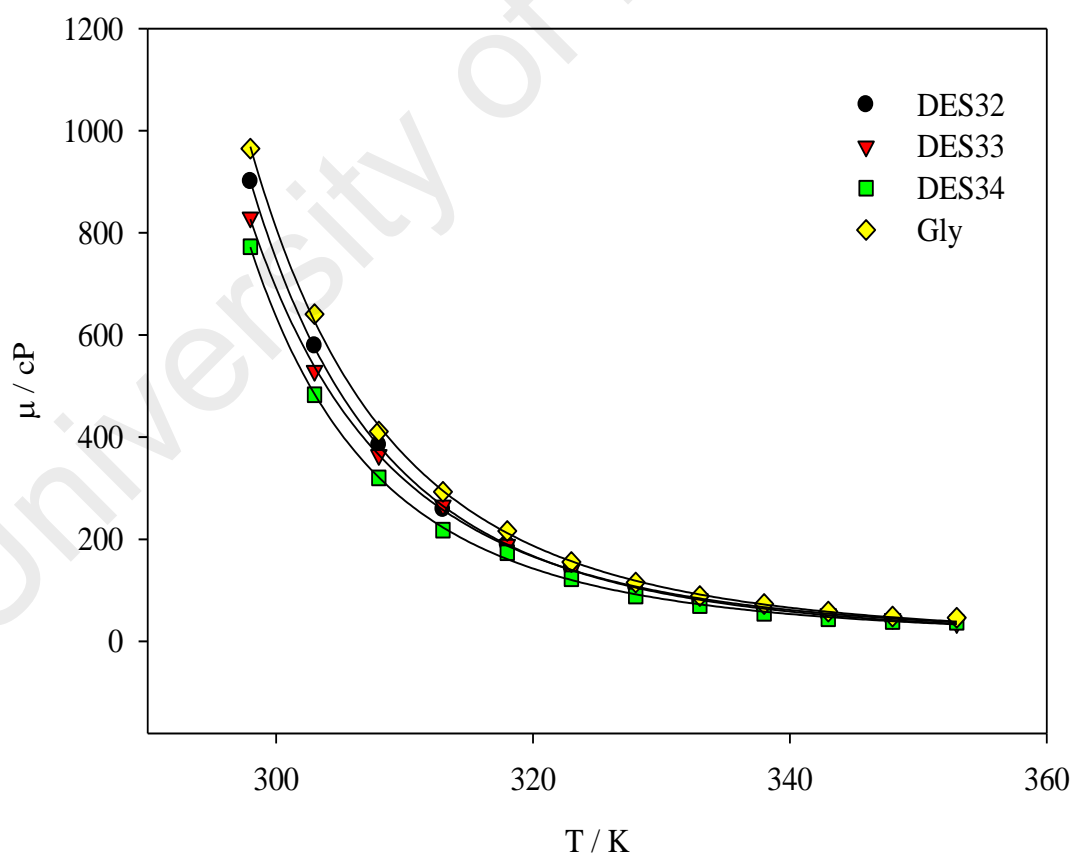


Figure 4.5: Variation of viscosity with temperature for the Gly based DESs with different molar ration

Table 4.4: Viscosity–temperature model parameters and regression coefficients.

DES	μ°	$\frac{E_\mu}{RT}$	R ²
DES2	0.00117	3342.611	0.99683
DES13	0.00087	3417.681	0.98475
DES23	1.032E-06	6081.017	0.98775
DES32	1.829E-06	5932.574	0.98654
DES33	1.664E-06	5922.586	0.99393
DES34	1.539E-06	5907.275	0.98333
EG	0.02184	2051.497	0.99221
DEG	0.00107	3031.144	0.99717
TEG	0.00062	3286.513	0.99749
Gly	1.829E-06	5932.574	0.98654

4.3.4 Conductivity

Conductivity plays a significant role in electrochemical applications. It is well known that the conductivity is increased with the rise of temperature due to the reduction of viscosity, which leads to increase molecular mobility. Herein, the conductivity was measured as a function of temperature at a range from 298 K to 348 K. Figure 4.6 illustrates the trend of the conductivity increment with the rising of temperature for DES2, DES13, and DES23. Owing to the large amount of salt and hence, the ionic conductivity of EG, the conductivity of DES2 was the highest with 7500 $\mu\text{S}/\text{cm}$ at 348 K, which is close to that of Tetrabutylammonium Chloride: EG with a molar ratio of 1:4 as reported by Mjalli (2014) (Jibril et al., 2014). While the conductivities of DES13 and DES23 are much less than that of DES2, the reason behind that might be due to the amount of salt in these DESs and also the ionic species in their HBD.

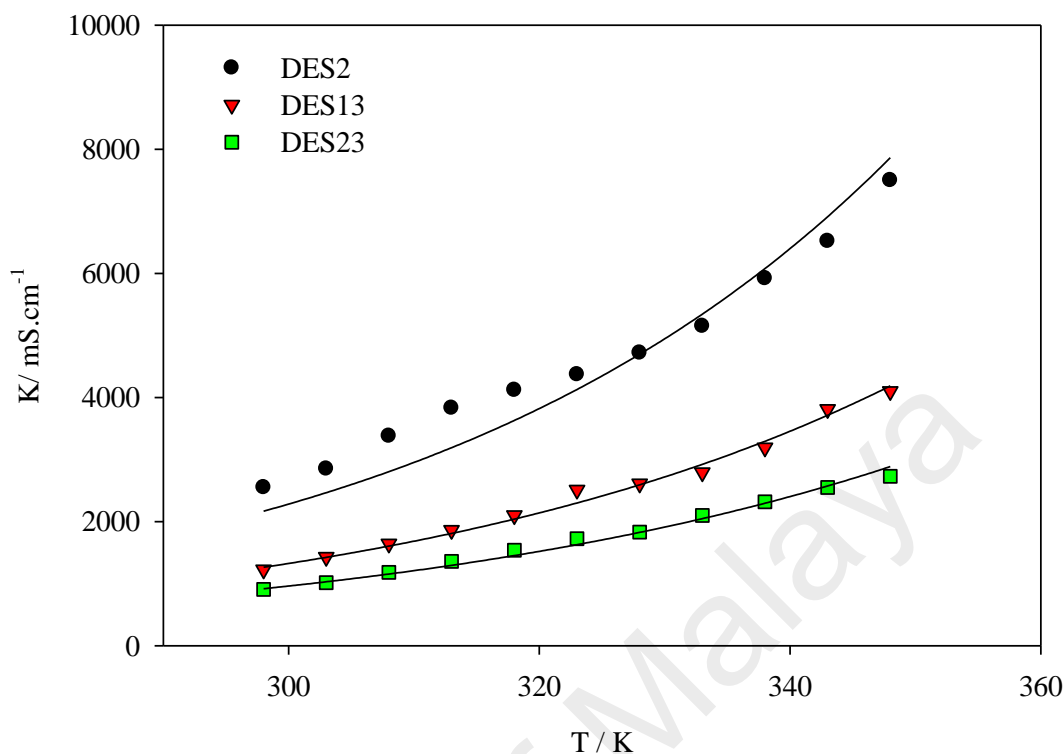


Figure 4.6: Variations of conductivities with temperature for glycols DESs systems

On the other hand, the conductivities of DES32, DES33 and DES34 were less than that of DES2 and DES23. Figure 4.7 shows electrical conductivity of BTAC:Gly-based DESs with different molar ratios.

The conductivities of these DESs increased by increasing the ratio of salt. The conductivity-temperature relationship is described well by Arrhenius equation Eq. 4.3:

$$K = K^{\circ} e^{-\frac{E_{\kappa}}{RT}} \quad (4.3)$$

Where K is the conductivity in $\mu S \cdot cm^{-1}$, K° is a constant, E_{κ} is the activation energy of conductivity, R is the gas constant and T is the temperature in Kelvin. The value of R^2 is more than 0.98 for all DESs. Table 4.5 lists the values of K° , E_{κ} , and R^2 .

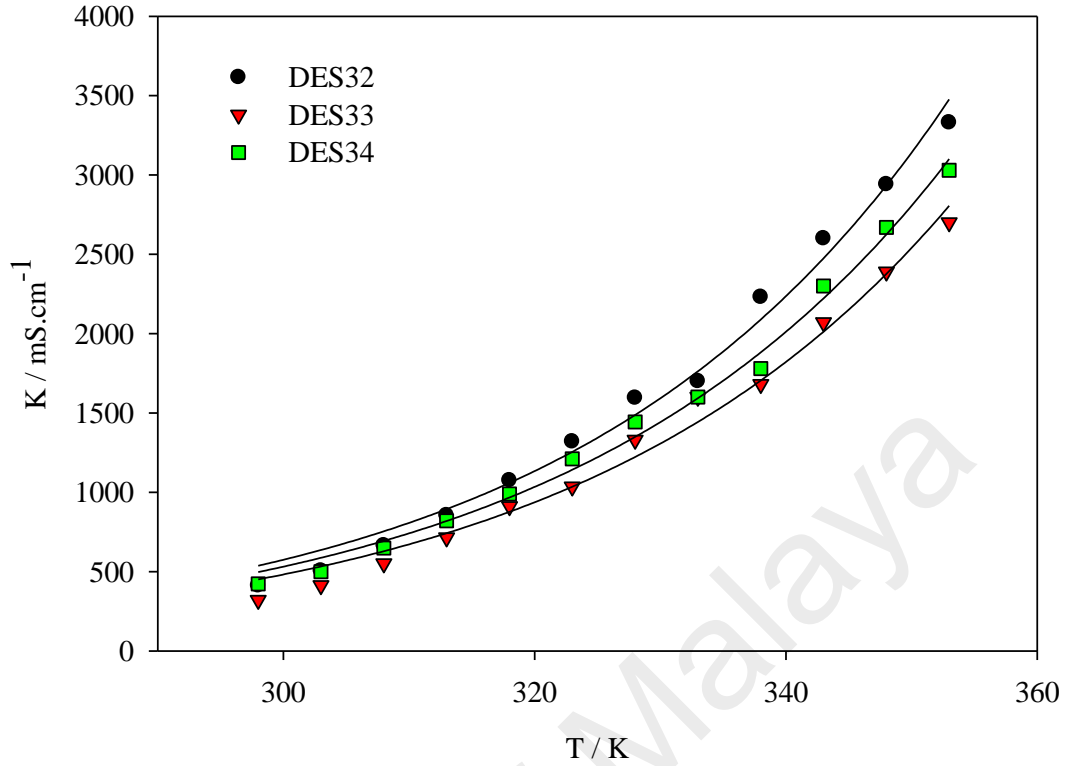


Figure 4.7: Variation of conductivity with temperature for the Gly based DESs with different molar ratio

Table 4.5: Conductivity–temperature model parameters and regression coefficients.

DES	K°	$-\frac{E_k}{RT}$	R^2
DES2	3E+06	-2099.15	0.9882
DES13	5E+06	-2456.05	0.9930
DES23	2E+06	-2321.19	0.9969
DES32	3E+08	-4048.3	0.9942
DES33	3E+08	-4053.02	0.9904
DES34	1E+08	-3771.25	0.9957

4.3.5 Surface tension

The cohesive force between the molecules that results from an imbalance of intermolecular attractive forces in the liquid is known as surface tension. It is crucial for many industries to know the surface tension. In this study, the surface tension was measured at different temperatures between 298-348 K. For the glycols systems, the surface tension of DES2 was the most sensitive to temperature, and had the highest surface tension at 298 K and the lowest at 348 K among other DESs. Figure 4.8 shows the surface tension behavior of each DES toward temperature. The surface tension of DES13 and DES23 was close to that of tetrapropylammonium bromide: EG with molar ratios of 1:3, 1:4, and 1:5 reported by Baba Jibril et al. (2014) (Jibril et al., 2014).

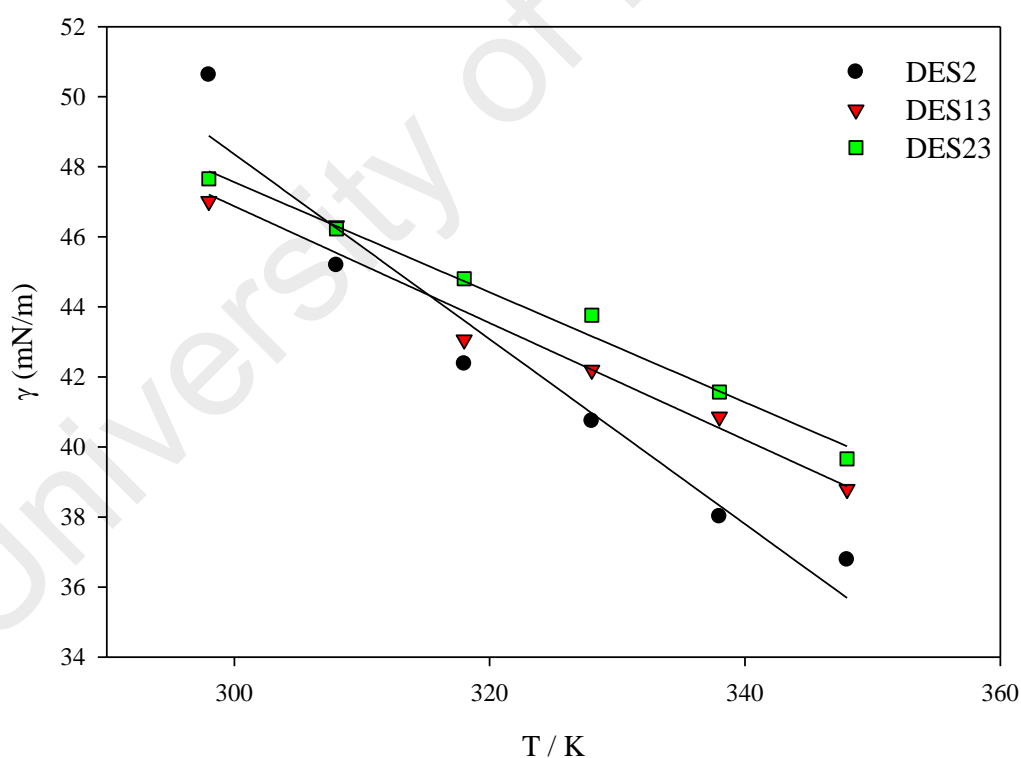


Figure 4.8: Variations of surface tension with temperature for glycols DESs systems

On the other hand, the surface tension of Gly based DESs with different molar ratio showed that by increasing the salt ratio in the mixture, the surface tension decreased. This

is due to the breaking of the intermolecular forces of Gly (Andrew P Abbott et al., 2011). Figure 4.9 showed the trend in surface tension of the Gly-based DESs system with respect to temperature. Surface tension could be expected to follow trends similar to those of viscosity, since it is a measure of how strong the intermolecular forces are in the liquid (Andrew P Abbott et al., 2011); however, the surface tension correlation with temperature showed a linear form and fitted well in Eq. 4.4.

$$\gamma = a + b(T) \quad (4.4)$$

Where γ is the surface tension, T is the temperature in Kelvin, and a and b is constant.

Table 4.6 lists the values of a , b , and the regression coefficient for all DESs.

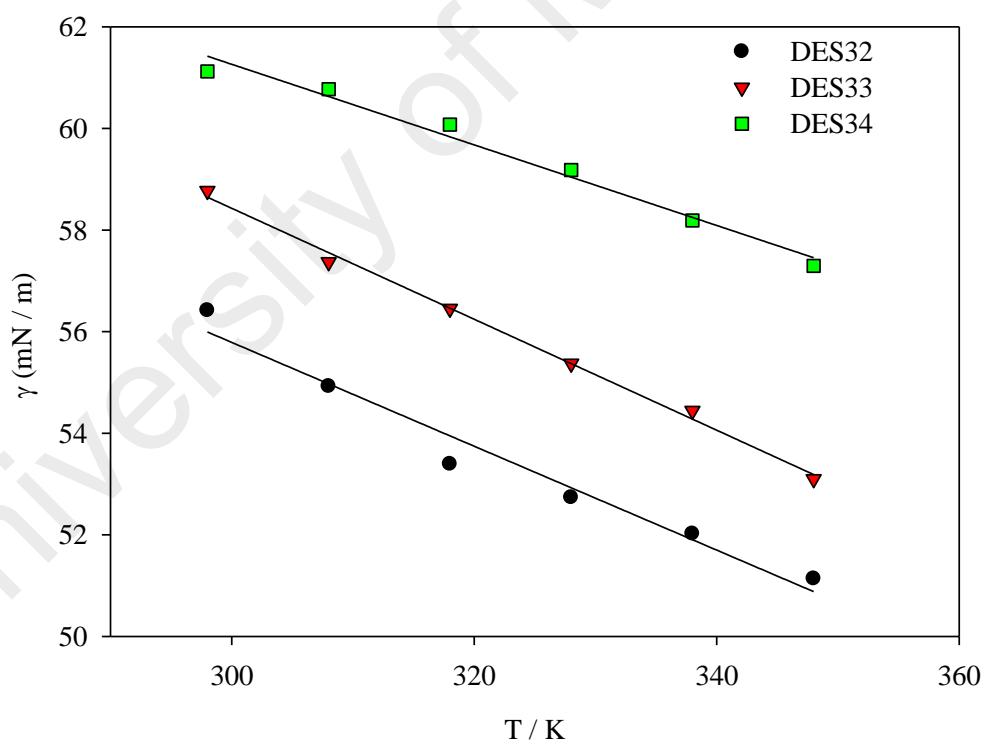


Figure 4.9: Variation of Surface tension with temperature for the Gly based DESs with different molar ration

Table 4.6: Surface tension–temperature model parameters and regression coefficients.

DES	a	b	R ²
DES2	127.5575	-0.2640	0.9457
DES13	96.8976	-0.1667	0.9717
DES23	94.6994	-0.1571	0.9874
DES32	86.4582	-0.1022	0.9678
DES33	91.1897	-0.1092	0.9959
DES34	85.0613	-0.0793	0.9807

4.3.6 FTIR

FTIR is essential to study the functional groups of any new solvent via identifying the functional groups in the molecule. FTIR is usually utilized to study the interaction of different groups in order to analyze and identify the structure of the material (Yue et al., 2012). As indicated in Figure 4.10d, all DESs systems have a very similar spectrum because all HBDs have an extensive presence of O-H, C-H and C-C stretching. The presence of water is obviously predicted through stretching bond between 3200-3600 cm⁻¹ where the O-H functional group existence is usually indicated (J. Luo et al., 2012; B. C. Smith, 1998; B. Stuart, 2005). The N-H stretching overlapped with the O-H stretching, also the C-H stretching found in the same region of O-H stretching between 3000 to 3100 cm⁻¹ (B. C. Smith, 1998; B. Stuart, 2005). The Cl⁻ presence can be seen in the range of 600-800 cm⁻¹ in all DESs systems (B. C. Smith, 1998). Figure 4.10, 4.11, and 4.12 shows the spectrum of the glycols DESs systems, HBDs, and the salt. Figure 4.13 shows the spectrum of the Gly-based DESs at different molar ratios along with the Gly and the salt spectrum. Furthermore, Table 4.7 lists all the wave numbers found in the DESs and the functional groups associated with them.

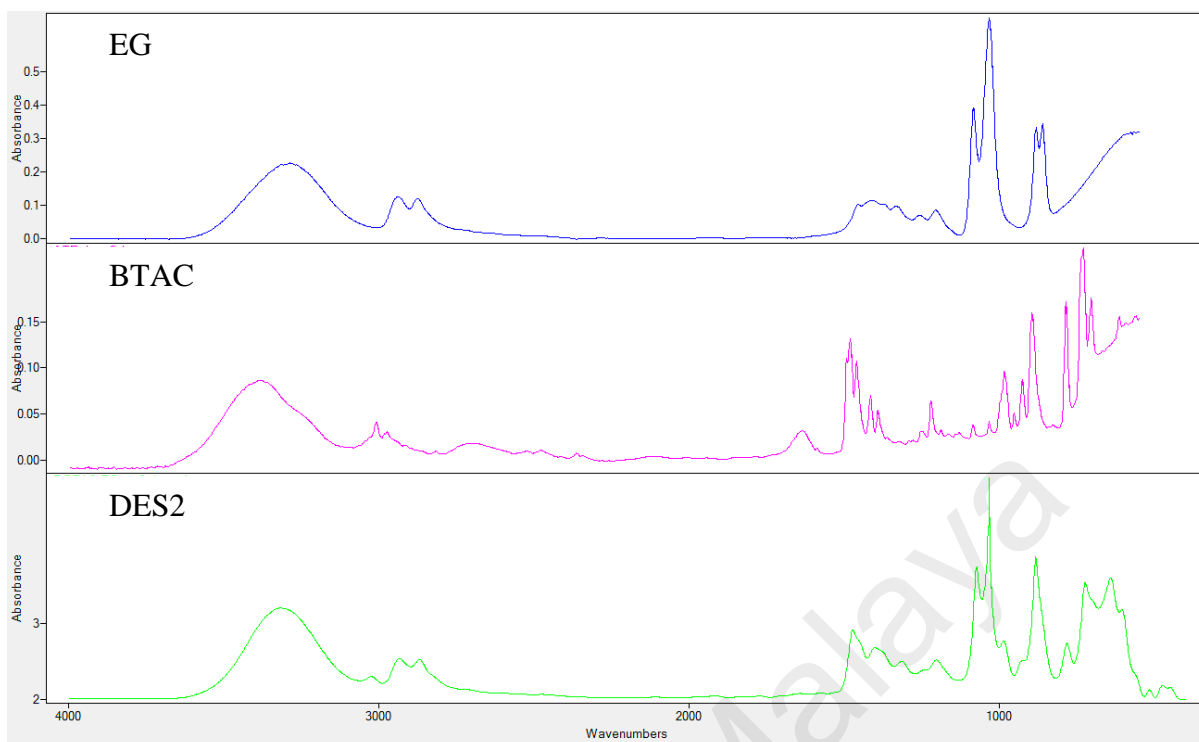


Figure 4.10: FTIR spectrum of EG, BTAC and DES23

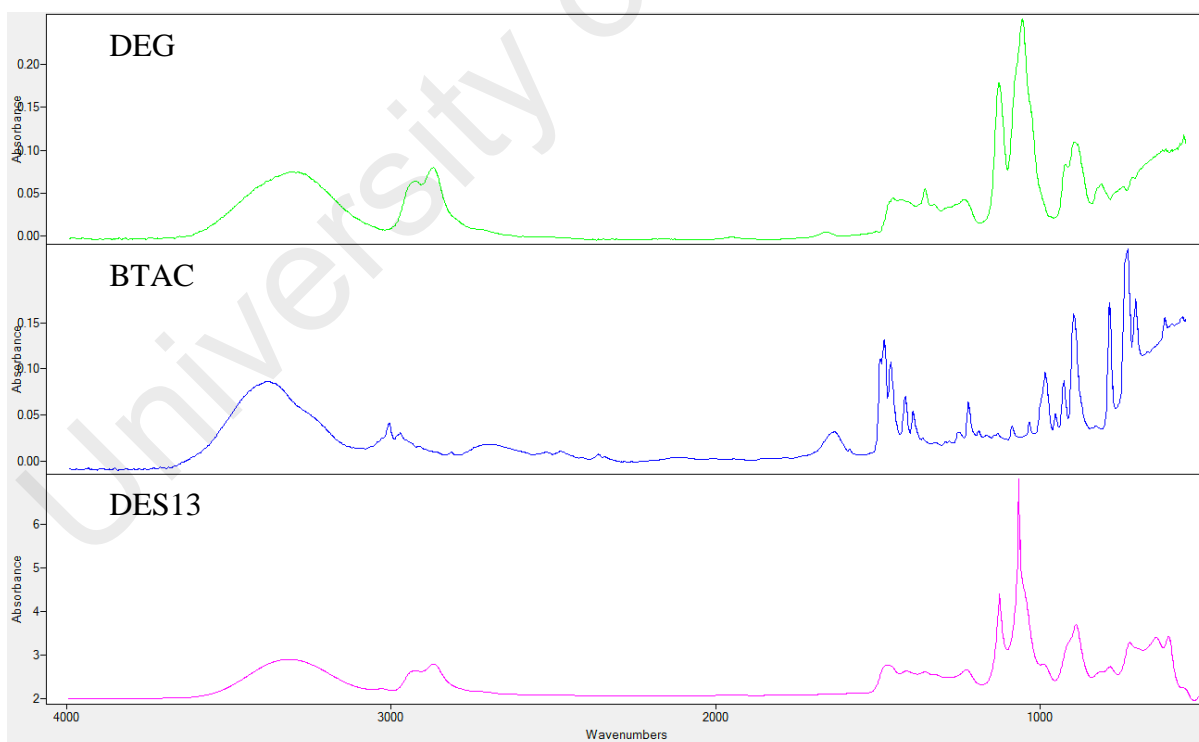


Figure 4.11: FTIR spectrum of DEG, BTAC and DES13

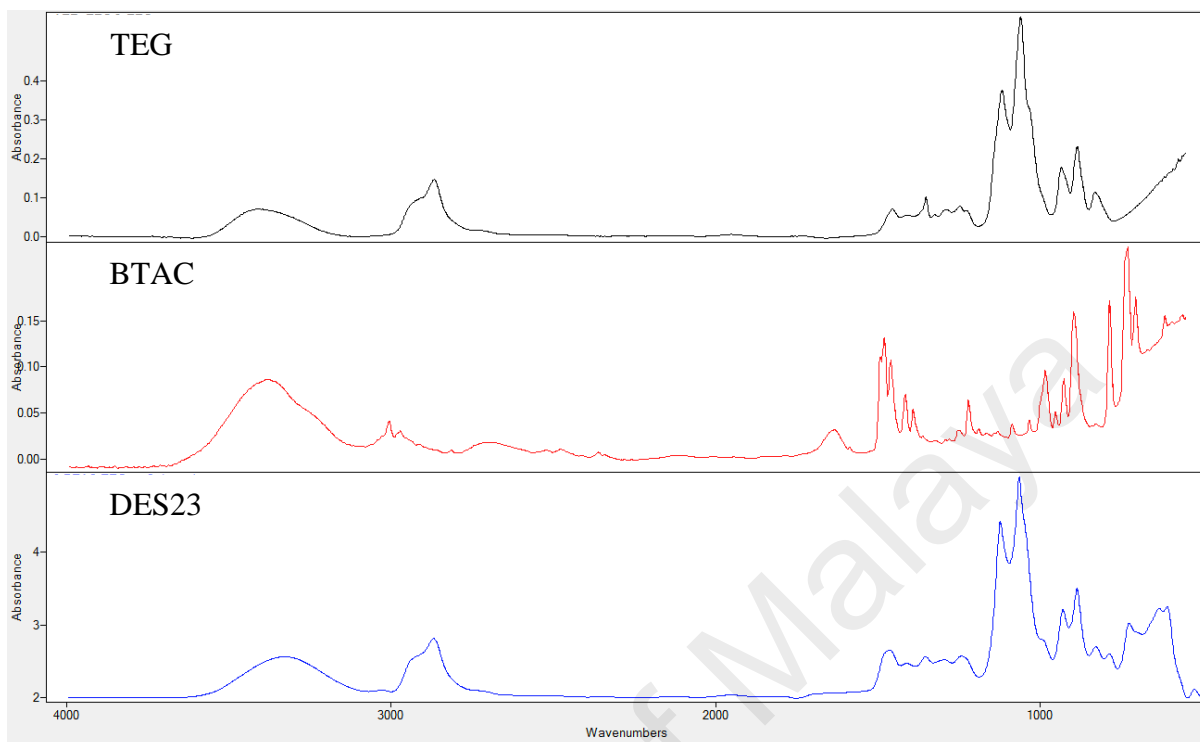


Figure 4.12: FTIR spectrum of TEG, BTAC, and DES13

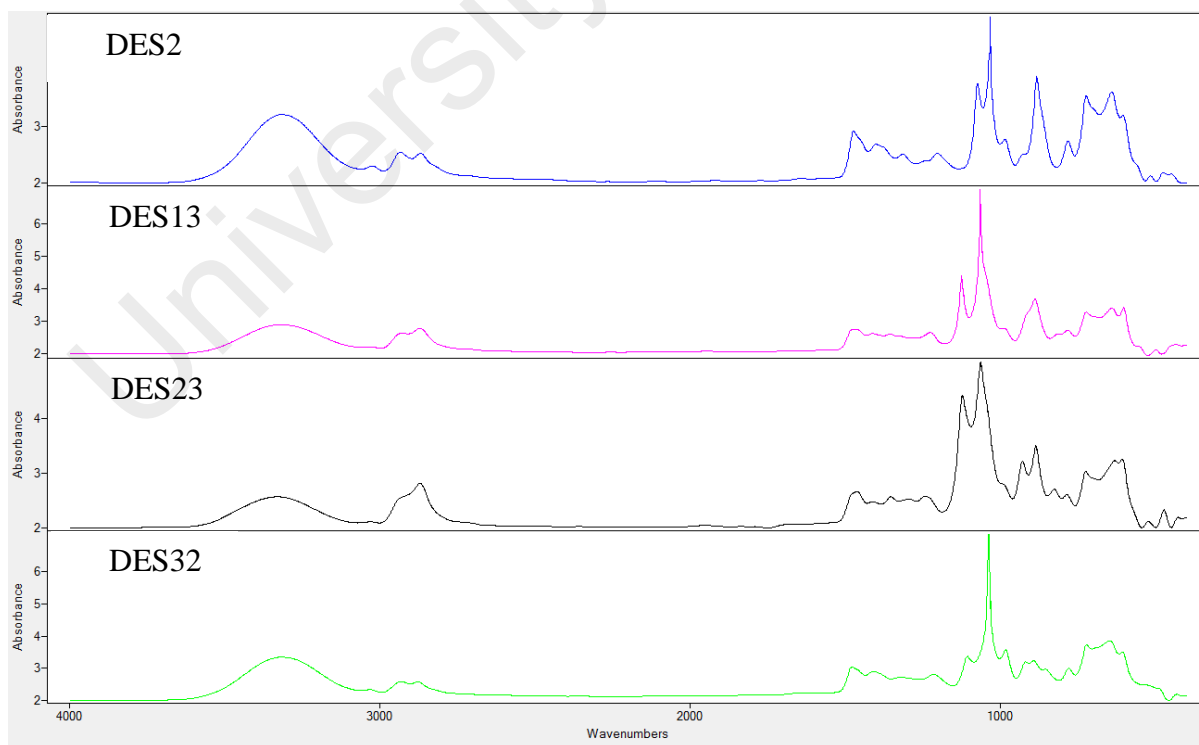


Figure 4.13: FTIR spectrum for Gly DESs system with different molar ratio, Gly and BTAC salt

4.4 Summary

Deep eutectic solvents (DESs) occupy a strategic place as an analogue to ionic liquids due to their availability, non or less toxicity, biodegradability, recyclability, flammability, and low price compared to other types of conventional ionic liquids. In this study, four new DES systems were successfully synthesized based on BTAC and four different types of HBD named EG, DEG, TEG and Gly. 40 different DESs were synthesized based on different molar ratios (1-10) for each DESs system. The first stable ratio of each system was chosen to investigate the physical properties with respect to temperature, including density, viscosity, conductivity, and surface tension. Moreover, the freezing point of each DES was conducted. Furthermore, the effect of molar ratio was also investigated for the Gly-based DESs system. Additionally, an FTIR has been utilized in order to identify the functional groups associated with the synthesis of these novel DESs. The results showed that these new DESs have a great potential in many applications, especially environmental applications.

Table 4.7: Functional groups of the novel DESs

Wave number (cm^{-1})	DESs	Functional group	Reference
3300	DES2, DES13, DES23, DES32	O-H and N-H	(B. C. Smith, 1998; B. Stuart, 2005)
3030	DES2,DES13, DES23, DES32	C-H	(B. C. Smith, 1998; B. Stuart, 2005)
2930	DES2, DES13, DES32	CH ₂ Asymmetric	(B. C. Smith, 1998)

Table 4.7 continued

2869	DES2, DES13, DES23	CH ₂ Symmetric	(B. C. Smith, 1998; B. Stuart, 2005)
1470	DES2, DES13, DES23, DES32	C-CH Asymmetric	(B. C. Smith, 1998; B. Stuart, 2005)
1400	DES2, DES13, DES23, DES32	C-N stretching, =C-H in- plane bending (Alkenes)	(B. C. Smith, 1998; B. Stuart, 2005)
1350	DES13, DES23	Aromatic nitro compound NO ₂ symmetric stretching	(B. Stuart, 2005)
1270-1300	DES2, DES13, DES23	Nitrate NO ₂ symmetric stretching	(B. Stuart, 2005)
1240	DES23	C-O stretching	(B. Stuart, 2005)
1200-1225	DES13, DES23	In-plane C-H bending	(B. Stuart, 2005)
1122	DES13, DES23	C-N stretching	(B. C. Smith, 1998)
1073	DES2, DES32	C-O stretch	(B. C. Smith, 1998)
1064	DES13, DES23	C-O stretch	(B. C. Smith, 1998)
1033	DES2, DES32	O-C-C stretch	(B. C. Smith, 1998)
985	DES32	(Vinyl) out of plane C-H bend	(B. C. Smith, 1998)

Table 4.7 continued

928	DES23	C-O and C-C stretches	(B. C. Smith, 1998)
882	DES2, DES13	C-O out-of-plane bend	(B. C. Smith, 1998)
782	DES2, DES13, DES23	C-X stretch, C-Cl bond	(B. C. Smith, 1998)
779	DES32	(Meta) out of plane C-H bending	(B. C. Smith, 1998)
647	DES32	C-Cl bond	(B. C. Smith, 1998)

CHAPTER 5: LEAD REMOVAL FROM WATER BY CHOLINE CHLORIDE BASED DEEP EUTECTIC SOLVENTS FUNCTIONALIZED CARBON NANOTUBES

5.1 Introduction

The presence of lead in water causes a variety of health problems and has gained enormous concern worldwide due to its specific effects on children (Ngueta et al., 2014). Exposure to lead affects the nervous system and can cause brain disorders (Gad & Pham, 2014). Lead presence in water is often due to the corrosion of plumbing materials or to waste disposal associated with certain industries (Tong et al., 2000).

Many techniques have been proposed to reduce lead contamination in water. Adsorption is considered as the most effective method for removal of lead ions (H. J. Wang et al., 2007). Different types of adsorbents have been used to remove Pb(II) from water. Examples include rice husks, maize cobs, sawdust (Abdel-Ghani et al., 2007), aquatic plant (Axtell et al., 2003), kaolinitic clay, giru clay (Orumwense, 1996), and granulated blast-furnace slag (Dimitrova & Mehandgiev, 1998). Furthermore, the most useable adsorbent is activated carbon, which can originate from different sources (Goel et al., 2005; Imamoglu & Tekir, 2008; Netzer & Hughes, 1984; Sekar et al., 2004; Tao et al., 2015). Nanoparticles have been found to be effective adsorbents for many pollutants due to their unique features, including small size, catalytic potential, high reactivity, and large surface area (Ali, 2012). In the field of water treatment, carbon nanotubes (CNT) are the most commonly used nanomaterial.

Due to their extraordinary physical, electrical, and chemical properties, CNTs have many promising applications in material science, electrical engineering, environmental engineering, and medical science. Accordingly, CNTs have been employed to remove many different pollutants (Ibrahim, Hayyan, AlSaadi, Hayyan, & Ibrahim, 2016),

including dioxin (Long & Yang, 2001), nitrogen, methane (Bienfait et al., 2004), ammonia (Bauschlicher & Ricca, 2004b), hydrogen (A. C. Dillon, 1997), and ozone (Yim & Liu, 2004), from air, and cadmium (Ruthiraan et al., 2015), Copper (N. M. Mubarak, Sahu, Abdullah, Jayakumar, & Ganesan, 2015), zinc (N. M. Mubarak et al., 2013), lead (Nabisab Mujawar Mubarak, Sahu, Abdullah, & Jayakumar), 1,2-dichlorobenzene (Peng et al., 2003), fluoride (Y.-H. Li, Wang, Zhang, et al., 2003), and trihalomethanes (C. Lu et al., 2005) from water. Therefore, CNTs as an adsorbent have interested researchers worldwide, which has resulted in more publications than any other adsorbent (Ali, 2012). However, CNTs have many drawbacks, including solubility, aggregation, and difficulty of manipulation, which impose a large limitation on the applications of CNTs. On the other hand, CNTs have shown a great affinity for interaction with different compounds (Ihsanullah et al., 2016). With this in mind, functionalization is the key to enhancing the activity of CNTs.

Many studies have reported utilizing convenient functionalization methods of CNTs to be used as Pb(II) absorber. Examples include nitric acid functionalized CNTs (H. J. Wang et al., 2007), manganese oxide-CNTs (CNTs/MnO₂) nanocomposite (Salam, 2013; S.-G. Wang et al., 2007), alumina coated CNTs (V. K. Gupta et al., 2011), sugarcane bagasse/CNTs composite (Hamza et al., 2013), and titanium dioxide/CNTs (TiO₂/CNT) nanocomposite (X. Zhao et al., 2010). Consequently, the need for new types of economical and environmentally friendly functionalization agents is crucial for many applications (M. Hayyan, Abo-Hamad, et al., 2015a; Martínez et al., 2003).

Recently, there has been increasing interest in the area of ionic liquids analogues, i.e. deep eutectic solvents (DESs), which were introduced by Abbot et al. in 2003 (Andrew P. Abbott et al., 2003) as a cheaper replacement for developed ionic liquids (ILs). Substantially, DESs consist of two or more compounds, with the mixtures of these

components have a melting point lower than that of the individual compounds (Andrew P. Abbott, Boothby, et al., 2004; M. Hayyan et al., 2010). The physicochemical properties of DESs are comparatively similar to those of conventional ILs. However, DESs have many advantages over conventional ILs. These advantages can be summarized as the simplicity of synthesis, the variety of the physical properties with different molar ratios, and the reasonable price of components (M. Hayyan, M. A. Hashim, M. A. Al-Saadi, et al., 2013; M. Hayyan, M. A. Hashim, A. Hayyan, et al., 2013). Based on the previous advantages, fast development and a wide range of potential application have appeared in many studies covering the physicochemical properties of these solvents, as well as applying them in many applications (E. L. Smith et al., 2014).

In the last decade, ILs and DESs have shown great potential in nanotechnology synthesis and applications. The first combination of nanotechnology and ionic liquids was presented by Deshmukh et al. (2001) (Deshmukh et al., 2001). Consequently, DESs have been involved in many nanotechnology related applications (Abo-Hamad et al., 2015).

DESs have excellent potential as functionalization agents, unlike conventional harsh acidic oxidative functionalization, to play a major role in attaching useful functional groups to the surface of CNTs without damage and through environmental relatively friendly process.

In this study, choline chloride (ChCl) and six hydrogen bond donors (HBDs) namely, glycerol (Gly), ethylene glycol (EG), diethylene glycol (DEG), triethylene glycol (TEG), urea (U), and malonic acid (MA) were used to synthesis six DESs systems. Subsequently, as a novel functionalization agent for CNTs, the synthesized DESs were utilized to study influences on this process. A comprehensive characterization of the functionalized CNTs was conducted by deferent analytical techniques, including FTIR, RAMAN, XRD, FESEM, EDX, BET surface area, Zeta potential, and TGA. Then, the DES-CNT models

were used as adsorbents for Pb(II) ions in aqueous solution. In addition, an optimization study was performed in order to find the optimum conditions for Pb(II) sorption onto the novel adsorbent. Moreover, kinetics and isotherm studies were also performed at different removal conditions.

5.2 Experiment

5.2.1 Chemicals and materials

MWCNTs with specifications of D×L 6-9 nm × 5 μm >95% (carbon) was supplied by SIGMA-ALDRICH. ChCl, MA, Gly, EG, TEG, DEG, sulfuric acid H₂SO₄ (95%-97%), nitric acid HNO₃ (65%), potassium permanganate KMnO₄, sodium hydroxide pellets, and hydrochloric acid (36.5-38%) were also supplied by SIGMA-ALDRICH. Lead standard solution of 1000 mg/L was supplied by MERCK.

5.2.2 Synthesis of DES

The DESs were synthesized by mixing ChCl with each HBD using magnetic stirring at 400 rpm and 80 °C until the DES fluid in the mixing bottle became a homogeneous liquid without any precipitate. Table 5.1 gives the synthesis details of each DES. After synthesis, all DESs were kept in well-sealed cups and in a desiccator to avoid humidity effects.

5.2.3 Oxidation and acidification of MWCNT

Pristine MWCNTs (P-CNTs) were dried over night at 100 °C. Half of the dried P-CNTs were oxidized using KMnO₄ via sonication for two hours to produce K-CNTs (AlSaadi, Al Mamun, Alam, Amosa, & Atieh, 2016). Two types of acids were used separately during the acidification process. Firstly, P-CNTs were refluxed in HNO₃ (65%) for one hour at 140 °C to produce N-CNTs. The rest of the P-CNTs was refluxed with H₂SO₄ (50%) for one hour to produce S-CNTs. For all, the functionalized CNTs were

washed and filtrated using a vacuum pump and a PTFE 0.45 μm membrane repeatedly using distilled water until the filtrate water pH was neutral.

Table 5.1: List of the synthesized DESs used as functionalization agents.

Salt	HBD	Molar ratio		Ref.
		Salt	HBD	
ChCl	Gly	1	2	(AlOmar, Hayyan, et al., 2016; M. Hayyan et al., 2010)
	EG	1	2	(Andrew P. Abbott et al., 2006)
	TEG	1	3	(M. Hayyan, Aissaoui, et al., 2015)
	DEG	1	3	(G. Li, Deng, Chen, Shan, & Ai, 2014)
	U	1	2	(Andrew P. Abbott et al., 2003)
	MA	1	1	(Andrew P. Abbott, Boothby, et al., 2004)

5.2.4 Functionalization by DES

200 mg from each of P-CNTs, K-CNTs, N-CNTs, and S-CNTs was sonicated in 7ml of DES for three hours at 65 °C. The mixture was then washed with distilled water several times and filtered using a PTFE 0.45 μm membrane until the filtrate water became neutral. Table 5.2 lists the functionalization details and the abbreviations for each sample.

5.2.5 Characterization of functionalized CNT

The adsorbents were characterized using Raman spectroscopy (Renishaw System 2000 Raman Spectrometer) to obtain Raman shift spectra for all adsorbents. The surface modification and the functional groups that resulted from the functionalization processes were studied using Fourier transform infrared (FTIR) spectroscopy PerkinElmer® FTIR

spectrometer. The structural phases of the functionalized CNTs were investigated using X-ray powder diffraction (XRD). The thermal stability of the new adsorbent was studied using thermogravimetric analysis (TGA) and differential thermogravimetry (DTG) by Thermal Analyzer (STA-6000, PerkinElmer®). Furthermore, the surface charge was estimated by conducting the zeta potential using Zetasizer (Malvern, UK). A fully Automated Gas Sorption System (micromeritics, TriStar II 3020, USA) was used to study the selected samples surface area based on the method of Brunauer-Emmett-Teller (BET). Field-Emission Scanning Electron Microscope (JEOL Ltd, Japan. JSM-6700F) was used to obtain high resolution images in nano size for studying the morphology of all selected samples along with energy-dispersive X-ray spectrometer (EDX).

Table 5.2: Functionalized CNTs classification and abbreviation

DES	CNT based adsorbents			
	P-CNTs	K-CNTs	N-CNTs	S-CNTs
ChCl:Gly	PGly-CNTs	KGly-CNTs	NGly-CNTs	SGly-CNTs
ChCl:EG	PEG-CNTs	KEG-CNTs	NEG-CNTs	SEG-CNTs
ChCl:TEG	PTEG-CNTs	KTEG-CNTs	NTEG-CNTs	STEG-CNTs
ChCl:DEG	PDEG-CNTs	KDEG-CNTs	NDEG-CNTs	SDEG-CNTs
ChCl:U	PU-CNTs	KU-CNTs	NU-CNTs	SU-CNTs
ChCl:MA	PMA-CNTs	KMA-CNTs	NMA-CNTs	SMA-CNTs

5.2.6 Adsorption experiments

5.2.7 Screening of different adsorbents

A sample of 10 mg from each of the 28 prepared adsorbents, listed in Table 5.2, was exposed to a batch shake flask adsorption process with Pb(II) as the dissolved heavy metal ion. The Pb (II) stock solution with a concentration of 5 mg/L and pH of 2.7 was prepared

using deionized water. The flasks were placed in a mechanical shaker system for 30 min at room temperature with a shaking speed of 180 rpm. The adsorbent with the highest removal efficiency was chosen for further studies.

5.2.8 Optimization of Pb (II) removal

Response surface methodology (RSM) was employed to optimize the conditions of Pb(II) removal. Central composite design (CCD) was selected using the software Design Expert V7.0. The effects and interactions of three parameters were investigated in this study, specifically pH (3 to 8), contact time (5 to 15 min), and adsorbent dosage (5 to 20 mg). Removal percentage (%) and uptake capacity, q (mg/g), were adopted as the response functions. Table 5.3 shows the design of experiments in terms of the actual parameters of each run. The optimization was performed at initial concentration of 10 mg/L. The agitation speed was fixed at 180 rpm.

5.2.9 Adsorption isotherm and kinetics

The isotherm studies were performed at 13 initial concentrations to determine the equilibrium concentration while the variations of concentration with time were observed for kinetics studies for three initial concentrations, 5, 10 and 20 mg/L, at pH 2.7. To perform adsorption equilibrium isotherm experiments, the various Pb (II) initial concentrations were 3, 5, 10, 15, 20, 25, 30, 35, 40, 45, 50, 55 and 60 mg/L at the following conditions: pH (2.7 and 5), adsorbent dosage of 5 mg, and agitation speed 180 rpm. The linearized Langmuir and Freundlich isotherms models were used for the fitting of the experimental data (Eq. 1 and Eq. 2), respectively.

$$\frac{C_e}{q_e} = \frac{1}{K_a Q_m} + \left(\frac{1}{Q_m}\right) * C_e \quad \dots\dots\dots (1)$$

$$\ln q_e = \ln K_F + \frac{1}{n} \ln C_e \quad \dots\dots\dots (2)$$

Where C_e is the initial equilibrium concentration and q_e is the amount of Pb(II) on the adsorbent. K_a and Q_m are the adsorption equilibrium constant and the maximum adsorption capacity, respectively. K_F and n are the Freundlich isotherm constants.

Table 5.3: List of design of experiments runs and the actual values obtained from each response

run	pH	Dosage	Contact time	Response (1)	Response (2)
				Removal (%)	Uptake capacity
1	7	20	5	43.94125	23.855
2	3	12.5	10	47.98531	21.308
3	3	20	15	75.17809	19.425
4	7	5	15	75.153	97.97
5	7	20	15	75.5202	24.5
6	5	12.5	15	79.29417	36.292
7	3	5	15	15.33838	23.94
8	7	5	5	21.29743	93.57
9	5	5	10	80.34398	91.2
10	5	12.5	10	87.84901	37.824
11	3	5	5	8.426091	17.73
12	5	12.5	5	74.35783	35.408
13	5	20	10	91.15479	24.01
14	7	12.5	10	62.5459	38.776

To determine the kinetics model that fit with the adsorption system of Pb (II) in aqueous solution, three kinetics models were investigated, namely a pseudo-first-order, pseudo-second-order, and intraparticle diffusion model. Table 5.4 shows a linearized schematic of each technique performed to determine the kinetics coefficients, the

equilibrium capacities, and the correlation coefficients (R^2).

Table 5.4: Kinetics models equations and parameters

Model	Plot	Intercept	Slope	Parameters
Pseudo-First-Order Adsorption Kinetics	$\ln(q_e - q_t)$ vs time (t).	$\ln q_e$	$-K_1$	$K_1 = -\text{slope}$ $q_e = e(\text{intercept})$
	$\ln(q_e - q_t) = \ln q_e - K_1 t$			
Pseudo-Second-Order Adsorption Kinetics	$\frac{t}{q_t}$ vs t	$\frac{1}{K_2 q_e^2}$	$\frac{1}{q_e}$	$q_e = 1/(\text{slope})$ $K_2 = \frac{\text{Slope}^2}{\text{Intercept}}$
	$\frac{t}{q_t} = \frac{1}{K_2 q_e^2} + \frac{1}{q_e} t$			
Intraparticle Diffusion	q_t vs $t^{0.5}$	c	K_d	$K_d = \text{slope}$
	$q_t = K_d t^{\frac{1}{2}} + c$			

Where C_0 is the initial concentration, q_e is the equilibrium adsorption capacity, K_1 rate constant of Pseudo-First-Order, K_2 rate constant of Pseudo-Second-Order, K_d is rate constant of Intraparticle Diffusion

5.3 Results and discussion

Primary screening showed that adsorbent samples KTEG-CNTs, KU-CNTs, and K-CNTs recorded the highest Pb(II) removal rates at 94.7, 84.96, and 74.44%, respectively. Figure 5.1 illustrates the screening study for the adsorption of Pb(II). The presence of MnO_2 on the surface of the CNTs caused a significant increase in adsorption capacity and further functionalization with DESs containing TEG or U led to further surface sorption activity.

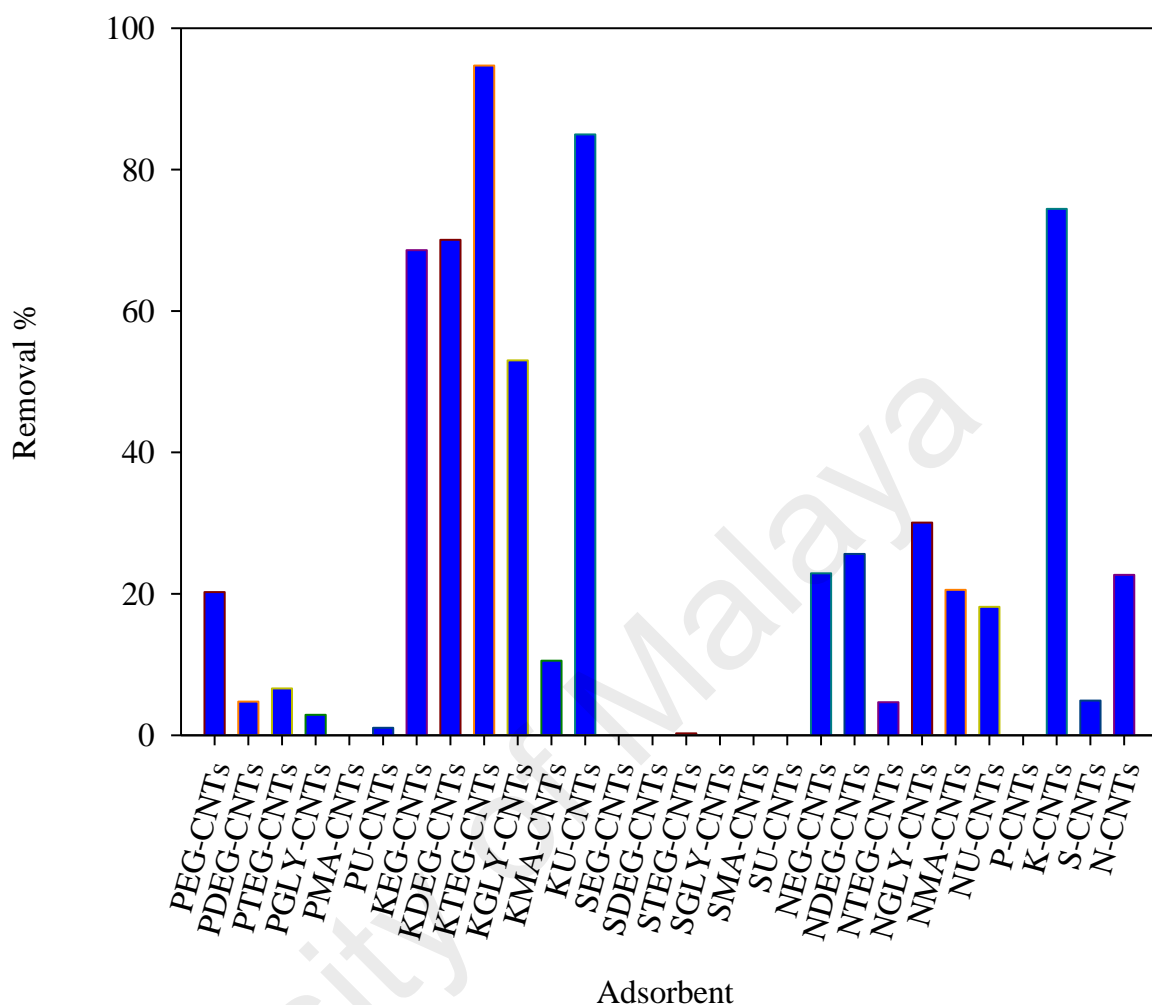


Figure 5.1: Screening study for the best Pb(II) absorber

5.3.1 Characterization of DES-functionalized CNT

5.3.1.1 Raman spectroscopy

It is well known that Raman spectroscopy works very well for CNT characterization. Three major bands are usually detected in multi wall CNTs. Specifically the G-band at $1500-1600\text{ cm}^{-1}$, the D-mode at 1350 cm^{-1} , and the D' mode at approximately 1615 cm^{-1} (Jorio, Saito, Dresselhaus, & Dresselhaus, 2004). The degree of functionalization can be

indicated by comparing the intensity of the D band (I_D) to that of the G band (I_G) (Aitchison, Ginic-Markovic, Matisons, Simon, & Fredericks, 2007). In the graphite sheet, the movement of two neighboring atoms in opposite direction produces Raman effect known as G mode. (Hiura, Ebbesen, Tanigaki, & Takahashi, 1993). While, the D mode is resulted from the sp^3 -hybridized carbon atoms in the nanotube sidewalls (Bahr et al., 2001). The D band, G band, and D' band positions are listed in Table 5.5, along with the intensity of each peak, the full-width at half maximum (FWHM), and the I_D/I_G ratio (R). Herein, the R of P-CNTs was found to be 1.12. After oxidation with $KMNO_4$, the intensity ratio increased to 1.16, and in the sequence functionalization step, the R of KTEG-CNTs was found to be 1.26. Consequently, the formation of new functional groups had obviously occurred. Figure 5.2a shows the positions and the intensity of both the D and G band. On the other hand, the D' band appeared as a weak shoulder of the G-band at higher frequencies. The D' band cannot be found in pure graphite. However, it can be detected in intercalated graphite and MWCNTs (C. S. Kumar, 2012). Moreover, the disorder and defects produces the D' band as double resonance feature (Kordás et al., 2006). Figure 5.2b shows the D' shift, which further confirms the functionalization effects on the CNTs.

Table 5.5: Raman spectroscopy bands intensities and locations

	D band			G band			D' band		I_D/I_G
	Wave No.	FWHM	Intensity	Wave No.	FWHM	Intensity	Wave No.	Intensity	
P-CNTs	1351	58.97	1890	1592	72.8	1681	1605	1541	1.12
K-CNTs	1354	55.4	1370	1592	67.4	1161	1612	937	1.18
KTEG-CNTs	1352	56.15	1573	1592	66.59	1244	1612	1012	1.26

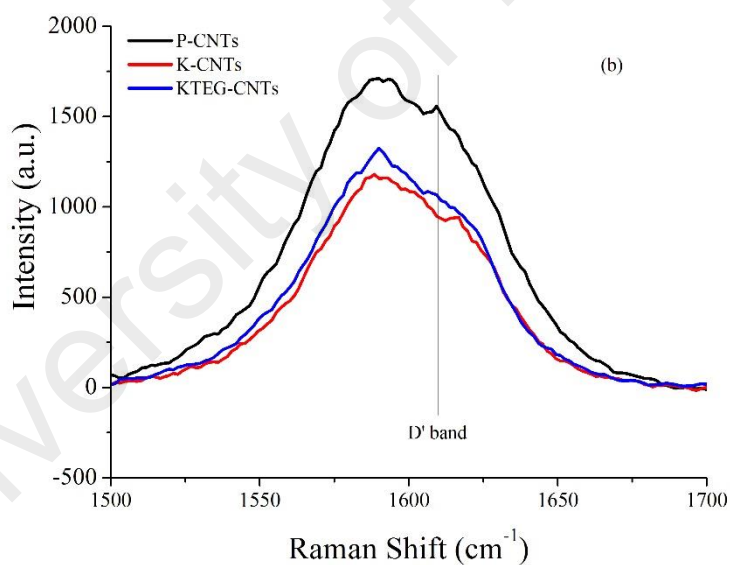
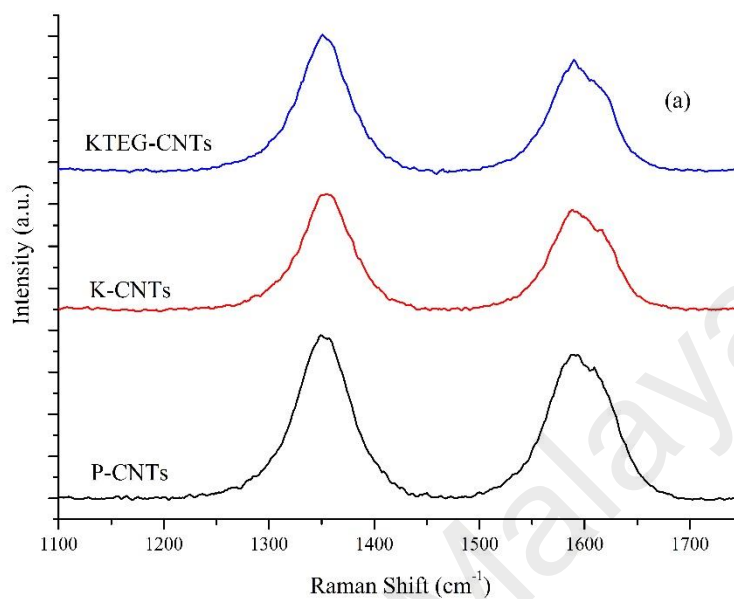


Figure 5.2: Raman spectroscopy of P-CNTs, K-CNTs and KTEG-CNTs for a) D band and G band, and b) D' band shift

5.3.1.2 Surface chemistry analysis (FTIR)

The adsorption behavior of any adsorbent is influenced by the chemical reactivity of its surface, especially when chemically bonded oxygen exists on the surface, which

occurs in the form of various functional groups (Kandah & Meunier, 2007; S. Yang, Li, Shao, Hu, & Wang, 2009). Fourier transforms infrared (FTIR) spectroscopy is a common procedure to study surface chemistry, in terms of probing functional groups. P-CNTs before and after each functionalization step (K-CNTs and KTEG-CNTs) was inspected to detect the formation of new functional groups. Figure 5.3 shows the FTIR profile for P-CNTs, K-CNTs, and KTEG-CNTs. The existence of O-H stretching is noticeable in the peaks around 3500 cm^{-1} for K-CNTs and KTEG-CNTs. The intense bands in the initial region between ($3000\text{-}3600\text{ cm}^{-1}$) contain -OH groups, C-H, and H-C=O groups at 2800 . The medium region contained several peaks, CO_2 , carbonyl groups, and aliphatic carboxylic acids at 2400 , 2300 , and 1580 cm^{-1} wave numbers. The final region below 1400 cm^{-1} and it is known as a fingerprint region and contains indications for the presence of N-H, CO_2 , C=O (B. C. Smith, 1998). The N-H stretching was detected through a very strong peak at 3198 cm^{-1} for KTEG-CNTs. Carboxylates groups show a strong, characteristic asymmetric stretching absorption from the CO_2 group in the $1650\text{-}1540\text{ cm}^{-1}$ region. The corresponding symmetric stretching absorption occurs at approximately $1450\text{-}1360\text{ cm}^{-1}$. Relatively strong rocking in and out of plane deformation absorptions are observed in the $770\text{-}400\text{ cm}^{-1}$ region. In addition, the C-Cl bond may overlap with other CO groups between 600 and 700 cm^{-1} . Evidently several functional groups were formed on the surface of P-CNTs during the first oxidation step. In addition, the surface of K-CNTs with DES functionalization provides various adsorption sites and increases the adsorption capacity of Pb (II) ions.

5.3.1.3 XRD analysis

Figure 5.4 shows the XRD patterns of P-CNTs, K-CNTs, and KTEG-CNTs. The P-CNTs patterns comply with previously published research where the (002) peak is found at approximately 2θ of 26 , which corresponds to the concentric cylinder structure of P-CNTs (D. Zhang, Shi, Fang, Li, & Dai, 2005). However, the intensity of (002) was

reduced in the K-CNTs pattern due to the extensive presence of MnO_2 , which caused the CNT to form a non-stoichiometric, amorphous shape (S.-G. Wang et al., 2007). After functionalization by DES, the (002) peak had almost disappeared in KTEG-CNTs patterns.

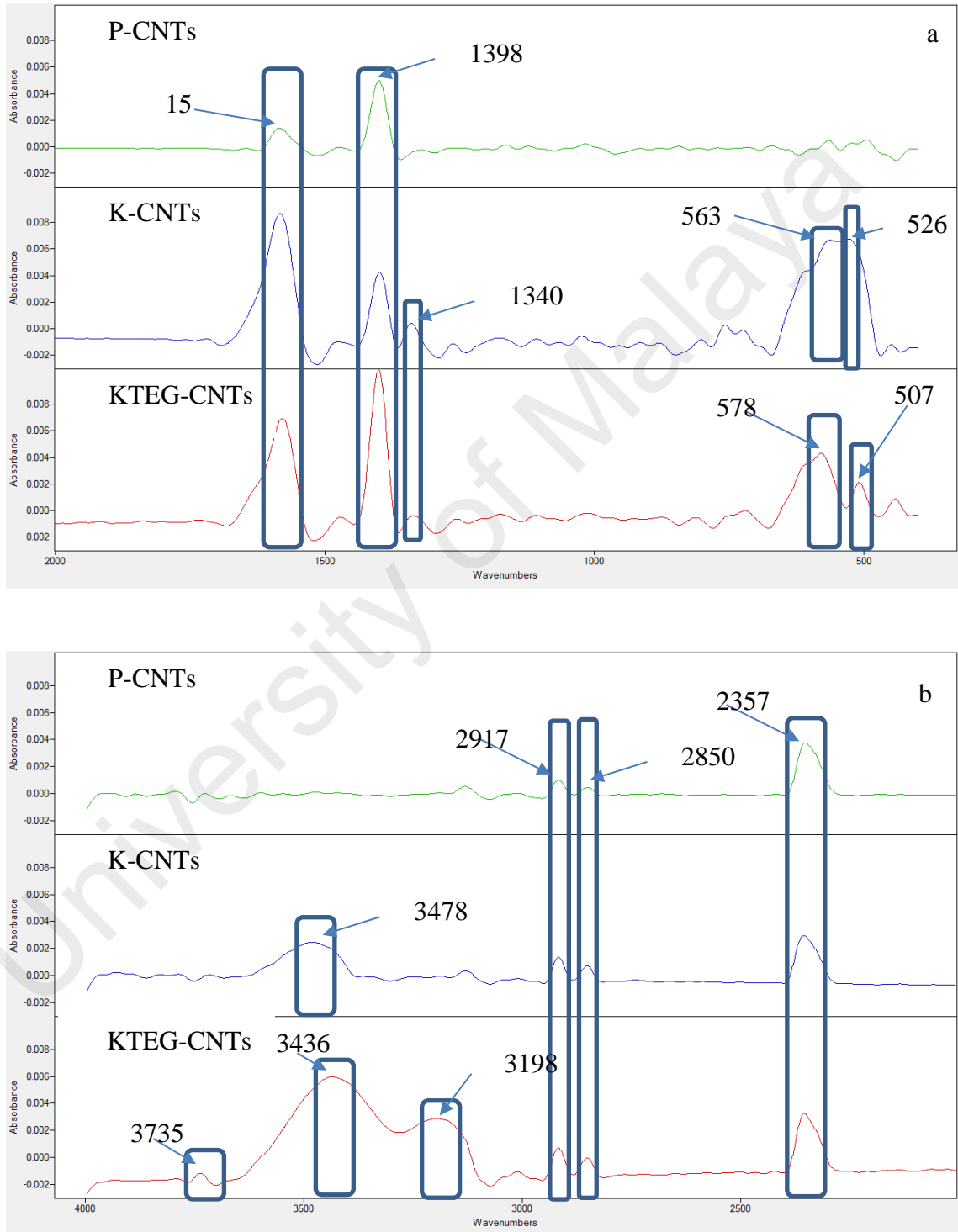


Figure 5.3: FTIR spectrum for P-CNTs, K-CNTs and KTEG-CNTs, a) from 400 to 2000 cm^{-1} , and b) from 2000 to 4000 cm^{-1} , waver number

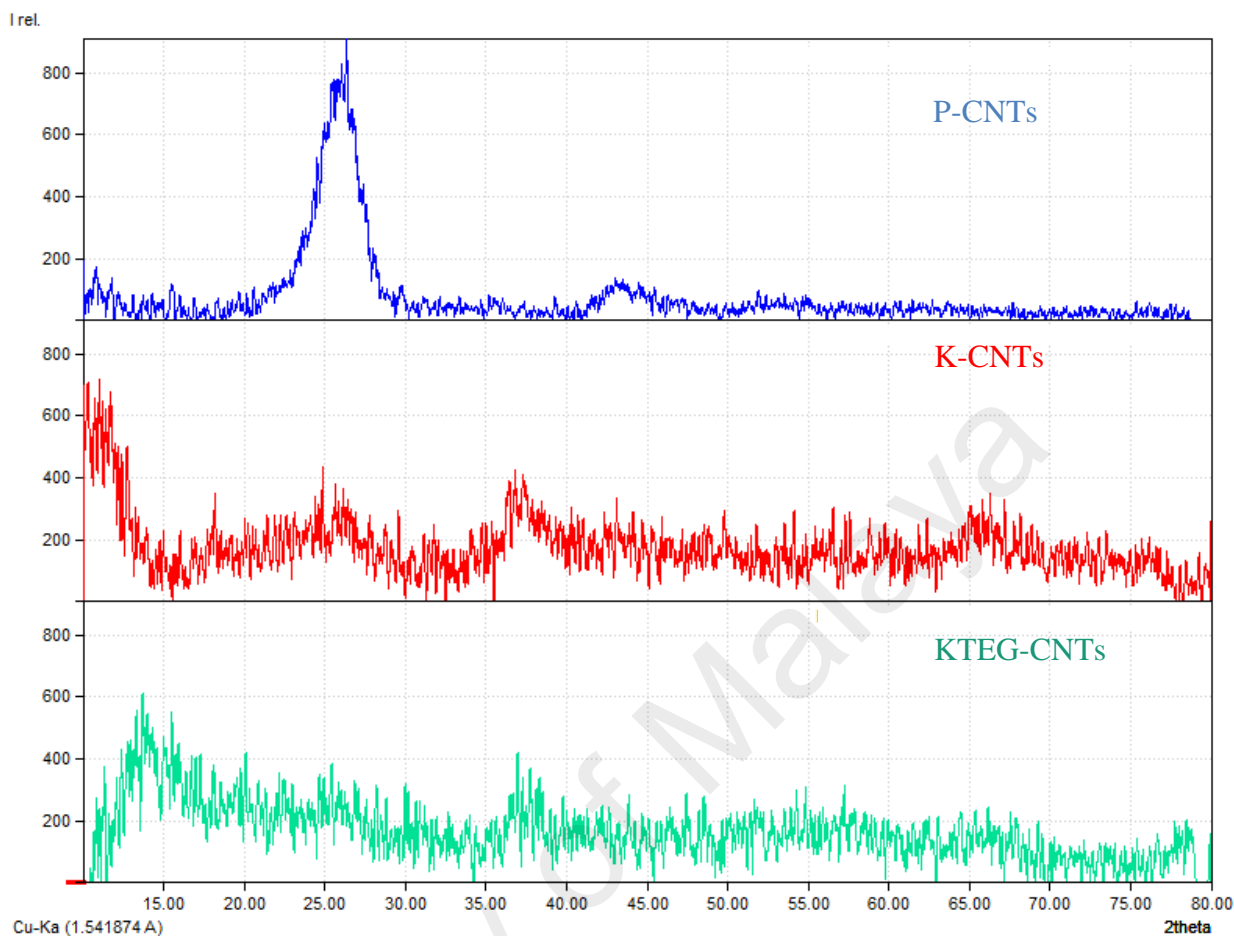


Figure 5.4: X-ray diffraction patterns for P-CNTs, K-CNTs and KTEG-CNTs

5.3.1.4 FESEM and EDX

Figure 5.5 shows the FESEM images for P-CNTs, K-CNTs and K TEG-CNTs. The figures show that the presence of MnO_2 is embedded inside the CNTs where no powder of MnO_2 appeared in K-CNTs image. Furthermore, the effect of DESs functionalization is slightly observable. In addition, EDX study was conducted for KTEG-CNTs after the adsorption of Pb(II) . The results proved the hypothesis of MnO_2 decomposition on the surface of CNTs where the weight percentage of MnO_2 was about 65 %, this results agrees with TGA results. In addition, the traceable amount of Cl^- was also confirmed even after Pb(II) removal. Figure 1C (Appendix C) shows the EDX spectrum for KTEG-CNTs.

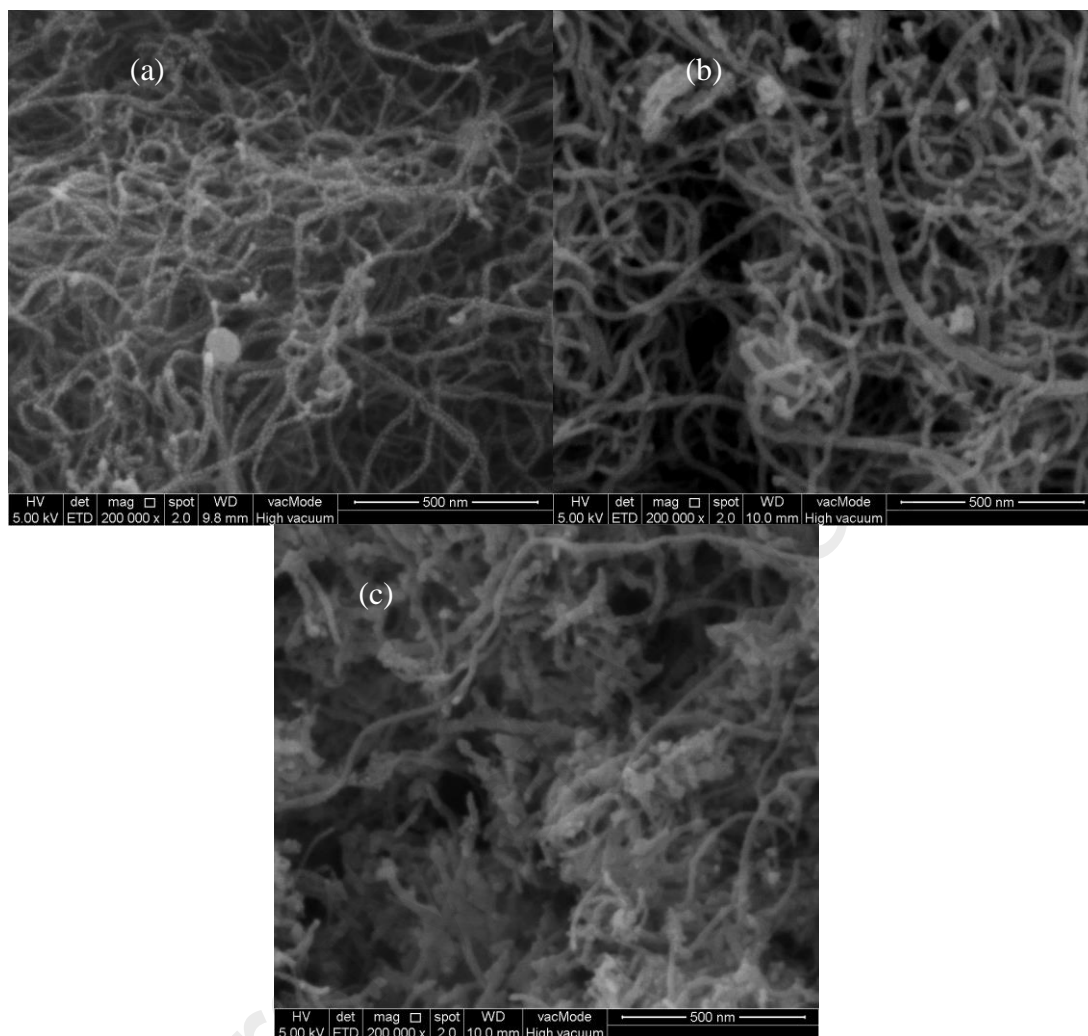


Figure 5.5: FESEM images for a) P-CNTs, b) K-CNTs and c) KTEG-CNTs

5.3.1.5 Zeta potential

The surface electric charge potential of the solid particle is important to identify characteristics of surface behavior in aqueous solutions and evaluate the suspension stability. To compare the stability of different particles in suspension, absolute values of zeta potential is usually adopted (Z. Sun et al., 2008). There are many factors affecting the zeta potential, including particle surface charges, pH, conductivity, ion concentration, and temperature (Simate, Iyuke, Ndlovu, & Heydenrych, 2012). Herein, 2.5 mg of P-

CNTs, K-CNTs and KTEG-CNTs was separately dispersed in 5 mL of deionized water for zeta potential measurement. The results showed that the absolute values of zeta potential increased from 5.5 to 45.81 for P-CNTs and K-CNTs, respectively (AlOmar, Alsaadi, Hayyan, Akib, & Hashim, 2016). The obvious increment in absolute value of zeta potential could be due to the presence of oxygen-containing functional groups on the surface, such as carbonyl groups and aliphatic carboxylic acids surface, which increased the hydrophilicity of the adsorbent. This, in turn, resulted in an increase in the electronegativity, which affects the adsorption mechanism. On the other hand, the absolute zeta potential value after the functionalization with TEG-based DES slightly decreased to 43.41, compared with that of K-CNTs. As a result, these adsorbents are suitable for water suspensions with excellent stability. According to ASTM standards, the criterion for “good stability” requires a zeta potential of absolute value above 40 mV (Fan et al., 2012).

5.3.1.6 Thermogravimetric analyses (TGA)

The thermal gravimetric analysis was conducted at a starting temperature of 25 °C and an ending temperature of 800 °C with a heating rate of 10 degrees per min (°C/min). The experiments were conducted under air flow rate of 50 mL/min. In order to confirm that gravimetric changes occurred on different samples of CNTs during the process of functionalization and adsorption P-CNTs, K-CNTs, KTEG-CNTs, and KTEG-CNTs after Pb(II) absorption (KTEG-CNTs-Pb) were selected for TGA analysis. Figure 5.6 shows the initial gradual weight change, which was reduced by 7%, 5%, and 2% for K-CNTs, KTEG-CNTs and KTEG-CNTs-Pb, respectively, at approximately 100 °C. This is an indication of moisture evaporation. After 100 °C, the weight of these samples remained at a constant reduction level until the initial temperature of combustion was reached. Then a steep drop in the weight took place as the temperature increased. The combustion profile of the samples suggested higher thermal stability and purity for P-

CNTs compared to K-CNTs and KTEG-CNTs. The onset of P-CNTs combustion was 556 °C, while K-CNTs had onset of oxidation at 270 °C due to the presence of MnO₂ embedded in the surface of CNT and acting as an active catalyst for oxidization. On the other hand, the onset of oxidation temperature for KTEG-CNTs was 314 °C. The 50 °C difference between K-CNTs and KTEG-CNTs is an indication of the TEG functionalization effects on the stability. The presence of Pb after adsorption further reduced the oxidation catalytic activity of the MnO₂ impeded in the surface. It was observed that weight loss stops after the higher limit temperature of combustion and some residual material remains for all samples. These residues indicate the carbon purity of the samples. P-CNTs left 0% residue. K-CNTs, KTEG-CNTs, and KTEG-CNTs-Pb left residues of 65.21%, 59.75%, and 62.41%, respectively. The highest percentage of residue was observed for K-CNTs, indicating the presence of functional MnO₂ attached to the CNT surface. This percentage decreased in the case of KTEG-CNTs due to the presence of carbon containing functional groups embedded by TEG based DES, which had been oxidized. Table 5.6 lists the weight percentage of all contained materials in each sample. Subsequently, KTEG-CNTs-Pb which left with around 4% more than KTEG-CNTs, due to the Pb(II) ions absorbed on the surface of the KTEG-CNTs.

Table 5.6: Weight percentage of each material based on TGA analysis.

Sample	CNT W (%)	MnO₂ W (%)	DES W (%)	Pb (II) W (%)
P-CNTs	100	0	0	0
K-CNTs	34.79	65.21	0	0
KTEG-CNTs	34.79	59.75	5.46	0
KTEG-CNTs-Pb	34.79	59.75	2.8	2.66

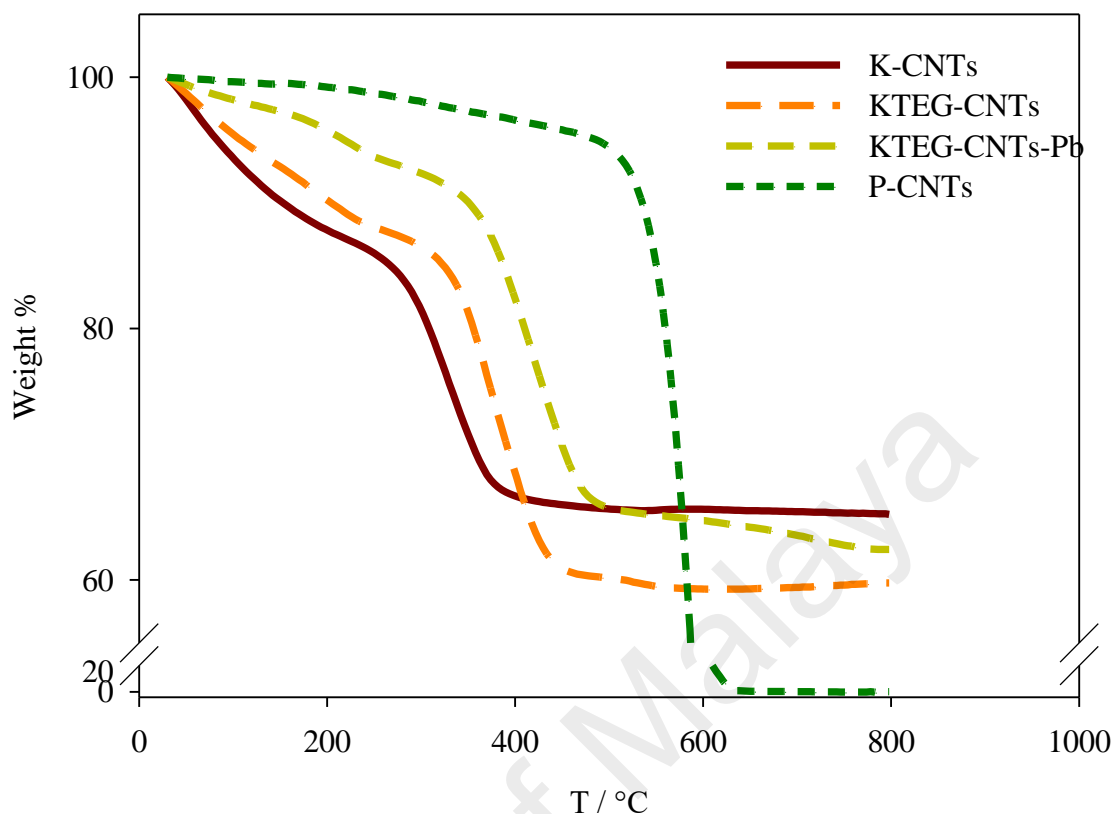


Figure 5.6: TGA curves for P-CNTs, K-CNTs, KTEG-CNTs and KTEG-CNTs-Pb

5.3.1.7 BET surface area

The BET surface area for P-CNT, K-CNT and KTEG-CNT were investigated. The results showed that the surface area increased significantly after each functionalization step. Table 5.7 list the BET surface area, total pore volume and the average pore diameter. the pore volume was decreased after the functionalization by KMnO_4 which is a further proof the MnO_2 was embedded inside the pore hole of P-CNTs.

Table 5.7: BET surface area and pore volume and diameter of all adsorbents

Property	P-CNT	K-CNT	KTEG-CNT
BET Surface Area (m^2/g)	123.543	158.934	176.0556
Total pore volume (cm^3/g)	0.620782	0.453468	0.6519
Average Pore Diameter (Å)	20.4994	114.1271	148.1243

5.3.2 Optimization study

Analysis of variance (ANOVA) modeling for the two responses, removal (%) and uptake capacity (q) of KTEG-CNTs, showed that the Model F-values were 577.09 and 217.06, which implies that both models are significant. There is only a 0.01% and 0.05% chance that a "Model F-Value" this large could occur due to noise for each response, respectively. Values of "Prob > F" less than 0.05 indicate that the model terms are significant. For the first response (removal %) the cases A, B, C, AB, AC, BC, A², C², ABC, A²B, and A²C, all are significant model terms. However, for the case of uptake capacity, only B, AB, A², B², C², A²B, and AB₂ are significant model terms. Table 5.8 and Table 5.9 listed the P-values, F- values, and the square mean for both removal (%) and uptake capacity, respectively.

Figure 5.7 shows the theoretical values plotted versus the experimental values for the removal percentage and uptake capacity of TEG-CNT. It is clear that the theoretical values predicted by the models developed in this study were in close agreement with the experimental values, indicating that both models have successfully created correlation between the process variables in both models.

5.3.2.1 Effects of Optimization Variables on Adsorption of Pb(II)

Figures 5.8a and 5.8b show the interaction effects between contact time and pH on removal (%) and uptake capacity of Pb(II), respectively. Both removal (%) and uptake capacity increased with time since the system did not approach equilibrium. The removal (%) increased with increasing pH and reached a maximum at pH 5, followed by a decrease with increasing pH. A similar trend was observed for the uptake capacity, where it reached the maximum at pH 5 then became constant.

Table 5.8: Reduced Cubic Model Analysis of variance (ANOVA) for Pb (II) removal (%) on KTEG-CNTs

Source	Sum of Squares	df	Mean Square	F Value	p-value Prob > F
Model	10000.15	11	909.1046	577.9552	0.0001
A	357.5563	1	357.5563	227.3132	0.0006
B	24.40957	1	24.40957	15.51817	0.0291
C	59.9881	1	59.9881	38.13691	0.0085
AB	106.8798	1	106.8798	67.94787	0.0037
AC	651.407	1	651.407	414.1263	0.0003
BC	63.43643	1	63.43643	40.32915	0.0079
A ²	2577.398	1	2577.398	1638.558	< 0.0001
C ²	215.8147	1	215.8147	137.2023	0.0013
ABC	101.1265	1	101.1265	64.2903	0.0040
A ² B	217.5322	1	217.5322	138.2942	0.0013
A ² C	183.5276	1	183.5276	116.6761	0.0017
R-Squared 0.957, Adj R-Squared 0.923, Pred R-Squared 0.9825, Adeq Precision 74.259					
A: pH , B: adsorbent dosage and C: Contact time					

It is well-known that heavy metals precipitate at high pH values (Jiang, Gao, Yu, Chen, & Deng, 2007; W. Yang et al., 2013a), hence, a part of Pb in solution precipitated in a form of Pb(OH)₂ due the effect of OH⁻ anions present in the solution (V. K. Gupta et al., 2011). Herein, the initial concentration measurement was taken after adjusting the pH. Consequently, the effects of precipitation will be at a minimum upon removal and uptake capacity of KTEG-CNTs. Regardless the precipitation phenomena, the increase in pH results in a reduction in total number of H⁺ cations, which are in competition with Pb

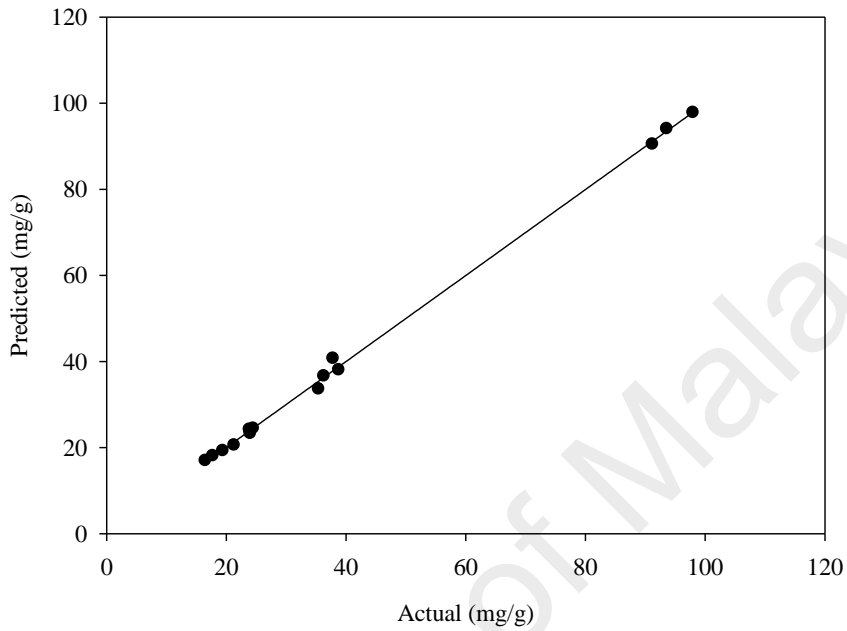
(II) cations for occupation of the active sites on adsorbent. Moreover, high pH enhances the surface charge of the adsorbents (Y.-H. Li, Ding, et al., 2003).

Table 5.9: Reduced Cubic Model Analysis of variance (ANOVA) for uptake capacity of KTEG-CNTs

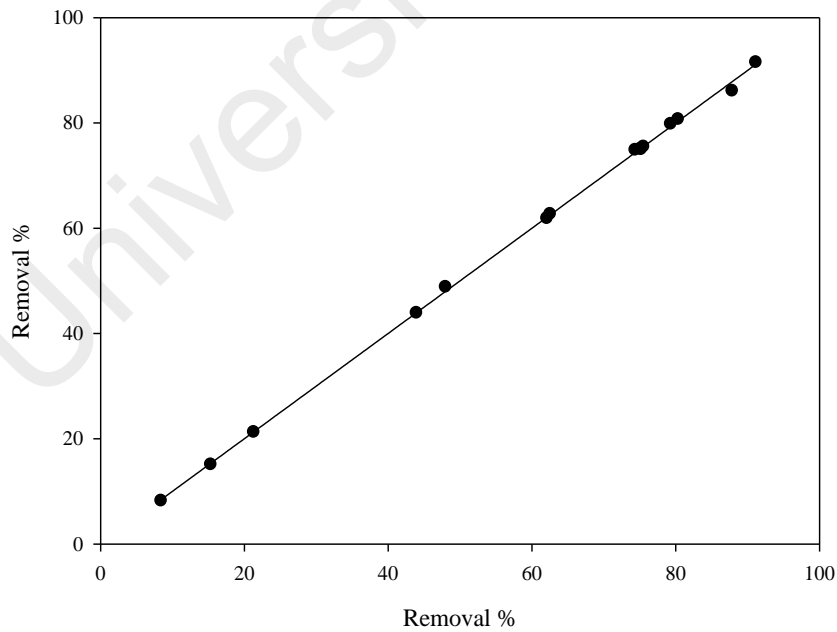
Source	Sum of Squares	df	Mean Square	F Value	p-value Prob > F
Model	11713.73	11	1064.885	217.0564	0.0005
A	15.35957	1	15.35957	3.130755	0.1750
B	3049.809	1	3049.809	621.6453	0.0001
C	17.64984	1	17.64984	3.597584	0.1541
AB	333.842	1	333.842	68.04733	0.0037
AC	2.103813	1	2.103813	0.428822	0.5593
BC	6.17322	1	6.17322	1.258293	0.3437
A ²	334.8036	1	334.8036	68.24333	0.0037
B ²	847.2145	1	847.2145	172.6885	0.0010
C ²	80.71442	1	80.71442	16.45209	0.0270
A ² B	358.9058	1	358.9058	73.15611	0.0034
AB ²	213.6312	1	213.6312	43.54463	0.0071
R-Squared 0.9987, Adj. R-Squared 0.9941, Pred. R-Squared 0.9031, Adeq. Precision 40.800					
A: pH , B: adsorbent dosage and C: Contact time					

Figures 5.9a and 5.9b show the effect of pH and adsorbent dosage on the removal (%) and the uptake capacity at constant contact time. The increase in adsorbent amount leads to increasing active sites concentration, which helps adjust the adsorption solution electrostatic charge to an adsorption preferred level by removing the competitive H⁺ cations. By fixing pH and contact time, the adsorbent dosage linearly increases the

removal. Meanwhile, the uptake capacity has decreased due to increasing the adsorbent dosage. This may be due to conglomeration or overlapping of the active adsorption sites with the increase in adsorption dosage (Asmaly et al., 2015).

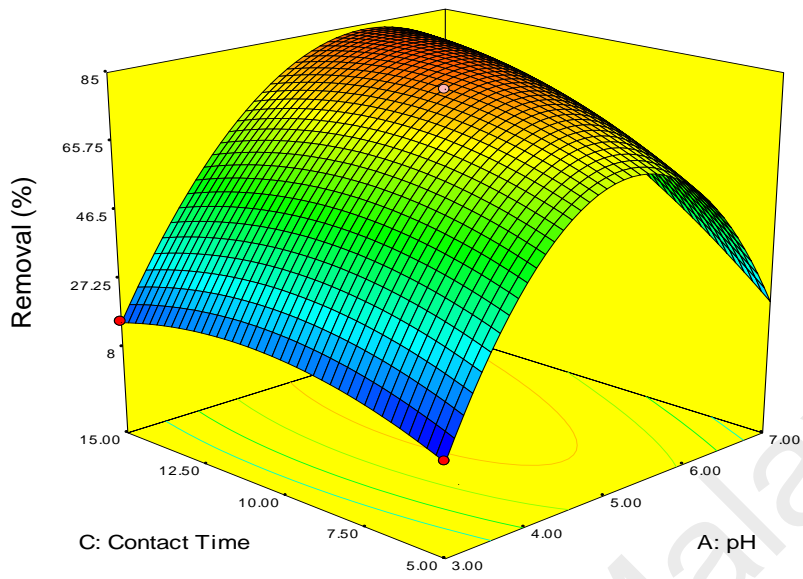


(b) Uptake capacity

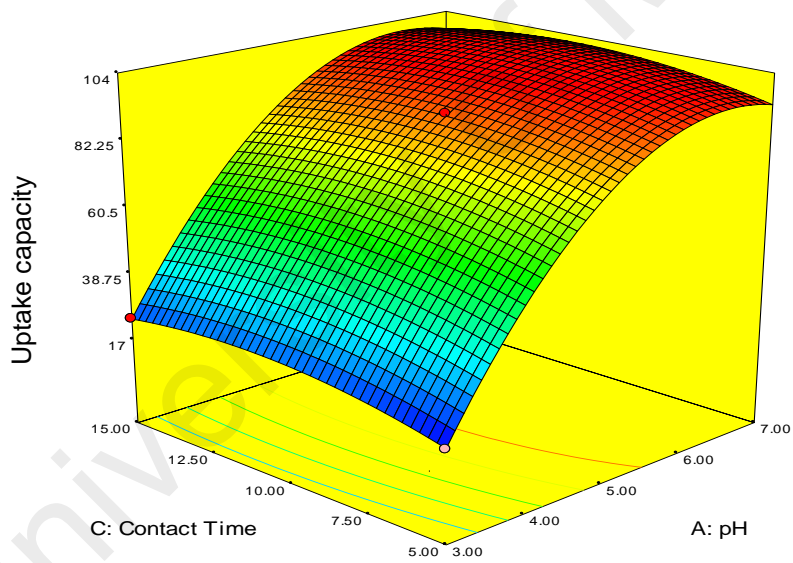


(a) Removal (%)

Figure 5.7: Theoretical Vs Experimental values for a) removal (%) of Pb(II) and b) uptake capacity of KTEG-CNTs

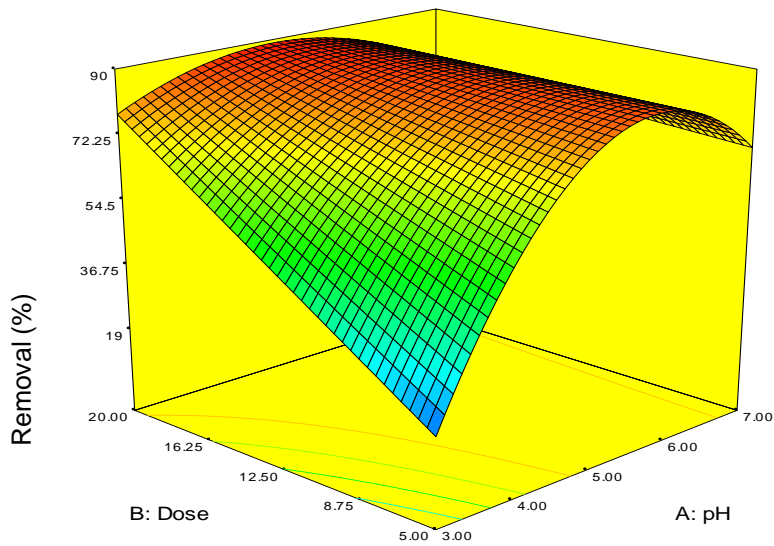


(a) Removal (%)

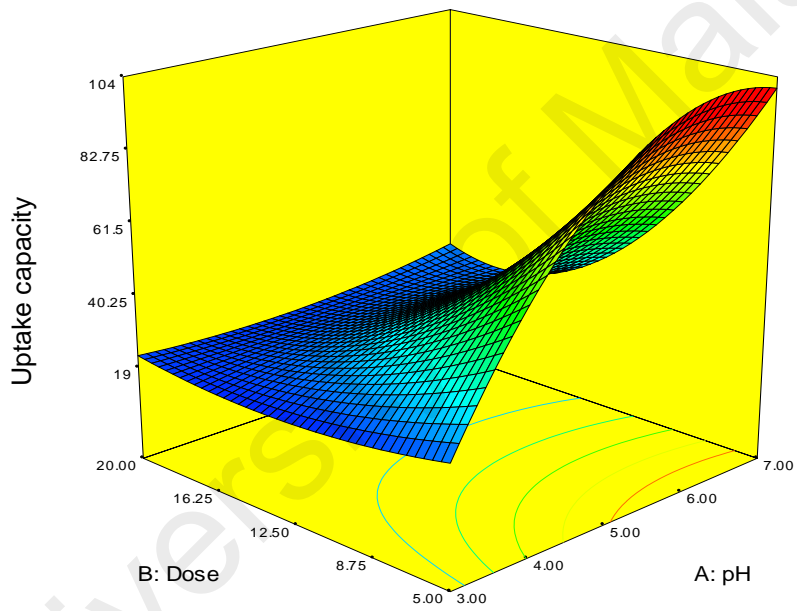


(b) Uptake capacity

Figure 5.8: Surface response representation of, a) Pb(II) removal (%) interaction with pH and contact time and b) uptake capacity of KTEG-CNTs interaction with pH and contact time, by fixing the adsorbent dose to the optimum



(a) Removal (%)



(b) uptake capacity

Figure 5.9: Surface response representation of a) Pb(II) removal (%) interaction with pH and adsorbent dosage and b) uptake capacity of KTEG-CNTs interaction with pH and adsorbent dosage, by fixing contact time to the optimum

5.3.3 Kinetics study

Kinetics studies were executed at pH 2.7 to eliminate the precipitation effects and with initial concentrations of 5, 10, and 20 mg/L. The adsorbent dosage was 5 mg and the agitation speed was 180 rpm for all concentrations. A contact time of 9 hours was used to ensure that the reactions reached equilibrium. The data sets presented in Figures 5.10, 5.11, and 5.12 show three kinetics models: pseudo-first-order, pseudo-second-order, and intraparticle diffusion, respectively. The values of the correlation coefficients R^2 for the data sets were considered as indications of conformity between experimental data and the corresponding values predicted by each model, as shown in Table 5.10. The kinetics of Pb (II) sorption on KTEG-CNTs followed the pseudo-second-order with more conformity, compared to pseudo-first-order and intraparticle diffusion models at all concentrations. The R^2 of the pseudo-second-order was 0.999, 0.998, and 0.996 for 5, 10, and 20 mg/L concentrations, respectively. In the case of pseudo-first-order, the R^2 was less than 0.9. Similarly, the intraparticle diffusion kinetics model did not fit the experimental data, since the R^2 was less than 0.9. Based on this observation, it can be claimed that the adsorption reaction of Pb(II) ions on KTEG-CNTs is quantitatively described by a pseudo-second-order kinetics model. these findings agree with many previously investigated CNT-based adsorbents (Gong et al., 2014; Z.-H. Huang et al., 2012; Pyrzynska & Stafiej, 2012; C. Zhang et al., 2012).

Table 5.10: Adsorption kinetics constants and correlation coefficient for each model

C0 (mg/L)	Pseudo-first- order			Pseudo-second-order			Intraparticle	
	q_e (mg/g)	K_1 (min ⁻¹).	R^2	q_e (mg/g)	K_2 (g/mg.min)	R^2	K_d (g/mg.min ^{0.5})	R^2
5	49.5	0.003098	0.8909	49.5087	0.004486	0.9999	0.692169	0.7271
10	66.52917	0.005136	0.8906	100.2279	0.000255	0.9985	2.164832	0.8215
20	100.10836	0.003564	0.9148	186.1126	0.000158	0.9967	3.520684	0.7264

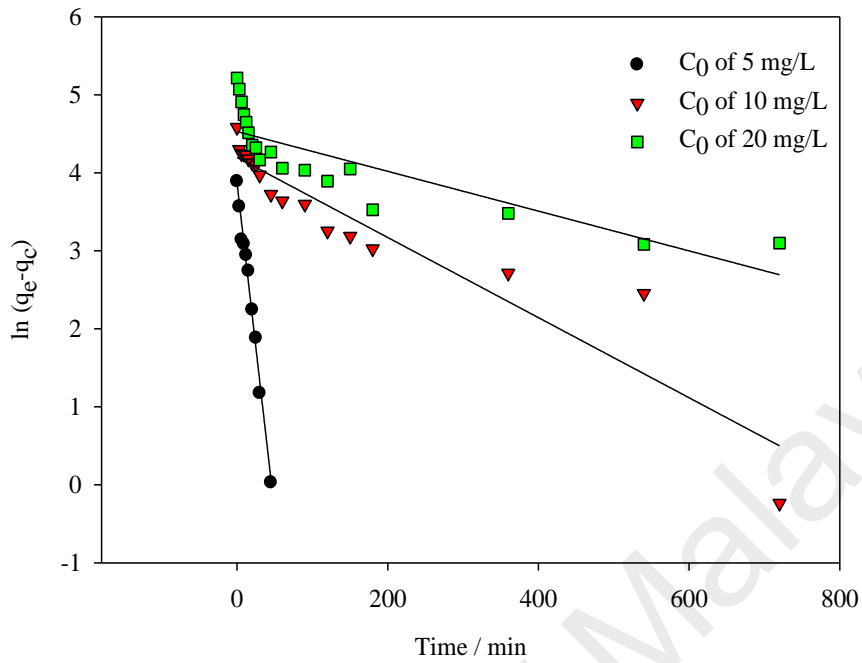


Figure 5.10: Pseudo-first-order adsorption kinetics at different initial concentrations

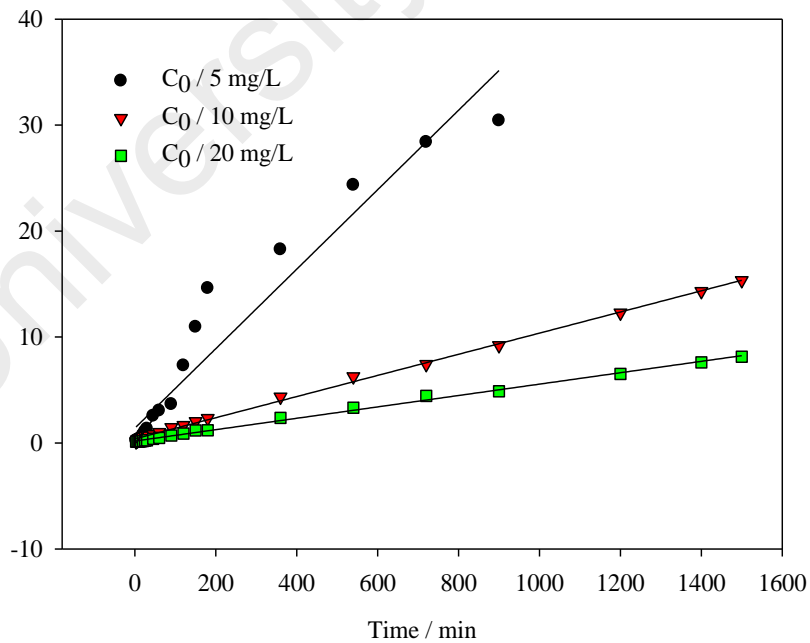


Figure 5.11: Pseudo-second-order adsorption kinetics at different initial concentrations

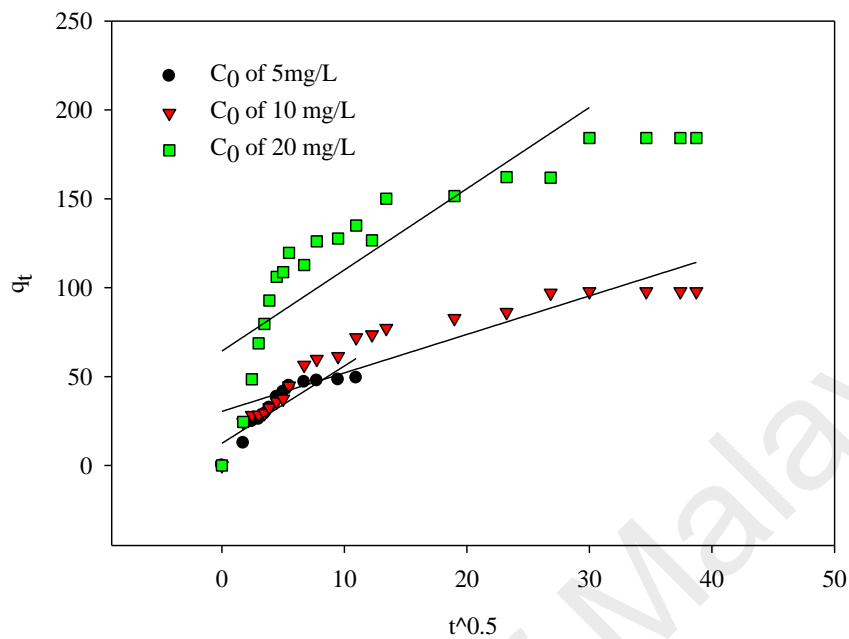


Figure 5.12: Intraparticle diffusion adsorption kinetics at different initial concentrations

5.3.4

5.3.5 Isotherm study

Figures 5.13 and 5.14 show the plots of the linearized Langmuir model (Eq. 1) at pH 2.7 and pH 5, respectively. Figures 5.15 and 5.16 plots the linearized Freundlich isotherm model (Eq 2) at pH 2.7 and pH 5, respectively. Both models can describe the behavior of Pb (II) adsorption onto KTEG-CNTs for both pH conditions, especially since, the R^2 for all models are above 0.94. Table 5.11 lists the values of the isotherm constants for both Langmuir and Freundlich isotherms models, alongside the correlation coefficients for each model and the maximum adsorption capacity. The maximum adsorption capacity of KTEG-CNTs for Pb (II) was significantly increased by increasing pH from 2.7 to 5. It is

well known that increasing of Pb sorption by increasing pH is due to the increase in the electrostatic interaction between the Pb ions and the surface of the adsorbent (Hamza et al., 2013; Salam, 2013; H. J. Wang et al., 2007). Moreover, in media with a pH >6, the dominant Pb species is Pb(II). At a pH above 7, two forms of Pb species dominate the solution, in form of Pb(OH)⁺ and Pb(OH)₂ (V. K. Gupta et al., 2011). However, in the case of Pb(II) sorption on the surface of KTEG-CNTs, the increasing in the maximum adsorption capacity by increasing pH may be due to the reduction of H⁺ ions in the solution. Also, the multilayer adsorption of Pb(II) might be contributed to this increment.

Table 5.11: Isotherm models constants and the maximum adsorption capacity

Adsorption Isotherm Model Adsorbent	pH	Langmuir			Freundlich			Reference
		q_m (mg/g)	K_L (l/mg)	R^2	n	K_f (mg/g)	R^2	
KTEG-CNTs	2.7	122.1	4.314	0.995	2.779	31.66	0.984	Present work
KTEG-CNTs	5	288.4	1.484	0.964	5.355	147.1	0.984	Present work
CNF-PAC ^a	5	100	0.4	0.998	-	27.5	0.808	(Ahmed, Abdullah-Al-Mamun, Ma'an Fahmi, Iameel, & AlSaadi, 2010)
CS-CNT-H ^b	5	158.7	0.247	0.996	4.599	59.5	0.993	(Gong et al., 2014)
MPTS-CNTs/Fe ₃ O ₄ ^c	6.5	65.40	0.045	0.993	2.204	7.284	0.952	(C. Zhang et al., 2012)
HNO ₃ -CNT ^d	7	117.6	0.003	0.933	0.407	5.493	0.988	(Tofighy & Mohammadi, 2011)

^a Carbon nanofiber impregnated on powder activated carbon, ^b acid treated cup-stuck carbon nanotubes, ^c thiol-functionalized superparamagnetic carbon nanotubes, ^d carbon nanotubes oxidized with concentrated nitric acid.

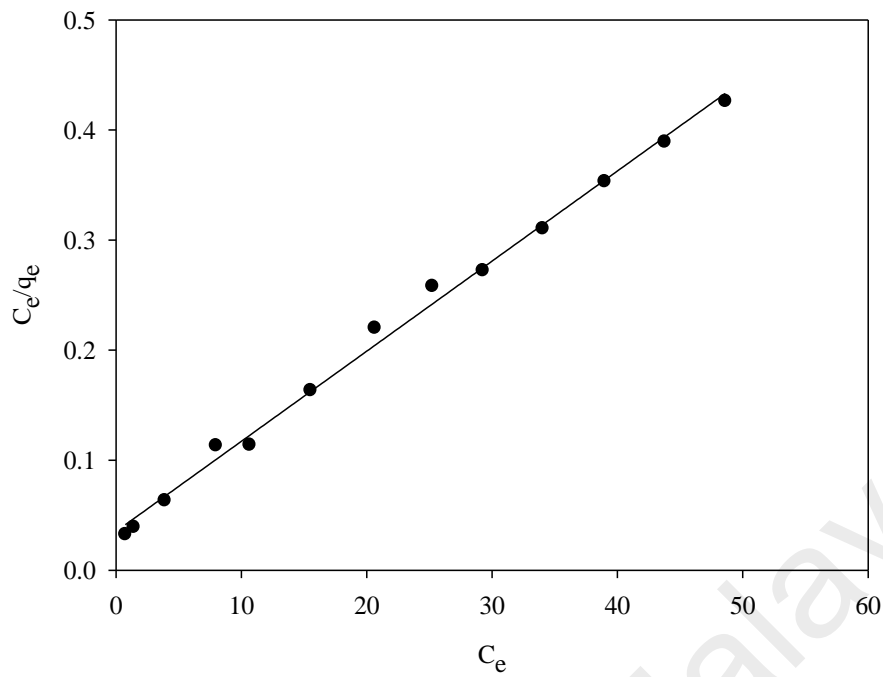


Figure 5.13: Langmuir isotherm model plot of Pb(II) sorption on KTEG-CNTs surface at pH 2.7.

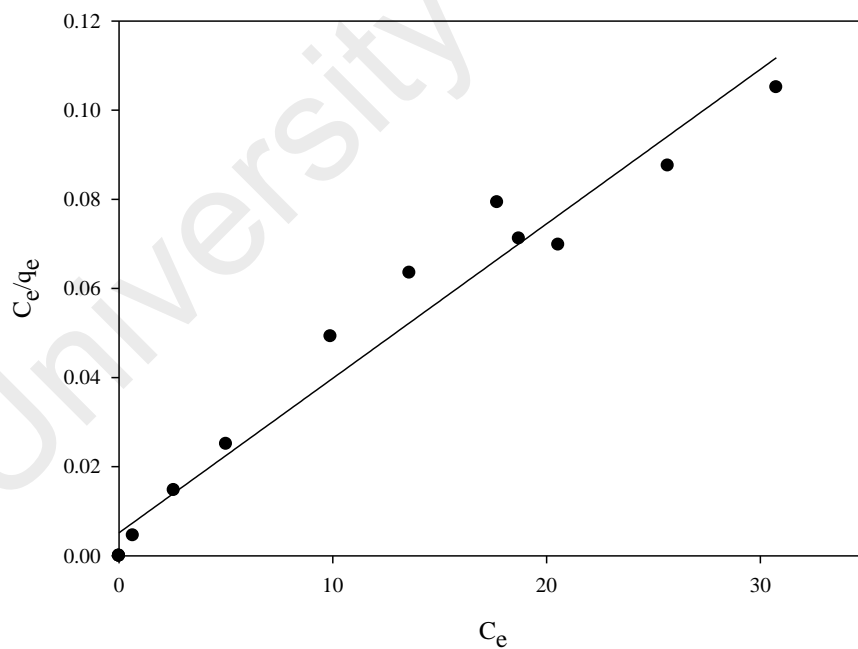


Figure 5.14: Langmuir isotherm model plot of Pb(II) sorption on KTEG-CNTs surface at pH 5.

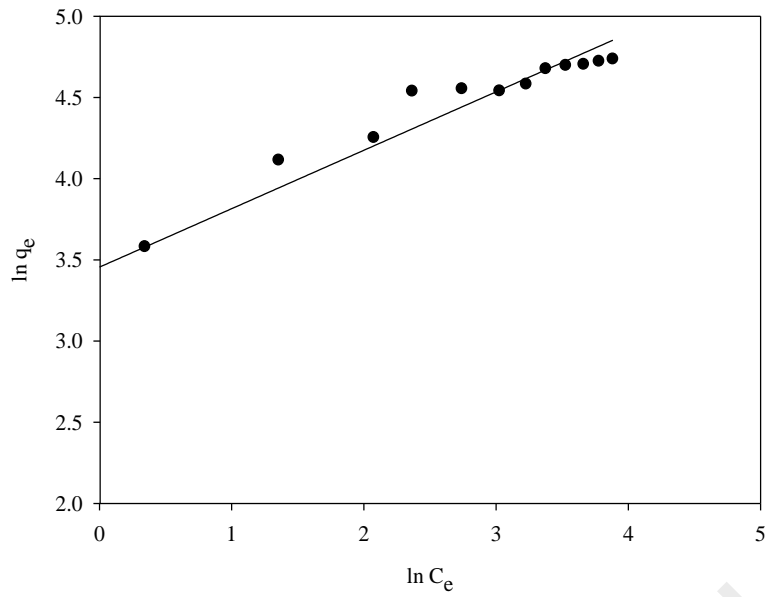


Figure 5.15: Freundlich isotherm model plot of Pb(II) sorption on KTEG-CNTs surface at pH 2.7.

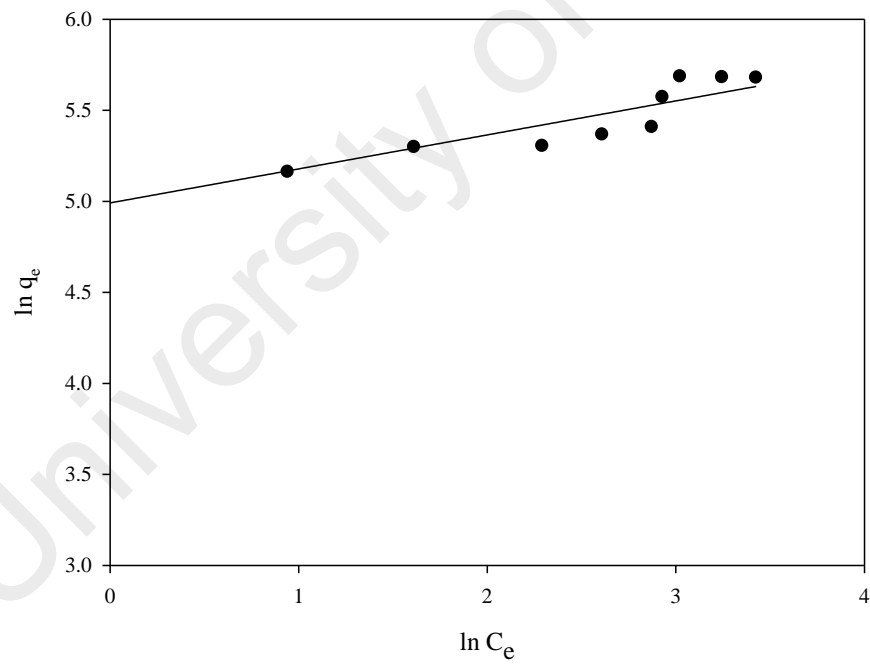


Figure 5.16: Freundlich isotherm model plot of Pb(II) sorption on KTEG-CNTs surface at pH 5.

5.4 Summary

Six different choline chloride based DESs were used as functionalization agents for pristine CNTs, KMnO_4 treated CNTs, HNO_3 treated CNTs, and H_2SO_4 treated CNTs. The capability of the functionalized CNTs to absorb Pb(II) from water was measured. The new adsorbents were characterized using Raman spectroscopy, FTIR, XRD, FESEM, EDX, BET, TGA, and Zeta potential. Screening studies were conducted for all adsorbents to discover the adsorbent with the highest removal percentage, which was then selected for further optimization studies. The optimum Pb(II) removal conditions were found, through RSM techniques, to be pH 5 with an adsorbent dosage of 5 mg and contact time of 15 min. Langmuir isotherm was used to approximate the data with maximum adsorption capacity of 288.4 mg/g for CNTs functionalized with KMnO_4 and TEG-based DES (KTEG-CNTs). The Pb(II) adsorption system fitted excellently to a pseudo-second order kinetics model.

CHAPTER 6: FUNCTIONALIZATION OF CNTS SURFACE WITH PHOSPHONUM BASED DEEP EUTECTIC SOLVENTS FOR ARSENIC REMOVAL FROM WATER

6.1 Introduction

Heavy metals contaminants in water have been the focus of world concern due to their effects on human life, in addition to causing damage in other organisms (Danil de Namor et al., 2012). One of the most toxic heavy metal is arsenic (As), which has been recognized as a deadly poison since ancient times due to causing severe side effects and lethality. It exists in many forms with varying toxicity levels. Toxicity of As species follows the trend: arsenite > arsenate > monomethyl arsenic acid (MMA) > dimethyl arsenic acid (DMA) (Ali, 2012). Many water resources have been contaminated either naturally or by human activities (Black, 1999; Mandal & Suzuki, 2002). The maximum arsenic level in the drinking water is 10 µg/L, as recommended by the World Health Organization (WHO) (Smedley & Kinniburgh, 2001; B. S. Tawabini et al., 2011).

Many conventional methods have been used to remove As from water. Examples of such include coagulation (P. R. Kumar et al., 2004), precipitation (Bissen & Frimmel, 2003), ion exchange (J. Kim & Benjamin, 2004), reverse osmosis (Ning, 2002), and oxidation (Gihring et al., 2001). However, these techniques have significant drawbacks (Payne & Abdel-Fattah, 2005; Tuutijärvi et al., 2009) and, therefore, the need for new alternative or modified technologies is imperative. Adsorption has been considered as one of the most effective techniques to remove As ions since it excels at separation of small amounts of pollutant from a large amount of solution (Ali, 2012).

In the last decade, nanotechnology has conquered almost all fields of science. Nanoparticles have been proposed as the most effective adsorbents for many pollutants, due to their unique features, small size, catalytic potential, high reactivity, and large

surface area (Ali, 2012). In the field of water treatment, carbon nanotubes (CNTs) are the most widely used nanomaterials. CNTs are extensively utilized to remove various kinds of pollutant (Ibrahim et al., 2016; Ihsanullah et al., 2016). However, significant limitations in the application of CNTs have been imposed because of many flaws in solubility, aggregation, and difficulty in manipulation. On the other hand, CNTs have shown a great affinity for interaction with different compounds, especially after surface functionalization (Y.-P. Sun et al., 2002; Thostenson et al., 2001). Oxidative functionalization can enhance CNTs surface charge, but requires the use of strong acids and environmentally unfavourable chemicals. Consequently, the need for new types of economical and environmentally friendly functionalization agents is crucial for the development of new applications (M. Hayyan, Abo-Hamad, et al., 2015a; Martínez et al., 2003).

The ionic liquids analogues, i.e. deep eutectic solvents (DESs), were introduced by Abbot et al. in 2003 (Andrew P. Abbott et al., 2003) as a cheaper replacement for developed ionic liquids (ILs). Substantially, DESs consist of two or more compounds. The mixture of these components have a melting point lower than that of the individual compounds (Andrew P. Abbott, Boothby, et al., 2004; M. Hayyan et al., 2010). DESs are considered to be the fourth generation of ILs, even though they are not entirely composed of ionic species (Cvjetko Bubalo et al., 2015b). Correspondingly, DESs have many advantages over conventional ILs, which can be summarized as simplicity of synthesis, variety of the physical properties with different molar ratios and reasonable price of components (M. Hayyan, M. A. Hashim, M. A. Al-Saadi, et al., 2013; M. Hayyan, M. A. Hashim, A. Hayyan, et al., 2013). Recently, ILs and DESs have been applied in many nanotechnologies related fields (Abo-Hamad et al., 2015).

In this study, two phosphonium based salts, namely methyl triphenyl phosphonium bromide (MTPB) and benzyl triphenyl phosphonium chloride (BTPC), were separately mixed with glycerol (Gly), which acts as a hydrogen bond donor (HBD), to form DESs. Subsequently, the synthesized DESs were used as novel functionalization agents for CNTs. The DES-functionalized CNTs were used as an adsorbent of As^{3+} ions from water. Response surface methodology (RSM) was employed to find the optimum operation conditions for As^{3+} adsorption on these novel adsorbents. Moreover, kinetics and isotherm studies were also performed at the potential optimum conditions.

6.2 Experimental methodology

6.2.1 Chemicals and materials

Multi-wall carbon nanotubes (MWCNTs) with specifications of D 6-9 nm \times L 5 μm , >95% carbon, Gly, 65% nitric acid (HNO_3), potassium permanganate (KMnO_4), sodium hydroxide pellets, and hydrochloric acid (36.5-38%) were all supplied by SIGMA-ALDRICH. MTPB, BTPC with >99% purity, and an arsenic standard solution of 1000 mg/L were supplied by Merck, Germany.

6.2.2 Synthesis of DESs

The DESs were synthesized by mixing each salt with Gly using magnetic stirring at 400 rpm and 80 $^\circ\text{C}$ until the DES became a homogeneous mixture without any precipitate. The molar ratio was chosen in concordance with our previous study (AlOmar, Hayyan, et al., 2016). Table 6.1 lists the synthesis details of each DES. All DESs were kept in well-sealed cups in a desiccator to avoid humidity effects.

Table 6.1: List of the synthesized DESs used for functionalization.

Salt	HBD	Molar ratio		DES
		Salt	HBD	abbreviation
MTPB	Gly	1	3	M
BTBC	Gly	1	16	B

6.2.3 Oxidation and acidification of MWCNTs

After drying the pristine MWCNTs (P-CNTs) overnight at 100 °C, two different oxidations methods were conducted. The first involved oxidation by KMnO_4 via sonication for two hours to produce K-CNTs (AlSaadi et al., 2016). The second method was performed by acidify the P-CNTs via refluxing with 65% HNO_3 for one hour at 140 °C to produce N-CNTs. For both methods, the functionalized CNTs was repeatedly washed by distilled water and filtered with a vacuum system using a PTFE 0.45 μm membrane until the filtrate water pH was neutral.

6.2.4 Functionalization by DES

200 mg of P-CNTs, K-CNTs, and N-CNTs were individually sonicated in 7ml of MTPB-based DES (M) and BTBC-based DES (B) DESs separately for three hours at 65 °C. The mixture was then washed with distilled water several times and filtered using a PTFE 0.45 μm membrane until the filtrate water was neutral. Figure 6.1 demonstrates the functionalization process and gives the abbreviation of each adsorbent.

6.2.5 Characterization of functionalized CNTs

All adsorbents were characterized using Raman spectroscopy (Renishaw System 2000 Raman Spectrometer) to obtain Raman shift spectra. The surface modification and functional groups that resulted from the functionalization processes were conducted using

Fourier transform infrared (FTIR) spectroscopy via a PerkinElmer® FTIR spectrometer. The structure phases were analyzed using X-ray powder diffraction (XRD) Shimadzu XRD 6000. The thermal stability of the new adsorbents was also investigated using thermogravimetric analysis (TGA) and differential thermogravimetry (DTG) with a Thermal Analyzer (STA-6000, PerkinElmer®). Furthermore, the surface charge was measured by conducting the zeta potential using Zetasizer (Malvern, UK). A fully Automated Gas Sorption System (micromeritics ASAP2020, TRISTAR II 3020 Kr) was used to study the selected samples surface area based on the method of Brunauer-Emmett-Teller (BET). A Field-Emission Scanning Electron Microscope (Quanta FEG 450, EDX-OXFORD) was used to obtain high resolution nano-sized images for studying the morphology of all selected samples, along with an energy-dispersive X-ray spectrometer (EDX).

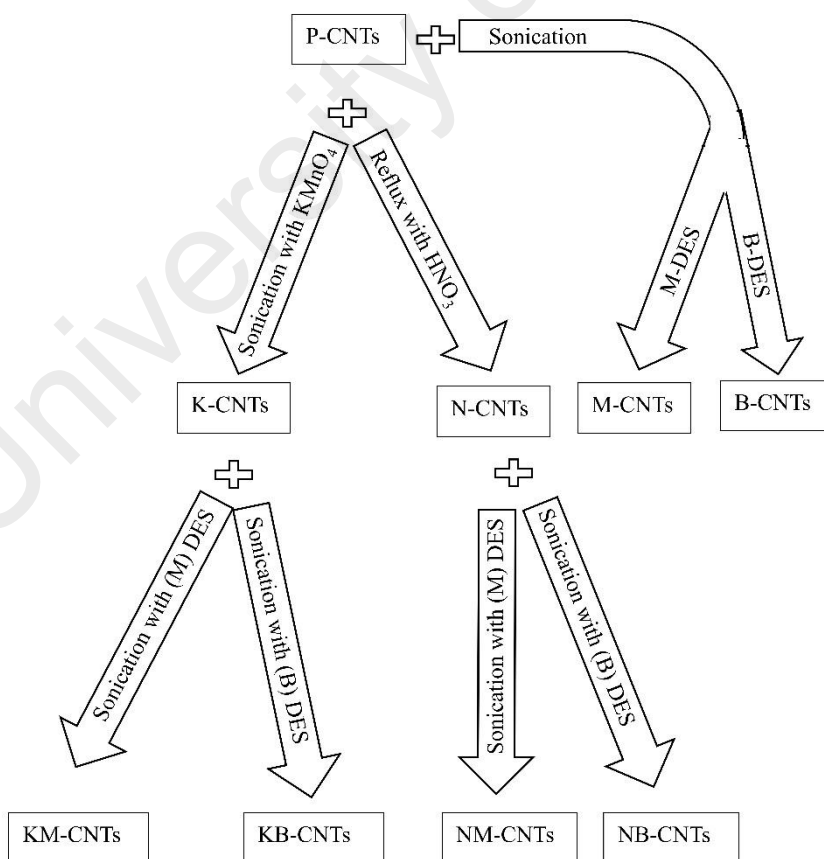


Figure 6.1: Functionalization process and the abbreviation of each adsorbent

6.2.6 Adsorption experiments

A sample of 10 mg from each of the 9 prepared adsorbents (listed in Figure 6.1) was applied in batch adsorption of As^{3+} . Distilled water was used to prepare As^{3+} stock solution at 5 mg/L concentration and pH of 2.7. The experiments were conducted using 50 ml of contaminated water in a 250 ml flask with 10 mg of adsorbent. The flask was shaken using a mechanical system for 30 min at room temperature and an agitation speed of 180 rpm. The adsorbent with the highest removal efficiency was chosen for further studies. The same screening experiments were repeated but at pH 6.0.

6.3 Result and Discussion

The results obtained from the primary screening show that the KM-CNTs achieved the highest removal percentage at pH 2.7. On the other hand, KB-CNTs recorded the highest removal at pH 6. Figure 6.2 illustrates the screening study for the adsorption of As^{3+} .

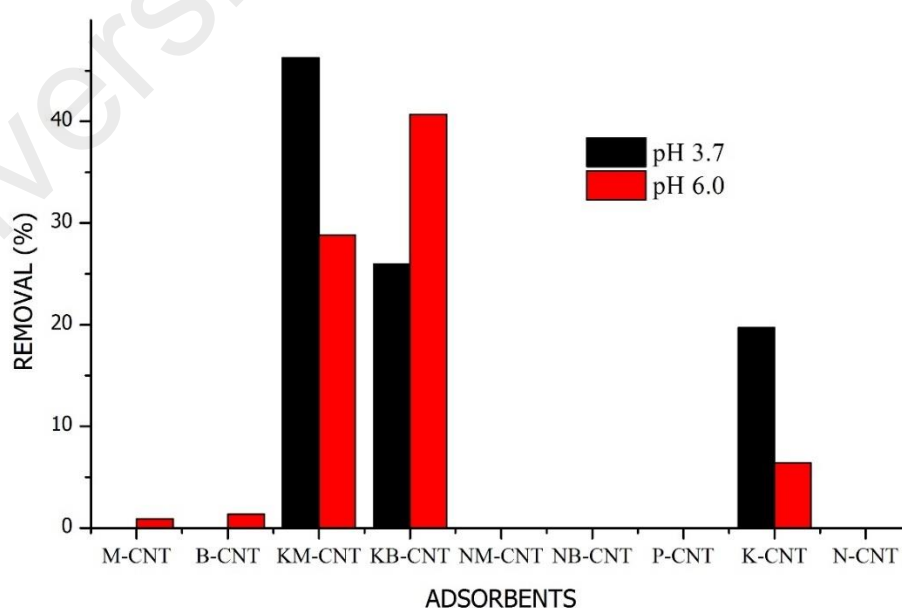


Figure 6.2: Screening for best adsorbent of As^{3+}

6.3.1 Characterization of DES-functionalized CNTs

6.3.1.1 Raman spectroscopy

Raman spectroscopy is considered to be an essential characterization for Carbon based materials, due to its ability to indicate the degree of functionalization by comparing the intensity of D band (I_D) to that of G band (I_G) (Aitchison et al., 2007). The G mode corresponds to the movement in opposite directions of two neighbouring carbon atoms in a graphite sheet (Hiura et al., 1993). The D mode is caused by sp^3 -hybridized carbon atoms in the nanotube sidewalls (Bahr et al., 2001). The D band is usually detected at 1350 cm^{-1} wavelength, the G-band is usually detected in the $1500\text{-}1600\text{ cm}^{-1}$ range, and the D' mode is found at approximately 1615 cm^{-1} (Jorio et al., 2004). These wavelengths usually appear in multiwall CNTs. While in single wall CNTs, the radial breathing mode (RBM) can be detected in the range of $100\text{-}400\text{ cm}^{-1}$. Figure 6.3 shows the positions and intensities of both the D and G bands for P-CNTs, K-CNTs, KM-CNTs, and KB-CNTs.

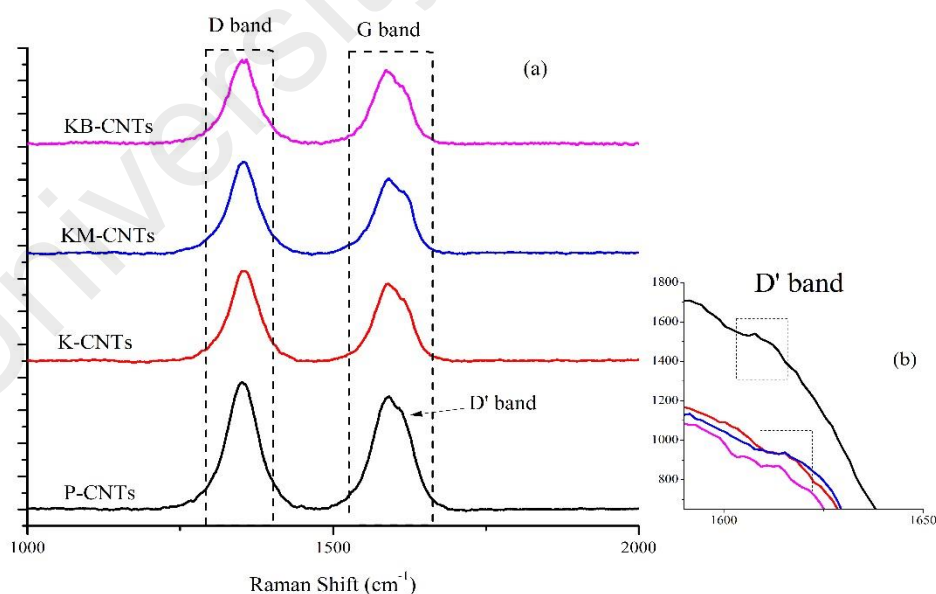


Figure 6.3: Raman spectroscopy, a) D band and G band location and intensity, b) D' band

In this study, the I_D/I_G ratio of P-CNTs was 1.11. Adding new functional groups by the oxidation with $KMnO_4$ resulted in an increase in I_D/I_G to 1.16. Subsequently, introducing new functional groups increased the deformation on the surface of CNTs, resulting in an increase in the I_D/I_G ratio to 1.22 for KM-CNTs. By contrast, the KB-CNTs I_D/I_G was 1.14. This difference may be due to a higher level of covalent functionalization on the surface of the KM-CNTs with carboxylic functional groups or other Sp^3 groups. Subsequently, the FTIR findings confirm the presence of Sp^3 covalent functionalization. The D band, G band, and D' band positions are listed in Table 6.2, along with the intensity of each peak, the full-width at half maximum (FWHM), and the I_D/I_G values. Additionally, the D' band, which is usually displayed as a weak shoulder of the G-band at higher frequencies, cannot be found in pure graphite. However, it can be observed in intercalated graphite and MWCNTs (C. S. Kumar, 2012). Furthermore, it is considered to be a double resonance feature generated by disorder and defects. Figure 2b shows the D' shift, which confirms the functionalization effects on the CNTs (Kordás et al., 2006).

Table 6.2: Intensity of Raman bands and the I_D/I_G ratios

Sample	D band			G band			D' band		I_D/I_G
	Wave No.	FWHM	Intensity	Wave No.	FWHM	Intensity	Wave No.	Intensity	
P-CNTs	1355	58.97	1903	1589	72.8	1710	1608	1539	1.11
K-CNTs	1355	55.4	1368	1590	67.4	1171	1614	946	1.16
KM-CNTs	1356	54.1	1398	1590	67.5	1144	1615	944	1.22
KB-CNTs	1358	54.6	1264	1587	68.4	1105	1612	876	1.14

6.3.1.2 Surface chemistry analysis (FTIR)

Fourier transforms infrared (FTIR) spectroscopy is an adaptable technique that determines the surface chemistry, specifically in terms of functional groups. In order to study the formation of new functional groups at each functionalization step, the surfaces of P-CNTs, K-CNTs, KM-CNTs, and KB-CNTs were investigated.

Figure 6.4 shows the FTIR profile for P-CNTs, K-CNTs, KM-CNTs, and KB-CNTs. The presence of O-H stretching is obvious in the peaks around 3400 cm^{-1} for all functionalized samples except KM-CNTs. However, in the region between ($3000\text{-}3600\text{ cm}^{-1}$), the O-H and C-H may overlap. The intense band in the first region contains signal of CH_2 asymmetric and symmetric at 2920 and 2850 respectively. Furthermore, symmetric and asymmetric vibrations of C-H groups at 2800 cm^{-1} also detectable. The second region contains several peaks that indicate the presence of carboxylates groups (asymmetric CO_2 stretch), carbonyl groups, and aliphatic carboxylic acids at 2400 and 1580 cm^{-1} wave numbers. The third region, under 1400 cm^{-1} , is usually denoted as a fingerprint region and contains indications of the presence of CO_2 and $\text{C}=\text{O}$ (B. C. Smith, 1998). In addition, the presence of phosphonium functional groups in a form of PO_4^{3-} are shown by the bend at $500\text{-}600\text{ cm}^{-1}$. The C-Br and C-Cl bond is located in the range of $500\text{-}570$ or $600\text{-}800\text{ cm}^{-1}$ for KM-CNTs and KB-CNTs, respectively. The bands representing rocking in and out of plane are usually located in the $770\text{-}400\text{ cm}^{-1}$ region, which might overlap with the range of carboxylates groups, and show a strong, characteristic asymmetric stretching absorption from the CO_2 group in the $1575\text{-}1585\text{ cm}^{-1}$ region. Based on the forgoing, each functionalization process added several function groups to the surface of P-CNTs. The presence of DESs as a functionalization agent also increased the active sites on the surface and improved the adsorption of As^{3+} .

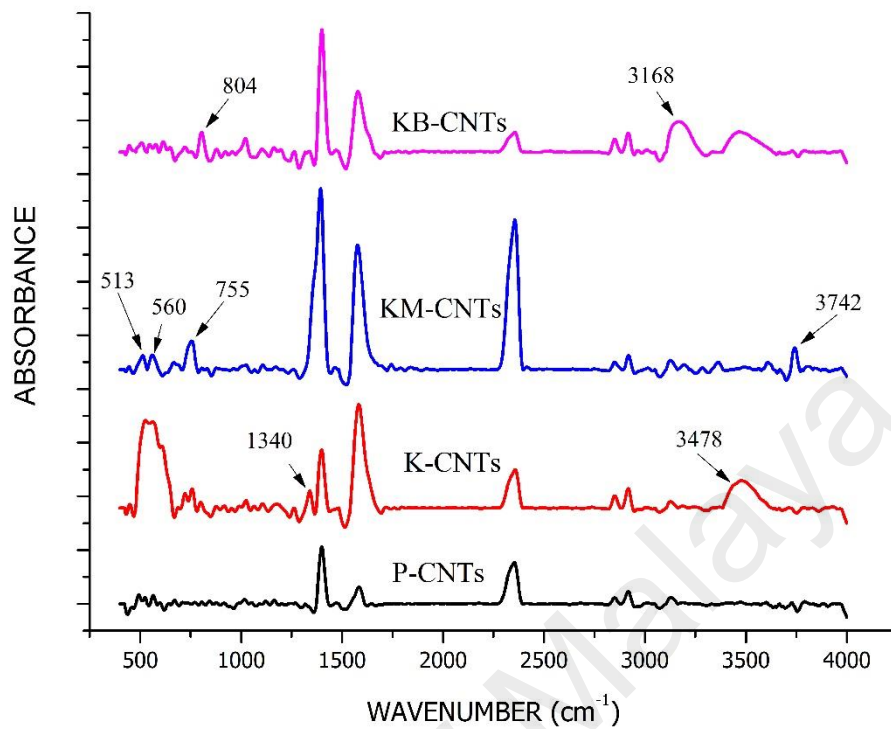


Figure 6.4: FTIR spectroscopy for P-CNTs, K-CNTs, KM-CNTs and KB-CNTs

6.3.1.3 XRD analysis

Figure 6.5 shows the XRD patterns of P-CNTs, K-CNTs, KM-CNTs, and KB-CNTs. The (002) and (001) peaks representing the hexagonal graphite structure and the concentric cylinder structure are located at 2θ around 26° and 42° , respectively, in P-CNTs patterns (D. Zhang et al., 2005). The (002) was reduced in the K-CNTs pattern due to the extensive presence the of MnO_2 , which, by its deposition, destroys the hexagonal graphite structure of CNTs through wrapping the CNTs into a non-stoichiometric amorphous shape (S.-G. Wang et al., 2007). The DESs functionalization increased the wrapping around the CNT edges. The patterns of KM-CNTs and KB-CNTs are almost identical.

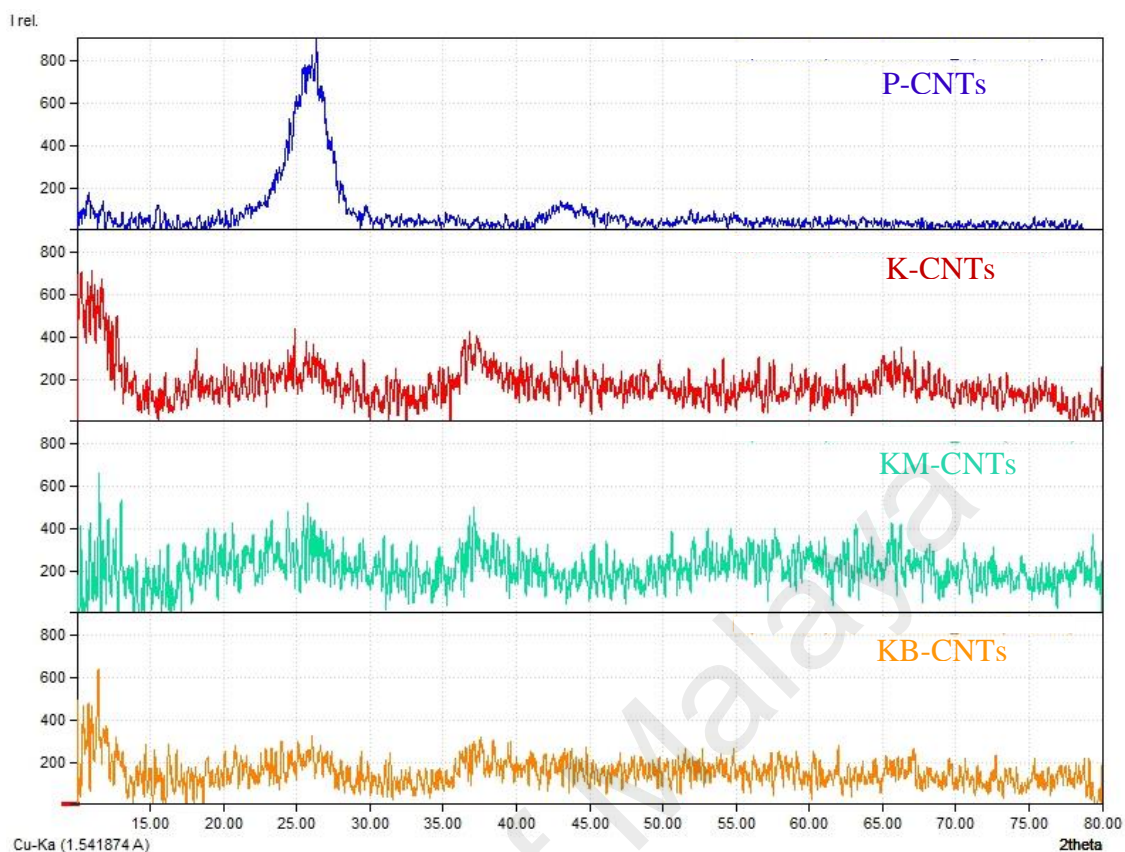


Figure 6.5: XRD patterns for P-CNTs, K-CNTs, KM-CNTs and KB-CNTs

6.3.1.4 EDX analysis and FESEM

EDX studies were conducted on KM-CNTs and KB-CNTs after adsorption of As^{3+} . The results supported the hypothesis of MnO_2 decomposition on the surface of CNTs when the weight percentage of MnO_2 was approximately 65 %. This results agrees with the TGA results. In addition, the presence of Cl^- and Br^- was also confirmed, even after removal of As^{3+} . Figures 1D and 2D (Appendix D) shows the EDX spectrum for KM-CNTs and KB-CNTs, respectively. Moreover, figure 6.6 shows representative high magnification FESEM images for P-CNTs, K-CNTs, KM-CNTs, and KB-CNTs. The presence of MnO_2 embedded inside the CNT is also demonstrated. Furthermore, the effect of DESs functionalization is slightly observable.

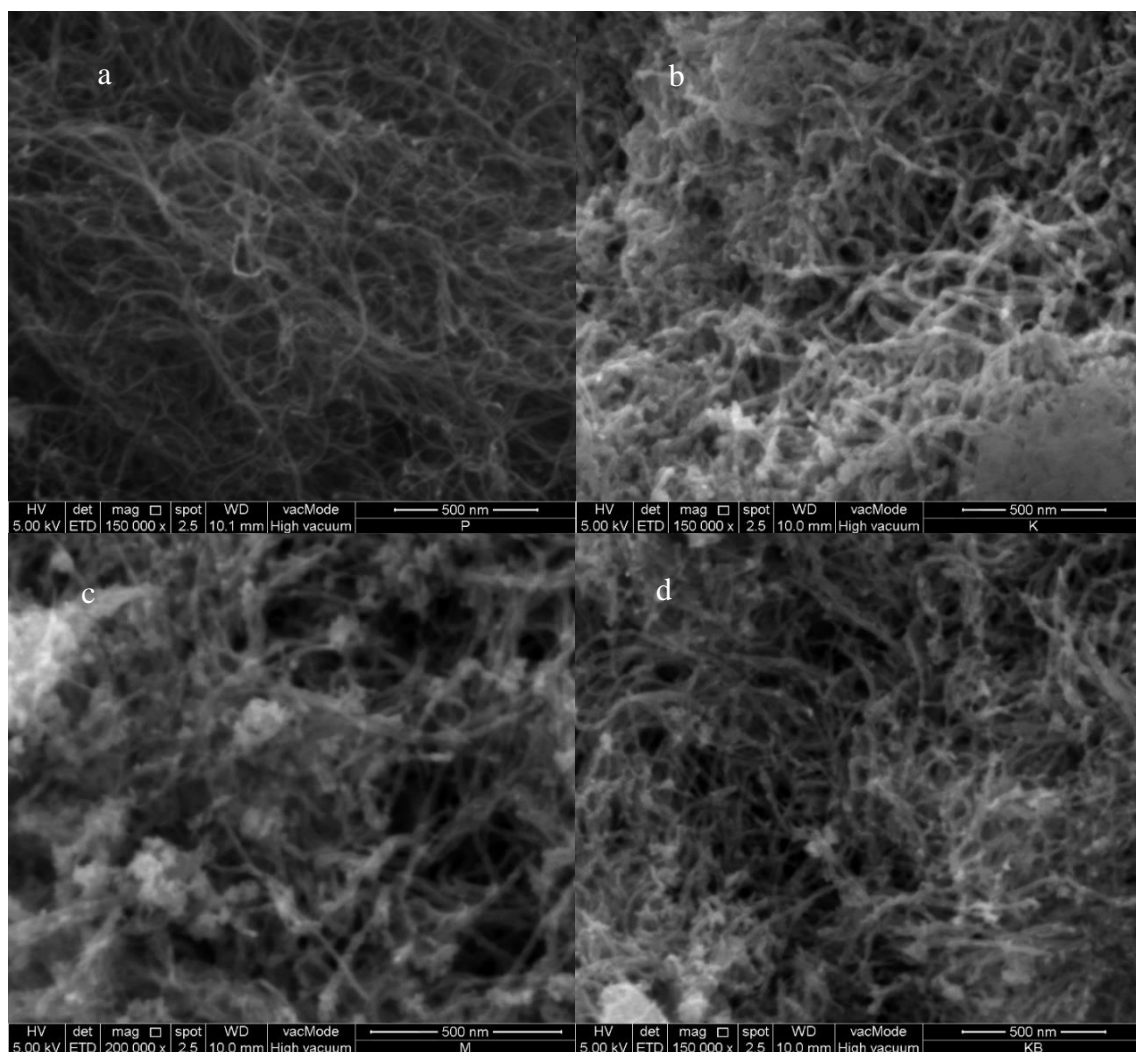


Figure 6.6: FESEM image for a) P-CNTs, b) K-CNTs, C) KM-CNTs, and d) KB-CNTs

6.3.1.5 BET surface area

In this study, the surface area for P-CNTs, K-CNTs, KM-CNTs, and KB-CNTs were investigated using BET methodology. The BET was measured according to ASTM D 3663-3 reapproved (ISO second edition 1-09-2010). Table 6.3 presents a summary of the surface area results. The surface area increased significantly with each functionalization step. The surface area of the KM-CNTs was higher than that of KB-CNTs, which was also reflected in the maximum adsorption capacity and corroborates the isotherm results.

Table 6.3: Comparative BET summary result for all adsorbent

Property	P-CNTs	K-CNTs	KM-CNTs	KB-CNTs
BET Surface Area (m ² /g)	123.543	158.934	205.500	174.772
Total pore volume (cm ³ /g)	0.620	0.453	0.668	0.642
Average Pore Diameter (Å)	20.499	114.127	130.214	147.019

6.3.1.6 Thermogravimetric analyses (TGA)

TGA analysis was performed for P-CNTs, K-CNTs, KM-CNTs, and KB-CNTs. In addition, the analysis was conducted before and after adsorption process. KM-CNTs-As and KB-CNTs-As refer to the after adsorption samples corresponding to KM-CNTs and KB-CNTs. TGA analysis was conducted with a starting temperature of 25 °C and an ending temperature of 800 °C with a heating rate of 10 degrees per min (°C/min). The experiments were conducted under aerobic conditions with a flow rate of 50 mL/min. Figure 6.7 shows the TGA curves for all samples. The combustion profiles of the samples suggested higher thermal stability and purity for P-CNTs compared to the functionalized CNTs. The onset of P-CNTs combustion was 556 °C, while K-CNTs had an onset of oxidation at 270 °C. This reduction indicates the effects of MnO₂ embedded in the CNTs and acting as an active catalyst for oxidization. On the other hand, the effect of DESs functionalization is observable for KM-CNTs and KB-CNTs, which had onsets of combustion at 327 °C and 365 °C, respectively. The presence of As³⁺ after adsorption further reduced the oxidative catalytic activity of the MnO₂. It was observed that weight loss stopped after the higher limit temperature of combustion and some residual material remained for all samples. These residues indicated the carbon purity of the samples. P-CNTs left 0% residue. K-CNTs, KM-CNTs, KB-CNTs, KM-CNTs-As, and KB-CNTs-As left residues of 65.21%, 56.76%, 62.72%, 60.74%, and 64.62%, respectively.

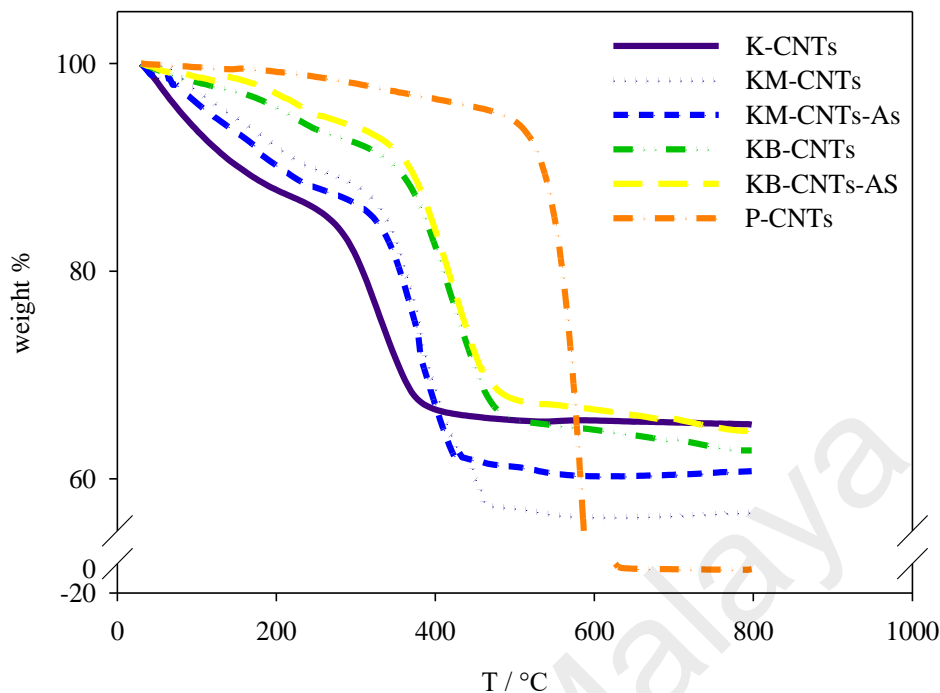


Figure 6.7: TGA graph of P-CNTs, K-CNTs, KM-CNTs, KB-CNTs and (KM-CNTs-As and KB-CNTs-As) after adsorption

6.3.1.7 Zeta potential

Studying the electric charge potential of a solid particle surface is essential to discover characteristics explain its behaviour in aqueous environment and predict its suspension stability. Absolute values can be used to quantitatively compare various stability of particle dispersions (Z. Sun et al., 2008). Numerous factors influence the zeta potential, including particle surface charges, and the environmental conditions of the suspension, such as pH, conductivity, ion concentration, and temperature (Simate et al., 2012). Herein, dispersions of P-CNTs, K-CNTs, KM-CNTs, and KB-CNTs was prepared separately in deionized water at 2.5 mg/ml for zeta potential measurements. The results showed that the absolute zeta potential values increased from 5.5 to 45.81 mV for P-CNTs and K-CNTs, respectively. This significant increase indicates that the presence of

oxygen-containing functional groups on the surface, such as carbonyl groups and aliphatic carboxylic acids, increased the hydrophilicity of the adsorbent and resulted in an increase in electronegativity, which plays an important role in the adsorption mechanism. The absolute zeta potential value for the KB-CNTs slightly decreased to 45.34 mV, compared with that of K-CNTs. On the other hand, the zeta potential of KM-CNTs was 39.78 mV. It is well known that the electronic surface charge affects the dispersion of the particles in any solvent (P.-C. Ma, Siddiqui, Mäder, & Kim, 2011). Based on this fact, these adsorbents are believed to form water suspensions with very good stability. According to ASTM standards, the criterion for “good stability” requires a zeta potential with an absolute value above 40 mV (Fan et al., 2012).

6.3.2 Optimization study

In order to optimize the conditions for the removal of As^{3+} , response surface methodology (RSM) was adopted using the Design Expert V7.0 software package. Central composite design (CCD) was used to conduct the experiments. The effect and interaction of three parameters, specifically pH (3 to 8), contact time (5 to 55 min), and adsorbent dosage (5 to 20 mg), were investigated. Removal percentage (%) and uptake capacity q (mg/g) were adopted as the response functions. Tables 1D and 2D show the experimental design in terms of the actual parameters of each run and the responses of each run for KM-CNTs and KB-CNTs, respectively. The optimization was performed at As^{3+} initial concentration of 1 mg/L with a fixed agitation speed of 180 rpm.

The highest removal response was observed with KM-CNTs (95.52%) at pH 3, 55 min contact time, and 20 mg adsorbent dosage. While for KB-CNTs, the highest observed removal was 92.52% at pH 5.5, 55 min contact time, and an adsorbent dosage of 20 mg. The removal percentage and uptake capacity of both KM-CNTs and KB-CNTs were in accordance with the variance models for the two responses. The Model F-values of all

models for both adsorbents implied that all models were significant. Table 3D and Table 4D lists the P-values, F-values, and the square mean for both removal percentage and uptake capacity, respectively, of KM-CNTs. There is only a 0.01% and 0.01% chance that a "Model F-Value" this large could occur due to noise for both removal percentage and uptake capacity of KM-CNTs. While these values were 0.01 and 0.03 with KB-CNTs as the adsorbent. Table 5D and 6D lists the P-values, F-values, and the square mean for removal percentage and uptake capacity, respectively, of KB-CNTs.

Figure 6.8 (a and b) and 6.9 (a and b) show the theoretical values plotted versus the experimental values for removal percentage and adsorption capacity for both adsorbents. These graphs clearly demonstrate that the theoretical values predicted by the models developed in this study were quite close to the experimental values, indicating that both models successfully achieved correlation between the process variables. The correlation coefficient R^2 for both responses indicated that the quality of the models were excellent. In the case of KM-CNTs, the R^2 for removal and uptake capacity were 0.9820 and 0.9995, respectively. The R^2 of removal and uptake capacity for KB-CNTs were 0.9862 and 0.9703, respectively.

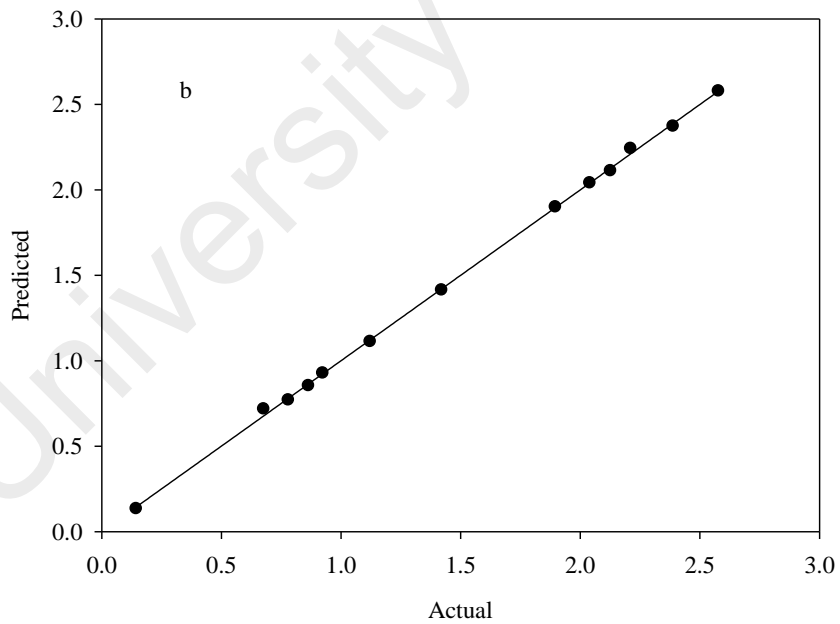
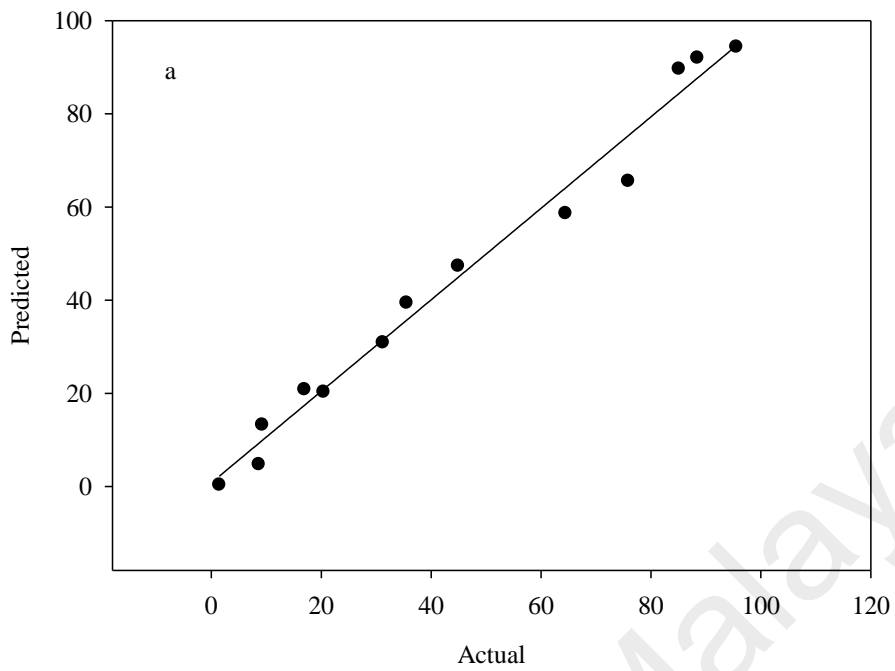


Figure 6.8: Theoretical vs experimental data for a) As^{+3} removal (%) and b) uptake capacity (mg/g) on KM-CNTs adsorbent

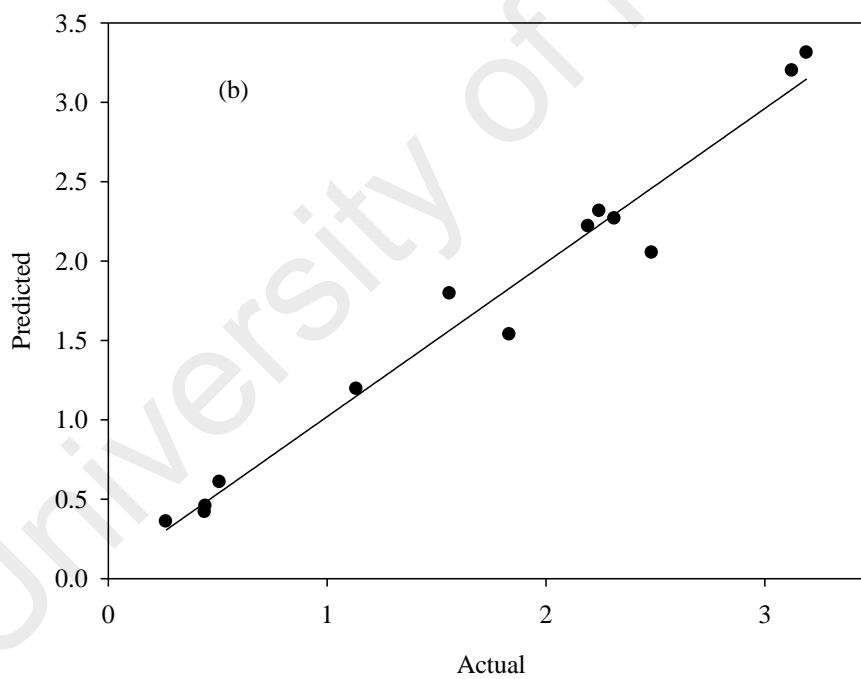
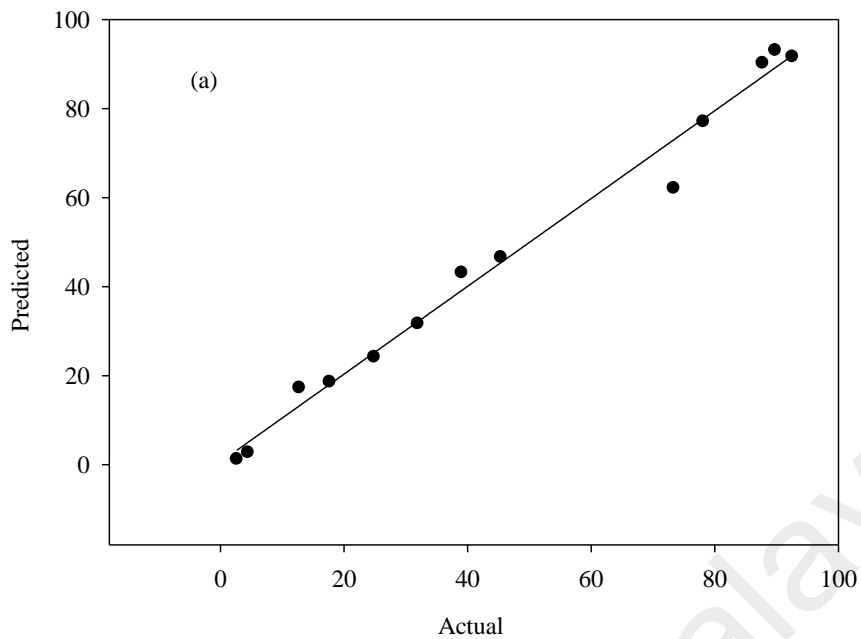


Figure 6.9: Theoretical vs experimental data for a) As^{+3} removal (%) and b) uptake capacity (mg/g) on KB-CNTs adsorbent

Figures 6.10 (a and b) and 6.11 (a and b) show the interaction effects between contact time and pH on removal and uptake capacity for both KM-CNTs and KB-CNTs. Both removal and uptake capacity increased with time since the system did not approach equilibrium. The effect of pH was slightly observable for KM-CNTs. Meanwhile, for KB-CNTs, the removal percentage increased with increasing pH. However, by fixing the contact time, increases in pH decreased the removal percentage at low adsorption dosages. The same behaviour was observed with the uptake capacity response.

For both adsorbents, contact time showed a significant impact on the removal percentage and the uptake capacity. The removal percentage and the uptake capacity increased linearly with time (figures 6.10a and 6.11 (a and b)). While, figure 6.10b shows an exponential increment of uptake capacity with contact time. Based on the ANOVA model Eq. 6.1, 6.2, 6.3 and 6.4, the statistical model reveals that the contact time linearity in some cases and the nonlinearity in others attributed to two effects. The first is the interaction between contact time and pH, and the second is the limitation of time points which did not show the nonlinearity in the linear cases.

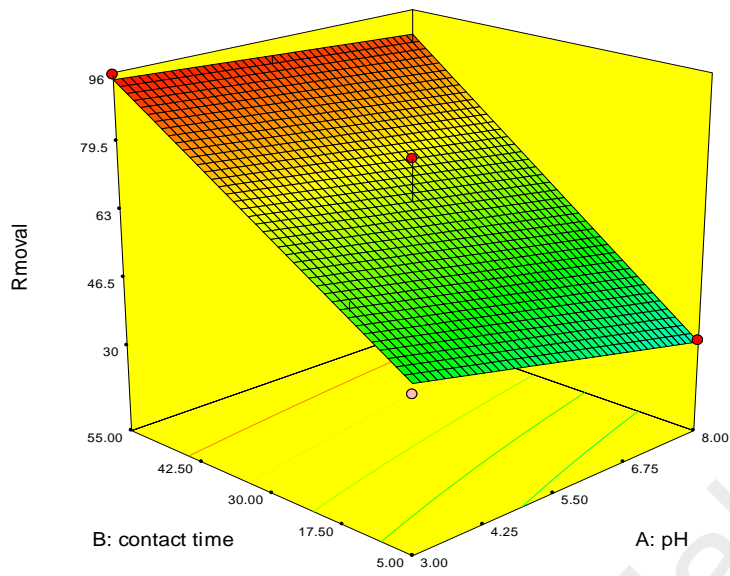
$$As^{3+} \text{ removal (\%)} \text{ on KM - CNTs} = 39.42 - 2.29A + 18.58B + 26.16C + 2.93AC - 3.02AC + 7.87BC \quad \dots\dots\dots (6.1)$$

$$\text{Adsorption capacity of KM - CNTs} = 1.41 - 0.04A + 0.84 + 0.49 + 0.23AB - 0.11AC + 0.14B^2 - 0.21ABC - 0.45B^2C \quad \dots\dots\dots(6.2)$$

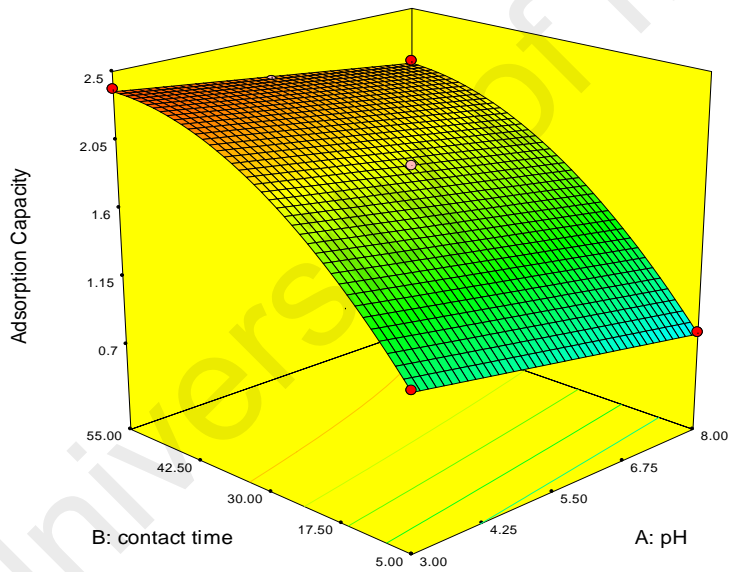
$$As^{3+} \text{ removal (\%)} \text{ on KB - CNTs} = 43.18 + 0.34A + 25.86B + 18.97C + 7.72AB - 6.63AC + 3.68BC \quad \dots\dots\dots(6.3)$$

$$\text{Adsorption capacity of KB - CNTs} = 1.8 - 5.797 \times 10^{-4}A + 1.19B - 0.26C + 0.22AB - 0.17AC - 0.46BC \quad \dots\dots\dots(6.4)$$

Where A,B, and C refer to pH, contact time and adsorbent dosage respectively.

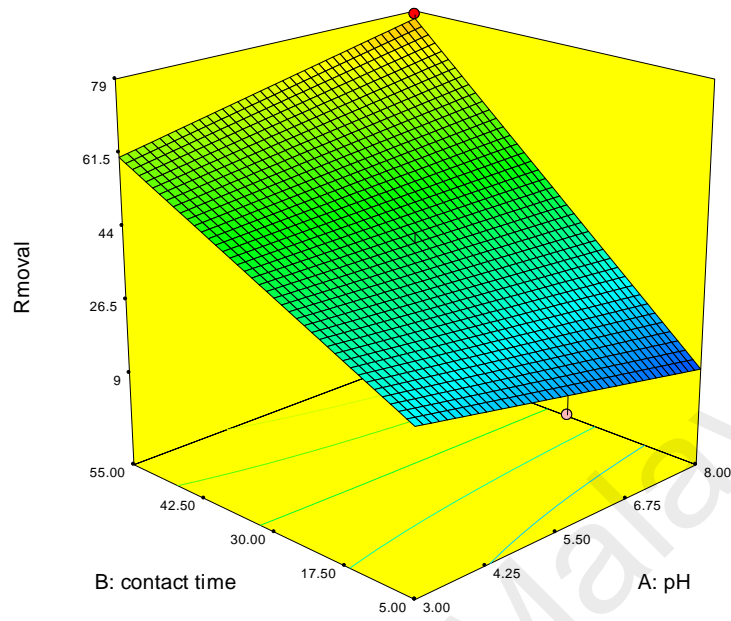


a) Removal %

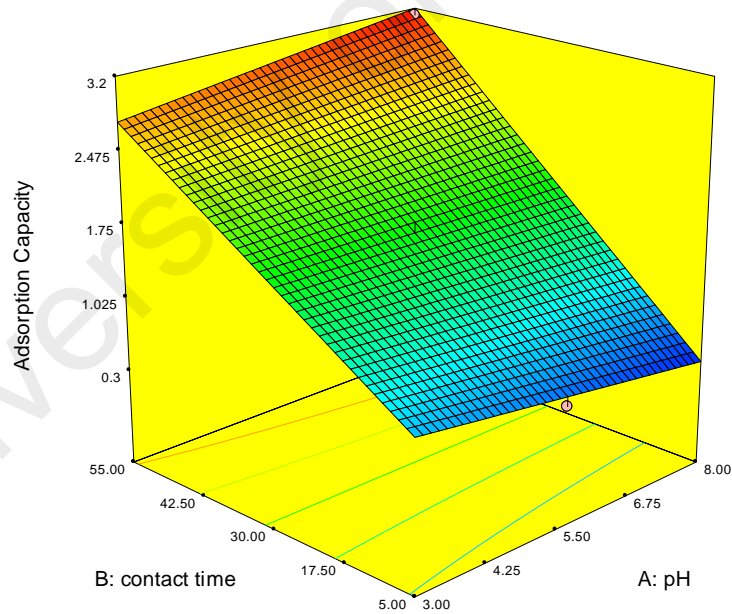


b) Uptake Capacity

Figure 6.10: Surface response representation of a) Removal (%) of As^{+3} versus contact time and pH by fixing adsorbent dosage to the optimum value and b) uptake capacity of KM-CNTs versus contact time and pH by fixing adsorbent dosage to the optimum value.



a) Removal %



b) Uptake Capacity

Figure 6.11: Surface response representation of a) Removal (%) of As^{+3} versus contact time and pH by fixing adsorbent dosage to the optimum value and b) uptake capacity of KB-CNTs versus contact time and pH by fixing adsorbent dosage to the optimum value.

6.3.3 Kinetics study

To investigate the kinetic rates that fit with the adsorption of As³⁺ in an aqueous solution, three kinetics models were examined, specifically pseudo-first order, pseudo-second order and intraparticle diffusion models. Table 6.4 shows the linearized forms of the techniques performed to determine the kinetics constants, equilibrium capacities, and correlation coefficients (R²).

Table 6.4: Linearized forms of kinetics models and their parameters

Model	Plot	Intercept	Slope	Parameters
Pseudo-First-Order Adsorption Kinetics $\ln(q_e - q_t) = \ln q_e - K_1 t$	$\ln(q_e - qt)$ vs time (t).	$\ln q_e$	$-K_1$	$K_1 = -\text{slope}$ $q_e = e(\text{intercept})$
Pseudo-Second-Order Adsorption Kinetics $\frac{t}{q_t} = \frac{1}{K_2 q_e^2} + \frac{1}{q_e} t$	$\frac{t}{q_t}$ vs t	$\frac{1}{K_2 q_e^2}$	$\frac{1}{q_e}$	$q_e = 1/(\text{slope})$ $K_2 = \frac{\text{Slope}^2}{\text{Intercept}}$
Intraparticle Diffusion $q_t = K_d t^{0.5} + c$	qt vs $t^{0.5}$	c	K_d	$K_d = \text{slope}$

Where q_e is the equilibrium adsorption capacity, K_1 Rate constant of Pseudo-First-Order, K_2 Rate constant of Pseudo-Second-Order, K_d is Rate constant of Intraparticle Diffusion

An initial concentration of 1 mg/L was applied in the kinetics study. The adsorbent dosage was 20 mg and the agitation speed was 180 rpm. The optimum pH for each adsorbent was used in this study, which was 3.0 and 6.0 for KM-CNTs and KB-CNTs, respectively. The experiment reached equilibrium after 150 min for both adsorbents. The data sets are plotted in Figures 6.12 and 6.13 and show the pseudo-second order kinetic models for KM-CNTs and KB-CNTs, respectively. The values of the correlation coefficients (R²) of the data sets were considered as indications of conformity between the experimental data and the corresponding values predicted by each model. Pseudo-second order rate equations describe the kinetics of both adsorbents with increased conformity compared to the pseudo-first order and intraparticle diffusion models, since

the R^2 of the pseudo-second order was 0.9966 and 0.9921 for KM-CNTs and KB-CNTs, respectively. Table 6.5 shows a comparison of the different correlation coefficients (R^2) obtained from each kinetic model. The results of the kinetic study demonstrate that the adsorbent and the adsorbate concentrations are involved in the rate determining step, which indicates that the rate limiting step may be chemisorption. This agrees with previous observations in many kinds of CNT-based adsorbents (Sheng et al., 2012; B. S. Tawabini et al., 2011; Z. S. Veličković et al., 2013).

Table 6.5: Experimental values of constants of adsorption kinetics models

Adsorbent	Pseudo-first- order			Pseudo-second-order			Intraparticle	
	q_e (mg/g)	K_1 (min^{-1})	R^2	q_e (mg/g)	K_2 (g/mg.min)	R^2	K_d (g/mg.min ^{0.5})	R^2
KM-CNTs	1.74	-0.002	0.777	2.19	0.113	0.996	4.83	0.595
KB-CNTs	1.04	0.035	0.843	2.20	0.089	0.992	5.00	0.642

6.3.4 Adsorption mechanism

It is well known that MWCNTs and their modified allotropes have heterogeneous surface which offers a platform for the probability of multi mechanisms. Based on the characterization, the surface consists of several active sites such as, oxygen containing functional groups, metal oxide imbedded between the exfoliated graphene layers on the surface of CNTs, and the defects of the graphene network on the surface. Consequently, each site can play a different role in the mechanism. Herein, the As^{3+} could form complexation with oxygen containing groups and ion exchange process takes place with H^+ . Furthermore, OH^- ions in the solution play positive role in consuming H^+ which led to enhance the adsorption of As^{3+} with the increase of pH. However, further increase in pH leads to excess amount of OH^- which forms complexations with As^{3+} in the solution and reduces the rate of direct surface adsorption but the As^{3+} removed in a form of

precipitated hydroxide. In addition, As^{3+} could form complexation with MnO_2 embedded within the graphene layers of external CNTs walls. In case of using KM-CNTs, the precipitated complexes of As^{3+} were not attached to the surface of the adsorbent while attached to the KB-CNTs surface. This is probably occurring due to the electrostatic charges.

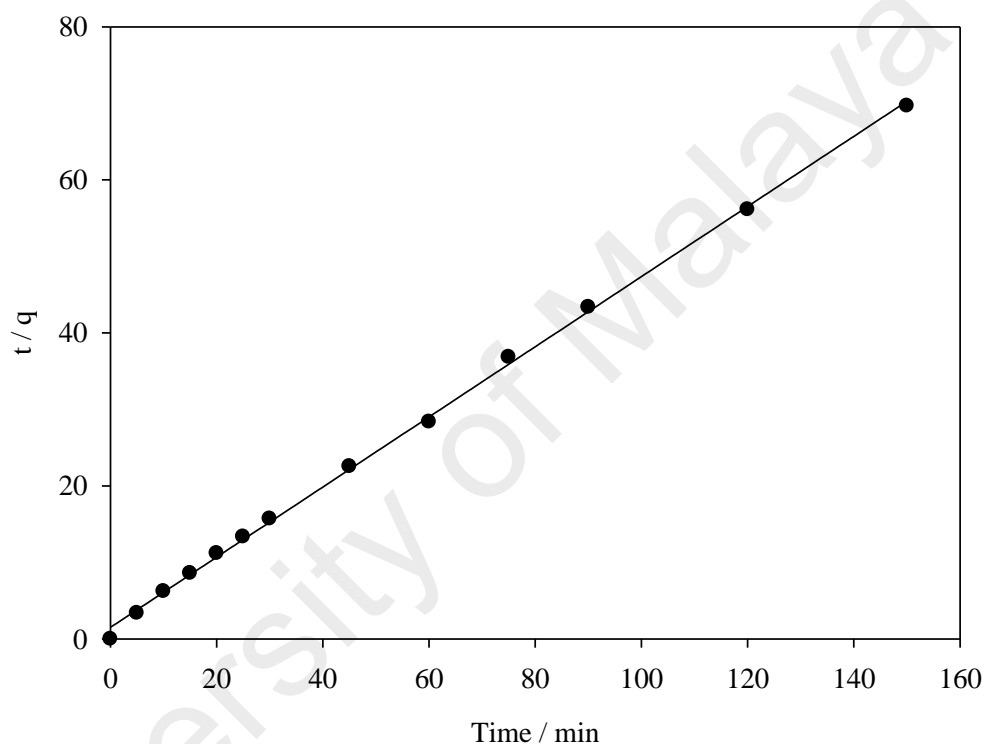


Figure 6.12: Pseudo-second-order kinetic model for As^{3+} adsorption on KM-CNTs surface

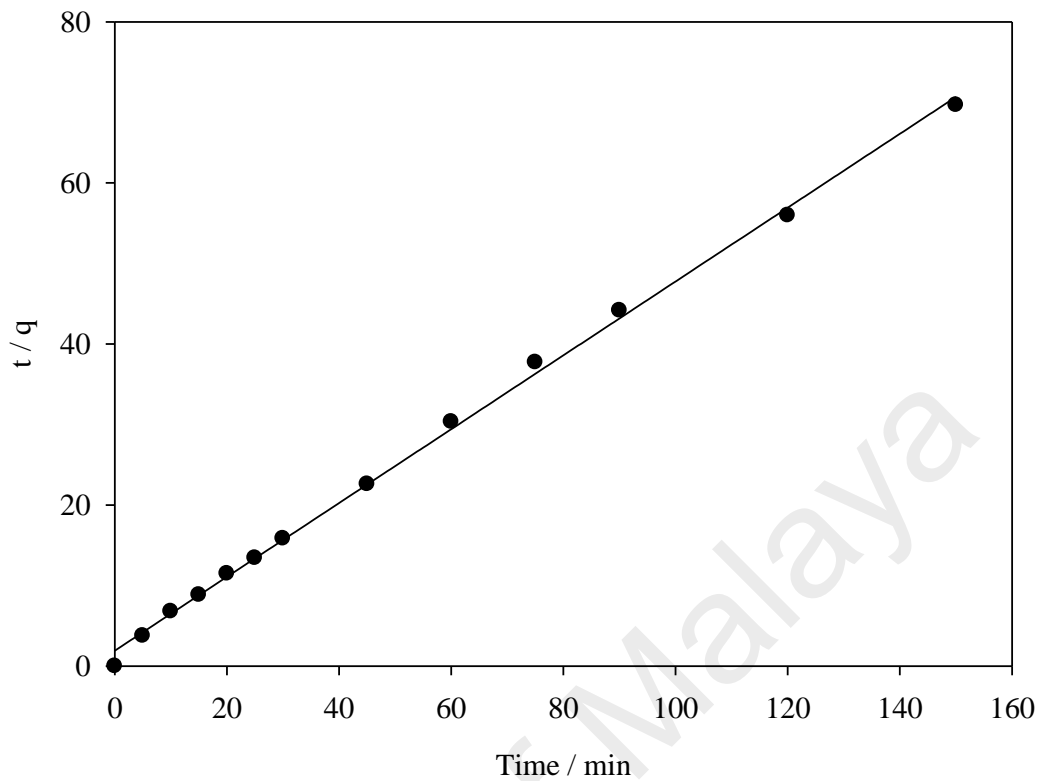


Figure 6.13: Pseudo-second-order kinetic model for As³⁺ adsorption on KB-CNTs surface

6.3.5 Isotherm study

Studying the equilibrium adsorption is crucial in the design of adsorption systems. Taking into consideration the optimum conditions obtained from the optimization study, 20 mg of adsorbents and pHs of 3.0 and 6 was used for KM-CNTs and KB-CNTs, respectively. 14 As³⁺ initial concentrations (1, 3, 5, 10, 15, 20, 25, 30, 35, 40, 45, 50, 55, and 60 mg/L) were employed to investigate the adsorption isotherm for each adsorbent. Langmuir and Freundlich isotherm models were applied for both adsorbents in this study. The linearized form of these models are described by Eq. 6.5 and Eq. 6.6.

$$\frac{C_e}{q_e} = \frac{1}{K_a Q_m} + \left(\frac{1}{Q_m}\right) * C_e \quad \dots\dots\dots (6.5)$$

$$\ln q_e = \ln K_F + \frac{1}{n} \ln C_e \quad \dots\dots\dots (6.6)$$

Where C_e is the initial equilibrium concentration and q_e is the amount of As^{3+} on the surface of the adsorbent. K_a and Q_m are the adsorption equilibrium constant and the maximum adsorption capacity, respectively. K_F and n are the isotherm constants for the Freundlich isotherm model.

Figure 6.14 and 6.15 show the plots for the Langmuir isotherm equation for KM-CNTs and KB-CNTs, respectively. Figure 6.16 and 6.17 show the plot of the Freundlich isotherm for KM-CNTs and KB-CNTs, respectively. The Freundlich model described the data derived from the adsorption of As^{3+} on KM-CNTs better than Langmuir model. The larger correlation coefficient observed in the Freundlich model indicates that the adsorption of As^{3+} occurs on a heterogeneous surface with interaction between adsorbed molecules with a nonuniform distribution of heat of sorption over the surface (Ghaedi, Hassanzadeh, & Kokhdan, 2011). Conversely, the Langmuir model described the data obtained from the As^{3+} sorption on KB-CNTs, which indicate a monolayer coverage of As^{3+} ions on the surface of the KB-CNTs (Langmuir, 1916). Table 6.6 lists the values of the isotherm constants for both Langmuir and Freundlich isotherms models, alongside the correlation coefficients for each model and the maximum adsorption capacity.

Table 6.6: Isotherm models parameters and comparison of adsorption capacity of other adsorbents

Adsorption Isotherm Model	Langmuir				Freundlich			Reference
Adsorbent	pH	q_m (mg/g)	K_L (l/mg)	R^2	n	K_f (mg/g)	R^2	
KM-CNTs	3	23.40	6.23	0.959	3.98	7.79	0.973	Present work
KB-CNTs	6	14.23	3.00	0.992	6.17	7.23	0.970	Present work
e-MWCNTs*	4	12.17	24.11	0.948	2.77	5.52	0.991	(Z. S. Veličković et al., 2013)
Fe-MCNTs**	8	4.00	1.35	0.996	3.24	2.09	0.987	(B. S. Tawabini et al., 2011)

* e-MWCNT refer to aminofunctionalized CNT, ** Fe-MCNTs refer to iron oxide modified CNT,

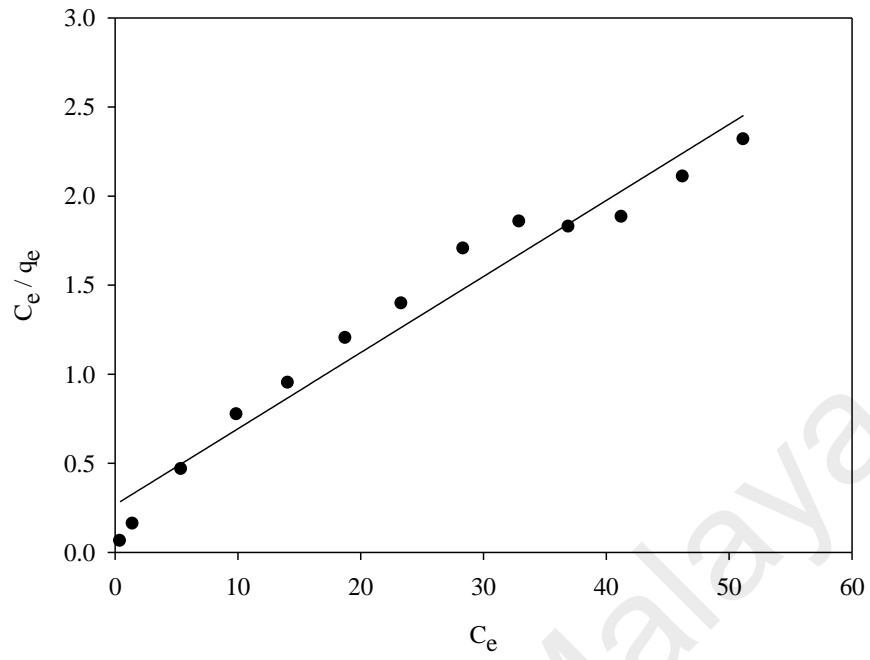


Figure 6.14: Linear form of Langmuir adsorption isotherm for As³⁺ on KM-CNTs surface

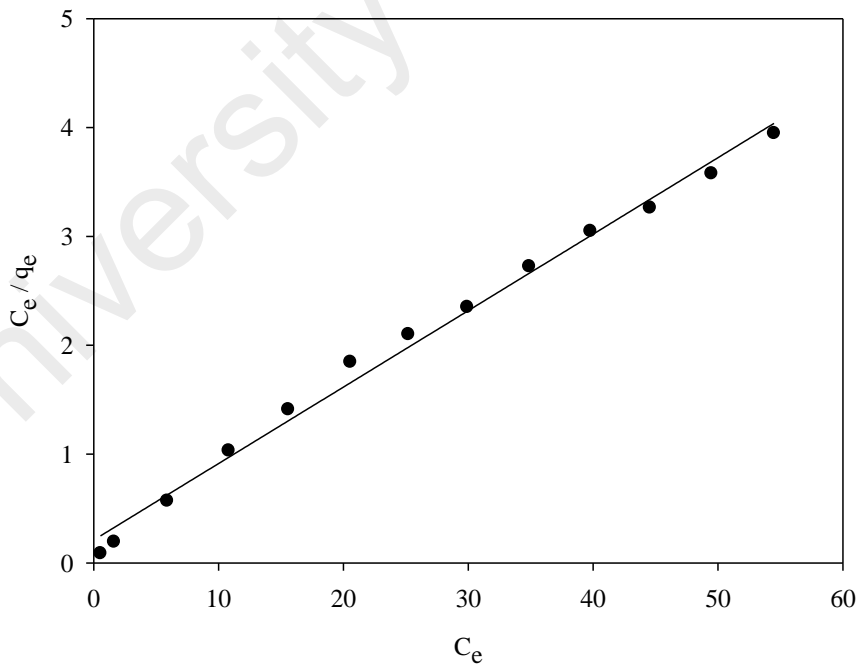


Figure 6.15: Linear form of Langmuir adsorption isotherm for As³⁺ on KB-CNTs surface

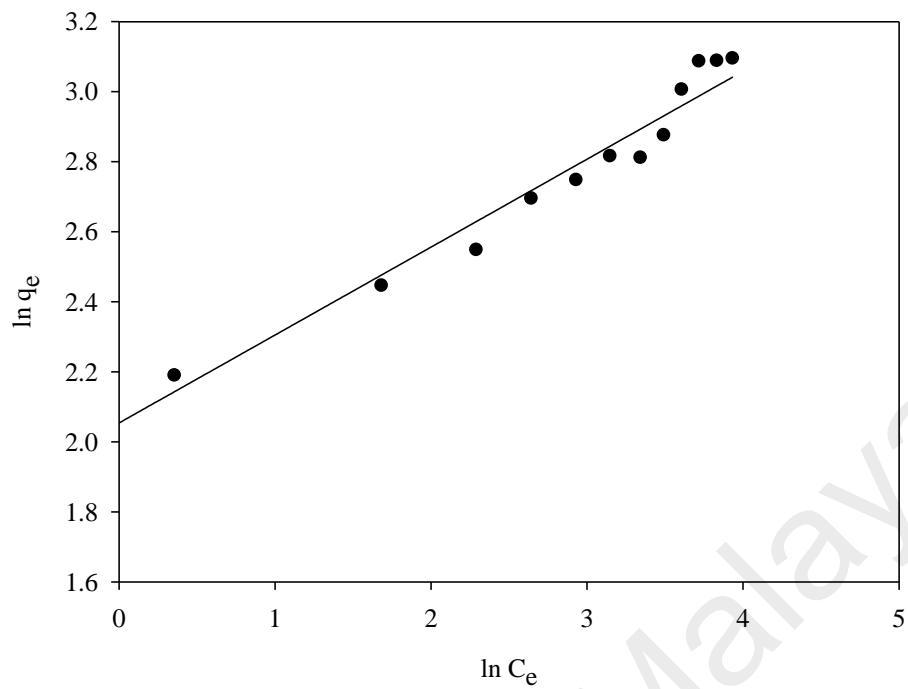


Figure 6.16: Linear form of Freundlich adsorption isotherm for As³⁺ on KM-CNTs surface

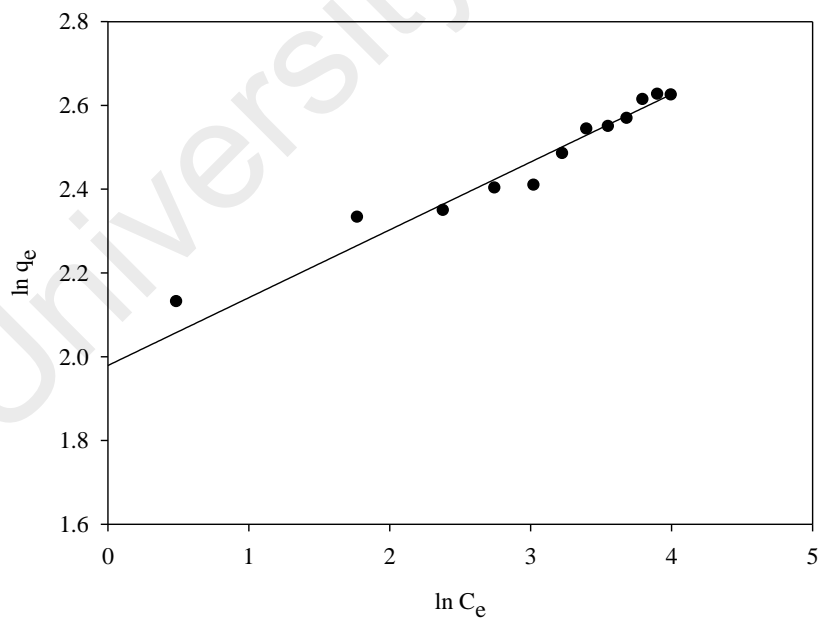


Figure 6.17: Linear form of Freundlich adsorption isotherm for As³⁺ on KB-CNTs surface

6.4 Summary

Novel adsorbents for As^{3+} were developed using two DESs systems as functionalization agents of CNTs. A screening study was conducted to select the best DES-CNTs adsorbents from each DESs systems. The new adsorbents were characterized using Raman spectroscopy, FTIR, XRD, TGA, Zeta potential, EDX, FESEM, and BET. The surface area increased significantly after functionalization with DESs. The removal conditions were optimized using RSM. Pseudo-second order kinetics describe the adsorption rate order for both adsorbents. Langmuir and Freundlich models best describe the isotherm of KB-CNTs and KM-CNTs, respectively. The maximum adsorption capacity observed in these experiments was 23.4 mg/g for KM-CNTs, which consists of CNTs functionalized with KMnO_4 and MTPB based DES.

University of Malaysia

CHAPTER 7: N,N-DIETHYLETHANOLAMMONIUM CHLORIDE BASED DES-FUNCTIONALIZED CARBON NANOTUBES FOR ARSENIC REMOVAL FROM AQUEOUS SOLUTION

7.1 Introduction

The presence of arsenic (As) in water, in any oxidation state form, is considered very harmful to humankind and other living organisms. The As contamination in Drinking water has been proposed to cause skin cancer and kidney cancers, and lung, bladder and other internal tumors, vascular diseases, and diabetes (Ihsanullah et al., 2016). The order of toxicities for arsenic species is as follows: arsenite (As^{3+}) > arsenate (As^{5+}) > monomethyl arsenic acid (MMA) > dimethyl arsenic acid (DMA) (Duffus, 2002). Water resources may be become contaminated by As either from natural deposits in the earth or through human activities (Black, 1999; Ihsanullah et al., 2016; Mandal & Suzuki, 2002). The maximum levels of As allow in drinking water is 10 $\mu\text{g/l}$ according to the World Health Organization (WHO) (Smedley & Kinniburgh, 2001; B. S. Tawabini et al., 2011). The contamination of As in water have been reduced using several chemical methods i.e. coagulation, precipitation, ion exchange, reverse osmosis, oxidation, and adsorption (Al-Mamun et al., 2009). However, these techniques have some limitations (Payne & Abdel-Fattah, 2005; Tuutijärvi et al., 2009). Therefore, the new alternative or modified technologies can be highly expected. Adsorption can be considered one of the most effective techniques for removal of As ions, since it is the best in term of separation for small amount of pollutant from large amounts of solution (Ali, 2012; Sheng et al., 2012). Various adsorbents i.e. Ferrihydrite (Raven, Jain, & Loepfert, 1998), Activated Alumina Grains (T.-F. Lin & Wu, 2001), Iron oxide uncoated sand (V. K. Gupta, Saini, & Jain, 2005), have been used to remove all forms of As ions for solution. These adsorbents still have some problems concerning the low adsorption capacity and difficulty of separating adsorbents from aqueous solutions. Carbon nanotubes (CNTs) have proven to be the excellent adsorbent

for many pollutant, including cadmium, zinc, lead, 1,2-dichlorobenzene, fluoride, and trihalomethanes (Ibrahim et al., 2016). However, the CNTs have many problems like solubility, aggregation, and difficulty of manipulation even though they have many extraordinary physicochemical properties. But CNTs have shown a great affinity for interaction with a variety of different compounds. Enhances CNTs surface with active functional groups to increase the adsorption capacity. However, functionalization with conventional agents can be ineffective or involve chemicals that are harmful for environment. Consequently, the new types of economical and environmentally friendly functionalization agents needed for many applications (M. Hayyan, Abo-Hamad, et al., 2015a; Martínez et al., 2003). Including As removal from aqueous solution (AlOmar, Alsaadi, Hayyan, Akib, & Hashim, 2016).

Due to the large amount of interest in the ionic liquids analogues, i.e. deep eutectic solvents (DESs), which were introduced as a cheaper replacement for developed ionic liquids (ILs) by Abbot et al. in 2003 (Andrew P. Abbott et al., 2003). they have been used in a large number of applications (E. L. Smith et al., 2014). Recently, ILs and DESs have been applied in many nanotechnology related fields, such as media for synthesis of nanoparticles, electrolyte for nanostructure sensors, and electrolyte for nanoparticle deposition (Abo-Hamad et al., 2015).

In this work, ammonium based DESs composed of N,N-diethylethanolammonium chloride (DAC), with glycerol (Gly) as hydrogen bond donor (HBD), are used as functionalization agents of CNTs. Subsequently, a novel DES/CNTs combination was utilized as an adsorbent of As^{3+} ions from water. The adsorbent was characterized using Raman spectroscopy, XRD diffraction, FTIR, and Zeta potential. An optimization study was performed using Response surface methodology (RSM) to optimize the removal

conditions for As^{3+} adsorption. Moreover, kinetics and isotherm studies were also performed at the potential optimal conditions.

7.2 Materials and methods

7.2.1 Chemicals and materials

MWCNTs with specifications of D 6-9 nm \times L 5 μm >95% (carbon) were supplied by SIGMA-ALDRICH. Glycerol, sulfuric acid (95%-97%), nitric acid (65%), potassium permanganate, sodium hydroxide pellets, and hydrochloric acid (36.5-38%) were also supplied by SIGMA-ALDRICH. N,N-diethyl ethanol ammonium chloride and As^{3+} 1000 mg/L standard solution were supplied by MERCK.

7.2.2 Synthesis of DES

To prepare DESs, DAC was mixed with Gly at a molar ratio of 1:2 using magnetic stirring at 400 rpm and 80 °C until the mixture became homogeneous solution. Later, all DESs were stored in well-sealed cups and placed in a desiccator to avoid humidity effects. The details of stability and physical properties of this DES were reported in our previous study (AlOmar, Hayyan, et al., 2016).

7.2.3 Oxidation and acidification of MWCNTs

Two types of conventional functionalization were applied to oxidize the pristine MWCNTs (P-CNTs) in order to prepare them for use in subsequent functionalization steps. The P-CNTs were dried overnight at 100°C. Later, the P-CNTs were sonicated in a solution of KMnO_4 , in order to produce KMnO_4 based CNTs (K-CNTs). The P-CNTs were refluxed with HNO_3 (65%) for 1h at 140°C to produce HNO_3 based CNTs (N-CNTs). All the functionalized CNTs were washed with distilled water and filtrated with a vacuum pump by several times using a PTIF 0.45 μm membrane. Functionalization by DES

Seven ml of DAC-based DES was added to 200 mg each of P-CNTs, K-CNTs, and N-CNTs and heated to 65°C with sonication for 3 hours to produce (PD-CNTs), (KD-CNTs), and (ND-CNTs), respectively. The mixture was then washed with distilled water by several times and filtered using a 0.45 µm membrane until reaching neutral water. Later, all CNTs samples were dried overnight under vacuum at 100°C and then kept in well-sealed cups in a desiccator. The prepared CNTs samples are listed in Table 1E (Appendix E).

7.2.4 Characterization of functionalized CNTs

High resolution nano-sized images were taken along with an energy-dispersive X-ray spectrometer (EDX) using a Field-Emission Scanning Electron Microscope (Quanta FEG 450, EDX-OXFORD). The surface modifications and functional groups were identified using Fourier transform infrared (FTIR) spectroscopy. Raman spectroscopy (Renishaw System 2000 Raman Spectrometer) was used to obtain Raman shift spectra for all adsorbents to evaluate the degree of functionalization. The structure phases were analyzed using an X-ray powder diffraction (XRD) Shimadzu XRD 6000XRD. A fully Automated Gas Sorption System (micromeritics ASAP2020, TRISTAR II 3020 Kr) was used to study the surface area of the selected samples based on Brunauer-Emmett-Teller (BET) method. Furthermore, the surface charge was measured by conducting zeta potential experiments using a Zetasizer (Malvern, UK). The arsenic concentration was measured using Inductive Coupled Plasma (ICP-OES) with an Optima 7000DV PerkinElmer®.

7.2.5 Adsorption studies

Primary, batch adsorption experiments were carried out in 250 ml flasks. Two sets of stock solution were prepared at pH 2.7 and pH 6.0. Next, 10 mg of P-CNTs, K-CNTs, N-CNTs, PD-CNTs, KD-CNTs, and ND-CNTs were added to 50 ml of As³⁺ stock solution with a concentration of 5 mg/l. The flasks were agitated at 180 rpm for 30 min

at room temperature. The adsorbent with the highest removal % was chosen for further study.

7.3 Results and discussion

The results obtained from the primary screening show that KD-CNTs recorded the highest removal percentage at pH 6.0 and this effect increased significantly by increasing pH. The removal percentage of As^{3+} by each adsorbent are listed in Table 7.1.

Table 7.1: Screening study for the removal of As^{3+}

Adsorbent		P-CNTs	K-CNTs	N-CNTs	D-CNTs	KD-CNTs	ND-CNTs
Removal (%)	pH 2.7	0	19.7	0	0	12.29	0
	pH 6.0	0	8.3	0	0	33.99	0

7.3.1 Characterization of the adsorbent

Knowing the zeta potential of nanoparticles is essential to understanding the charge of the surface and the long term stability of the nanoparticle suspension in aqueous solution. Absolute values can be used to quantitatively compare the various stabilities of particle dispersions (Z. Sun et al., 2008). It is well known that there are many factors affecting zeta potential measurements, including particle surface charges, pH, conductivity, ion concentration, and temperature (Simate et al., 2012). Herein, 2.5 mg of each adsorbent was dispersed in 5 ml of deionized water for zeta potential measurement. The absolute zeta potential value increased from 5.5 to -45.81 mV for P-CNTs and K-CNTs, respectively (AlOmar, Alsaadi, Hayyan, Akib, & Hashim, 2016). High zeta potential value is an indication of the electro kinetical stability of the particles, where those with a low zeta potential tend to coagulate (B. S. Tawabini et al., 2011). By addition of oxygen-containing functional groups, such as carbonyl groups and aliphatic carboxylic acids surface, on the surface of CNTs by functionalization with $KMnO_4$ or acid refluxing, the surface electronegativity increased. Consequently, the hydrophilicity of the adsorbent

increased, and that is reflected in the adsorption mechanism. Furthermore, functionalization with DAC based DES decreased the absolute zeta potential value to -37.6 mV. This reduction may be due to the reduction of oxygen functional groups through formation of new groups.

7.3.1.1 Raman spectroscopy

Raman spectroscopy is a very valuable technique for the characterization of carbon-based nanomaterials. Herein, Raman spectroscopy was used to analyze P-CNTs, K-CNTs, and KD-CNTs. Figure 7.1 shows the two major characteristic bands, namely the G-band, which usually detected at 1500-1600 cm^{-1} , and the D-band at 1350 cm^{-1} . The D band is attributed to the presence of amorphous or disordered carbon in the CNT samples, which is caused by the sp^3 -hybridized carbon atoms in the nanotube sidewalls (Bahr et al., 2001; Datsyuk et al., 2008). The G-band corresponds to the movement in opposite directions of two neighboring carbon atoms in a graphite sheet. (Hiura et al., 1993) The third characteristic band, known for carbon based nanostructure, is the D', which appears as weak shoulder of the G-band at higher frequencies and is considered to be a double resonance feature originating from disorder and defects. It worth mentioning that the D' band is undetectable in pure graphite. However, it can be observed in intercalated graphite and MWCNTs (C. S. Kumar, 2012). The degree of functionalization can be determined by comparing the intensity of the D-band (I_D) to that of the G-band (I_G) (Aitchison et al., 2007). In this study, the I_D/I_G ratio increased significantly with KMnO_4 functionalization, and also after the sequence functionalization step with DAC-based DES. Table 7.2 lists the values of I_D/I_G for each P-CNTs, K-CNTs, and KD-CNTs.

Table 7.2: I_D/I_G intensity ratios of each adsorbent

sample	P-CNTs	K-CNTs	KD-CNTs
I_D/I_G	1.1	1.16	1.2

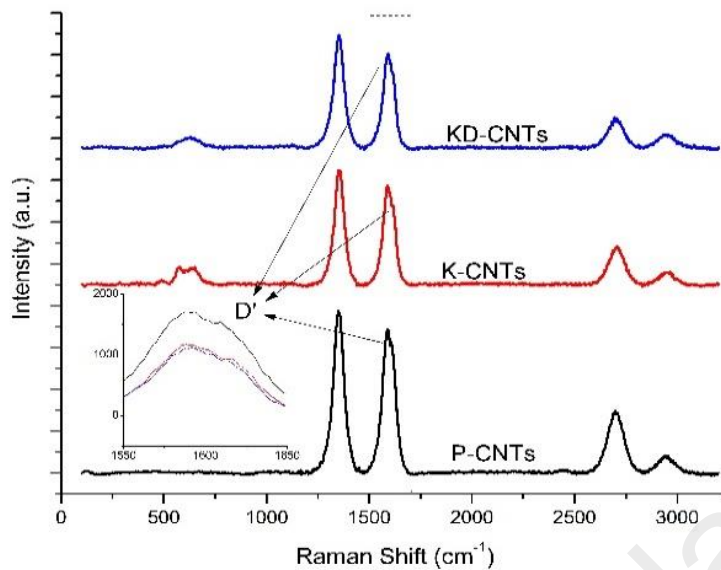


Figure 7.1: Raman spectroscopy of P-CNTs, K-CNTs and KD-CNTs

7.3.1.2 XRD analysis

Figure 7.2 shows the XRD patterns of P-CNTs, K-CNTs, and KD-CNTs. (002) and (001), representing the hexagonal graphite structure and the concentric cylinder structure, respectively, are located at 2θ around 26° and 42° in P-CNTs patterns (D. Zhang et al., 2005). The (002) was reduced in the K-CNTs pattern due to the extensive presence of (MnO_2), which indicated that deposition of MnO_2 destroys the hexagonal graphite structure of CNTs by wrapping the CNTs into non-stoichiometric, amorphous shapes (S.-G. Wang et al., 2007). The DES functionalization has increased the wrapping around the CNT edges.

7.3.1.3 FTIR analysis

Figure 7.3 shows the FTIR spectrum for P-CNTs, K-CNTs, and KD-CNTs. After functionalization with DAC based DES, the results demonstrate the detection of N-H stretches in the range of 3207 cm^{-1} and stretches for aromatic NH_2 located at 3445 cm^{-1} ,

which overlapped with the O-H functional group (B. C. Smith, 1998). In addition, the presence of C-Cl bonds may overlap with other CO groups between 600 and 700 cm^{-1} . Meanwhile the presence of O-H in K-CNTs is located at 3478 cm^{-1} . The presence of new functional groups after functionalization with DES provides various adsorption sites and increases the adsorption capacity for As^{+3} .

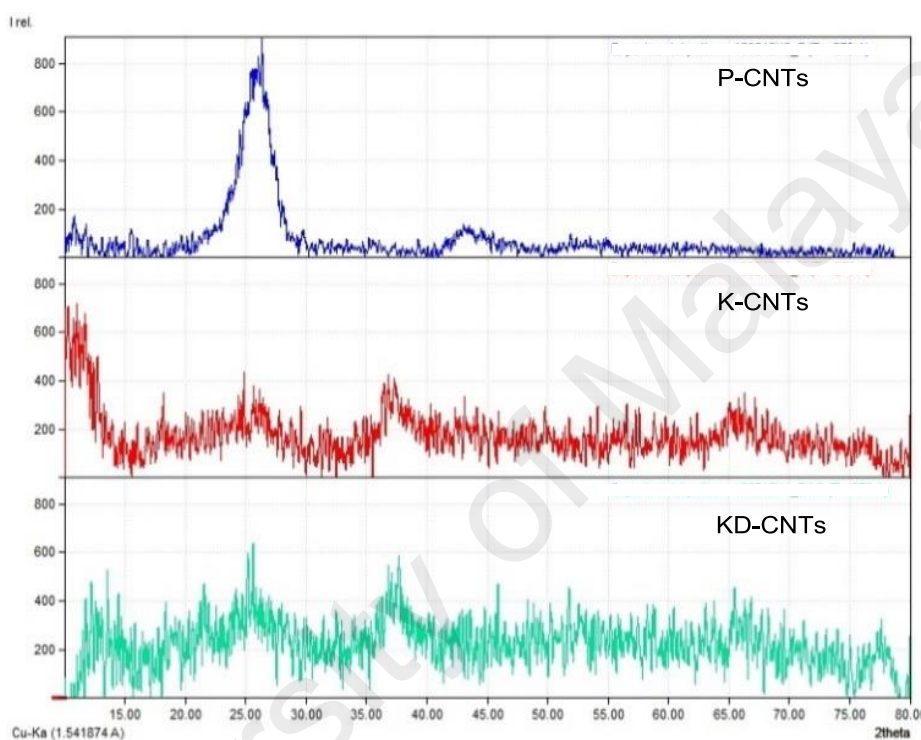


Figure 7.2: XRD patterns of P-CNTs, K-CNTs and KKD-CNTs

7.3.1.4 FESEM and EDX

Figure 7.4 shows the FESEM images for P-CNTs, K-CNTs, and KD-CNTs. The presence of MnO_2 is not observable in splatted powder or the crystal form, but is embedded within the CNT surface structure, as we can clearly observe in the FESEM images. On the other hand, EDX studies were conducted for KD-CNTs after As^{3+} adsorption. The presence of Mn is observable and weight % complies with the results obtained from the TGA analysis. In addition, a traceable amount of As^{3+} , Cl^- , O, and N were also observed in the EDX spectrum. Figure 1E shows the EDX spectrum of KD-CNTs after adsorption.

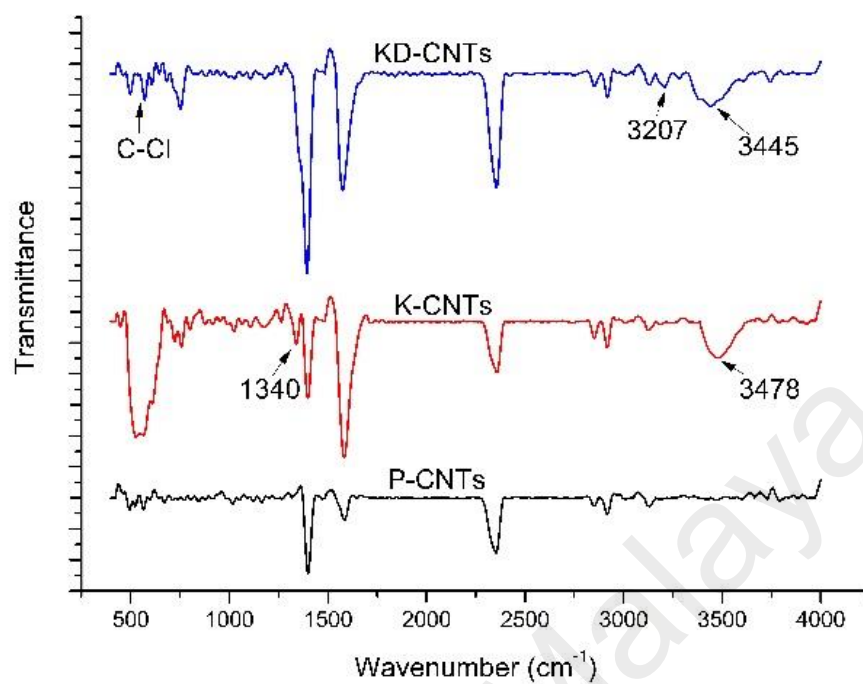


Figure 7.3: FTIR spectrum for each adsorbent

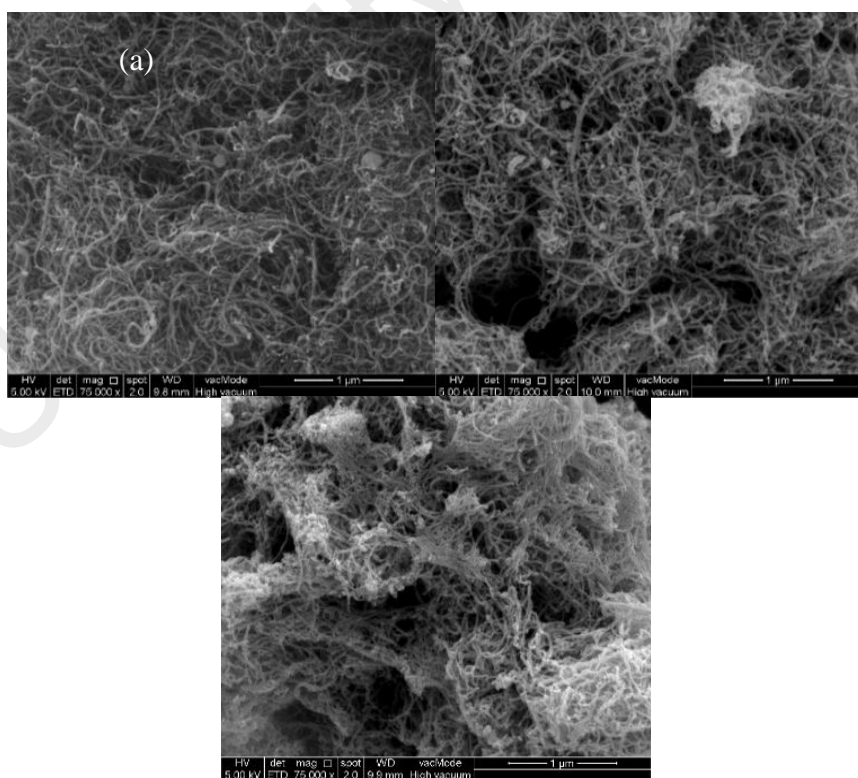


Figure 7.4: FESEM images of a) P-CNTs, b) K-CNTs and c) KD-CNTs

7.3.1.5 BET surface area

BET isotherm studies were conducted for P-CNTs, K-CNTs, and KD-CNTs. The results showed that the surface area increased after each functionalization step, due to the functional groups attached to the surface of the adsorbent. Table 7.3 lists the BET surface areas, total pore volumes, and the average pore diameter. The pore volumes decreased after functionalization by KMnO_4 , which may be attributed to the presence of MnO_2 partially occupying the space between the CNT surfaces after being embedded within the external surface layers. But the initial pore volume increased again after functionalization with DES, resulting in additional distance gained through charge repulsion from the presence of functional groups with similar electrostatic charges.

Table 7.3: BET surface area and pore volume and diameter of all adsorbents

Property	P-CNTs	K-CNTs	KD-CNTs
BET Surface Area (m^2/g)	123.543	158.934	200.583
Total pore volume (cm^3/g)	0.620	0.453	0.648
Average Pore Diameter (\AA)	20.499	114.127	129.411

7.3.2 Optimization studies

An estimation of the regression empirical relationship was performed to describe removal percentage and adsorption capacity of As^{3+} using Response surface methodology (RSM). Central composite design (CCD) was employed using the Design Expert V7.0 software package. The effects and interactions of three parameters were investigated in this study, specifically pH (3 to 8), contact time (5 to 55 min), and adsorbent dosage (5 to 20 mg). The initial concentration and the agitation speed were fixed to 1 mg/l and 180 rpm, respectively. Table 2E lists the design of the experimental runs in terms of the actual parameters, alongside the removal percentage response and the adsorption capacity response.

Analysis of variance (ANOVA) modeling for removal response and adsorption capacity of KD-CNTs response with both models indicates significant due to the Model F-values, which were 44.81 and 64.30, respectively. There is only a 0.01% and 0.28% chance that a "Model F-Value" this large could occur due to noise for each response, respectively. Eq. 7.1 and Eq. 7.2 described the removal of As³⁺ and the adsorption capacity of the KD-CNTs models, respectively. Table 3E and Table 4E listed the P-values, F-values, and the square mean for both removal and adsorption capacity. Figure 7.5 shows the theoretical values plotted versus the experimental values for the removal percentage and adsorption capacity of KD-CNTs. The R² were 0.9782 and 0.9948 for each model, respectively. It is clear that the theoretical values predicted by the models developed in this study were in close agreement with the experimental values, indicating that both models have successfully created correlation between the process variables.

$$As^{3+} \text{ removal} = 41.81 + 0.45A + 17.17B + 29.44C + 1.08AB + 2.36AC + 5.81BC \quad (7.1)$$

$$KD - CNTs \text{ (Adsorption capacity)} = 0.36 - 0.34A + 0.49B + 0.98C + 0.015AB + 0.37AC - 0.17BC + 0.44A^2 - 0.72C^2 - 0.57A^2C \quad (7.2)$$

Where A, B, C refer to pH, contact time, and adsorbent dosage, respectively.

Generally, increasing pH of the solution lead to enhance the surface charge of the adsorbent, electrical double layer and the affinity of metal ion to form seeds of hydroxide which subjected to electrostatic attraction to the surface of the adsorbent. Figure 6 illustrates the effects of pH on removal percentage, meanwhile, Figures 7 and 8 show 3D response surfaces to represent the interaction effect between contact time and adsorbent dosage with pH, respectively, on the adsorption capacity. These observations demonstrate that there is a significant effect for pH on adsorption capacity. By fixing the adsorbent

dosage to the maximum, the adsorption capacity will increase with increasing pH until reaching the optimum pH, where it starts to decrease. On the other hand, by fixing the contact time to the maximum, the interaction of adsorbent dosage and pH shows that, at low adsorbent dosage, the pH has a significant effect on the adsorption capacity. At high adsorbent dosage, the effect of pH decreased and almost vanished.

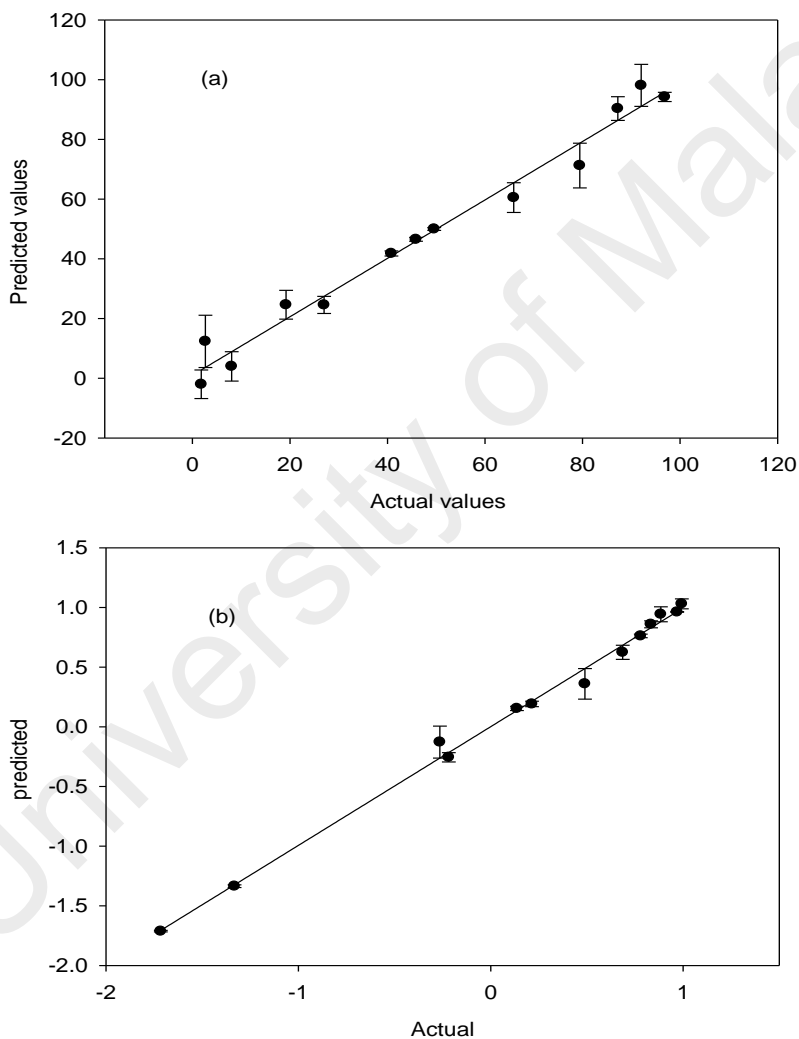


Figure 7.5: Theoretical values vs actual values for a) removal response and b) adsorption capacity response

The optimization functions were set to control the software selection for the optimum adsorption process conditions values, specifically pH, contact time, and adsorbent dosage. The adsorption variables values were set to be in range. Meanwhile, the two responses, removal percentage of As^{3+} and adsorption capacity of KD-CNTs, were set to the maximum values. Several potential solutions for optimum conditions for As^{3+} adsorption were given by the statistical analysis of CCD. Based on this analysis, the optimum conditions were found to be pH 6.0, adsorbent dosage of 20 mg, and contact time of 55 min, with a desirability of 0.986.

Design-Expert® Software

Rmoval



X1 = A: pH

X2 = B: contact time

Actual Factor

C: dose = 20.00

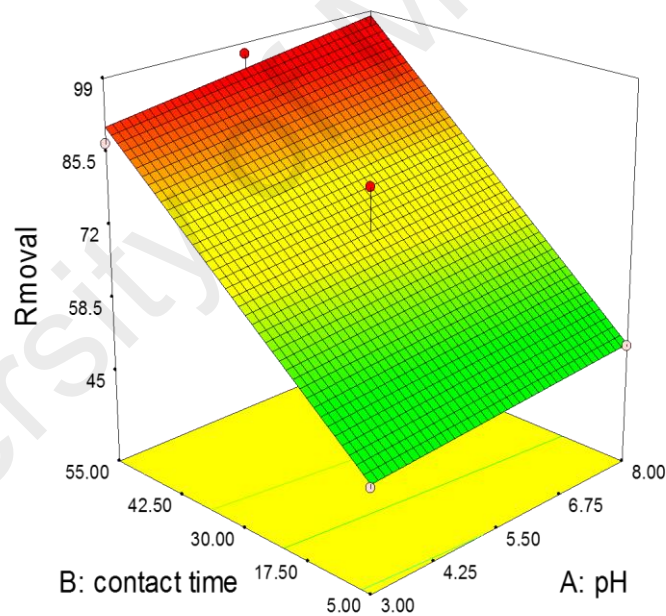


Figure 7.6: pH and contact time effect on the removal of As^{3+}

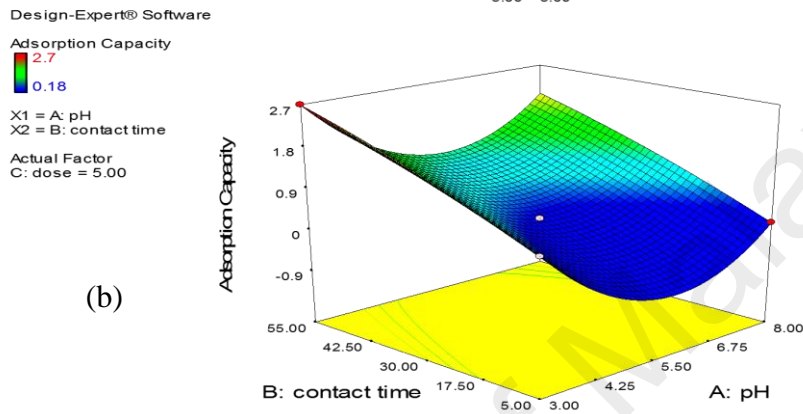
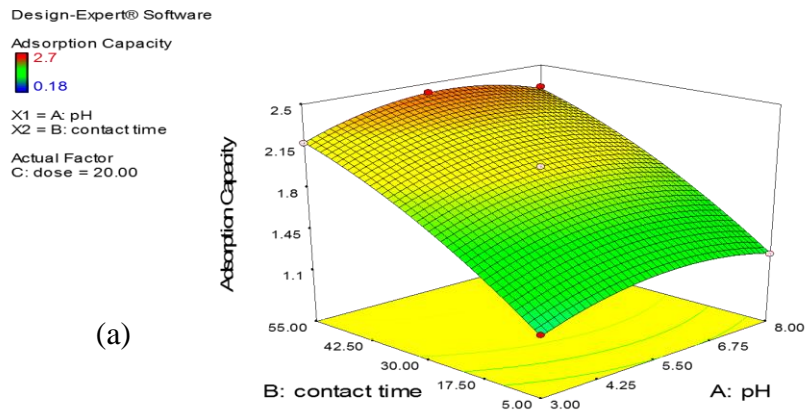


Figure 7.7: The effect of pH and contact time on the adsorption capacity of KD-CNTs at a) maximum adsorbent dosage and b) minimum adsorbent dosage

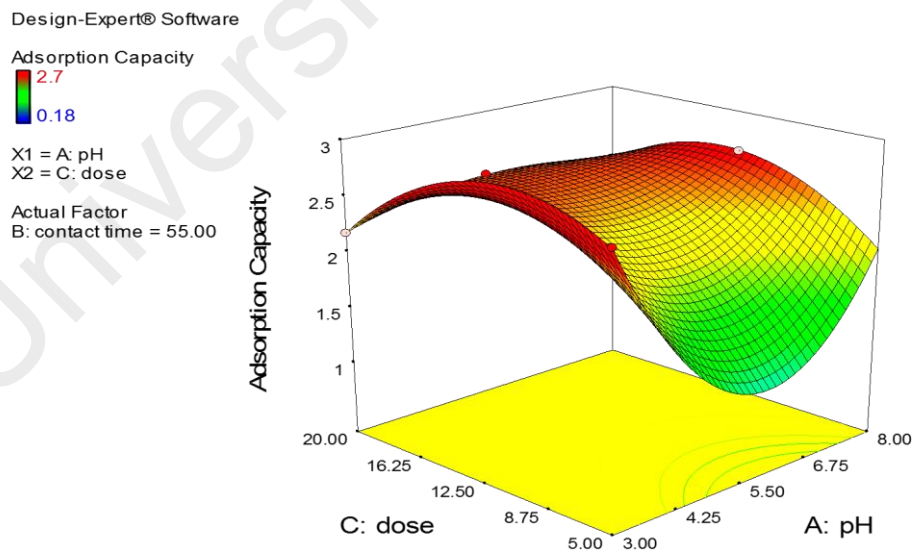


Figure 7.8: The effect of pH and adsorbent dosage on the adsorption capacity of KD-CNTs at the optimum contact time

7.3.3 Kinetics study

Adsorption kinetics are considered to be one of the most essential characteristics overseeing the rate of ions transferred from the solute to the adsorbent surface, which, furthermore, represents the efficiency of the adsorption process and, hence, determines its potential applications. Pseudo-first-order and pseudo-second-order models were applied to investigate the adsorption kinetics of As^{3+} on the surface of KD-CNTs. The linear form (Eq. 7.3) of the pseudo-first-order model described by Lagergren was used to plot the kinetics.

$$\ln(q_e - q_t) = \ln q_e - K_1 t \quad (7.3)$$

Where k_1 and q_e are the slope and intercept calculated by plotting, $\ln(q_e - q_t)$ vs *time* (t), respectively. a pseudo-second-order model was also used to study the adsorption kinetics, as described in Eq. 7.4.

$$\frac{t}{q_t} = \frac{1}{K_2 q_e^2} + \frac{1}{q_e} t \quad (7.4)$$

Where q_e is calculated as $1/(\text{slope})$ and k_2 is calculated as $(\text{Slope})^2/\text{intercept}$. The slope and the intercept were determined from the plot of t/q_t vs t . In addition, q_e and q_t refer to the adsorption uptake at equilibrium and at time t , respectively.

The conditions applied during kinetic studies were those obtained from the optimization study, i.e. 1 mg/l initial concentration, 20 mg adsorbent dosage, pH 6.0, and agitation speed of 180 rpm. The contact time was 5.5 hours to ensure that the reactions reached equilibrium. Figure 7.9 shows the plot of pseudo-second-order kinetics model. The values of correlation coefficient R^2 of the data sets were considered as indications of conformity between the experimental data and the corresponding values, as predicted by each model. Herein, the pseudo-second order rate equation describes the adsorption

kinetics of As^{3+} onto KD-CNTs with an R^2 of 0.991. Meanwhile, the pseudo-first-order kinetics model did not fit the adsorption data, since the R^2 was 0.604. The results of the kinetics studies indicate that both the adsorbent and the adsorbate concentrations are involved in the rate determining step, which indicates that the rate-limiting step may be chemisorption. This agreed with observations from many CNTs-based adsorbent systems (Gong et al., 2014; Sheng et al., 2012; B. S. Tawabini et al., 2011; Z. S. Veličković et al., 2013).

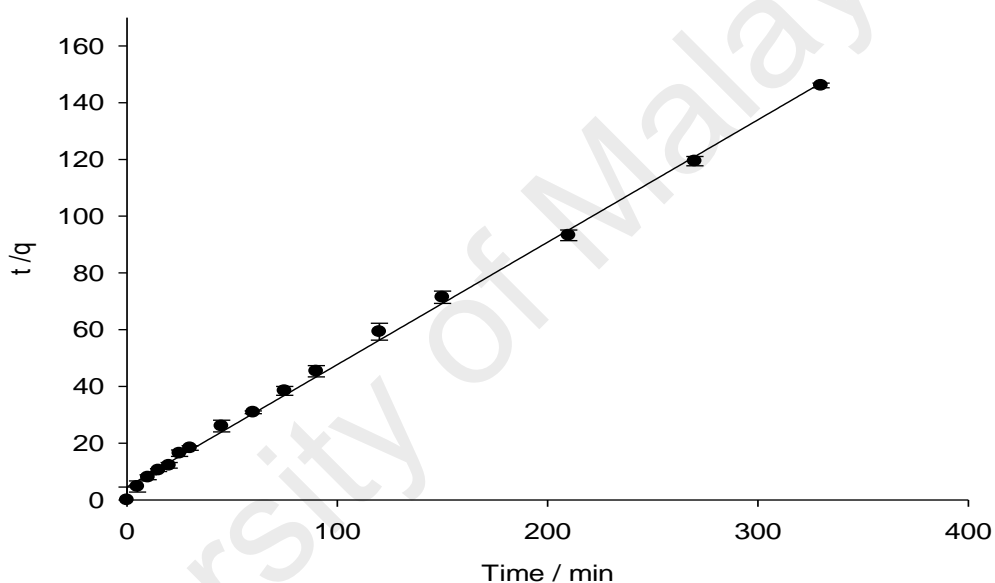


Figure 7.9: Plot of pseudo-second-order kinetics model

7.3.4 Isotherm study

Isotherm studies are essential for any novel adsorbents to investigate the adsorption mechanism, which can be used for future design purposes. Langmuir and Freundlich isotherms adsorption models are the most common isotherm models, which quantify the amount of metal ion adsorbed at equilibrium (q_e) and the solution concentration at equilibrium (C_e) (X. Liu et al., 2009). Herein, 14 As^{3+} initial concentrations (1, 3, 5, 10, 15, 20, 25, 30, 35, 40, 45, 50, 55, and 60 mg/L) were employed to investigate the

adsorption isotherm of KD-CNTs. The adsorbent dosage and pH were used at the values indicated in the optimization study.

The Langmuir adsorption isotherm can be described in the linearized form (Eq. 7.5) (Langmuir, 1916).

$$\frac{C_e}{q_e} = \frac{1}{K_a Q_m} + \left(\frac{1}{Q_m}\right) * C_e \quad (7.5)$$

Where C_e is the initial equilibrium concentration, and q_e is the amount of metal ions adsorbed on the surface of the adsorbent. K_a and Q_m are the adsorption equilibrium constant and the maximum adsorption capacity, respectively.

The Freundlich model is described by a linearized form (Eq. 7.6). (Al Mamun, Ahmed, AlKhatib, Jameel, & AlSaadi, 2015; Freundlich & Hatfield, 1926)

$$\ln q_e = \ln K_F + \frac{1}{n} \ln C_e \quad (7.6)$$

Where q_e is the uptake of the adsorbent and K_F and n are isotherm constants.

The Langmuir isotherm model describes the adsorption of As^{3+} onto the surface of KD-CNTs very well, as the correlation coefficients R^2 were found to be 0.99, which indicates a monolayer coverage of As^{3+} ions on the surface of the KD-CNTs. (Langmuir, 1916) On the other hand, the corresponding R^2 for the Freundlich isotherm model was 0.95. Figures 7.10 and 7.11 show plots of the Langmuir and Freundlich isotherm models, respectively. Moreover, Table 7.4 lists the values of the isotherm constants for both models, R^2 , the maximum adsorption capacity, and a comparison of the maximum adsorption capacity with previously published results.

Table 7.4: Isotherm models parameters and comparison of adsorption capacity of other adsorbents

Adsorption Isotherm Model		Langmuir			Freundlich			Reference
Adsorbent	pH	qm (mg/g)	KL (l/mg)	R ²	n	Kf (mg/g)	R ²	
KD-CNTs	6	17.1	4.0	0.995	3.3	5.4	0.956	Present work (Z. S. Veličković et al., 2013)
e-MWCNTs*	4	12.1	24.1	0.948	2.8	5.5	0.991	
Fe-MCNTs**	8	4.0	1.3	0.996	3.2	2.0	0.987	(B. S. Tawabini et al., 2011)

*e-MWCNT refer to aminofunctionalized CNT, **Fe-MCNTs refer to iron oxide modified CNT

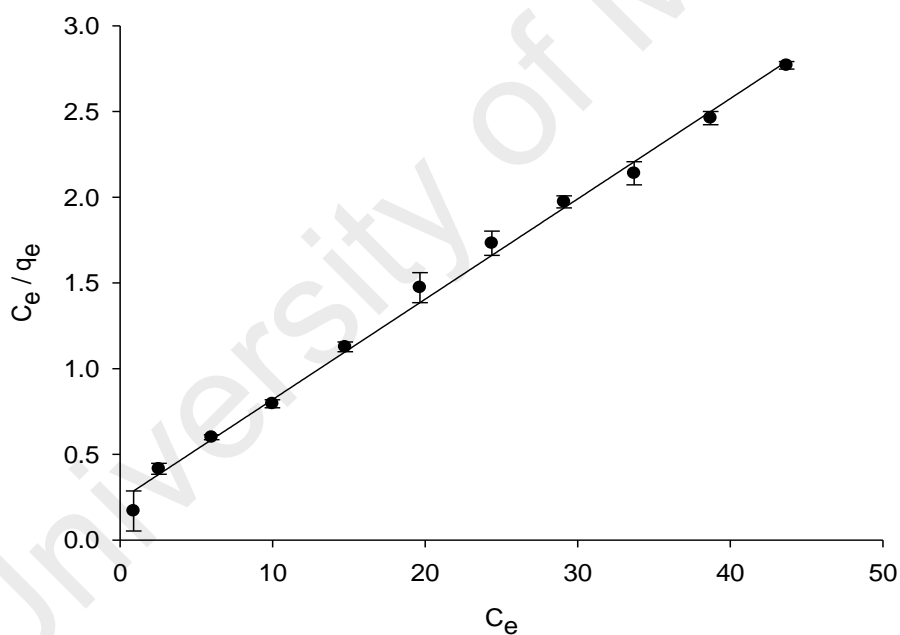


Figure 7.10: Linear form of Langmuir isotherm model

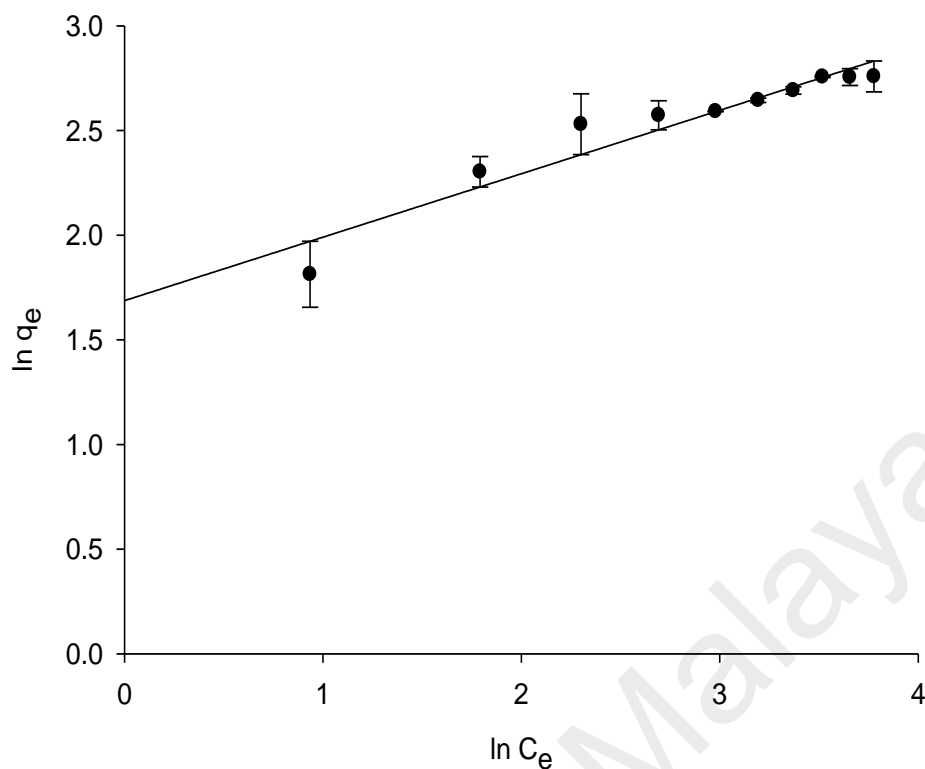


Figure 7.11: Linear form of Freundlich isotherm model

7.4 Summary

N,N-diethyl ethanol ammonium chloride based DES was introduced as a functionalization agent of CNTs . Raman spectroscopy, FTIR, XED, zeta potential, FESEM, and EDX were used to characterize the new adsorbent. Later, a novel DES-CNTs combination was used as an As^{3+} adsorbent. The removal conditions were optimized using RSM. A pseudo-second order equation describes the adsorption rate order. The maximum adsorption capacity of CNTs functionalized with $KMnO_4$ and DAC-DES was 17.085 mg/g and isotherm data fitted well with the Langmuir isotherm model.

CHAPTER 8: ALLYL TRIPHENYL PHOSPHONIUM BROMIDE BASED DES-FUNCTIONALIZED CARBON NANOTUBES FOR THE REMOVAL OF MERCURY FROM WATER

8.1 Introduction

Mercury (Hg) is a heavy metal which exists in liquid or vapour phase at room temperature. It is considered to be one of the most toxic element in nature. It mainly affects the neurologic, gastrointestinal (GI), and renal organ systems. Hg can be found in three forms, specifically metallic element, organic salt, and inorganic salt (Goldman et al., 2001). This element also exists in seawater, fresh water, and soil (Martha H. Keating, December 1997). It is extremely hazardous, even at low concentrations, and hence the maximum allowable concentration of Hg in water, according to the World Health Organization (WHO), is $1 \mu\text{g L}^{-1}$ (Mohan et al., 2001),

Different techniques have been utilized to decrease Hg concentrations in water. Examples include solvent extraction, precipitation, ion-exchange, reverse osmosis, membrane separation, coagulation, and photoreduction. However, most of these methods require either high-energy or a large quantities of chemicals (F.-S. Zhang et al., 2005). Adsorption processes have been commonly applied in industrial applications, and are consequently the most studied technique for Hg removal from water (Chiarle et al., 2000).

Carbon nanotubes (CNTs) have been shown to be an excellent adsorbent for many pollutants (Ibrahim et al., 2016), including cadmium (Ruthiraan et al., 2015), zinc (N. M. Mubarak et al., 2013), lead (Y.-H. Li et al., 2002), copper (N. M. Mubarak et al., 2015), 1,2-dichlorobenzene (Peng et al., 2003), fluoride (Y.-H. Li, Wang, Zhang, et al., 2003), and trihalomethanes (C. Lu et al., 2005). However, despite all the extraordinary physicochemical properties of CNTs, they have many flaws with regards to solubility, aggregation, and difficulty of manipulation. On the other hand, CNTs have shown a great

affinity for interaction with different compounds (Andrews et al., 2002; Hirsch & Vostrowsky, 2005; Ihsanullah et al., 2016; T. Lin et al., 2003; N. M. Mubarak et al., 2014; Y.-P. Sun et al., 2002) .. Consequently, the need for new types of economical and environmentally friendly functionalization agents is crucial in many applications (M. Hayyan, Abo-Hamad, et al., 2015a; Martínez et al., 2003).

Recently, deep eutectic solvents (DESs) have gain great interest, owing to their involvement in many applications (E. L. Smith et al., 2014). DESs are involved in nanotechnology through many approaches, such as media for synthesis of nanoparticles (Chakrabarti et al., 2015; F. Chen et al., 2013; Jia et al., 2015; Mohammad Karimi et al., 2016; Xiong et al., 2015; Xu et al., 2016), electrolyte in nanostructure sensors (Zheng et al., 2014), and electrolyte in nanoparticle deposition (Andrew P. Abbott et al., 2009; Andrew P. Abbott et al., 2012; C. Gu & J. Tu, 2011; X. Guo et al., 2014; Renjith et al., 2014; Wei, Fan, Tian, et al., 2012; Wei, Fan, Wang, et al., 2012; Wei et al., 2013; You et al., 2012).

In this work, we introduce a novel Hg^{2+} adsorbent based on DES-functionalized CNTs. Allyl triphenyl phosphonium bromide (ATPB) based DES was successfully synthesised by using glycerol (Gly) as the hydrogen bond donor (HBD). Subsequently, the novel DES/CNT combination was characterized using Raman spectroscopy, XRD diffraction, FTIR, FESEM, TEM, EDX, TGA, BET surface area, and zeta potential. An optimization study was performed using Response surface methodology (RSM) to optimize the removal conditions for Hg^{2+} adsorption. Moreover, kinetics and isotherm studies were also performed according at the potential optimal conditions.

8.2 Experiment

8.2.1 Chemicals and materials

MWCNTs with specifications of D×L 6-9 nm × 5 μm >95% (carbon) were supplied by SIGMA-ALDRICH. Gly, nitric acid (65%), potassium permanganate, sodium hydroxide pellets, and hydrochloric acid (36.5-38%) were also supplied by SIGMA-ALDRICH. ATPB and 1000 mg L⁻¹ mercury standard solution was supplied by MERCK.

8.2.2 Functionalization of CNTs

Two types of primary oxidation were performed to oxidize the surface of the pristine CNTs (P-CNTs). The first involved sonication with KMnO₄ for 2 h at 65 °C (AlSaadi et al., 2016). The resulting oxidized CNTs are referred to as K-CNTs in this study. The second method involved refluxing with HNO₃ (65%) for 1 h at 140 °C, and the resulted acidified CNTs are referred to as N-CNTs in this study.

The DESs were synthesized by mixing ATPB with Gly (HBD) using magnetic stirring at 400 rpm and 80 °C until the DES became homogeneous liquid without any visual precipitate. The details of synthesis, characterization, and choosing of molar ration is based on our previous study (AlOmar, Hayyan, et al., 2016). Next, functionalization with DESs was performed by sonicating 200 mg of P-CNTs, K-CNTs, and N-CNTs separately with 7 ml of DES for 3 h at 65 °C. The resulting functionalized CNTs are referred to as PA-CNTs, KA-CNTs, and NA-CNTs, respectively. It should be noted that after each functionalization step, the functionalized CNTs were repeatedly washed and filtered using a vacuum pump and a PTFE 0.45 μm membrane with distilled water until the filtrate water pH was neutral.

8.2.3 Characterization of functionalized CNTs

To obtain Raman shift spectra, all adsorbents were characterized using Raman spectroscopy (Renishaw System 2000 Raman Spectrometer). Fourier transform infrared

(FTIR) spectroscopy, via a PerkinElmer® FTIR spectrometer, was used to study the surface modifications and functional groups that resulted from the functionalization processes. The structure phases were analyzed using an X-ray powder diffraction (XRD) Shimadzu XRD 6000. Furthermore, the surface charge was measured by conducting zeta potential tests using a Zetasizer (Malvern, UK). A fully Automated Gas Sorption System (micromeritics ASAP2020, TRISTAR II 3020 Kr) was used to study the selected samples surface area, based on the method of Brunauer-Emmett-Teller (BET). A Field-Emission Scanning Electron Microscope (Quanta FEG 450, EDX-OXFORD) was used to obtain high resolution nano-sized images for studying the morphology of all selected samples, along with an energy-dispersive X-ray spectrometer (EDX). The functionalization effect on the CNTs layers was explored using Transmission electron microscopy (TEM). Finally, the effect of thermal oxidation was investigated using thermogravimetric analysis (TGA) and differential thermogravimetry (DTG) with a Thermal Analyzer (STA-6000, PerkinElmer®).

8.2.4 Adsorption experiments

Initially, 10 mg of P-CNTs, K-CNTs, N-CNTs, PA-CNTs, KA-CNTs and NA-CNTs were individually added to 50 ml of Hg^{2+} stock solution at a concentration of 5 mg L^{-1} , in a 250 ml flask. The screening study was carried out at two pHs, 2.0 and 6. The flasks were placed in a mechanical shaker system for 30 min at room temperature at a shaking speed of 180 rpm. The adsorbent with the highest removal percentage was chosen for further studies.

8.3 Result and discussion

Figure 8.1 plots the removal percentage of each adsorbent according to the primary screening study. The results demonstrated that functionalization with ATPB-based DES significantly increases the removal percentage at both pH (2.0 and 6.0). The removal

percentage increased with increasing pH, indicating that removal may be pH dependent.

KA-CNTs achieve the highest removal percentage compared to the other adsorbent.

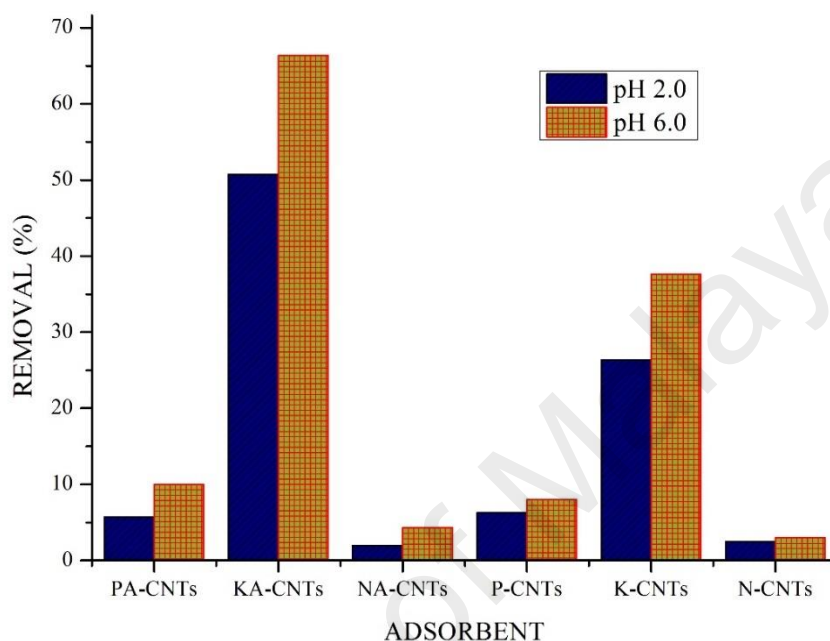


Figure 8.1: Screening study for all adsorbents

8.3.1 Characterization of DES-functionalized CNTs

Figure 8.2 (a, b, and c) show the FESEM images for P-CNTs, K-CNTs, and KA-CNTs. The presence of MnO_2 is not observed in a powder form, indicating that it was embedded within the surface layers of the CNTs. These results are confirmed by the TEM analysis. Figure 8.2 (d, e, and f) shows that the MnO_2 has destroyed the hexagonal graphite sheets of the CNTs by exfoliating parts of the CNTs layers and embedding them between them. Moreover, the ATPB-DES functional groups are obvious in both FESEM and TEM images where the agglomeration of KA-CNTs was observable and the TEM results revealed that the KA-CNTs have added more layers on the surface of CNTs.

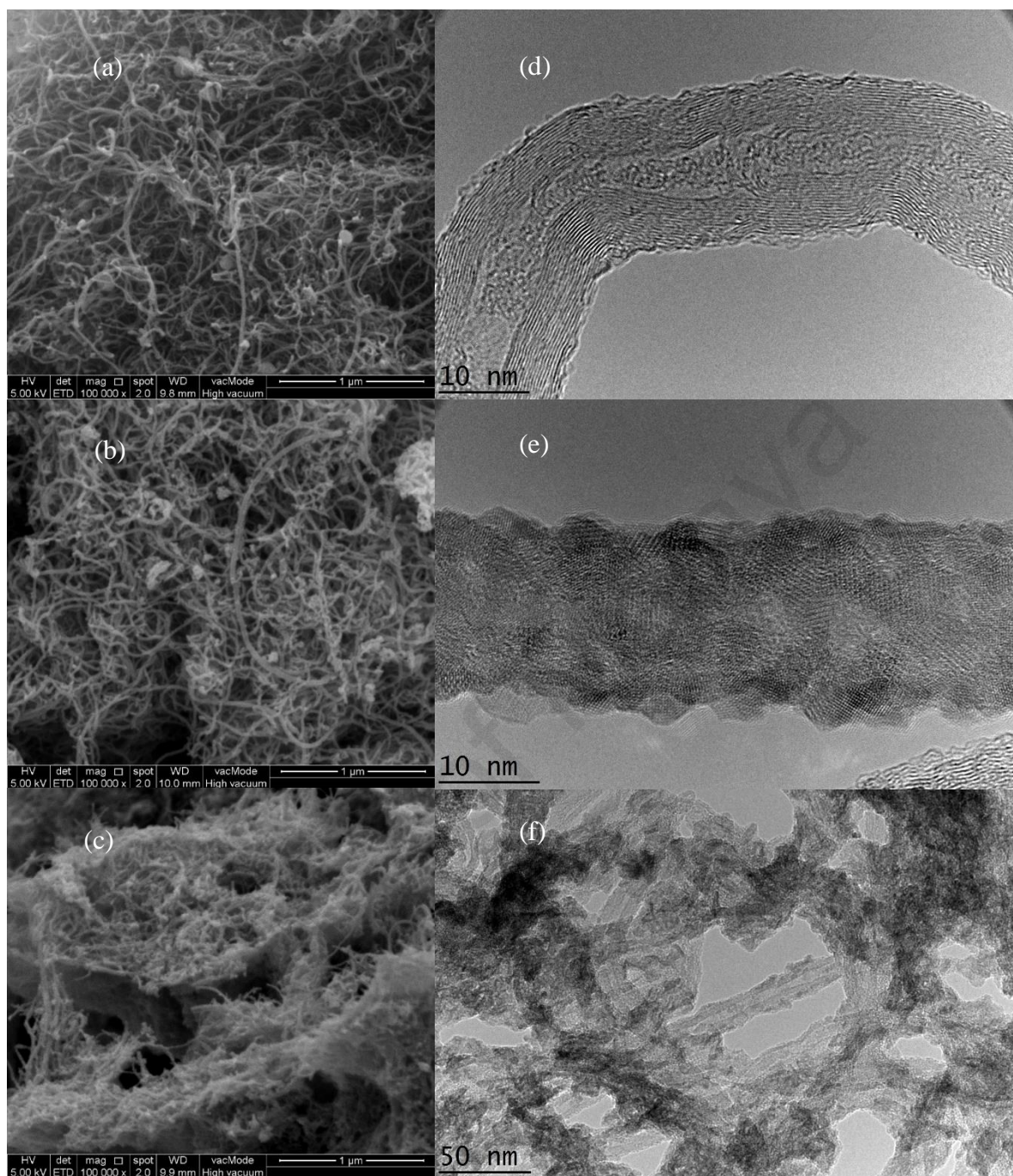


Figure 8.2: FESEM images of a) P-CNTs, b) K-CNTs, c) KA-CNTs, and TEM images of d) P-CNTs, e) K-CNTs, f) KA-CNTs

The TGA analysis was compatible with results obtained from TEM and FESM. Figure 8.3 shows the TGA analysis for P-CNTs, K-CNTs, KA-CNTs and the after adsorption samples which referred as KA-CNTs-Hg. The analysis was carried out under oxygen to

investigate the oxidation level of CNTs. The catalytic activity of oxygen functional groups decreased the composition point from 556 °C to 270 °C for P-CNTs and K-CNTs respectively (AlOmar, Alsaadi, Hayyan, Akib, Ibrahim, et al., 2016). The ash content of K-CNTs remain as a residues materials was 65.21% which indicates the amount of MnO₂ in the composite. Meanwhile, this amount was reduced after the functionalization by DES, the weight difference indicates the functional groups percentage resulted from DES functionalization, hence, the amount of MnO₂ was reduced to 53.757%. Finally, after the adsorption of Hg²⁺ the residues materials remain almost the same 53.8%, which indicates that the metals percentage in the CNTs materials. In addition, EDX studies were conducted for KA-CNTs-Hg. Traceable amounts of Br⁻ and P confirmed the presence of DESs functional groups on the surface of the CNTs. Figure 1F (Appendix F) shows the EDX spectrum for KA-CNTs.

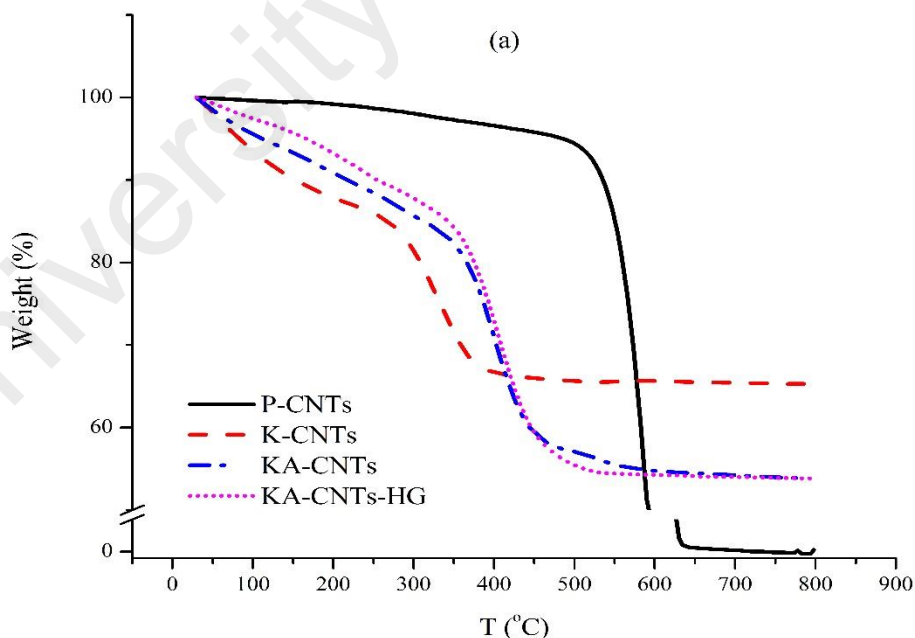


Figure 8.3: TGA curves of P-CNTs, K-CNTs, KA-CNTs and KA-CNTs-HG

The XRD results demonstrated a typical spectrum of P-CNT profile. In which, (002) at 2θ around 26° represents the hexagonal graphite structure. While (001) at 2θ around 42° represents the concentric cylinder structure. (D. Zhang et al., 2005). Figure 8.4 shows the XRD spectrum, which demonstrated that, after the functionalization by KMnO_4 , the peaks almost completely disappeared. That indicated the deposition of MnO_2 which destroys the hexagonal graphite structure of the CNTs by contorting its surface into a non-stoichiometric, amorphous shape (S.-G. Wang et al., 2007). The presence of MnO_2 is revealed also by the two weak peaks at 2θ around 38° and 65° in K-CNTs pattern which can be indexed as (201/111) and (021/311), respectively (Xia, Wang, Lin, & Lu, 2012; H. T. Zhu et al., 2008). The ATPB-DES functionalization increased the wrapping around the CNT edges.

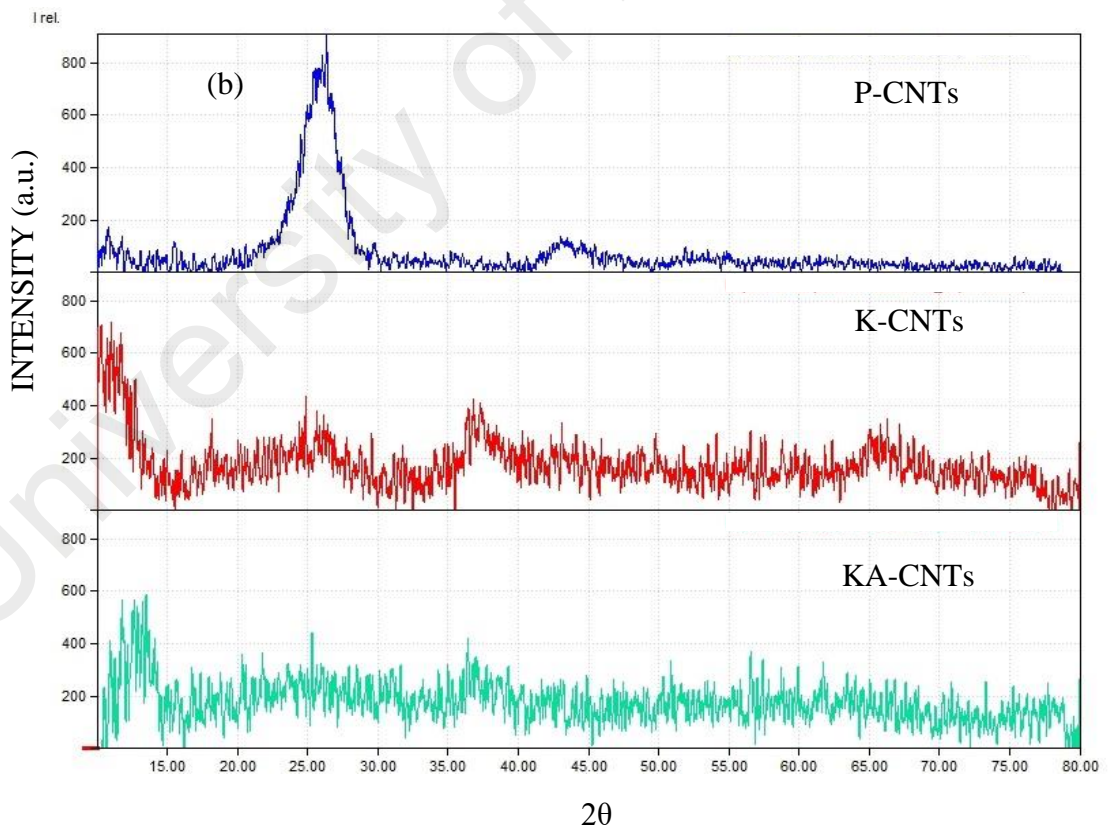


Figure 8.4: XRD spectrum of P-CNTs, K-CNTs and KA-CNTs

Figure 8.5 shows the FTIR spectrum of P-CNTs, K-CNTs, and KA-CNTs. The results revealed that the O-H stretch disappeared after functionalization with ATPB-DES. The presence of OH⁻ is probably due to adsorbed water on the hydrophilic CNTs surface and that was noticeable in the case of K-CNTs. The functionalization with ATPB-DES reduced the hydrophilicity and enhanced the drying process of the sample, this was the reason behind the disappearing of OH⁻ from the FT-IR spectrums of KA-CNTs and P-CNTs. The presence of PO₄³⁻ was observable in the 500-600 cm⁻¹ range and the C-Br stretch is also detected in the 550-650 cm⁻¹ range (B. C. Smith, 1998).

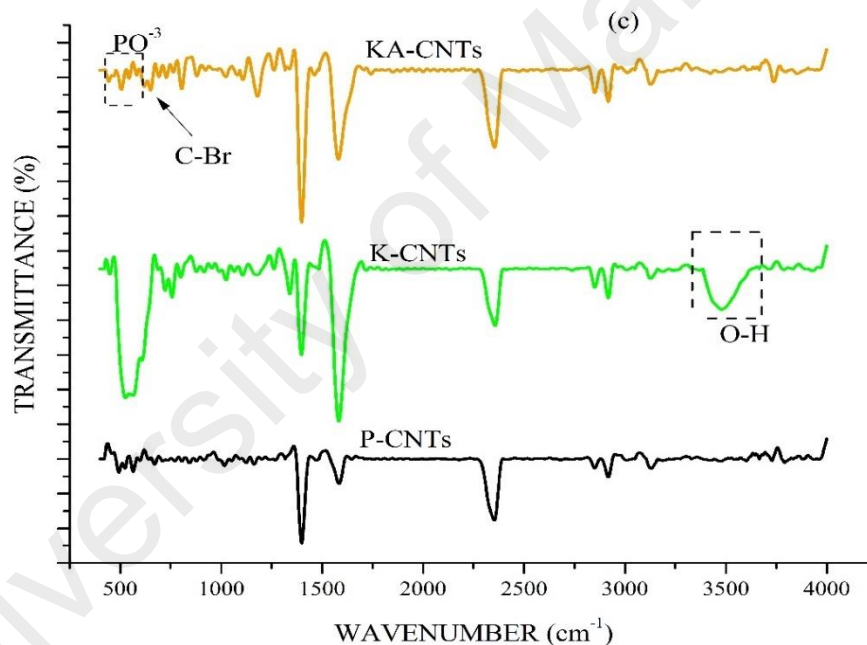


Figure 8.5: FTIR spectrum of P-CNTs, K-CNTs and KA-CNTs

Raman spectroscopy is considered to be essential for characterization of Carbon based materials, due to the ability to indicate the degree of functionalization by comparing the intensity of D band (I_D) to that of G band (I_G) (Aitchison et al., 2007). Herein, the I_D/I_G ratio of P-CNTs, K-CNTs, and KA-CNTs was found to be 1.11, 1.16, and 1.18, respectively. The I_D/I_G increased after each functionalization step, due to higher levels of

covalent functionalization on the surface of the KA-CNTs with carboxylic functional groups or other Sp^3 groups. Which was confirmed by the FTIR spectrum. Figure 8.6 show the major Raman peaks. Additionally, the D' band, which is usually displayed as a weak shoulder of the G-band, occurs at higher frequencies. It cannot be found in pure graphite. However, it can be observed in intercalated graphite and MWCNTs (C. S. Kumar, 2012). Furthermore, the D' band is considered to be a double resonance feature generated by disorder and defects (Kordás et al., 2006). Furthermore, two peaks were noticeable for k-CNTs at around 575 and 650 cm^{-1} which probably take place corresponding to the presence on MnO_2 (Ogata, Komaba, Baddour-Hadjean, Pereira-Ramos, & Kumagai, 2008). After ATPB-DES functionalization, these peaks were almost disappeared except for a small hump due to the excessive functionalization and wrapping of CNTs which was supported by the TEM results.

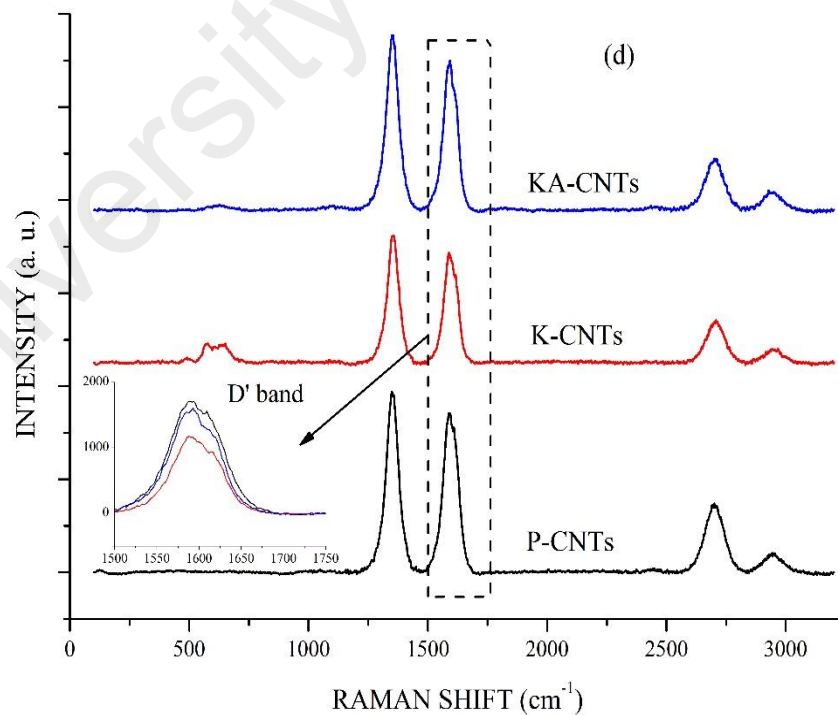


Figure 8.6: Raman Spectrum of P-CNTs, K-CNTs and KA-CNTs

It is well known that the surface charge of an adsorbent greatly influences the adsorption processes, especially for the sorption of heavy metals. It is well known that there are many factors affecting zeta potential measurements, including particle surface charges, pH, conductivity, ion concentration, and temperature (Simate et al., 2012). Herein, 2.5 mg of each adsorbent was dispersed in 5 ml of deionized water for zeta potential measurements. The absolute zeta potential increased significantly from 5.5 to 45.81 mV for P-CNTs and K-CNTs, respectively (AlOmar, Alsaadi, Hayyan, Akib, & Hashim, 2016). Therefore, the oxygen-containing functional groups, such as carbonyl groups and aliphatic carboxylic acids, added to the surface led to an increase in the hydrophilicity of the adsorbent. The zeta potential slightly increased to 52.3 mV after addition of new functional groups by ATPB-DES to the surface. According to ASTM standards, the criterion for “good stability” requires a zeta potential with an absolute value above 40 mV (Fan et al., 2012). Based on that, our novel adsorbents can form water suspensions with very good stability and offers suitable contact with the aqueous solution.

The BET surface areas of P-CNTs, K-CNTs, and KA-CNTs were calculated using nitrogen adsorption/desorption, according to ASTM D 3663-3 reapproved (ISO second edition 1-09-2010), and were found to be 123.54, 158.93, and 199.366 m² g⁻¹, respectively. This showed that functionalization with ATPB-DES improved the surface area, which is considered to be a key factor for any adsorbent. It worth mentioning that the pore volume decreased from 0.62 to 0.45 cm³ g⁻¹ after functionalization with KMnO₄. In addition, the pore size diameters increased significantly after each functionalization step, and were found to be 20.49, 114.12, and 127.34 Å, respectively.

8.3.2 Leaching study

In order to evaluate the stability of functionalized CNTs as an adsorbent, a leaching study was performed. Herein, KA-CNTs were shaken in various pH solutions at 180 rpm.

later, the Mn concentration was measured from each solution with respect to time as seen in Figure 8.7. The leaching of Mn accrued at pH 3.0 and below. Meanwhile, at pH more than 3.0 there was no trace of Mn in the solution after 7 h. However, at pH 1.3 the leaching of Mn reached the equilibrium state after 4.5 h with Mn concentration of 25 mg L^{-1} . These results indicate that the ion exchange between Mn and Hg as an adsorption mechanism was in very low level which was also supported by the EDX results which was performed after adsorption. In addition, there was very low trace of Mn ions in the water after applying KA-CNTs as an adsorbent of Hg^{2+} .

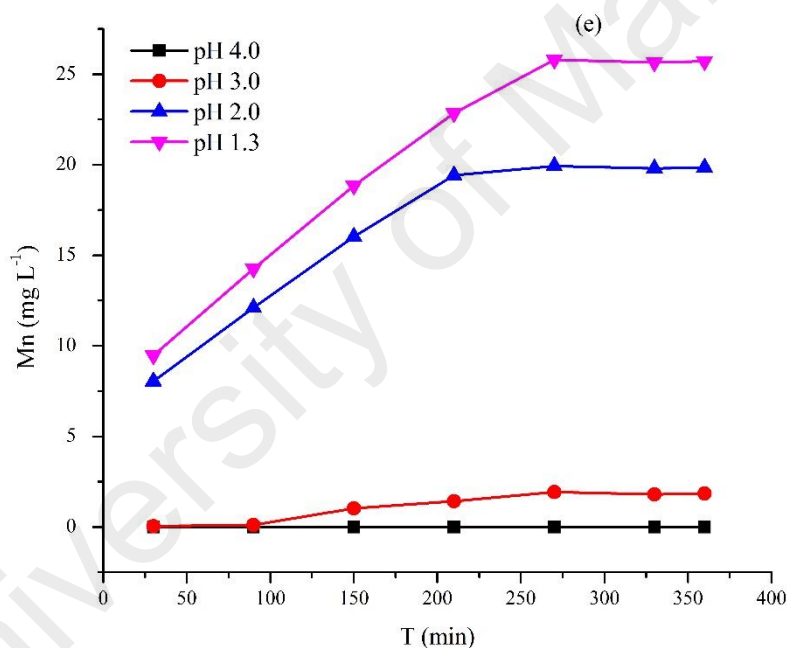


Figure 8.7: Leaching of Mn at different pH with respect to time

8.3.3 Optimization

Response surface methodology (RSM) was utilized to optimize the conditions of Hg^{2+} removal. Central composite design (CCD) was selected using the software Design Expert V7.0. In this study, three dependent variables were adopted, specifically pH (3 to 8), contact time (5 to 55 min), and adsorbent dosage (5 to 20 mg). The initial concentration

and agitation speed were fixed to 3 mg L⁻¹ and 180 rpm, respectively. The removal percentage (R%) and the adsorption capacity (Q) were taken as the response functions of the optimization study. Table 1F (Appendix F) lists the experimental design runs, in terms of the actual parameters, together with the experimental values of each response.

The analysis of variance (ANOVA) modelling for the R% model and Q of the KA-CNTs model were both significant. Both models are represented by Eq. 8.1 and Eq. 8.2, which are the regression equations for R% and Q, respectively. Table 2F and Table 3F listed the P-values, F- values, and the square mean for both R% and Q, respectively. The correlation coefficients R² values were 0.9974 and 0.9909 for both R% and Q. Figure 2F (a and b) plot the theoretical values versus the experimental values for R% and Q, respectively, which clearly show that the theoretical values predicted by the models developed in this study were close to the experimental values, indicating that both models have successfully achieved correlation between the process variables in both models.

$$Hg^{2+} \text{ removal } \% = 91.22 + 2.17A + 8.28B - 0.18C + 6.24AB - 0.52AC - 4.04BC - 18.32A^2 + 4.24ABC + 2.11A^2C \quad (8.1)$$

$$KA - CNTs \text{ adsorption capacity} = 11.47 + 0.43A + 1.93B - 10.16C + 0.66AB - 0.32AC - 1.67BC - 3.60A^2 + 5.54C^2 + 2.35A^2C \quad (8.2)$$

Where A, B, and C are representing pH, contact time, and adsorption capacity, respectively.

Several potential solutions for optimal conditions were obtained from the statistical model of CCD for Hg²⁺ adsorption on KA-CNTs. A set of constrains, presented in Table 4F, was developed to control the software selection for the optimal adsorption process condition values. Based on the forgoing, the optimal Hg²⁺ adsorption conditions were found to be at a pH around 5.5, with a contact time of 28 min, and an adsorbent dosage of 5 mg. The interaction of pH with the adsorbent dosage shows that the R% is pH dependent, where the removal increased by increasing pH until it reached the maximum at pH around 5.5. Upon further increases in pH, the removal percentage began dropping.

Figure 8.8a shows the effect of pH on the removal at a fixing contact time. On the other hand, Figure 8.8b shows the effect of pH and contact time by fixing the adsorbent dosage, which clearly showed that the contact time has a significant impact on the R% of Hg^{2+} . A similar phenomenon was observed for Q in term of contact time. However, the adsorbent dosage has a significant effect on the Q for Hg^{2+} absorption. Figure 8.8c and d shows the interaction of pH, with contact time and with the adsorbent dosage, respectively, and their influence on the Q.

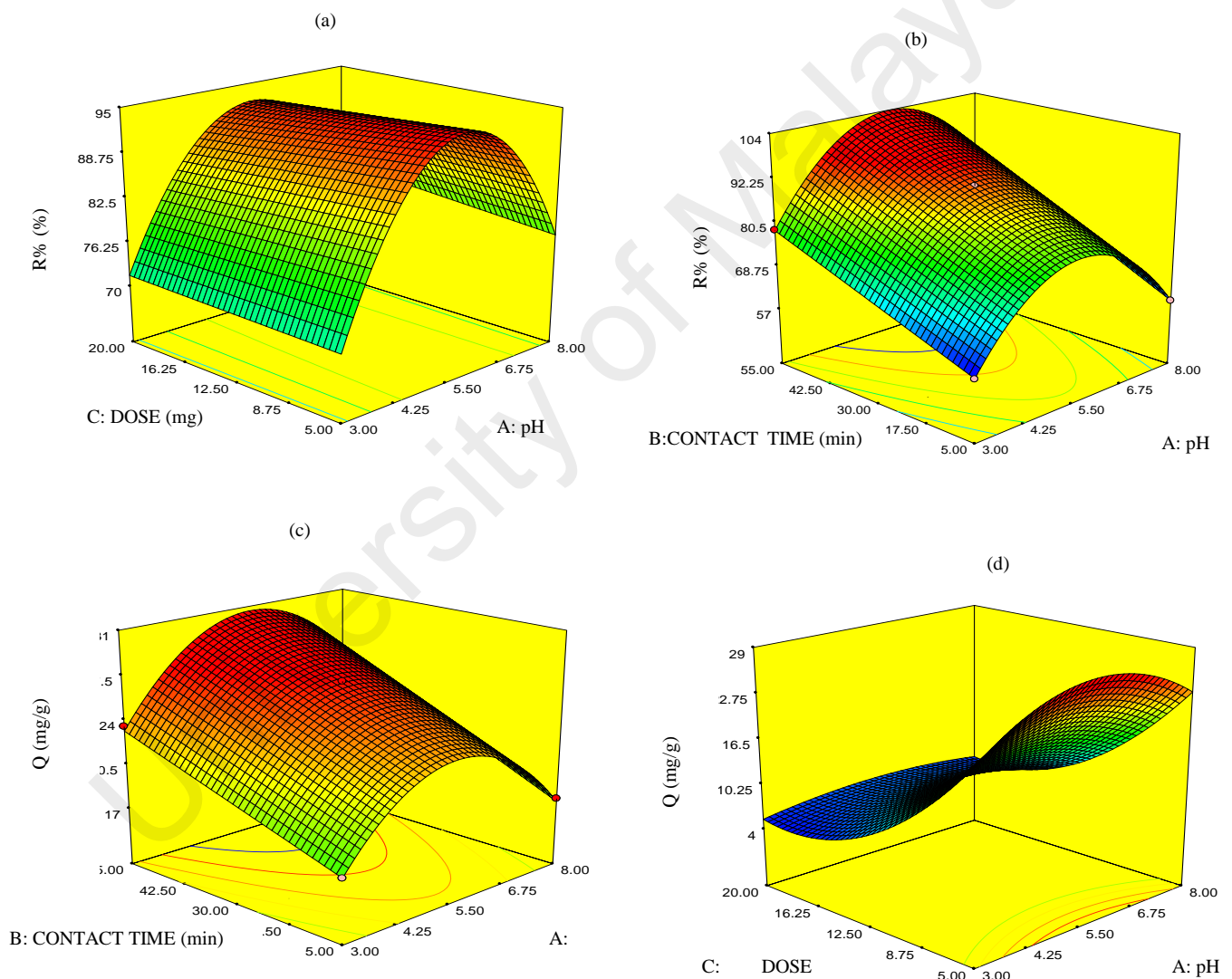


Figure 8.8: a) effect and interaction of pH and adsorbent dosage on the removal percentage, b) effect and interaction of pH and contact time on the removal percentage of, c) effect and interaction of pH and contact time on the adsorption capacity of KA-CNTs, and d) the effect and interaction of pH and adsorbent dosage on the adsorption capacity of KA-CNTs

8.3.4 Kinetics and Isotherm studies

The kinetics of Hg^{2+} adsorption were determined in order to understand the adsorption behaviour of KA-CNTs. The same experimental procedure as in the previous sections was adopted. The optimal conditions were used in this study, which were pH 5.5, adsorbent dosage of 5 mg, agitation speed of 180 rpm, and initial concentration of 3 mg L^{-1} . The reaction was considered fast where it reached equilibrium in approximately 1 h. However, in order to ensure that equilibrium was reached, the experiments were conducted for 2.5 h. The experimental data was analysed using three kinetics models, i.e. pseudo-first-order, pseudo-second-order and intraparticle diffusion.

The values of the correlation coefficients, R^2 , for the data sets were considered as indications of conformity between the experimental data and the corresponding values predicted by each model. Table 8.1 lists the R^2 and the constants coefficients for each model. Based on these results, the adsorption kinetics of KA-CNTs clearly followed the pseudo-second order model with greater conformity, compared to the pseudo-first-order and intraparticle diffusion models, since R^2 was found to be 0.9999 for pseudo-second order. These findings agree with previous research on CNTs-based adsorbents (Gong et al., 2014; C. Zhang et al., 2012). Figure 8.9 plots the experimental data according to the linearized pseudo-second-order model.

Table 8.1: Experimental values of constants of adsorption kinetics models

Experimental (q)	Pseudo-first- order			Pseudo-second-order			Intraparticle	
	q_e (mg/g)	K_1 (min^{-1})	R^2	q_e (mg/g)	K_2 (g/mg.min)	R^2	K_d (g/mg.min ^{0.5})	R^2
14.998	14.56	-5×10^{-4}	0.717	15.17	0.04	0.999	3.11	0.862

The proposed mechanism is illustrated in Eq. 8.3, 8.4, and 8.5. The Hg^{2+} could form complexation with oxygen containing groups and ion exchange process takes place with

H⁺. On the other hand, OH⁻ ions in the solution play positive role in consuming H⁺ and this is the reason behind the enhancement of adsorption with the increase of pH to certain point (in our case pH 5.5). however, further increase in pH leads to excess amount of OH⁻ which forms complexations with Hg in the solution and reduces the rate of adsorption on the surface.

It is well known that MWCNTs and their modified allotropes have heterogeneous surface which gives the probability of multi mechanisms to take place (P. H. Chen et al., 2014; Hadavifar, Bahramifar, Younesi, & Li, 2014).

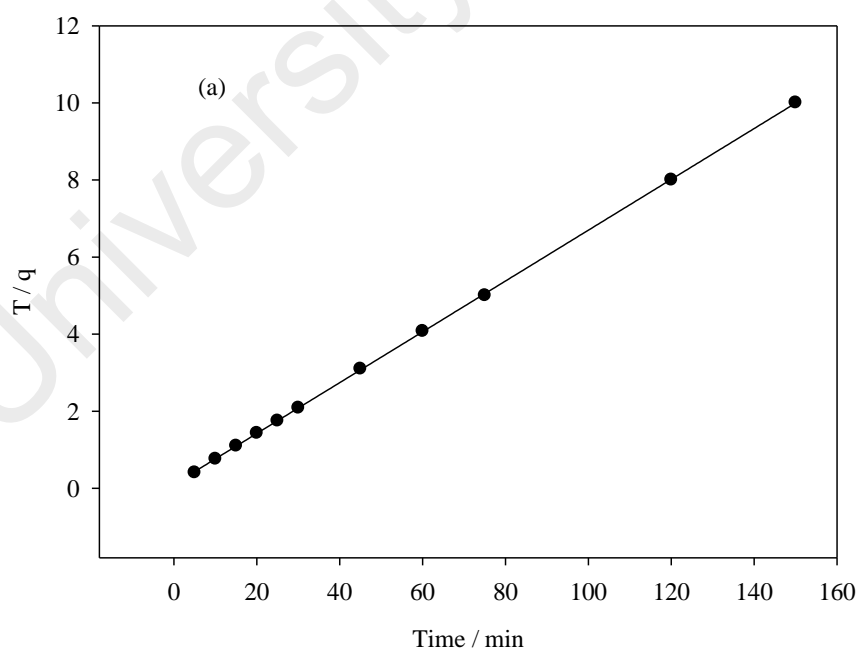
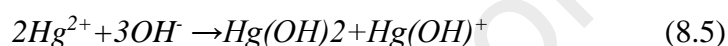
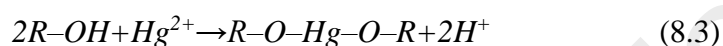


Figure 8.9: Pseudo-second order adsorption kinetics

The Langmuir and Freundlich isotherm models were used to describe the adsorption of Hg^{2+} onto the surface of KA-CNTs. Herein, 16 Hg^{2+} initial concentrations (1, 3, 5, 10, 15, 20, 25, 30, 35, 40, 45, 50, 55, 60, 65, and 70 mg L^{-1}) were employed to investigate the adsorption isotherm of KA-CNTs. The adsorbent dosage (5 mg) and pH (5.5) were used, in agreement with the optimization study.

Figure 8.10 and 8.11 plots the Langmuir and Freundlich equations, respectively. The Freundlich isotherm equation was found to be a better fit for the adsorption of Hg^{2+} onto KA-CNTs. The correlation coefficient (R^2) of the Freundlich equation was found to be 0.9583. Meanwhile, the experimental data did not fit the Langmuir isotherm equation. Therefore, the adsorbed Hg^{2+} occurs as a heterogeneous surface with interaction between adsorbed molecules with a nonuniform distribution of heat of sorption over the surface (Ghaedi et al., 2011). Table 8.2 lists the Langmuir and Freundlich models together with previous researches findings.

Table 8.2: Isotherm models parameters and comparison of adsorption capacity of other adsorbents

Adsorption Isotherm Model		Langmuir			Freundlich			Reference
Adsorbent	pH	q_m (mg/g)	K_L (l/mg)	R^2	n	K_f (mg/g)	R^2	
KA-CNTs	5.5	250.5	14.16	0.773	2.17	33.72	0.958	Present work
^a MWCNTs-SH	-	84.66	0.31	0.945	0.30	30.92	0.926	(Hadavifar et al., 2014)
^b SiO ₂ -CNT	5-6	250	0.14	0.982	1.50	34.8	0.992	(Saleh, 2015)
^c CNT-S	6	151.51	0.31	0.994	1.83	1.24	0.936	(A. Gupta et al., 2014)
^d COOH-MWCNT	4.3	127.60	0.19	0.990	1.17	18.04	0.968	(P. H. Chen et al., 2014)
^e MPTS-CNTs/Fe ₃ O ₄	6.5	65.52	0.03	0.992	2.26	7.62	0.984	(C. Zhang et al., 2012)

^asodium 2-mercaptoethanol functionalized CNT, ^bSilica combined with 2 % functionalized CNT, ^csulfur incorporated MWCNT, ^dpre-treated MWCNT in acidic $\text{KMnO}_4/\text{H}_2\text{SO}_4$ solution, ^eThiol-functionalized multiwall carbon nanotube/magnetite nanocomposites.

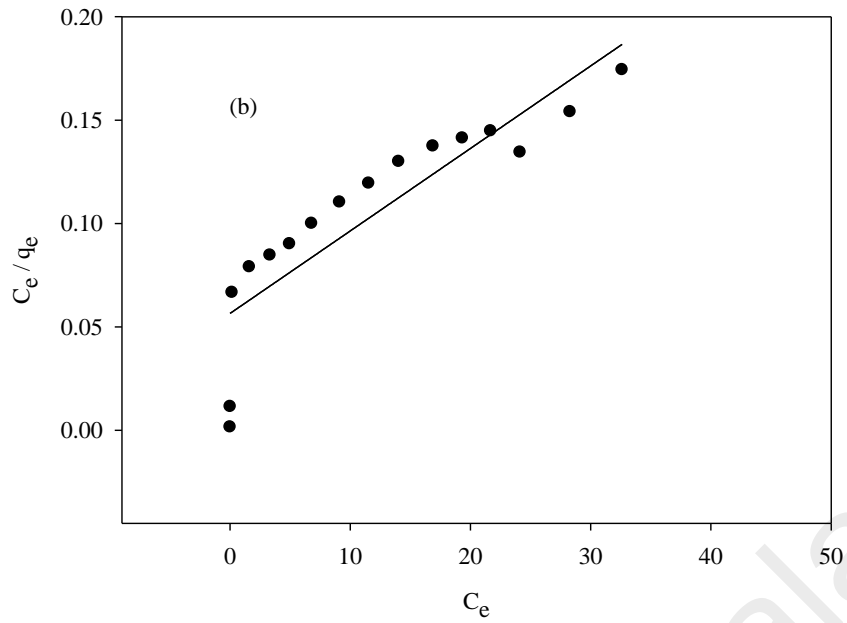


Figure 8.10: Linear form of Langmuir isotherm model for the Hg^{2+} adsorption onto KA-CNTs

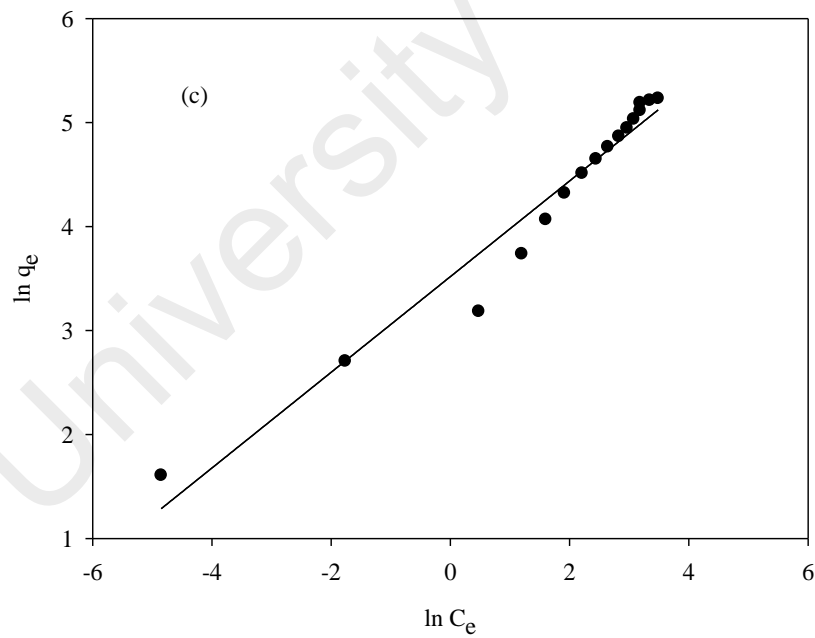


Figure 8.11: Linear form of Freundlich isotherm model for the Hg^{2+} adsorption onto KA-CNTs

8.3.5 Desorption and regeneration

Knowing the reversibility of an adsorbent is crucial to determine the practical application of it. Herein, the optimum removal conditions were used to adsorb 3 mg L^{-1} of Hg^{2+} until reaching equilibrium. Then the adsorbent was collected and dried over night at 100°C . The used KA-CNTs were mixed with different pH solutions by adding 5 mg of KA-CNTs to 50 ml of each solution and agitated at 180 rpm. The Hg concentration was measured in the solutions with respect to time. Eq. 8.6 calculated the Hg^{2+} desorption percentage $D\%$. Figure 8.12 plots the $D\%$ of Hg^{2+} at different pH with respect to time. The $D\%$ reached 10 % after been shaken in neutral water for 7 h, meanwhile, the $D\%$ reached 99 % after 30 min shaking in pH 1.3 solution. the adsorbent recovered was successfully reused three times with 70 % efficiency.

$$D\% = q_D/q_E \times 100\% \quad (8.6)$$

Where $D\%$ is the desorption of Hg^{2+} , q_D and q_E are referring to the amount of Hg^{2+} desorption with respect to time and the amount of adsorption at equilibrium respectively.

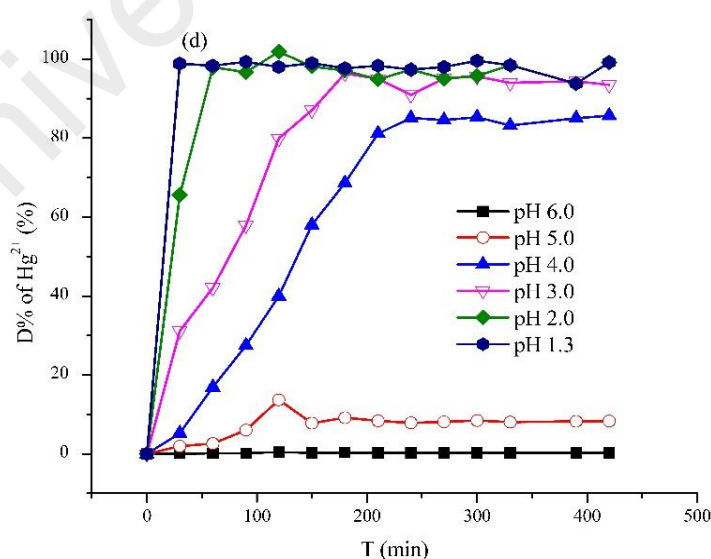


Figure 8.12: Desorption of Hg^{2+} at different pH

8.4 Summary

A novel Hg^{2+} adsorbent was successfully prepared using Allyl triphenyl phosphonium bromide (ATPB) based DES as a functionalization agent of CNTs. The novel adsorbent was characterized using Raman spectroscopy, FTIR, XED, FESEM, EDX, BET, TGA, TEM, and Zeta potential. An optimization study was performed utilizing RSM techniques. The optimum removal conditions were found to be pH 5.5, contact time of 28 min, and adsorbent dosage of 5 mg. The Freundlich isotherm was used to approximate the data with a maximum adsorption capacity of 186.97 mg g^{-1} for CNTs functionalized with KMnO_4 and a ATPB based DES (KA-CNTs). The Hg^{2+} adsorption system fitted excellently to a pseudo-second order kinetics model.

University of Malaya

CHAPTER 9: NOVEL DEEP EUTECTIC SOLVENT-FUNCTIONALIZED CARBON NANOTUBES ADSORBENT FOR MERCURY REMOVAL FROM WATER

9.1 Introduction

It is well known that mercury (Hg) is one of the most toxic elements in nature. Mercury exposure in humans is closely tied to extensive damage to the kidneys, reproductive systems, immune, hematologic, cardiovascular, respiratory system, and the brain (Ihsanullah et al., 2016). The three forms of Hg present in nature are metallic element, organic salt, and inorganic salt (Goldman et al., 2001). Hg usually exists in seawater, fresh water, and in soil (*Mercury Study Report to Congress*, December 1997). In addition, Hg is a waste product associated with many industries, including production of chlor-alkali, fossil fuels, various switches, and wiring devices, measuring and control devices, lighting, and dental work (A. Gupta et al., 2014). According to the World Health Organization (WHO), the maximum allowable concentration of Hg in water is 1µg/l. This value is due to its extremely hazardous effects, even at low concentrations (Mohan et al., 2001).

Many conventional techniques have been utilized to reduce Hg concentrations in water, including solvent extraction, precipitation, ion-exchange, reverse osmosis, membrane separation, coagulation, and photoreduction (Bandaru et al., 2013). However, most of these methods have drawbacks such as high energy requirements or their association with large quantities of environmentally hazardous chemicals (F.-S. Zhang et al., 2005). As a result, Hg removal from water using the adsorption technique proved to be the most applicable on an industrial scale (Chandra & Kim, 2011; Chiarle et al., 2000).

Recently, nanoparticles have been introduced as extremely effective adsorbents for many pollutants, due to their unique features, small size, catalytic potential, high

reactivity, and large surface area (Ali, 2012). Carbon nanotubes (CNTs) have attracted the most attention in the field of water remediation, which includes removal of cadmium (T. Lin et al., 2003), zinc (C. Lu & Chiu, 2006), lead (Y.-H. Li et al., 2002), 1,2-dichlorobenzene (Peng et al., 2003), fluoride (T. Lin et al., 2003), and trihalomethanes (C. Lu et al., 2005). However, CNTs have yet to be fully optimized in terms of solubility, aggregation, and difficulty in manipulation. On the other hand, CNTs have shown a great affinity for interaction with different compounds, especially after surface functionalization (Andrews et al., 2002; Fischer, 2002; Hirsch & Vostrowsky, 2005; T. Lin et al., 2003; X. Lu & Chen, 2005; Niyogi et al., 2002; Y.-P. Sun et al., 2002; Thostenson et al., 2001). Oxidative functionalization can enhance the surface charge of CNTs, but requires the use of strong acids and environmentally unfavorable chemicals. Consequently, the need for new types of economical and environmentally friendly functionalization agents is crucial for the development of novel applications (M. Hayyan, Abo-Hamad, et al., 2015a; Martínez et al., 2003).

Recently, ionic liquids analogues, i.e., deep eutectic solvents (DESs) have been utilized in many different scientific fields. DESs were first introduced by Abbott et al. in 2003 as a cheaper replacement for developed ionic liquids (ILs) (Andrew P. Abbott et al., 2003). Some researchers consider DESs to be the fourth generation of ILs, even though they are not entirely composed of ionic species (Cvjetko Bubalo et al., 2015b). Substantially, DESs can be simply defined as a mixture of two or more compounds that has a melting point lower than that of each individual compound (Andrew P. Abbott, Boothby, et al., 2004; M. Hayyan et al., 2010). Regarding environmental safety, DESs have met many of the criteria necessary to be considered environmentally friendly solvents, including availability, biodegradability, recyclability, flammability, and relatively low price compared to other conventional solvents (Q. Zhang et al., 2012). Due to DESs physicochemical properties, they have been used in a variety of applications (Cooper et al.,

2004; A. Hayyan, M. Ali Hashim, et al., 2013; A. Hayyan et al., 2014; Leroy et al., 2012). Most recently, DESs have achieved wide-spread use in nanotechnology related fields, with uses such as media for synthesis of nanoparticles (Chakrabarti et al., 2015; F. Chen et al., 2013; Jia et al., 2015; Mohammad Karimi et al., 2016; Xiong et al., 2015; Xu et al., 2016), electrolyte in nanostructure sensors (Zheng et al., 2014), and electrolytes in nanoparticle deposition (Andrew P. Abbott et al., 2009; Andrew P. Abbott et al., 2012; C. Gu & J. Tu, 2011; X. Guo et al., 2014; Renjith et al., 2014; Wei, Fan, Tian, et al., 2012; Wei, Fan, Wang, et al., 2012; Wei et al., 2013; You et al., 2012). Based on these applications, DESs have the potential to be used as economically and environmentally friendly functionalization agents.

In this study, an ammonium based DES was synthesized using tetra-n-butyl ammonium bromide (TBAB) with glycerol (Gly) as the hydrogen bond donor (HBD). Later, this TBAB based-DES was utilized as a functionalization agent for CNTs, which were then used as an adsorbent agent for Hg^{2+} ions from water samples. In addition, the functionalized CNTs were fully characterized as the novel adsorbent in order to study the effect of TBAB based-DES on the CNT surface. This characterization includes Raman spectroscopy, XRD diffraction, FTIR, FESEM, EDX, BET surface area, and zeta potential. The optimal removal conditions for Hg^{2+} were determined using Response surface methodology (RSM). Moreover, kinetics and isotherm studies were also performed at the optimal conditions.

9.2 Experiments and Methods

9.2.1 Chemicals and materials

Multi wall carbon nanotubes with specifications of $D \times L$ 6-9 nm \times 5 μm >95% (carbon), TBAB, Gly, nitric acid (65%), potassium permanganate, sodium hydroxide

pellets, and hydrochloric acid (36.5-38%) were all supplied by SIGMA- ALDRICH. A 1000 mg/L mercury standard solution was supplied by MERCK.

9.2.2 Functionalization of CNTs

The surface of the pristine CNTs (P-CNTs) was functionalized by oxidation through to different procedures. The first procedure used sonication with KMnO_4 for 2 hr at 65 °C (AlSaadi et al., 2016). The resulting oxidized CNTs are referred to as K-CNTs in this study. The second method involved refluxing P-CNTs with HNO_3 (65%) for 1 hr at 140°C, the resulting acidified CNTs are referred to as N-CNTs in this study.

The DESs were synthesized by mixing TBAB with Gly (HBD) using magnetic stirring at 400 rpm and 80°C, until the DES became a homogeneous liquid without any precipitate. The details of synthesis, characterization, and molar ratio options are based on our previous study (AlOmar, Hayyan, et al., 2016). Next, functionalization with DESs was performed using sonication with 200 mg of P-CNTs, K-CNTs, and N-CNTs, separately, with 7 ml of DES for 3 hr at 65°C. The resulting functionalized CNTs will be referred as PT-CNTs, KT-CNTs, and NT-CNTs, respectively. It should be noted that after each functionalization step, the functionalized CNTs were repeatedly washed and filtered with distilled water, using a vacuum pump and a PTIF 0.45 μm membrane, until the filtrate water pH was neutral.

9.2.3 Characterization of functionalized CNTs

All adsorbents were characterized using a Renishaw System 2000 Raman Spectrometer to obtain Raman shift spectra. The surface modification and functional groups that resulted from the functionalization processes were studied using Fourier transform infrared (FTIR) spectroscopy via a PerkinElmer® FTIR spectrometer USA with a range of 400-4,000 wave number and four times repetitionreputation. The structural phases were analyzed using X-ray powder diffraction (XRD) with a Shimadzu

XRD 6000® at a scanning range of 2θ between 10° - 80° . Furthermore, the surface charge was measured by conducting zeta potential tests using a Zetasizer (Malvern, UK). For the purpose of measuring the zeta potential, 2.5 mg of each adsorbent was dispersed in 5 ml of deionized water and subjected to sonication for 1 hr before the measurement. A fully Automated Gas Sorption System (micromeritics ASAP2020, TRISTAR II 3020 Kr®, USA) was used to study the selected samples surface area, based on the Brunauer-Emmett-Teller (BET) method by adsorption-desorption of nitrogen gas at -200°C . A Field-Emission Scanning Electron Microscope (Quanta FEG 450, EDX-OXFORD) Thermo Fisher Scientific® USA was used to obtain high resolution nano-sized images for analysis of the morphology of all selected samples, along with an energy-dispersive X-ray spectrometer (EDX). Mercury ions were detected using ICP with an OES OPTIMA7000DV PerkinElmer® USA.

9.2.4 Adsorption experiments

A primary screening study was conducted to choose the adsorbent with the highest removal percentage. Samples consisting of 10 mg of each adsorbent (P-CNTs, K-CNTs, N-CNTs, PT-CNTs, KT-CNTs, and NT-CNTs) were applied in batch experiments. An Hg^{2+} stock solution with a concentration of 5 ppm and pH of 2.2 was prepared using distilled water. A similar screening experiment was repeated at pH 6.0. The experiments were conducted using 50 ml of contaminated water in a 250 ml flask with 10 mg of adsorbent. The flask was agitated using a mechanical system for 30 min at room temperature and an agitation speed of 180 rpm.

An estimation of the regression empirical relationship was conducted to assess the removal percentage (R) of Hg^{2+} and the adsorption capacity (Q) of KT-CNTs, utilizing response surface methodology (RSM). The central composite design (CCD) was selected using the Design Expert V7.0 software. The effects and interactions of three parameters

were investigated in this study, specifically pH (3 to 8), contact time (5 to 55 min), and adsorbent dosage (5 to 20 mg). The experimental design, in terms of the actual parameters, alongside R and Q responses, are listed in Table 1G (Appendix G). The optimization was performed at an initial concentration of 3 mg/L. The agitation speed was fixed at 180 rpm.

The rate of ion transfer from the solute to the adsorbent surface and associated parameters are crucial and can be determined by studying the adsorption kinetics. The efficiency of the adsorption process is indicated by the kinetic rate of the adsorption system and, hence, can determine its potential applications. In this study, the removal conditions obtained from the optimization study were applied in the most usable kinetics models, i.e. pseudo-first order, and pseudo-second order models. Eq. 9.1 and Eq. 9.2 describe the linear form of these two models, respectively.

$$\ln(q_e - q_t) = \ln q_e - K_1 t \quad (9.1)$$

$$\frac{t}{q_t} = \frac{1}{K_2 q_e^2} + \frac{1}{q_e} t \quad (9.2)$$

Where k_1 and q_e are the slope and intercept calculated by plotting, $\ln(q_e - q_t)$ vs time (t), respectively, for Eq. 9.1. q_e is calculated as $1/(\text{slope})$ and K_2 is calculated as $(\text{Slope})^2 / \text{intercept}$. The slope and the intercept can be determined from a plot of t/q_t vs t . The q_e and q_t refer to the adsorption uptake at equilibrium and at time t , respectively for Eq. 9.2.

To thoroughly investigate the adsorption mechanism, which can be used for design purposes, it is also essential to define the adsorption isotherm for any novel adsorbents. Herein, the optimal removal conditions were used with 16 initial Hg^{2+} concentrations (1, 3, 5, 10, 15, 20, 25, 30, 35, 40, 45, 50, 55, 60, 65, and 70 mg/L). The Langmuir and Freundlich isotherm models were used to describe the adsorption of Hg^{2+} on the novel adsorbent. Eq. 9.3 and Eq. 9.4 represent the linearized form of the Langmuir and

Freundlich models (Al Mamun et al., 2015; Freundlich & Hatfield, 1926; Langmuir, 1916), respectively.

$$\frac{C_e}{q_e} = \frac{1}{K_a Q_m} + \left(\frac{1}{Q_m}\right) * C_e \quad (9.3)$$

$$\ln q_e = \ln K_F + \frac{1}{n} \ln C_e \quad (9.4)$$

Where C_e is the initial equilibrium concentration, and q_e is the amount of Hg^{2+} absorbed on the surface of the adsorbent. K_a and Q_m are the adsorption equilibrium constant and the maximum adsorption capacity, respectively. In addition, q_e is the uptake of adsorbent. K_F and n are the isotherm constants for the Freundlich isotherm model.

The desorption and regeneration study was achieved by drying KT-CNTs overnight at 100 °C, which was primarily used to remove Hg^{2+} with initial concentration of 3 mg/L under the equilibrium optimal removal conditions. Subsequently, different pH solutions were used to desorb Hg^{2+} from KT-CNTs by adding 6 mg of the dried KT-CNT to 50 ml of each solution and shaken at 180 rpm. During the desorption experiment, the concentration was measured at different time intervals. Eq. 9.5 calculated the Hg^{2+} desorption percentage (D%)

$$D\% = q_D/q_E \times 100\% \quad (9.5)$$

where $D\%$ is the desorption of Hg^{2+} , and q_D and q_E are referring to the amount of Hg^{2+} desorption with respect to time and the amount of adsorption at equilibrium, respectively.

9.3 Results and discussion

The screening studies showed that the KT-CNTs recorded the highest removal, compared to other tested adsorbents. The significant effect of TBAB-based DES on the removal percentage can be seen at both pH 2.2 and pH 6.0. Figure 9.1 illustrates the screening studies for the adsorption of Hg^{2+} .

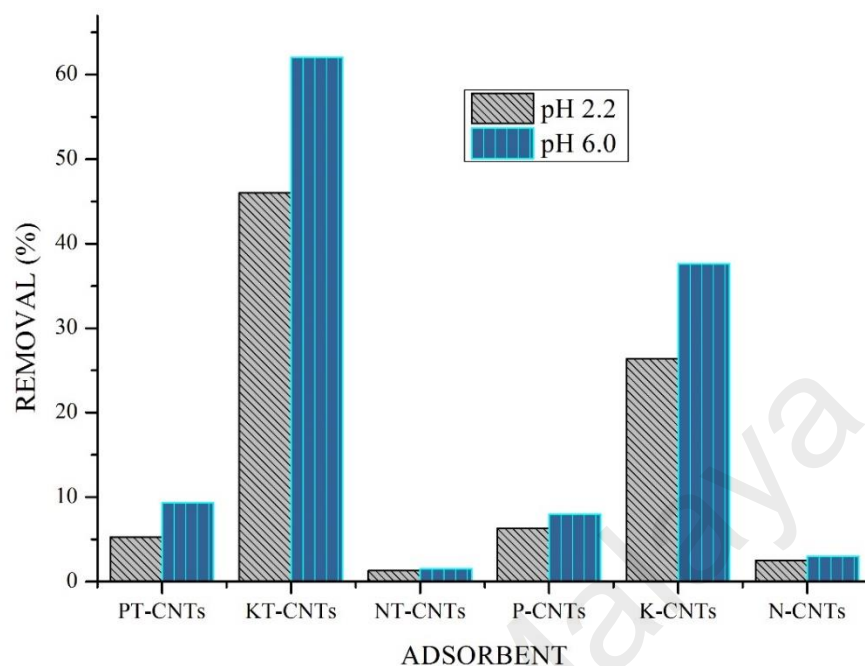


Figure 9.1: Primary screening study for all adsorbents

For carbon-based materials, Raman spectroscopy is considered to be an essential characterization due its ability to indicate the degree of functionalization by comparing the intensity of the D band (I_D) to that of the G band (I_G) (Aitchison et al., 2007). The I_D/I_G ratio was 1.11, 1.16, and 1.175 for P-CNTs, K-CNTs, and KT-CNTs, respectively. This increase demonstrates the high level of covalent functionalization on the surface of the KT-CNTs, through the addition of carboxylic functional groups or other Sp^3 groups. Furthermore, the third characteristic band known to indicate a carbon-based nanostructure is D' , which appeared as a weak shoulder of the G-band at higher frequencies and can be considered a double resonance feature originating from disorder and defects. It worth mentioning that the D' band is undetectable in pure graphite, however, it can be observed in intercalated graphite and MWCNTs (C. S. Kumar, 2012). On the other hand, the functionalization with $KMnO_4$ resulted in the presence of MnO_2 which was comfermed

by the two peaks at around 575 and 650 cm^{-1} in the K-CNTs spectrum (AlOmar et al., 2017; Ogata et al., 2008). Next, the additional functional groups that resulted from the functionalization with TBAB-DES reduced the intensity of these peaks and appeared as a small hump. Figure 9.2 shows the main Raman peaks.

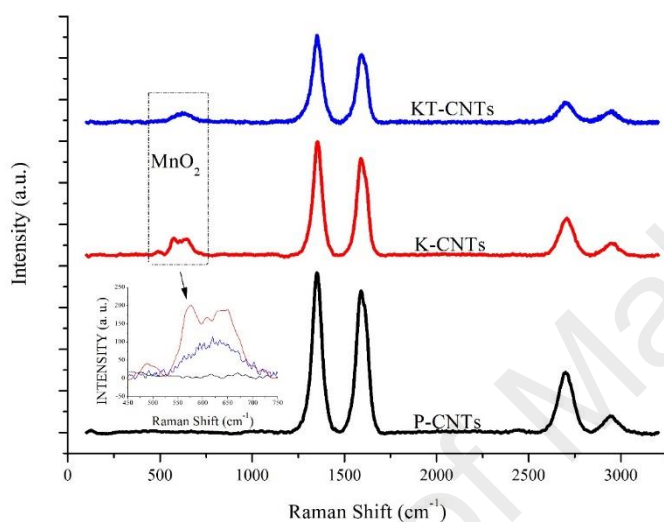


Figure 9.2: Raman Spectrum of P-CNTs, K-CNTs and KT-CNTs

Subsequently, FTIR analysis shows that functionalization with TBAB-based DES results in formation of new functional groups. The N-H stretch is present at wavenumber 3172 cm^{-1} in the KT-CNT spectrum (B. C. Smith, 1998). The presence of O-H is obvious in K-CNTs at 3478 cm^{-1} , however, this peak disappeared after application of DES as a functionalization agent which reduced the hydrophilicity of the surface. In addition, the presence of C-Br⁻ bonds can be observed in the range of 550 and 650 cm^{-1} for KT-CNTs. The presence of new chemical groups after functionalization with DES provides proof of modification and the creation of various adsorption sites, and increases the adsorption capacity for Hg^{2+} . Figure 3 shows the FTIR spectra for P-CNTs, K-CNTs, and KT-CNTs.

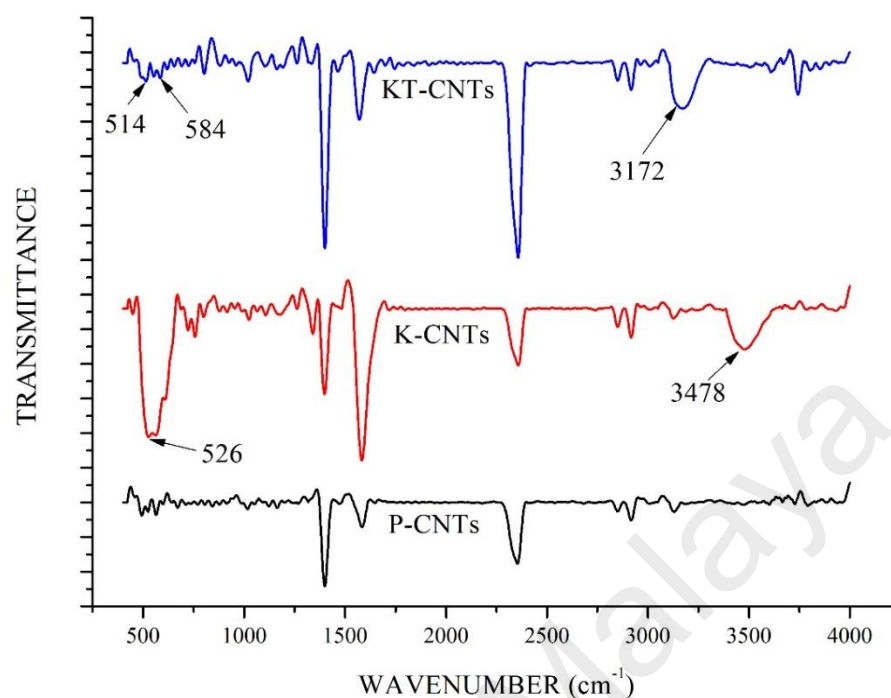


Figure 9.3: FTIR spectrum for P-CNTs, K-CNTs and KT-CNTs

The XRD results displayed a typical spectrum of P-CNTs, where (002) and (001), representing the hexagonal graphite structure and the concentric cylinder structure respectively, are located at 2θ around 26° and 42° , respectively in the P-CNTs patterns (D. Zhang et al., 2005). Figure 9.4 shows the XRD patterns of P-CNTs, K-CNTs, and KT-CNTs. After functionalization by KMnO_4 , the peaks almost completely disappeared, which indicates that the deposition of MnO_2 destroys the hexagonal graphite structure of the CNTs by conforming the CNTs into a non-stoichiometric, amorphous shape (S.-G. Wang et al., 2007). The presence of MnO_2 was identified by the two peaks at 2θ around 38° and 65° in K-CNTs pattern which can be indexed as (201/111) and (021/311), respectively (AlOmar et al., 2017). In the sequential functionalization step, the TBAB-based DES decreased the intensity of these peaks and the main peaks of CNTs were no longer present. This indicates the presence of more Sp^3 functional groups. Figure 9.5

shows the FESEM images for P-CNTs, K-CNTs, and KT-CNTs, indicating the presence of MnO₂ and, furthermore, the TBAB based DESs are barely observable in the FESEM images. Which indicates that the MnO₂ was embedded inside the CNTs. Furthermore, an EDX study for KT-CNTs after Hg²⁺ sorption was performed. Figure 1G shows the EDX spectrum of KT-CNTs after adsorption. Also, a traceable amounts of Hg²⁺, Br⁻, O, and N were also seen in the EDX spectrum.

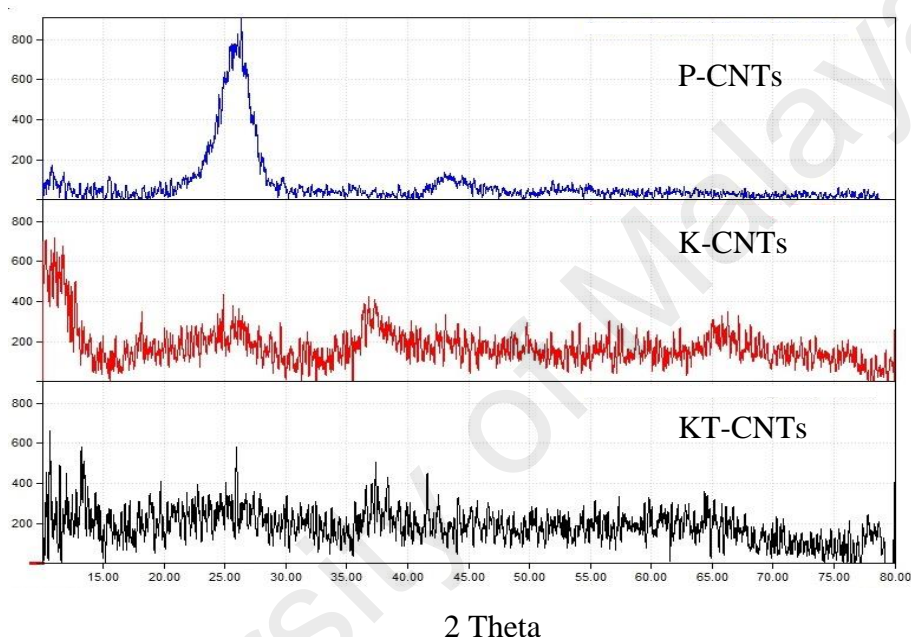


Figure 9.4: XRD pattern of P-CNTs, K-CNTs, and KT-CNTs

The zeta potential is the electrical potential between the bulk fluid and the surface across the dielectrical layer attached to the suspended particles in a solution. This potential is a source of balancing electrostatic force that keeps the micro or nano particles stable in suspension or emulsion. The absolute zeta potential was found to be 5.5, 45.81, and 59.7 for P-CNTs, K-CNTs, and KT-CNTs, respectively.

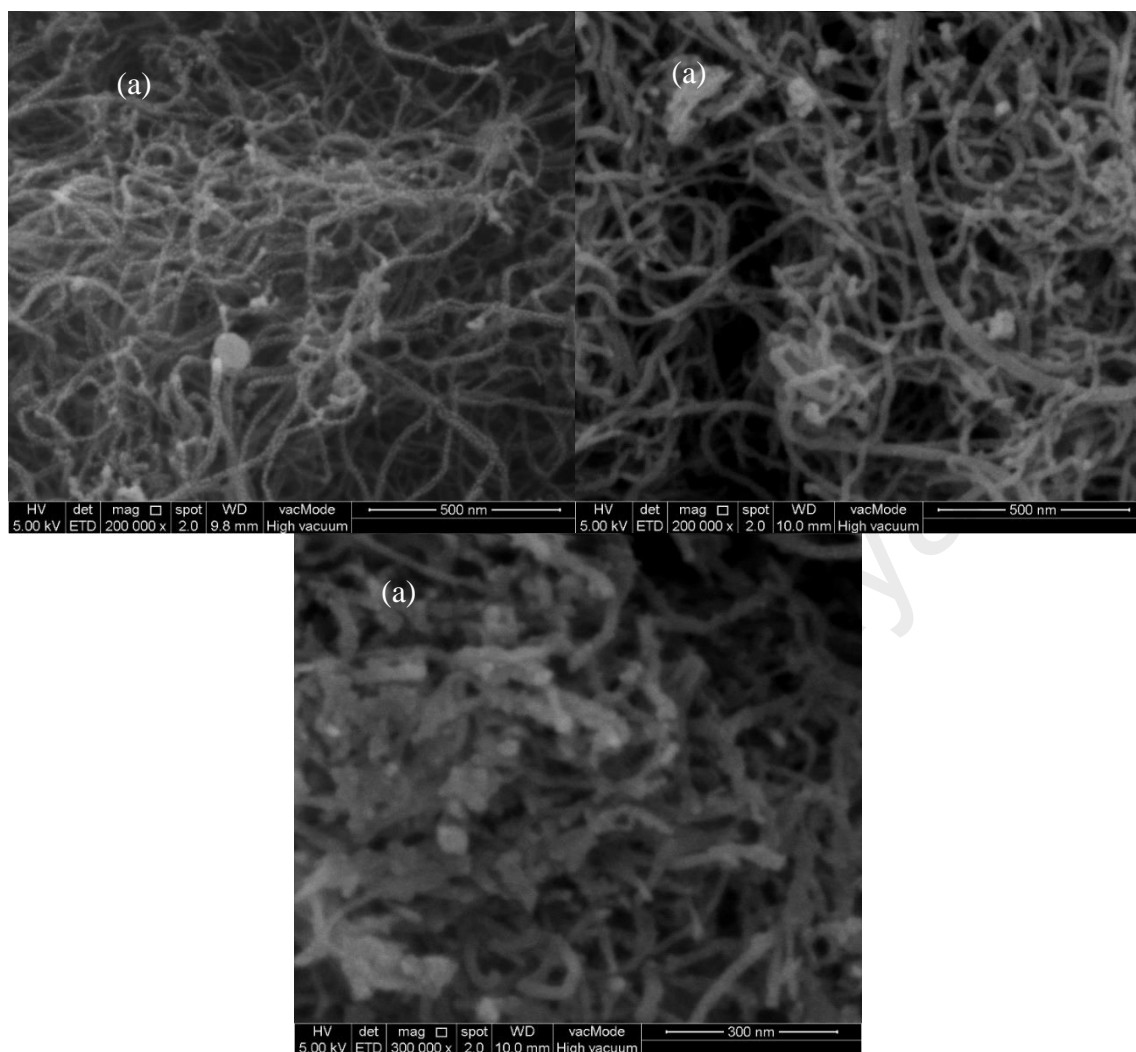


Figure 9.5: FESEM images for P-CNTs, K-CNTs and KT-CNTs

Functionalization with KMnO_4 resulted in the addition of new oxygen functional groups in form of carbonyl groups and aliphatic carboxylic acids. These functional groups increased the hydrophilicity of the surface, which resulted in increasing surface electronegativity, which plays an important role in the adsorption mechanism (AlOmar, Alsaadi, Hayyan, Akib, & Hashim, 2016; AlOmar, Alsaadi, Hayyan, Akib, Ibrahim, et al., 2016). The enhancement in the surface charge also comes from the formation of electronegative active sites, which were generated from the new functional groups and formed by using DESs as a functionalization agent, which significantly increased the zeta potential. It's worth mentioning that there are many factors affecting zeta potential measurements, including particle surface charges, pH, conductivity, ion concentration,

and temperature (Simate et al., 2012). On the other hand, the effect of TBAB-based DES functionalization on the BET surface area was significant, and which was found to be 123.54, 158.93, and 204.525 m²/g for P-CNTs, K-CNTs, and KT-CNTs, respectively. In addition, K-CNTs demonstrate a significant reduction in the pore volume, 0.45 cm³/g, as compared to P-CNTs, 0.62 cm³/g. Subsequently, the pore size diameters are believed to have increased significantly after each functionalization step, and these sizes were measured at 20.49, 114.12, and 124.8702 Å for P-CNTs, K-CNTs, and KT-CNTs, respectively.

The results obtained from the optimization study for both responses are listed in Table 1G. The highest R was measured at 96.3% under conditions of pH 5.5, contact time 55, and adsorbent dosage of 20 mg, and the highest Q was 16.44 mg/g at pH 5.5, contact time 30, and adsorbent dosage of 5 mg. The analysis of variance (ANOVA) of R and Q responses implies that both models are significant. Table 2G and Table 3G listed the P-values, F-values, and the square mean for both R and Q, respectively. Only a 0.01% and 1.1% chance that a "Model F-Value" this large could occur due to noise for both responses, respectively. These models can be used to successfully navigate the design space. The models are represented by the following formulas regression equations, Eq. 9.5 and Eq. 9.6. The correlation coefficients, R², was 0.9491 and 0.9978 for both R and Q, respectively.

$$Hg^{2+} \text{ removal } \% (R) = 98.04 + 17.08A + 3.33B + 1.62C - 1.93AB + 0.49AC - 0.55BC - 19.04A^2 - 0.061B^2 - 2.22C^2 \quad (9.6)$$

$$KT - CNTs \text{ adsorption capacity } (Q) = 26.16 + 12.65A + 1.11B - 22.64C + 0.63AB - 7.66AC - 0.92BC - 21.45A^2 + 12.69C^2 - 0.56ABC + 12.18A^2C \quad (9.7)$$

Where A, B and C represent pH, contact time, and adsorbent dosage, respectively.

The relationship between the theoretical values and experimental values was demonstrated in Figure 9.6 (a and b) for R and Q, respectively. Since the theoretical values predicted by the models developed in this study were quite close to the experimental values, it can be concluded that both models have successfully achieved correlation between the process variables.

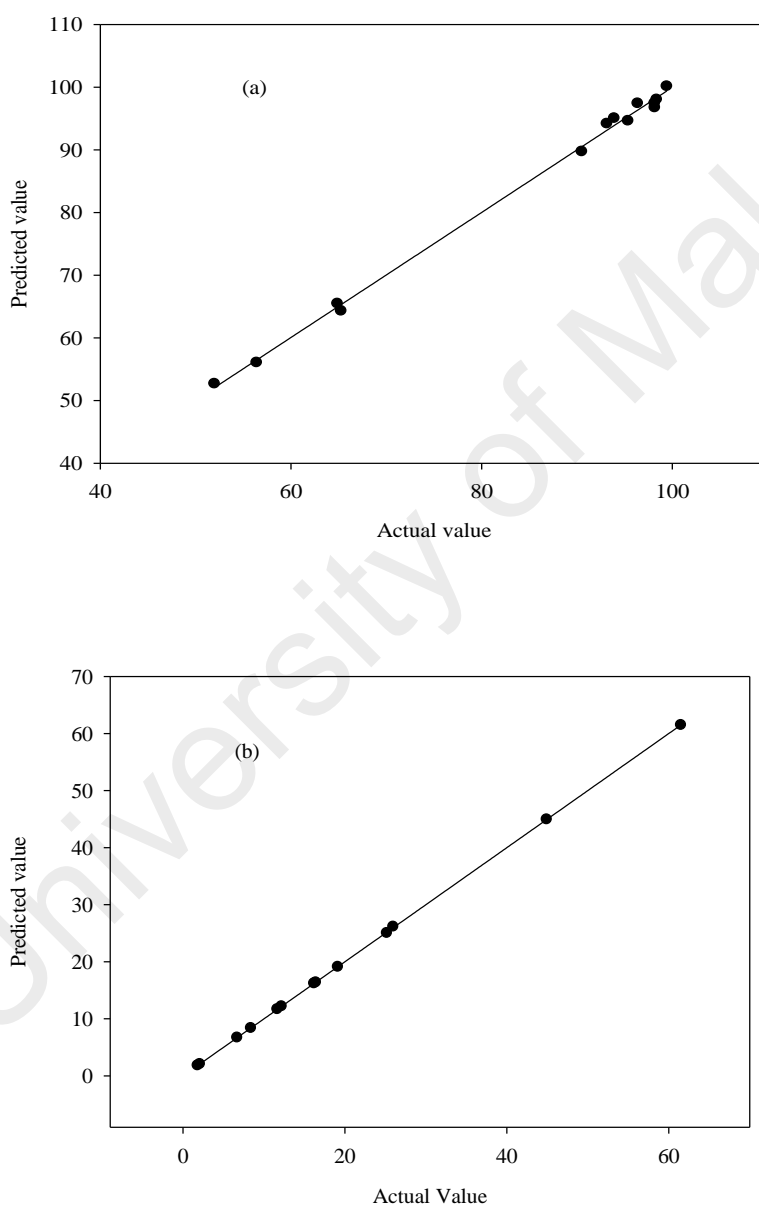


Figure 9.6: Theoretical vs experimental data for Hg²⁺ a) removal (%) and b) uptake capacity (mg/g) on KT-CNT adsorbent

Table 9.1 lists the restrictions developed to control the optimization solutions of the CCD software. The optimal removal conditions were found to be pH 6.4, an adsorbent dosage around 6.0 mg, and a contact time of 45 min. It is well known that the dominant Hg species at pHs between 5-8 are Hg^{2+} and $\text{Hg}(\text{OH})_2$. The surface charge of the adsorbent also increased inversely with relation to pH, which reduces the H^+ competition with Hg species. Herein, Figure 9.7 shows the effect of pH on R by fixing the adsorbent dosage to the optimal dose. At the optimum adsorbent dosage, the R increased gradually until it reached the optimal pH, at around 6.4, and then remain constant. Meanwhile, the contact time has a significant affect on R. Conversely, at a maximum adsorbent dosage of 20 mg, the effect of contact time is almost negligible, while the solution pH has a significant affect on the removal of Hg^{2+} . This may be due to the increase in the number of active sites, which makes the adsorption faster and, in turn, the effect of pH more obvious. Figure 9.8 shows the effect of pH on Hg removal by fixing the adsorbent dosage to the maximum. On the other hand, the adsorbent dosage has no significant effect on R, as demonstrated in Figure 9.9.

Table 9.1: Constraints for optimization process based on CCD for Hg^{2+} adsorption

Name	Goal	Lower limit	Upper limit	Importance
A	in range	3	8	3
B	in range	5	55	3
C	in range	5	20	3
R	maximize	51.98	99.43	5
Q	maximize	1.81	61.51	5

Design-Expert® Software

Rmoval
96.3
38.2

X1 = A: pH
X2 = B: contact time

Actual Factor
C: dose = 20.00

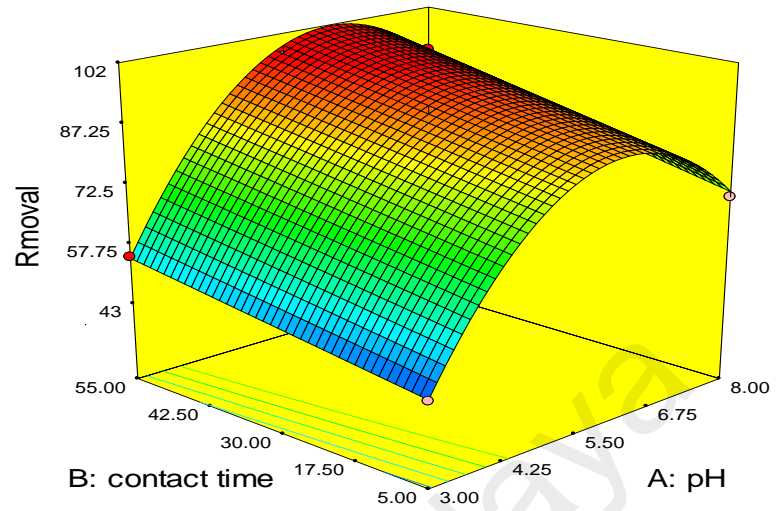


Figure 9.8: Effect of pH and contact time on the removal % at the optimum adsorbent dosage

Design-Expert® Software

Rmoval
99.4396
51.9814

X1 = A: pH
X2 = B: contact time

Actual Factor
C: dose = 5.16

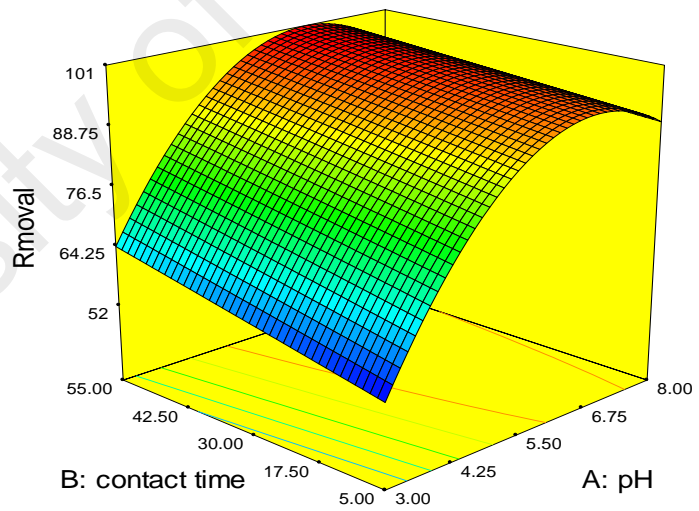


Figure 9.8: Effect of pH and contact time on the removal % at the maximum adsorbent dosage

Regarding the Q response, the effect of pH is also obvious, which can be seen in Figure 9.10. Meanwhile, the Q has increased with increasing contact time, due to an attempt to reach equilibrium. Also, Figure 9.11 demonstrates the effect of adsorbent dosage on Q , although it is well known that, Q increases with decreasing adsorbent

dosage.

Design-Expert® Software

R_{removal}
99.4396
51.9814

X1 = A: pH
X2 = C: dose

Actual Factor
B: contact time = 45.63

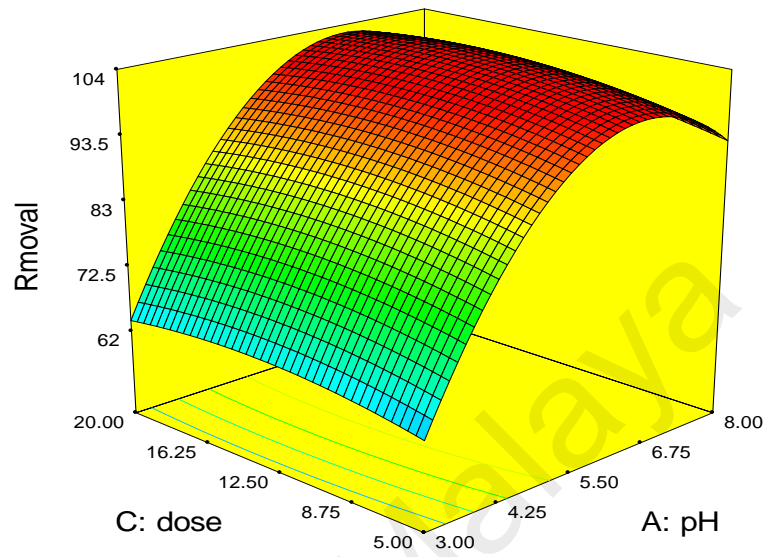


Figure 9.10: Effect of pH and adsorbent dosage on the removal %

Design-Expert® Software

Adsorption Capacity
61.51
1.815

X1 = A: pH
X2 = B: contact time

Actual Factor
C: dose = 5.16

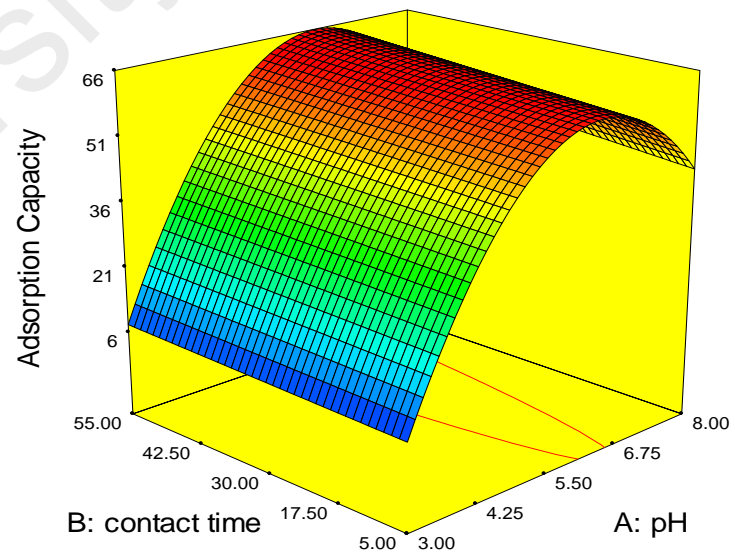


Figure 9.10: Effect of pH and contact time on the adsorption capacity of KT-CNTs

Design-Expert® Software

Adsorption Capacity



X1 = A: pH
X2 = C: dose

Actual Factor
B: contact time = 45.63

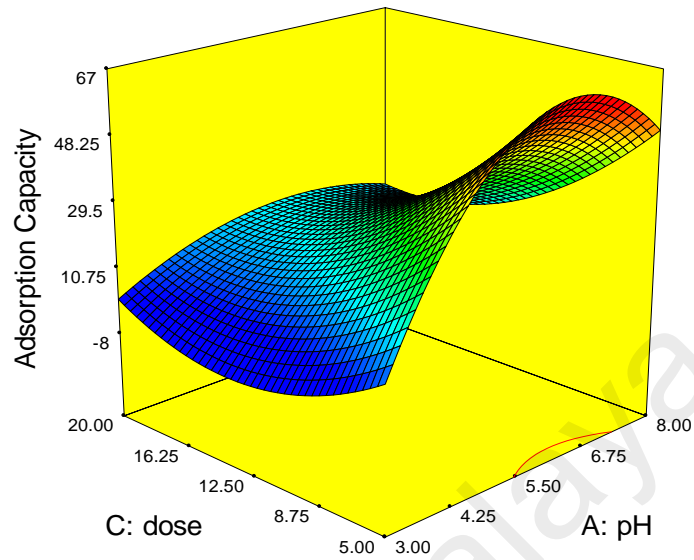


Figure 9.11: Effect of pH and adsorbent dosage on the adsorption capacity of KT-CNTs

The optimal removal conditions were used to study the adsorption kinetics and isotherms. Based on the values of the correlation coefficients, R^2 , was obtained by fitting the experimental data to the pseudo-first order and pseudo-second order kinetics models. Specifically, Hg^{2+} adsorption on the surface of KT-CNTs followed the pseudo-second order kinetics rate since the R^2 was found to be 0.997. On the other hand, the fitting of the pseudo-first order was very poor. Table 9.2 lists the R^2 and the constants coefficients for each model. These findings agree with previous research on CNTs-based adsorbents (Gong et al., 2014; C. Zhang et al., 2012). Figure 9.12 plots the experimental data according to the linearized pseudo-second order model.

Table 9.2: Experimental values of constants of adsorption kinetics models

Experimental (q)	Pseudo-first- order			Pseudo-second-order		
	q_e (mg/g)	K_1 (min ⁻¹)	R^2	q_e (mg/g)	K_2 (g/mg.min)	R^2
23.928	22.718	-0.00049	0.545	25.976	0.0037	0.997

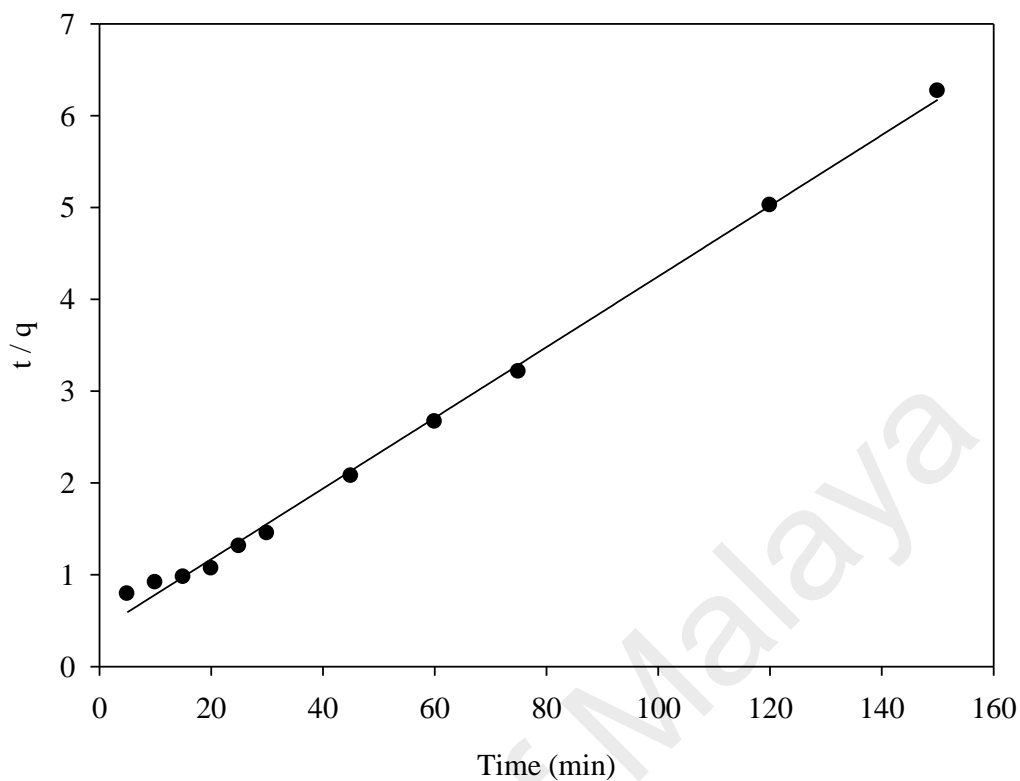
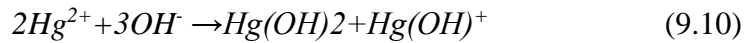
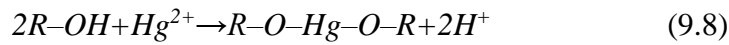


Figure 9.12: Pseudo-second-order adsorption kinetics model

MWCNTs and their modified allotropes have a heterogeneous surface. Therefore, the system probably follows multiple mechanisms of adsorption and surface reaction (P. H. Chen et al., 2014; Hadavifar et al., 2014).

The functional groups with high electronegativity present on the surface of MWCNTs, such as oxygen-containing groups or C-Br⁻ bonds, could form complexation with Hg²⁺ ions. Ion exchange processes could also take place with surface-attached H⁺ as well. That means, we are in front of two possible probabilities of two different surface reaction reactions, either complexation or proton exchange. On the other hand, OH⁻ ions in the solution play positive role in consuming H⁺, which is why there is enhanced adsorption with the increase of pH to certain point (in our case pH 6.4). However, a further increase in pH leads to an excess amount of OH⁻, which forms complexations with Hg in the

solution and reduces the rate of adsorption on the surface (Hadavifar et al., 2014). The mechanism that we expect is illustrated in Eq. 9.8, 9.9, and 9.10.



For the isotherm study, both the Langmuir and Freundlich isotherm models were found to be a fair fit to the experimental data. This behavior can be observed at low concentrations, where there is no contradiction between the two models. It is common in adsorption studies, as stated in many publications listed in Table 9.3, to have this kind of duality. However, the behavior of the adsorbate-adsorbent system at high concentrations deviates from the ideal gas model. Although the principal assumptions for Langmuir is monolayer-based and Freundlich is multilayer-based, both models can fit with the same set of data at low concentrations and high adsorption capacity for the adsorbent. Herein, the Freundlich isotherm model exhibited more conformity regarding the correlation coefficient, R^2 . Table 3 lists the values of R^2 and the isotherm constants for both the Langmuir and Freundlich isotherm models. The suitability of Freundlich model suggests that the adsorption system is heterogeneous by which the adsorption process takes place onto the adsorbent surface which contains different active sites with various affinities to Hg^{2+} ions and it gives consideration for the roughness of the surface as well as the multilayer approach. To reference the n value ($1 < n < 10$), the adsorptive behavior is dominated as a physisorption process and indicates the favorability of the Hg^{2+} adsorption on KT-CNTs (Saleh, 2015). Based on these results, the adsorption of Hg^{2+} occurs on a heterogeneous surface with interactions between the adsorbed molecules with a non-

uniform distribution of heat of sorption over the surface (Ghaedi et al., 2011). Furthermore, some monolayer coverage of Hg^{2+} ions on the surface of the KT-CNTs may be formed according to the Langmuir fitting data (Langmuir, 1916). Figure 9.13 and Figure 9.14 plot the linearized adsorption isotherm of KT-CNTs for both the Langmuir and Freundlich equations, respectively.

Table 9.3: Isotherm models parameters and comparison of adsorption capacity of other adsorbents

Adsorption Model	Isotherm	Langmuir			Freundlich			Reference
		qm (mg/g)	K_L (l/mg)	R2	n	K_f (mg/g)	R2	
KT-CNTs	6.5	177.7	9.77	0.949	2.69	37.9	0.976	Present work (Hadavifar et al., 2014) (Saleh, 2015) (A. Gupta et al., 2014) (P. H. Chen et al., 2014) (C. Zhang et al., 2012)
^a MWCNTs-SH		84.6	0.31	0.945	0.30	30.9	0.926	
^b SiO ₂ -CNT	5-6	250	0.14	0.982	1.50	34.8	0.992	
^c CNT-S	6	151.5	0.314 3	0.994	1.83	1.24	0.936	
^d COOH-MWCNT	4.3	127.6	0.19	0.990	1.17	18.0	0.968	
^e MPTS-CNTs/Fe ₃ O ₄	6.5	65.5	0.039	0.992	2.26	7.62	0.984	

^asodium 2-mercaptoethanol functionalized CNT, ^bSilica combined with 2 % functionalized CNT, ^csulfur incorporated MWCNT, ^dpre-treated MWCNT in acidic $KMnO_4/H_2SO_4$ solution, ^eThiol-functionalized multiwall carbon nanotube/magnetite nanocomposites.

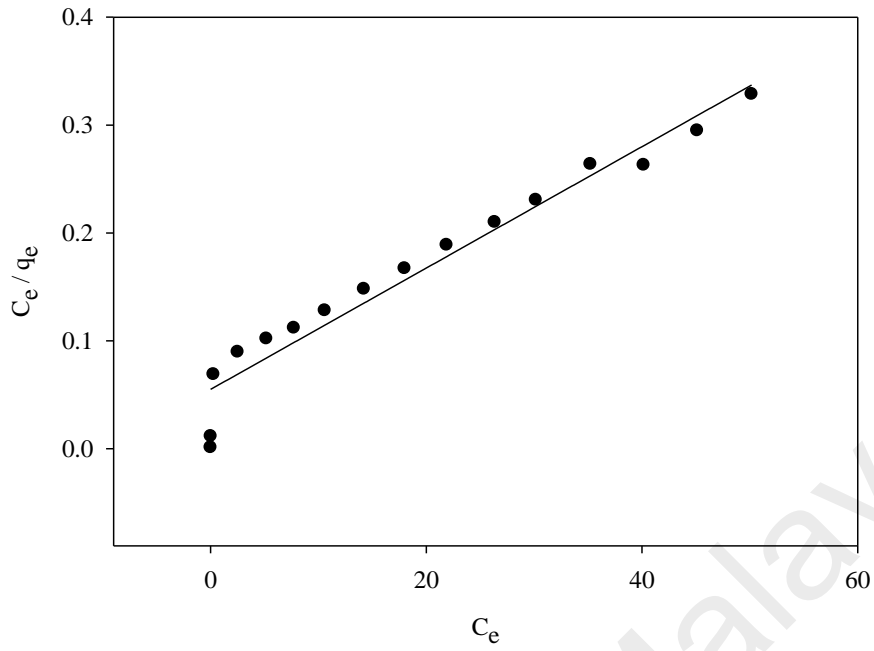


Figure 9.13: Langmuir adsorption isotherm model

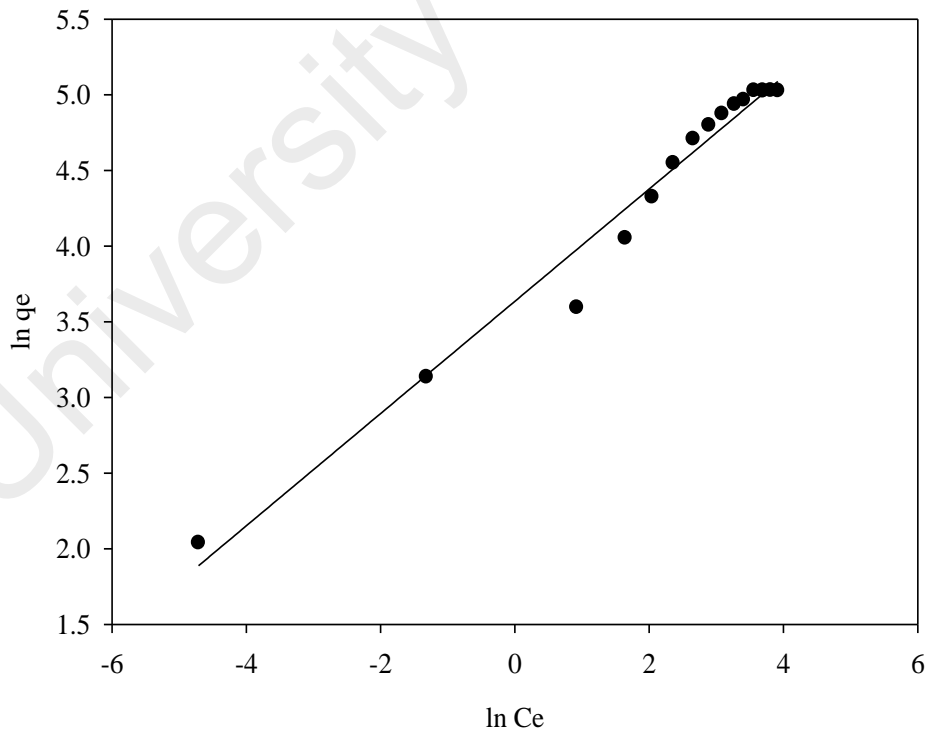
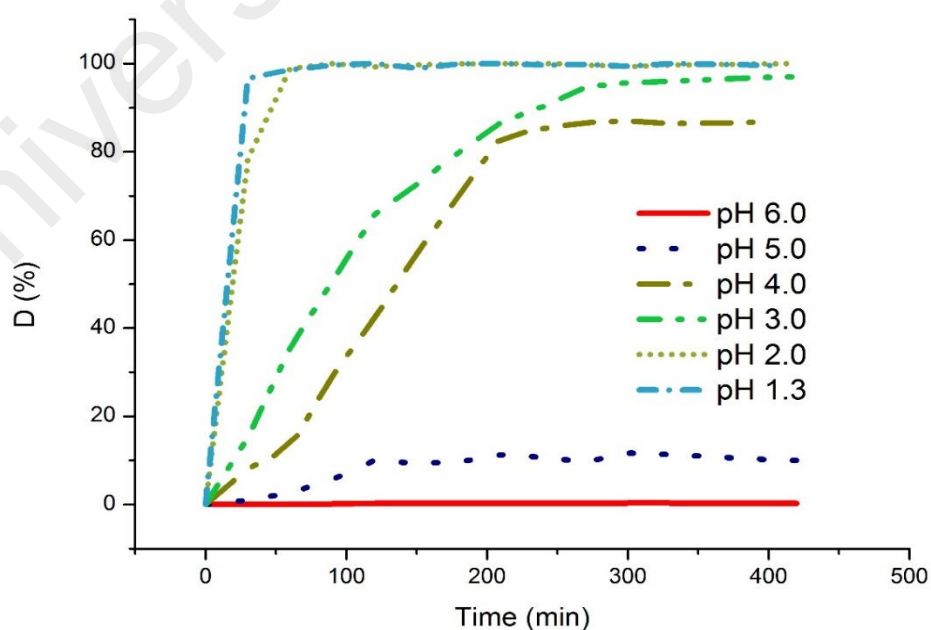


Figure 9.14: Freundlich adsorption isotherm model

The recyclability of an adsorbent is essential for practical applications. The simplicity of desorbing metal ions for many cycles of feasible reusability is one of the most important characteristics of a potential industrial adsorbent. The D% was only 10% at pH 5.0 after 3 hr and exceeds 80% at pH 3.0 after 3 hr. The D% was effective at $\text{pH} \leq 3.0$ as seen in Figure 9.15. The rate of desorption increases with the decrease of pH as demonstrated in Figure 9.16, where the slope of the curve before equilibrium starts with very low value at pH 4.0 and increases alongside the pH increase until it reaches the highest value at pH 1.3, almost vertical, when the spontaneous desorption takes place. The system reaches equilibrium at different concentrations and at different pHs, also in different equilibrium times. The fastest and highest desorption was seen at pH 1.3 with an equilibrium close to zero. To confirm the viability of regeneration, the recovered adsorbent from the desorption process was dried and reused multiple times. KT-CNTs were successfully reused five times, although the adsorption capacity decreased after each use until it reached 96 mg/g at round five.



9.15 desorption study of Hg^{2+} from KT-CNTs at different pHs

9.4 Summary

The Hg^{2+} ion was successfully removed from an aqueous solution by CNTs functionalized with DESs. The novel adsorbent exhibited great potential for Hg^{2+} removal, where the maximum adsorption capacity was found to be 177.76 mg/g, which lies in the highest range compared to the published data. The optimal removal conditions were found to be at pH 6.4, adsorbent dosage of 6.0 mg, and contact time of 45 min. A TBAB-based DESs was synthesized and was a sufficient functionalization agent for CNTs. The effect of TBAB-DES on the surface of CNTs and the enhancement was proved by investigation using Raman spectroscopy, FTIR, XED, Zeta potential, EDX, FESEM, and BET. The characterization showed that using a TBAB-based DES for functionalization resulted in significantly increasing the surface area of CNTs from 123.54 m^2/g to 204.525 m^2/g . In addition, the presence of new functional groups was detected by FTIR. The functionalized carbon nanomaterials were proven to be sufficient adsorbents for various contaminants, especially Hg^{2+} . With help of DESs, we managed to replace hazardous chemicals in the process of functionalization. These two findings can be a platform for future research and industrial implementation.

CHAPTER 10: CONCLUSION AND RECOMMENDATIONS

10.1 Conclusion

In this study, novel adsorbents were successfully prepared to remove three types of heavy metals, Pb^{2+} , As^{3+} , and Hg^{2+} . Firstly, new types of DESs were synthesized, based on different molar ratios, and subjected to screening studies in order to select the most stable molar ratio. The physical properties of these DESs were investigated. Later, three primary oxidized CNTs were prepared based on pristine CNTs (P-CNTs), specifically CNTs treated with $KmNO_4$ (K-CNTs), CNTs acidified by HNO_3 (N-CNTs), and CNTs acidified with H_2SO_4 (S-CNTs). Subsequently, the selected DESs were applied as functionalization agents for the four base CNTs. Later, screening studies involving patch adsorption experiments were performed for each heavy metal to select the most suitable adsorbent, based on the highest removal percentage obtained from the screening study. The selected adsorbents were characterized using Raman, FTIR, XRD, FESEM, EDX, BET surface area, TGA, TEM and zeta potential. An optimization study was performed for each adsorbent using surface response methodology (Central composite design (CCD)) to obtain the optimum removal conditions. Two responses were chosen for each adsorbent, including adsorption capacity and removal percentage. An empirical equation was developed based on the optimization studies using analysis of variance modelling (ANOVA) for each response. Kinetics and isotherm studies were performed for each adsorbent. Below are the main findings of this study:

1. Deep eutectic solvents (DESs) occupy a strategic place as an analogue to ionic liquids (ILs) due to their availability, lack of significant toxicity, biodegradability, recyclability, flammability, and low price compared to other types of conventional ionic liquids. Ten DESs systems were successfully synthesized based on different ammonium and phosphonium based salts and different hydrogen bond donors (HBDs). 110 different

DESs were synthesized based on different molar ratios (1-10) for each DES system. The first stable ratio of each system was selected to investigate the physical properties with respect to temperature, density, viscosity, conductivity, and surface tension. Moreover, a freezing point study was conducted for each DES. Additionally, FTIR was utilized to identify the functional groups associated with the synthesis of these novel DESs. The phosphonium based DESs have a higher density and viscosity compared to the ammonium based DESs. The effects of molar ratio on the physical properties was also investigated for the Gly: BTAC based DESs.

2. A primary oxidation was successfully performed by sonicating 200 mg of P-CNTs in 7 ml of 1 mol KMnO_4 solution for 2h at 65 °C. The second type of primary oxidation involved acidification of P-CNTs with HNO_3 or H_2SO_4 . P-CNTs were then refluxed in HNO_3 65% for 1 h at 140 °C. The second type of acidification was done by refluxing P-CNTs in H_2SO_4 (50%) for 1 h at 140 °C.
3. The selected DESs were used as functionalization agents for CNTs. Four types of base CNTs were used to be functionalized with DESs which are P-CNTs, K-CNTs, N-CNTs, and S-CNTs. A simple functionalization process was used that involved sonication of the base CNTs in each DES system for 3 h at 65 °C.
4. The resulting DES-CNTs combinations were successfully used as adsorbents of heavy metals ions, including Pb^{2+} , As^{3+} , and Hg^{2+} . A screening study was performed to find the best adsorbent for each heavy metal.
5. Characterization studies revealed the deposition of MnO_2 in the graphite sheets of CNTs. This was seen by TEM and FESEM imaging.

Furthermore, the XRD profile and Raman spectroscopy demonstrated the oxidation state of Mn on the surface of the CNTs. TGA analysis showed that the K-CNTs have more than 65% MnO₂. This was supported by the EDX results, where the percentage of Mn on the surface of the CNTs was approached 60%, depending on the type of DES used for the subsequent functionalization. After functionalization with DESs, new functional groups were formed. These were visualized using TEM and FESEM imaging. In addition, the XRD profile revealed that functionalization with DESs increased the coating of the functional groups on the surface of CNTs, which led to changes in the CNT structure by contorting its surface into a non-stoichiometric, amorphous shape. The surface area was improved significantly after functionalization with DESs. Lastly, the surface charge also increased with each functionalization step. All of these factors resulted in significant improvement on the surface of CNTs from the functionalization with DESs and a positive impact on the adsorption of heavy metals.

6. For the removal of Pb²⁺, six ChCl based DESs were synthesized and applied as functionalization agent to four based CNTs: P-CNTs, K-CNTs, N-CNTs, S-CNTs. Out of 28 adsorbents, the screening study revealed that K-CNTs functionalized with ChCl:TEG DES (KTEG-CNTs) were associated with the highest removal efficiency. Removal percentages and uptake capacities of Pb²⁺ on the novel selected adsorbents were optimized by RSM-CCD experimental design. The optimum conditions were found to be pH 5 with an adsorbent dosage of 5 mg and a contact time of 15 min. The maximum adsorption capacity of the selected adsorbent was found to be 288.4 mg/g. Both Langmuir and Freundlich adsorption isotherm

models described the adsorption isotherm. The kinetics study was described well by a pseudo-second order kinetics model.

7. For the removal of As^{3+} , three adsorbents were selected as the most suitable adsorbents, namely KM-CNTs, KB-CNTs and KD-CNTs, based on the screening study. Optimization studies were carried out utilizing RSM-CCD experimental designs to estimate the optimum removal conditions for each adsorbent. For KM-CNTs, the optimal removal conditions were pH 3.0, a contact time 55 min, and an adsorbent dosage of 20 mg. Meanwhile, when using KB-CNTs and KD-CNTs, the optimal pH was pH 6.0. The adsorption experimental data of all adsorbents fitted well with a pseudo-second-order kinetics model. In addition, the Langmuir and Freundlich equation described the adsorption isotherm models. The maximum adsorption capacity was 23.4, 14.23, 17 mg/g for KM-CNTs, KB-CNTs and KD-CNTs, respectively.
8. For the removal of Hg^{2+} , two adsorbents were selected, KA-CNTs and KT-CNTs based on the screening study. As per the optimization study, the optimal adsorption conditions were pH 5.5, a contact time of 28 min, and an adsorbent dosage of 5 mg for KA-CNTs. While the optimum removal conditions for KT-CNTs were at pH 6.4, an adsorbent dosage of 6.0 mg, and a contact time of 45 min. A pseudo-second order model accurately described the adsorption of Hg^{2+} for both adsorbents. On the other hand, a Freundlich isotherm was used to approximate the data with a maximum adsorption capacity of 186.97 mg/g for KA-CNTs. While, for KT-CNTs, both the Langmuir and Freundlich models fitted the isotherm data for KT-CNTs with a maximum adsorption capacity of 177.76 mg/g. The

desorption study revealed that KA-CNTs can be recycled and used three times with a 70% efficiency.

10.2 Recommendations

From the experience obtained through various stages of this study, many recommendations for further studies can be proposed and these proposals form in three distinct directions. The first involves DESs synthesis and characterization. The second consists of the functionalization processes, and finally future work should focus on water remediation. The following recommendations are proposed for future work:

1. For design purposes, a full rheological study is essential for different DESs as function of temperature. A determination of Newtonian or non-Newtonian behavior of each DES is very important, in addition to the phase changes that occur with temperature.
2. There are many other potential DESs can be explored using metal salts or organic salts.
3. The use of metal based DESs as functionalization agents is an interesting research pathway.
4. The uses of DESs as functionalization agents with other carbon based nanomaterials, i.e., graphene, SWCNTs, and other types of CNTs that are synthesized on different substrates, like activated carbon impregnated CNTs, warrant investigation.
5. The success of DES-CNTs adsorbent to remove Pb^{2+} , As^{3+} and Hg^{2+} gives a good indication if these adsorbents are useful in the removal of other types of heavy metals, such Cd, Cr, Ni, and Fe.
6. A column study can be performed to investigate the breakthrough conditions for adsorption processes.

7. A competition study can be carried out to determine the performance of each adsorbent with competitive ions.
8. Novel adsorbents can be used to remove other types of pollutant, such as organic compounds, dyes, and bio pollutants.
9. The DES-CNT adsorbents can be fixed in a packed bed filter to be used for continuous adsorption process in future investigations.

University of Malaya

REFERENCES

- A. C. Dillon, K. M. J., T. A. Bekkedahl, C. H. Kiang, D. S. Bethune & M. J. Heben. (1997). Storage of hydrogen in single-walled carbon nanotubes. *nature*, 386, 377-379.
- Abbott, A., Eardley, C., Farley, N. S., Griffith, G., & Pratt, A. (2001). Electrodeposition of aluminium and aluminium/platinum alloys from AlCl₃/benzyltrimethylammonium chloride room temperature ionic liquids. *Journal of Applied Electrochemistry*, 31(12), 1345-1350. doi:10.1023/A:1013800721923
- Abbott, A. P., Capper, G., Davies, D. L., Munro, H. L., Rasheed, R. K., & Tambyrajah, V. (2001). Preparation of novel, moisture-stable, Lewis-acidic ionic liquids containing quaternary ammonium salts with functional side chains. *Chemical Communications*(19), 2010-2011. doi:10.1039/B106357J
- Abbott, A. P., Capper, G., Davies, D. L., Rasheed, R. K., & Tambyrajah, V. (2003). Novel solvent properties of choline chloride/urea mixtures. *Chemical Communications*(1), 70-71. doi:10.1039/B210714G
- Abbott, A. P., Boothby, D., Capper, G., Davies, D. L., & Rasheed, R. K. (2004). Deep Eutectic Solvents Formed between Choline Chloride and Carboxylic Acids: Versatile Alternatives to Ionic Liquids. *Journal of the American Chemical Society*, 126(29), 9142-9147. doi:10.1021/ja048266j
- Abbott, A. P., Capper, G., Davies, D. L., & Rasheed, R. (2004). Ionic Liquids Based upon Metal Halide/Substituted Quaternary Ammonium Salt Mixtures. *Inorganic Chemistry*, 43(11), 3447-3452. doi:10.1021/ic049931s
- Abbott, A. P., Capper, G., Davies, D. L., & Rasheed, R. K. (2004). Ionic Liquid Analogues Formed from Hydrated Metal Salts. *Chemistry – A European Journal*, 10(15), 3769-3774. doi:10.1002/chem.200400127
- Abbott, A. P., & McKenzie, K. J. (2006). Application of ionic liquids to the electrodeposition of metals. *Physical Chemistry Chemical Physics*, 8(37), 4265-4279. doi:10.1039/B607329H
- Abbott, A. P., Capper, G., & Gray, S. (2006). Design of Improved Deep Eutectic Solvents Using Hole Theory. *ChemPhysChem*, 7(4), 803-806. doi:10.1002/cphc.200500489
- Abbott, A. P., Barron, J. C., Ryder, K. S., & Wilson, D. (2007). Eutectic-Based Ionic Liquids with Metal-Containing Anions and Cations. *Chemistry – A European Journal*, 13(22), 6495-6501. doi:10.1002/chem.200601738
- Abbott, A. P., Capper, G., McKenzie, K. J., & Ryder, K. S. (2007). Electrodeposition of zinc–tin alloys from deep eutectic solvents based on choline chloride. *Journal of Electroanalytical Chemistry*, 599(2), 288-294. doi:<http://dx.doi.org/10.1016/j.jelechem.2006.04.024>

- Abbott, A. P., Harris, R. C., & Ryder, K. S. (2007a). Application of Hole Theory to Define Ionic Liquids by their Transport Properties. *The Journal of Physical Chemistry B*, *111*(18), 4910-4913. doi:10.1021/jp0671998
- Abbott, A. P., Harris, R. C., & Ryder, K. S. (2007b). Application of Hole Theory to Define Ionic Liquids by their Transport Properties†. *The Journal of Physical Chemistry B*, *111*(18), 4910-4913. doi:10.1021/jp0671998
- Abbott, A. P., Griffith, J., Nandhra, S., O'Connor, C., Postlethwaite, S., Ryder, K. S., & Smith, E. L. (2008). Sustained electroless deposition of metallic silver from a choline chloride-based ionic liquid. *Surface and Coatings Technology*, *202*(10), 2033-2039. doi:<http://dx.doi.org/10.1016/j.surfcoat.2007.08.055>
- Abbott, A. P., El Ttaib, K., Frisch, G., McKenzie, K. J., & Ryder, K. S. (2009). Electrodeposition of copper composites from deep eutectic solvents based on choline chloride. *Physical Chemistry Chemical Physics*, *11*(21), 4269-4277. doi:10.1039/B817881J
- Abbott, A. P., Harris, R. C., Ryder, K. S., D'Agostino, C., Gladden, L. F., & Mantle, M. D. (2011). Glycerol eutectics as sustainable solvent systems. *Green Chemistry*, *13*(1), 82-90.
- Abbott, A. P., Ttaib, K. E., Frisch, G., Ryder, K. S., & Weston, D. (2012). The electrodeposition of silver composites using deep eutectic solvents. *Physical Chemistry Chemical Physics*, *14*(7), 2443-2449. doi:10.1039/C2CP23712A
- Abdel-Ghani, N. T., Hefny, M., & El-Chaghaby, G. A. F. (2007). Removal of lead from aqueous solution using low cost abundantly available adsorbents. *International Journal of Environmental Science & Technology*, *4*(1), 67-73. doi:10.1007/BF03325963
- Abdo, K. M. (2000). *NTP Technical Report on the Toxicity Studies of Benzyltrimethylammonium Chloride*. Retrieved from U.S. Department of Health and Human Services, Public Health Service, National Institutes of Health:
- Abo-Hamad, A., Hayyan, M., AlSaadi, M. A., & Hashim, M. A. (2015). Potential applications of deep eutectic solvents in nanotechnology. *Chemical Engineering Journal*, *273*, 551-567. doi:<http://dx.doi.org/10.1016/j.cej.2015.03.091>
- Addo Ntim, S., & Mitra, S. (2011). Removal of Trace Arsenic To Meet Drinking Water Standards Using Iron Oxide Coated Multiwall Carbon Nanotubes. *Journal of Chemical & Engineering Data*, *56*(5), 2077-2083. doi:10.1021/je1010664
- Addo Ntim, S., & Mitra, S. (2012). Adsorption of arsenic on multiwall carbon nanotube–zirconia nanohybrid for potential drinking water purification. *Journal of colloid and interface science*, *375*(1), 154-159. doi:<http://dx.doi.org/10.1016/j.jcis.2012.01.063>
- Ahmed, Y. M., Abdullah-Al-Mamun, S., Ma'an Fahmi, R., Jameel, A., & AlSaadi, M. A. (2010). Study of Pb Adsorption by Carbon Nanofibers Grown on Powdered Activated Carbon. *Journal of Applied Sciences*, *10*(17), 1983-1986.

- Aitchison, T. J., Ginic-Markovic, M., Matison, J. G., Simon, G. P., & Fredericks, P. M. (2007). Purification, Cutting, and Sidewall Functionalization of Multiwalled Carbon Nanotubes Using Potassium Permanganate Solutions. *The Journal of Physical Chemistry C*, *111*(6), 2440-2446. doi:10.1021/jp066541d
- Al-Mamun, A., Al-Khatib, M. A. F. R., Kadir, Z. A., Ahmed, Y. M., Mohammed, A., Alam, M., . . . Idris, A. (2009). Optimisation of arsenic adsorption from water by carbon nanofibres grown on powdered activated carbon impregnated with nickel.
- Al Mamun, A., Ahmed, Y. M., AlKhatib, M. a. F. R., Jameel, A. T., & AlSaadi, M. A. H. A. R. (2015). Lead Sorption by Carbon Nanofibers Grown on Powdered Activated Carbon — Kinetics and Equilibrium. *Nano*, *10*(02), 1550017. doi:doi:10.1142/S1793292015500174
- Ali, I. (2012). New Generation Adsorbents for Water Treatment. *Chemical Reviews*, *112*(10), 5073-5091. doi:10.1021/cr300133d
- Ali, I., & Gupta, V. K. (2007). Advances in water treatment by adsorption technology. *Nat. Protocols*, *1*(6), 2661-2667. doi:http://www.nature.com/nprot/journal/v1/n6/supinfo/nprot.2006.370_S1.html
- AlOmar, M. K., Alsaadi, M. A., Hayyan, M., Akib, S., & Hashim, M. A. (2016). Functionalization of CNTs surface with phosphonium based deep eutectic solvents for arsenic removal from water. *Applied Surface Science*, *389*, 216-226. doi:<http://dx.doi.org/10.1016/j.apsusc.2016.07.079>
- AlOmar, M. K., Alsaadi, M. A., Hayyan, M., Akib, S., Ibrahim, M., & Hashim, M. A. (2017). Allyl triphenyl phosphonium bromide based DES-functionalized carbon nanotubes for the removal of mercury from water. *Chemosphere*, *167*, 44-52. doi:<http://dx.doi.org/10.1016/j.chemosphere.2016.09.133>
- AlOmar, M. K., Alsaadi, M. A., Hayyan, M., Akib, S., Ibrahim, R. K., & Hashim, M. A. (2016). Lead removal from water by choline chloride based deep eutectic solvents functionalized carbon nanotubes. *Journal of Molecular Liquids*, *222*, 883-894. doi:<http://dx.doi.org/10.1016/j.molliq.2016.07.074>
- AlOmar, M. K., Hayyan, M., Alsaadi, M. A., Akib, S., Hayyan, A., & Hashim, M. A. (2016). Glycerol-based deep eutectic solvents: Physical properties. *Journal of Molecular Liquids*, *215*, 98-103. doi:<http://dx.doi.org/10.1016/j.molliq.2015.11.032>
- AlSaadi, M. A., Al Mamun, A., Alam, M. Z., Amosa, M. K., & Atieh, M. A. (2016). Removal of Cadmium from Water by CNT–PAC Composite: Effect of Functionalization. *Nano*, *11*(01), 1650011. doi:doi:10.1142/S1793292016500119
- Andjelkovic, I., Nestic, J., Stankovic, D., Manojlovic, D., Pavlovic, M. B., Jovalekic, C., & Roglic, G. (2013). Investigation of sorbents synthesised by mechanical–chemical reaction for sorption of As(III) and As(V) from aqueous medium. *Clean Technologies and Environmental Policy*, *16*(2), 395-403. doi:10.1007/s10098-013-0635-1

- Andrews, R., Jacques, D., Qian, D., & Rantell, T. (2002). Multiwall Carbon Nanotubes: Synthesis and Application. *Accounts of Chemical Research*, 35(12), 1008-1017. doi:10.1021/ar010151m
- Arnold, M. S., Green, A. A., Hulvat, J. F., Stupp, S. I., & Hersam, M. C. (2006). Sorting carbon nanotubes by electronic structure using density differentiation. *Nat Nano*, 1(1), 60-65. doi:http://www.nature.com/nnano/journal/v1/n1/suppinfo/nnano.2006.52_S1.html
- Asmaly, H. A., Abussaud, B., Ihsanullah, Saleh, T. A., Gupta, V. K., & Atieh, M. A. (2015). Ferric oxide nanoparticles decorated carbon nanotubes and carbon nanofibers: From synthesis to enhanced removal of phenol. *Journal of Saudi Chemical Society*, 19(5), 511-520. doi:<http://dx.doi.org/10.1016/j.jscs.2015.06.002>
- Axtell, N. R., Sternberg, S. P. K., & Claussen, K. (2003). Lead and nickel removal using *Microspora* and *Lemna minor*. *Bioresource Technology*, 89(1), 41-48. doi:[http://dx.doi.org/10.1016/S0960-8524\(03\)00034-8](http://dx.doi.org/10.1016/S0960-8524(03)00034-8)
- Bahr, J. L., Yang, J., Kosynkin, D. V., Bronikowski, M. J., Smalley, R. E., & Tour, J. M. (2001). Functionalization of Carbon Nanotubes by Electrochemical Reduction of Aryl Diazonium Salts: A Bucky Paper Electrode. *Journal of the American Chemical Society*, 123(27), 6536-6542. doi:10.1021/ja010462s
- Bandaru, N. M., Reta, N., Dalal, H., Ellis, A. V., Shapter, J., & Voelcker, N. H. (2013). Enhanced adsorption of mercury ions on thiol derivatized single wall carbon nanotubes. *Journal of Hazardous Materials*, 261, 534-541. doi:<http://dx.doi.org/10.1016/j.jhazmat.2013.07.076>
- Baughman, R. H., Zakhidov, A. A., & de Heer, W. A. (2002). Carbon Nanotubes--the Route Toward Applications. *Science*, 297(5582), 787-792. doi:10.1126/science.1060928
- Bauschlicher, C. W., & Ricca, A. (2004a). Binding of NH₃ to graphite and to a (9,0) carbon nanotube. *Physical Review B*, 70(11), 115409. doi:<https://doi.org/10.1103/PhysRevB.70.115409>
- Bauschlicher, C. W., & Ricca, A. (2004b). Binding of NH₃ to graphite and to a (9, 0) carbon nanotube. *Physical Review B*, 70(11), 115409.
- Bhatt, J., Mondal, D., Devkar, R. V., & Prasad, K. (2016). Synthesis of functionalized N-doped graphene DNA hybrid material in a deep eutectic solvent. *Green Chemistry*. doi:10.1039/C6GC00853D
- Bhushan, B., Kasai, T., Nguyen, C. V., & Meyyappan, M. (2004). Multiwalled carbon nanotube AFM probes for surface characterization of micro/nanostructures. *Microsystem Technologies*, 10(8), 633-639. doi:10.1007/s00542-004-0489-x
- Bienfait, M., Zeppenfeld, P., Dupont-Pavlovsky, N., Muris, M., Johnson, M. R., Wilson, T., . . . Vilches, O. E. (2004). Thermodynamics and structure of hydrogen, methane, argon, oxygen, and carbon dioxide adsorbed on single-wall carbon nanotube bundles. *Physical Review B*, 70(3), 035410.

- Bingöl, D., & Bozbaş, S. K. (2012). Removal of Lead (II) from Aqueous Solution on Multiwalled Carbon Nanotube by Using Response Surface Methodology. *Spectroscopy Letters*, 45(5), 324-329. doi:10.1080/00387010.2012.666697
- Bissen, M., & Frimmel, F. H. (2003). Arsenic - A review. Part II: Oxidation of arsenic and its removal in water treatment. *Acta Hydrochimica et Hydrobiologica*, 31(2), 97-107. doi:10.1002/ahch.200300485
- Black, B. (1999). *Arsenic: answers to questions commonly asked by drinking water professionals*: American Water Works Association.
- Boulos, R. A., Eroglu, E., Chen, X., Scaffidi, A., Edwards, B. R., Toster, J., & Raston, C. L. (2013). Unravelling the structure and function of human hair. *Green Chemistry*, 15(5), 1268-1273. doi:10.1039/C3GC37027E
- Brame, J., Li, Q., & Alvarez, P. J. J. (2011). Nanotechnology-enabled water treatment and reuse: emerging opportunities and challenges for developing countries. *Trends in Food Science & Technology*, 22(11), 618-624. doi:<http://dx.doi.org/10.1016/j.tifs.2011.01.004>
- Branco, L. C., Rosa, J. N., Moura Ramos, J. J., & Afonso, C. A. M. (2002). Preparation and Characterization of New Room Temperature Ionic Liquids. *Chemistry – A European Journal*, 8(16), 3671-3677. doi:10.1002/1521-3765(20020816)8:16<3671::AID-CHEM3671>3.0.CO;2-9
- Brown, P., Atly Jefcoat, I., Parrish, D., Gill, S., & Graham, E. (2000). Evaluation of the adsorptive capacity of peanut hull pellets for heavy metals in solution. *Advances in Environmental Research*, 4(1), 19-29. doi:[http://dx.doi.org/10.1016/S1093-0191\(00\)00004-6](http://dx.doi.org/10.1016/S1093-0191(00)00004-6)
- Chakrabarti, M. H., Manan, N. S. A., Brandon, N. P., Maher, R. C., Mjalli, F. S., AlNashef, I. M., . . . Nir, D. (2015). One-pot electrochemical gram-scale synthesis of graphene using deep eutectic solvents and acetonitrile. *Chemical Engineering Journal*, 274, 213-223. doi:<http://dx.doi.org/10.1016/j.cej.2015.03.083>
- Chandra, V., & Kim, K. S. (2011). Highly selective adsorption of Hg²⁺ by a polypyrrole-reduced graphene oxide composite. *Chemical Communications*, 47(13), 3942-3944. doi:10.1039/C1CC00005E
- Chen, C.-Y., Ozasa, K., Kitamura, F., Katsumata, K.-i., Maeda, M., Okada, K., & Matsushita, N. (2015). Self-organization of TiO₂ Nanobamboos by Anodization with Deep Eutectic Solvent. *Electrochimica Acta*, 153, 409-415. doi:<http://dx.doi.org/10.1016/j.electacta.2014.11.084>
- Chen, F., Xie, S., Zhang, J., & Liu, R. (2013). Synthesis of spherical Fe₃O₄ magnetic nanoparticles by co-precipitation in choline chloride/urea deep eutectic solvent. *Materials Letters*, 112, 177-179. doi:<http://dx.doi.org/10.1016/j.matlet.2013.09.022>
- Chen, J., Hamon, M. A., Hu, H., Chen, Y., Rao, A. M., Eklund, P. C., & Haddon, R. C. (1998). Solution Properties of Single-Walled Carbon Nanotubes. *Science*, 282(5386), 95-98. doi:10.1126/science.282.5386.95

- Chen, P. H., Hsu, C.-F., Tsai, D. D.-W., Lu, Y.-M., & Huang, W.-J. (2014). Adsorption of mercury from water by modified multi-walled carbon nanotubes: adsorption behaviour and interference resistance by coexisting anions. *Environmental Technology*, 35(15), 1935-1944. doi:10.1080/09593330.2014.886627
- Chen, S., Kobayashi, K., Miyata, Y., Imazu, N., Saito, T., Kitaura, R., & Shinohara, H. (2009). Morphology and Melting Behavior of Ionic Liquids inside Single-Walled Carbon Nanotubes. *Journal of the American Chemical Society*, 131(41), 14850-14856. doi:10.1021/ja904283d
- Chiarle, S., Ratto, M., & Rovatti, M. (2000). Mercury removal from water by ion exchange resins adsorption. *Water Research*, 34(11), 2971-2978. doi:[http://dx.doi.org/10.1016/S0043-1354\(00\)00044-0](http://dx.doi.org/10.1016/S0043-1354(00)00044-0)
- Coleman, J. N., Khan, U., & Gun'ko, Y. K. (2006). Mechanical Reinforcement of Polymers Using Carbon Nanotubes. *Advanced Materials*, 18(6), 689-706. doi:10.1002/adma.200501851
- Collins, P. G., & Avouris, P. (2000). Nanotubes for electronics. *Scientific american*, 283(6), 62-69.
- Cooper, E. R., Andrews, C. D., Wheatley, P. S., Webb, P. B., Wormald, P., & Morris, R. E. (2004). Ionic liquids and eutectic mixtures as solvent and template in synthesis of zeolite analogues. *nature*, 430(7003), 1012-1016. doi:http://www.nature.com/nature/journal/v430/n7003/supinfo/nature02860_S1.html
- Cui, H., Li, Q., Gao, S., & Shang, J. K. (2012). Strong adsorption of arsenic species by amorphous zirconium oxide nanoparticles. *Journal of Industrial and Engineering Chemistry*, 18(4), 1418-1427. doi:<http://dx.doi.org/10.1016/j.jiec.2012.01.045>
- Cvjetko Bubalo, M., Vidović, S., Radojčić Redovniković, I., & Jokić, S. (2015a). Green solvents for green technologies. *Journal of Chemical Technology & Biotechnology*, 90(9), 1631-1639. doi:10.1002/jctb.4668
- Cvjetko Bubalo, M., Vidović, S., Radojčić Redovniković, I., & Jokić, S. (2015b). Green Solvents for Green Technologies. *Journal of Chemical Technology & Biotechnology*, n/a-n/a. doi:10.1002/jctb.4668
- D'Agostino, C., Harris, R. C., Abbott, A. P., Gladden, L. F., & Mantle, M. D. (2011). Molecular motion and ion diffusion in choline chloride based deep eutectic solvents studied by 1H pulsed field gradient NMR spectroscopy. *Physical Chemistry Chemical Physics*, 13(48), 21383-21391. doi:10.1039/C1CP22554E
- Dai, B., Cao, M., Fang, G., Liu, B., Dong, X., Pan, M., & Wang, S. (2012). Schiff base-chitosan grafted multiwalled carbon nanotubes as a novel solid-phase extraction adsorbent for determination of heavy metal by ICP-MS. *Journal of Hazardous Materials*, 219-220(0), 103-110. doi:<http://dx.doi.org/10.1016/j.jhazmat.2012.03.065>
- Danil de Namor, A. F., El Gamouz, A., Frangie, S., Martinez, V., Valiente, L., & Webb, O. A. (2012). Turning the volume down on heavy metals using tuned diatomite.

A review of diatomite and modified diatomite for the extraction of heavy metals from water. *Journal of Hazardous Materials*, 241–242, 14-31.
doi:<http://dx.doi.org/10.1016/j.jhazmat.2012.09.030>

- Datsyuk, V., Kalyva, M., Papagelis, K., Parthenios, J., Tasis, D., Siokou, A., . . . Galiotis, C. (2008). Chemical oxidation of multiwalled carbon nanotubes. *Carbon*, 46(6), 833-840. doi:<http://dx.doi.org/10.1016/j.carbon.2008.02.012>
- Deng, M.-J., Chen, P.-Y., Leong, T.-I., Sun, I. W., Chang, J.-K., & Tsai, W.-T. (2008). Dicyanamide anion based ionic liquids for electrodeposition of metals. *Electrochemistry Communications*, 10(2), 213-216.
doi:<http://dx.doi.org/10.1016/j.elecom.2007.11.026>
- Deshmukh, R. R., Rajagopal, R., & Srinivasan, K. V. (2001). Ultrasound promoted C-C bond formation: Heck reaction at ambient conditions in room temperature ionic liquids. *Chemical Communications*(17), 1544-1545. doi:10.1039/B104532F
- Di, Z.-C., Ding, J., Peng, X.-J., Li, Y.-H., Luan, Z.-K., & Liang, J. (2006). Chromium adsorption by aligned carbon nanotubes supported ceria nanoparticles. *Chemosphere*, 62(5), 861-865.
doi:<http://dx.doi.org/10.1016/j.chemosphere.2004.06.044>
- Dimitrova, S. V., & Mehandgiev, D. R. (1998). Lead removal from aqueous solutions by granulated blast-furnace slag. *Water Research*, 32(11), 3289-3292.
doi:[http://dx.doi.org/10.1016/S0043-1354\(98\)00119-5](http://dx.doi.org/10.1016/S0043-1354(98)00119-5)
- Duffus, J. H. (2002). " Heavy metals" a meaningless term?(IUPAC Technical Report). *Pure and Applied Chemistry*, 74(5), 793-807.
- Duncan, T. V. (2011). Applications of nanotechnology in food packaging and food safety: barrier materials, antimicrobials and sensors. *Journal of colloid and interface science*, 363(1), 1-24.
- Ebbesen, T. W., & Ajayan, P. M. (1992). Large-scale synthesis of carbon nanotubes. *nature*, 358(6383), 220-222.
- El-Sheikh, A. H., Al-Degs, Y. S., Al-As'ad, R. M., & Sweileh, J. A. (2011). Effect of oxidation and geometrical dimensions of carbon nanotubes on Hg(II) sorption and preconcentration from real waters. *Desalination*, 270(1–3), 214-220.
doi:<http://dx.doi.org/10.1016/j.desal.2010.11.048>
- Esumi, K., Ishigami, M., Nakajima, A., Sawada, K., & Honda, H. (1996). Chemical treatment of carbon nanotubes. *Carbon*, 34(2), 279-281.
doi:[http://dx.doi.org/10.1016/0008-6223\(96\)83349-5](http://dx.doi.org/10.1016/0008-6223(96)83349-5)
- Fan, J., Shi, Z., Tian, M., Wang, J., & Yin, J. (2012). Unzipped Multiwalled Carbon Nanotube Oxide/Multiwalled Carbon Nanotube Hybrids for Polymer Reinforcement. *ACS Applied Materials & Interfaces*, 4(11), 5956-5965.
doi:10.1021/am301623t
- Feng, Q., Zhang, Z., Ma, Y., He, X., Zhao, Y., & Chai, Z. (2012). Adsorption and desorption characteristics of arsenic onto ceria nanoparticles. *Nanoscale Research Letters*, 7(1), 1-8. doi:10.1186/1556-276x-7-84

- Ferey, G. (2008). Hybrid porous solids: past, present, future. *Chemical Society Reviews*, 37(1), 191-214. doi:10.1039/B618320B
- Fischer, J. E. (2002). Chemical Doping of Single-Wall Carbon Nanotubes. *Accounts of Chemical Research*, 35(12), 1079-1086. doi:10.1021/ar0101638
- Freundlich, H., & Hatfield, H. S. (1926). Colloid and capillary chemistry.
- Fu, F., & Wang, Q. (2011). Removal of heavy metal ions from wastewaters: A review. *Journal of Environmental Management*, 92(3), 407-418. doi:<http://dx.doi.org/10.1016/j.jenvman.2010.11.011>
- Fukaya, Y., Iizuka, Y., Sekikawa, K., & Ohno, H. (2007). Bio ionic liquids: room temperature ionic liquids composed wholly of biomaterials. *Green Chemistry*, 9(11), 1155-1157. doi:10.1039/B706571J
- Gad, S. C., & Pham, T. (2014). Lead. In P. Wexler (Ed.), *Encyclopedia of Toxicology (Third Edition)* (pp. 61-65). Oxford: Academic Press.
- Ghaedi, M., Hassanzadeh, A., & Kokhdan, S. N. (2011). Multiwalled Carbon Nanotubes as Adsorbents for the Kinetic and Equilibrium Study of the Removal of Alizarin Red S and Morin. *Journal of Chemical & Engineering Data*, 56(5), 2511-2520. doi:10.1021/jc2000414
- Ghareh Bagh, F. S., Shahbaz, K., Mjalli, F. S., Hashim, M. A., & AlNashef, I. M. (2015). Zinc (II) chloride-based deep eutectic solvents for application as electrolytes: Preparation and characterization. *Journal of Molecular Liquids*, 204, 76-83. doi:<http://dx.doi.org/10.1016/j.molliq.2015.01.025>
- Ghorbel-Abid, I., & Trabelsi-Ayadi, M. (2015). Competitive adsorption of heavy metals on local landfill clay. *Arabian Journal of Chemistry*, 8(1), 25-31. doi:<http://dx.doi.org/10.1016/j.arabjc.2011.02.030>
- Ghosh, M. K., Poinern, G. E. J., Issa, T. B., & Singh, P. (2011). Arsenic adsorption on goethite nanoparticles produced through hydrazine sulfate assisted synthesis method. *Korean Journal of Chemical Engineering*, 29(1), 95-102. doi:10.1007/s11814-011-0137-y
- Gihring, T. M., Druschel, G. K., McCleskey, R. B., Hamers, R. J., & Banfield, J. F. (2001). Rapid arsenite oxidation by *Thermus aquaticus* and *Thermus thermophilus*: Field and laboratory investigations. *Environmental Science and Technology*, 35(19), 3857-3862. doi:10.1021/es010816f
- Goel, J., Kadirvelu, K., Rajagopal, C., & Kumar Garg, V. (2005). Removal of lead(II) by adsorption using treated granular activated carbon: Batch and column studies. *Journal of Hazardous Materials*, 125(1-3), 211-220. doi:<http://dx.doi.org/10.1016/j.jhazmat.2005.05.032>
- Gogotsi, Y. (2006). *Nanotubes and nanofibers*: CRC Press.
- Goldman, L. R., Shannon, M. W., & Health, t. C. o. E. (2001). Technical Report: Mercury in the Environment: Implications for Pediatricians. *Pediatrics*, 108(1), 197-205. doi:10.1542/peds.108.1.197

- Gong, J., Feng, J., Liu, J., Jiang, Z., Chen, X., Mijowska, E., . . . Tang, T. (2014). Catalytic carbonization of polypropylene into cup-stacked carbon nanotubes with high performances in adsorption of heavy metallic ions and organic dyes. *Chemical Engineering Journal*, 248(0), 27-40. doi:<http://dx.doi.org/10.1016/j.cej.2014.01.107>
- Gorke, J. T., Srienc, F., & Kazlauskas, R. J. (2008). Hydrolase-catalyzed biotransformations in deep eutectic solvents. *Chemical Communications*(10), 1235-1237. doi:10.1039/B716317G
- Gu, C.-D., & Tu, J.-P. (2011). Thermochromic behavior of chloro-nickel(II) in deep eutectic solvents and their application in thermochromic composite films. *RSC Advances*, 1(7), 1220-1227. doi:10.1039/C1RA00345C
- Gu, C., & Tu, J. (2011). One-Step Fabrication of Nanostructured Ni Film with Lotus Effect from Deep Eutectic Solvent. *Langmuir*, 27(16), 10132-10140. doi:10.1021/la200778a
- GU, C. D., MAI, Y. J., ZHOU, J. P., & TU, J. P. (2011). SnO₂ Nanocrystallite: Novel Synthetic Route From Deep Eutectic Solvent And Lithium Storage Performance. *Functional Materials Letters*, 04(04), 377-381. doi:doi:10.1142/S1793604711002251
- Guo, W., Hou, Y., Ren, S., Tian, S., & Wu, W. (2013). Formation of Deep Eutectic Solvents by Phenols and Choline Chloride and Their Physical Properties. *Journal of Chemical & Engineering Data*, 58(4), 866-872. doi:10.1021/je300997v
- Guo, X., Wang, S., Gong, J., Guo, J., Peng, L., & Ding, W. (2014). Characterization of highly corrosion-resistant nanocrystalline Ni coating electrodeposited on Mg–Nd–Zn–Zr alloy from a eutectic-based ionic liquid. *Applied Surface Science*, 313, 711-719. doi:<http://dx.doi.org/10.1016/j.apsusc.2014.06.060>
- Gupta, A., Vidyarthi, S. R., & Sankaramakrishnan, N. (2014). Enhanced sorption of mercury from compact fluorescent bulbs and contaminated water streams using functionalized multiwalled carbon nanotubes. *Journal of Hazardous Materials*, 274, 132-144. doi:<http://dx.doi.org/10.1016/j.jhazmat.2014.03.020>
- Gupta, K., Bhattacharya, S., Chattopadhyay, D., Mukhopadhyay, A., Biswas, H., Dutta, J., . . . Ghosh, U. C. (2011). Ceria associated manganese oxide nanoparticles: Synthesis, characterization and arsenic(V) sorption behavior. *Chemical Engineering Journal*, 172(1), 219-229. doi:<http://dx.doi.org/10.1016/j.cej.2011.05.092>
- Gupta, V. K., Agarwal, S., & Saleh, T. A. (2011). Synthesis and characterization of alumina-coated carbon nanotubes and their application for lead removal. *Journal of Hazardous Materials*, 185(1), 17-23. doi:<http://dx.doi.org/10.1016/j.jhazmat.2010.08.053>
- Gupta, V. K., Saini, V. K., & Jain, N. (2005). Adsorption of As(III) from aqueous solutions by iron oxide-coated sand. *Journal of colloid and interface science*, 288(1), 55-60. doi:<http://dx.doi.org/10.1016/j.jcis.2005.02.054>

- Gutiérrez, M. C., Carriazo, D., Tamayo, A., Jiménez, R., Picó, F., Rojo, J. M., . . . del Monte, F. (2011). Deep-Eutectic-Solvent-Assisted Synthesis of Hierarchical Carbon Electrodes Exhibiting Capacitance Retention at High Current Densities. *Chemistry – A European Journal*, 17(38), 10533-10537. doi:10.1002/chem.201101679
- Gutiérrez, M. C., Ferrer, M. L., Mateo, C. R., & del Monte, F. (2009). Freeze-Drying of Aqueous Solutions of Deep Eutectic Solvents: A Suitable Approach to Deep Eutectic Suspensions of Self-Assembled Structures. *Langmuir*, 25(10), 5509-5515. doi:10.1021/la900552b
- Hadavifar, M., Bahramifar, N., Younesi, H., & Li, Q. (2014). Adsorption of mercury ions from synthetic and real wastewater aqueous solution by functionalized multi-walled carbon nanotube with both amino and thiolated groups. *Chemical Engineering Journal*, 237, 217-228. doi:<http://dx.doi.org/10.1016/j.cej.2013.10.014>
- Hamel, A., Sacco, M., Mnasri, N., Lamaty, F., Martinez, J., De Angelis, F., . . . Charnay, C. (2014). Micelles into Glycerol Solvent: Overcoming Side Reactions of Glycerol. *ACS Sustainable Chemistry & Engineering*, 2(6), 1353-1358. doi:10.1021/sc500207r
- Hamon, M. A., Chen, J., Hu, H., Chen, Y., Itkis, M. E., Rao, A. M., . . . Haddon, R. C. (1999). Dissolution of Single-Walled Carbon Nanotubes. *Advanced Materials*, 11(10), 834-840. doi:10.1002/(SICI)1521-4095(199907)11:10<834::AID-ADMA834>3.0.CO;2-R
- Hamon, M. A., Hui, H., Bhowmik, P., Itkis, H. M. E., & Haddon, R. C. (2002). Ester-functionalized soluble single-walled carbon nanotubes. *Applied Physics A*, 74(3), 333-338. doi:10.1007/s003390201281
- Hamza, I. A. A., Martincigh, B. S., Ngila, J. C., & Nyamori, V. O. (2013). Adsorption studies of aqueous Pb(II) onto a sugarcane bagasse/multi-walled carbon nanotube composite. *Physics and Chemistry of the Earth, Parts A/B/C*, 66(0), 157-166. doi:<http://dx.doi.org/10.1016/j.pce.2013.08.006>
- Han, R., Zou, W., Li, H., Li, Y., & Shi, J. (2006). Copper(II) and lead(II) removal from aqueous solution in fixed-bed columns by manganese oxide coated zeolite. *Journal of Hazardous Materials*, 137(2), 934-942. doi:<http://dx.doi.org/10.1016/j.jhazmat.2006.03.016>
- Hawari, A. H., & Mulligan, C. N. (2006). Biosorption of lead(II), cadmium(II), copper(II) and nickel(II) by anaerobic granular biomass. *Bioresource Technology*, 97(4), 692-700. doi:<http://dx.doi.org/10.1016/j.biortech.2005.03.033>
- Hayyan, A., Ali Hashim, M., Mjalli, F. S., Hayyan, M., & AlNashef, I. M. (2013). A novel phosphonium-based deep eutectic catalyst for biodiesel production from industrial low grade crude palm oil. *Chemical Engineering Science*, 92(0), 81-88. doi:<http://dx.doi.org/10.1016/j.ces.2012.12.024>
- Hayyan, A., Hashim, M. A., Hayyan, M., Mjalli, F. S., & AlNashef, I. M. (2014). A new processing route for cleaner production of biodiesel fuel using a choline

chloride based deep eutectic solvent. *Journal of Cleaner Production*, 65(0), 246-251. doi:<http://dx.doi.org/10.1016/j.jclepro.2013.08.031>

Hayyan, A., Mjalli, F. S., AlNashef, I. M., Al-Wahaibi, T., Al-Wahaibi, Y. M., & Hashim, M. A. (2012). Fruit sugar-based deep eutectic solvents and their physical properties. *Thermochimica Acta*, 541, 70-75. doi:<http://dx.doi.org/10.1016/j.tca.2012.04.030>

Hayyan, A., Mjalli, F. S., AlNashef, I. M., Al-Wahaibi, Y. M., Al-Wahaibi, T., & Hashim, M. A. (2013). Glucose-based deep eutectic solvents: Physical properties. *Journal of Molecular Liquids*, 178, 137-141. doi:<http://dx.doi.org/10.1016/j.molliq.2012.11.025>

Hayyan, M., Abo-Hamad, A., AlSaadi, M., & Hashim, M. (2015a). Functionalization of graphene using deep eutectic solvents. *Nanoscale Research Letters*, 10(1), 1-26. doi:10.1186/s11671-015-1004-2

Hayyan, M., Abo-Hamad, A., AlSaadi, M. A., & Hashim, M. A. (2015b). Functionalization of graphene using deep eutectic solvents. *Nanoscale Research Letters*, 10(1), 1-26. doi:10.1186/s11671-015-1004-2

Hayyan, M., Aissaoui, T., Hashim, M. A., AlSaadi, M. A., & Hayyan, A. (2015). Triethylene glycol based deep eutectic solvents and their physical properties. *Journal of the Taiwan Institute of Chemical Engineers*, 50, 24-30. doi:<http://dx.doi.org/10.1016/j.jtice.2015.03.001>

Hayyan, M., Hashim, M. A., Al-Saadi, M. A., Hayyan, A., AlNashef, I. M., & Mirghani, M. E. S. (2013). Assessment of cytotoxicity and toxicity for phosphonium-based deep eutectic solvents. *Chemosphere*, 93(2), 455-459. doi:<http://dx.doi.org/10.1016/j.chemosphere.2013.05.013>

Hayyan, M., Hashim, M. A., Hayyan, A., Al-Saadi, M. A., AlNashef, I. M., Mirghani, M. E. S., & Saheed, O. K. (2013). Are deep eutectic solvents benign or toxic? *Chemosphere*, 90(7), 2193-2195. doi:<http://dx.doi.org/10.1016/j.chemosphere.2012.11.004>

Hayyan, M., Looi, C. Y., Hayyan, A., Wong, W. F., & Hashim, M. A. (2015). In Vitro and In Vivo Toxicity Profiling of Ammonium-Based Deep Eutectic Solvents. *PLoS ONE*, 10(2), e0117934. doi:10.1371/journal.pone.0117934

Hayyan, M., Mjalli, F. S., Hashim, M. A., & AlNashef, I. M. (2010). A novel technique for separating glycerine from palm oil-based biodiesel using ionic liquids. *Fuel Processing Technology*, 91(1), 116-120. doi:<http://dx.doi.org/10.1016/j.fuproc.2009.09.002>

Hiemenz, P. C., & Lodge, T. P. (2007). *Polymer chemistry*: CRC press.

Hirsch, A., & Vostrowsky, O. (2005). Functionalization of Carbon Nanotubes. In A. D. Schlüter (Ed.), *Functional Molecular Nanostructures* (Vol. 245, pp. 193-237): Springer Berlin Heidelberg.

- Hirsch, A., & Vostrowsky, O. (2007). Functionalization of Carbon Nanotubes *Functional Organic Materials* (pp. 1-57): Wiley-VCH Verlag GmbH & Co. KGaA.
- Hiura, H., Ebbesen, T. W., Tanigaki, K., & Takahashi, H. (1993). Raman studies of carbon nanotubes. *Chemical Physics Letters*, 202(6), 509-512. doi:[http://dx.doi.org/10.1016/0009-2614\(93\)90040-8](http://dx.doi.org/10.1016/0009-2614(93)90040-8)
- Ho, Y. S., & McKay, G. (1999). The sorption of lead(II) ions on peat. *Water Research*, 33(2), 578-584. doi:[http://dx.doi.org/10.1016/S0043-1354\(98\)00207-3](http://dx.doi.org/10.1016/S0043-1354(98)00207-3)
- Hone, J., Whitney, M., Piskoti, C., & Zettl, A. (1999). Thermal conductivity of single-walled carbon nanotubes. *Physical Review B*, 59(4), R2514-R2516.
- Hou, Y., Gu, Y., Zhang, S., Yang, F., Ding, H., & Shan, Y. (2008). Novel binary eutectic mixtures based on imidazole. *Journal of Molecular Liquids*, 143(2-3), 154-159. doi:<http://dx.doi.org/10.1016/j.molliq.2008.07.009>
- Huang, Y., Li, Y., Huang, Q., Cui, Z., Yu, D., Rajput, I. R., . . . Li, W. (2012). Effect of orally administered *Enterococcus faecium* EF1 on intestinal cytokines and chemokines production of suckling piglets. *Pak Vet J*, 32, 81-84.
- Huang, Z.-H., Zhang, F., Wang, M.-X., Lv, R., & Kang, F. (2012). Growth of carbon nanotubes on low-cost bamboo charcoal for Pb(II) removal from aqueous solution. *Chemical Engineering Journal*, 184(0), 193-197. doi:<http://dx.doi.org/10.1016/j.cej.2012.01.029>
- Hussein, A. K. (2015). Applications of nanotechnology in renewable energies—A comprehensive overview and understanding. *Renewable and Sustainable Energy Reviews*, 42(0), 460-476. doi:<http://dx.doi.org/10.1016/j.rser.2014.10.027>
- HWO. (2014) Progress on drinking water and sanitation
- Joint Monitoring Programme update 2014. *Vol. 2014 update* (pp. 6): world health organization
- Ibrahim, R. K., Hayyan, M., AlSaadi, M. A., Hayyan, A., & Ibrahim, S. (2016). Environmental application of nanotechnology: air, soil, and water. *Environmental Science and Pollution Research*, 1-35. doi:10.1007/s11356-016-6457-z
- Ihsanullah, Abbas, A., Al-Amer, A. M., Laoui, T., Al-Marri, M. J., Nasser, M. S., . . . Atieh, M. A. (2016). Heavy metal removal from aqueous solution by advanced carbon nanotubes: Critical review of adsorption applications. *Separation and Purification Technology*, 157, 141-161. doi:<http://dx.doi.org/10.1016/j.seppur.2015.11.039>
- Iijima, S. (1991). Helical microtubules of graphitic carbon. *nature*, 354(6348), 56-58.
- Imamoglu, M., & Tekir, O. (2008). Removal of copper (II) and lead (II) ions from aqueous solutions by adsorption on activated carbon from a new precursor hazelnut husks. *Desalination*, 228(1-3), 108-113. doi:<http://dx.doi.org/10.1016/j.desal.2007.08.011>

- Ji, L., Chen, W., Duan, L., & Zhu, D. (2009). Mechanisms for strong adsorption of tetracycline to carbon nanotubes: A comparative study using activated carbon and graphite as adsorbents. *Environmental Science & Technology*, 43(7), 2322-2327. doi:10.1021/es803268b
- Jia, H., An, J., Guo, X., Su, C., Zhang, L., Zhou, H., & Xie, C. (2015). Deep eutectic solvent-assisted growth of gold nanofoams and their excellent catalytic properties. *Journal of Molecular Liquids*, 212, 763-766. doi:<http://dx.doi.org/10.1016/j.molliq.2015.10.030>
- Jiang, Y., Gao, Q., Yu, H., Chen, Y., & Deng, F. (2007). Intensively competitive adsorption for heavy metal ions by PAMAM-SBA-15 and EDTA-PAMAM-SBA-15 inorganic-organic hybrid materials. *Microporous and Mesoporous Materials*, 103(1-3), 316-324. doi:10.1016/j.micromeso.2007.02.024
- Jibril, B., Mjalli, F., Naser, J., & Gano, Z. (2014). New tetrapropylammonium bromide-based deep eutectic solvents: Synthesis and characterizations. *Journal of Molecular Liquids*, 199, 462-469. doi:<http://dx.doi.org/10.1016/j.molliq.2014.08.004>
- Jorio, A., Saito, R., Dresselhaus, G., & Dresselhaus, M. S. (2004). Determination of nanotubes properties by Raman spectroscopy. *Philosophical Transactions of the Royal Society of London A: Mathematical, Physical and Engineering Sciences*, 362(1824), 2311-2336. doi:10.1098/rsta.2004.1443
- Justi, K. C., Fávere, V. T., Laranjeira, M. C. M., Neves, A., & Peralta, R. A. (2005). Kinetics and equilibrium adsorption of Cu(II), Cd(II), and Ni(II) ions by chitosan functionalized with 2[-bis-(pyridylmethyl)aminomethyl]-4-methyl-6-formylphenol. *Journal of colloid and interface science*, 291(2), 369-374. doi:<http://dx.doi.org/10.1016/j.jcis.2005.05.017>
- Kabbashi, N. A., Atieh, M. A., Al-Mamun, A., Mirghami, M. E. S., Alam, M. D. Z., & Yahya, N. (2009). Kinetic adsorption of application of carbon nanotubes for Pb(II) removal from aqueous solution. *Journal of Environmental Sciences*, 21(4), 539-544. doi:[http://dx.doi.org/10.1016/S1001-0742\(08\)62305-0](http://dx.doi.org/10.1016/S1001-0742(08)62305-0)
- Kadirvelu, K., Thamaraiselvi, K., & Namasivayam, C. (2001). Removal of heavy metals from industrial wastewaters by adsorption onto activated carbon prepared from an agricultural solid waste. *Bioresource Technology*, 76(1), 63-65. doi:[http://dx.doi.org/10.1016/S0960-8524\(00\)00072-9](http://dx.doi.org/10.1016/S0960-8524(00)00072-9)
- Kandah, M. I., & Meunier, J.-L. (2007). Removal of nickel ions from water by multi-walled carbon nanotubes. *Journal of Hazardous Materials*, 146(1-2), 283-288. doi:<http://dx.doi.org/10.1016/j.jhazmat.2006.12.019>
- Kaneko, K. (1994). Determination of pore size and pore size distribution. *Journal of Membrane Science*, 96(1), 59-89. doi:[http://dx.doi.org/10.1016/0376-7388\(94\)00126-X](http://dx.doi.org/10.1016/0376-7388(94)00126-X)
- Kareem, M. A., Mjalli, F. S., Hashim, M. A., & AlNashef, I. M. (2010). Phosphonium-Based Ionic Liquids Analogues and Their Physical Properties. *Journal of Chemical & Engineering Data*, 55(11), 4632-4637. doi:10.1021/je100104v

- Karimi, M., Eshraghi, M. J., & Jahangir, V. (2016). A facile and green synthetic approach based on deep eutectic solvents toward synthesis of CZTS nanoparticles. *Materials Letters*, *171*, 100-103. doi:<http://dx.doi.org/10.1016/j.matlet.2016.02.065>
- Karimi, M., Hesarakhi, S., Alizadeh, M., & Kazemzadeh, A. (2016). Synthesis of calcium phosphate nanoparticles in deep-eutectic choline chloride–urea medium: Investigating the role of synthesis temperature on phase characteristics and physical properties. *Ceramics International*, *42*(2, Part A), 2780-2788. doi:<http://dx.doi.org/10.1016/j.ceramint.2015.11.010>
- Karn, B., Kuiken, T., & Otto, M. (2009). Nanotechnology and in situ remediation: a review of the benefits and potential risks. *Environmental health perspectives*, 1823-1831.
- Karousis, N., Tagmatarchis, N., & Tasis, D. (2010). Current Progress on the Chemical Modification of Carbon Nanotubes. *Chemical Reviews*, *110*(9), 5366-5397. doi:10.1021/cr100018g
- Kim, E.-J., Lee, C.-S., Chang, Y.-Y., & Chang, Y.-S. (2013). Hierarchically Structured Manganese Oxide-Coated Magnetic Nanocomposites for the Efficient Removal of Heavy Metal Ions from Aqueous Systems. *ACS Applied Materials & Interfaces*, *5*(19), 9628-9634. doi:10.1021/am402615m
- Kim, J., & Benjamin, M. M. (2004). Modeling a novel ion exchange process for arsenic and nitrate removal. *Water Research*, *38*(8), 2053-2062. doi:10.1016/j.watres.2004.01.012
- Kiparissides, C., & Kammona, O. (2015). Nanotechnology Advances in Diagnostics, Drug Delivery, and Regenerative Medicine. *The Nano-Micro Interface: Bridging the Micro and Nano Worlds*, *16*, 1.
- Kobyas, M., Demirbas, E., Senturk, E., & Ince, M. (2005). Adsorption of heavy metal ions from aqueous solutions by activated carbon prepared from apricot stone. *Bioresource Technology*, *96*(13), 1518-1521. doi:<http://dx.doi.org/10.1016/j.biortech.2004.12.005>
- Kordás, K., Mustonen, T., Tóth, G., Jantunen, H., Lajunen, M., Soldano, C., . . . Ajayan, P. M. (2006). Inkjet Printing of Electrically Conductive Patterns of Carbon Nanotubes. *Small*, *2*(8-9), 1021-1025. doi:10.1002/sml.200600061
- Kosa, S. A., Al-Zhrani, G., & Abdel Salam, M. (2012). Removal of heavy metals from aqueous solutions by multi-walled carbon nanotubes modified with 8-hydroxyquinoline. *Chemical Engineering Journal*, *181–182*(0), 159-168. doi:<http://dx.doi.org/10.1016/j.cej.2011.11.044>
- Koziol, K., Vilatela, J., Moisala, A., Motta, M., Cunniff, P., Sennett, M., & Windle, A. (2007). High-Performance Carbon Nanotube Fiber. *Science*, *318*(5858), 1892-1895. doi:10.1126/science.1147635
- Kumar, C. S. (2012). *Raman spectroscopy for nanomaterials characterization*: Springer Science & Business Media.

- Kumar, P. R., Chaudhari, S., Khilar, K. C., & Mahajan, S. P. (2004). Removal of arsenic from water by electrocoagulation. *Chemosphere*, 55(9), 1245-1252. doi:10.1016/j.chemosphere.2003.12.025
- Langmuir, I. (1916). THE CONSTITUTION AND FUNDAMENTAL PROPERTIES OF SOLIDS AND LIQUIDS. PART I. SOLIDS. *Journal of the American Chemical Society*, 38(11), 2221-2295. doi:10.1021/ja02268a002
- Leroy, E., Decaen, P., Jacquet, P., Coativy, G., Pontoire, B., Reguerre, A.-L., & Lourdin, D. (2012). Deep eutectic solvents as functional additives for starch based plastics. *Green Chemistry*, 14(11), 3063-3066. doi:10.1039/C2GC36107H
- Li, G., Deng, D., Chen, Y., Shan, H., & Ai, N. (2014). Solubilities and thermodynamic properties of CO₂ in choline-chloride based deep eutectic solvents. *The Journal of Chemical Thermodynamics*, 75, 58-62. doi:<http://dx.doi.org/10.1016/j.jct.2014.04.012>
- Li, R., Chu, Q., & Liang, J. (2015). Electrodeposition and characterization of Ni-SiC composite coatings from deep eutectic solvent. *RSC Advances*, 5(56), 44933-44942. doi:10.1039/C5RA05918F
- Li, X., Hou, M., Han, B., Wang, X., & Zou, L. (2008). Solubility of CO₂ in a Choline Chloride + Urea Eutectic Mixture. *Journal of Chemical & Engineering Data*, 53(2), 548-550. doi:10.1021/je700638u
- Li, Y.-H., Ding, J., Luan, Z., Di, Z., Zhu, Y., Xu, C., . . . Wei, B. (2003). Competitive adsorption of Pb²⁺, Cu²⁺ and Cd²⁺ ions from aqueous solutions by multiwalled carbon nanotubes. *Carbon*, 41(14), 2787-2792. doi:[http://dx.doi.org/10.1016/S0008-6223\(03\)00392-0](http://dx.doi.org/10.1016/S0008-6223(03)00392-0)
- Li, Y.-H., Wang, S., Luan, Z., Ding, J., Xu, C., & Wu, D. (2003). Adsorption of cadmium(II) from aqueous solution by surface oxidized carbon nanotubes. *Carbon*, 41(5), 1057-1062. doi:[http://dx.doi.org/10.1016/S0008-6223\(02\)00440-2](http://dx.doi.org/10.1016/S0008-6223(02)00440-2)
- Li, Y.-H., Wang, S., Wei, J., Zhang, X., Xu, C., Luan, Z., . . . Wei, B. (2002). Lead adsorption on carbon nanotubes. *Chemical Physics Letters*, 357(3-4), 263-266. doi:[http://dx.doi.org/10.1016/S0009-2614\(02\)00502-X](http://dx.doi.org/10.1016/S0009-2614(02)00502-X)
- Li, Y.-H., Wang, S., Zhang, X., Wei, J., Xu, C., Luan, Z., & Wu, D. (2003). Adsorption of fluoride from water by aligned carbon nanotubes. *Materials Research Bulletin*, 38(3), 469-476. doi:[http://dx.doi.org/10.1016/S0025-5408\(02\)01063-2](http://dx.doi.org/10.1016/S0025-5408(02)01063-2)
- Lin, D., Tian, X., Li, T., Zhang, Z., He, X., & Xing, B. (2012). Surface-bound humic acid increased Pb²⁺ sorption on carbon nanotubes. *Environmental Pollution*, 167(0), 138-147. doi:<http://dx.doi.org/10.1016/j.envpol.2012.03.044>
- Lin, T.-F., & Wu, J.-K. (2001). Adsorption of Arsenite and Arsenate within Activated Alumina Grains: Equilibrium and Kinetics. *Water Research*, 35(8), 2049-2057. doi:[http://dx.doi.org/10.1016/S0043-1354\(00\)00467-X](http://dx.doi.org/10.1016/S0043-1354(00)00467-X)
- Lin, T., Bajpai, V., Ji, T., & Dai, L. (2003). Chemistry of Carbon Nanotubes. *Australian Journal of Chemistry*, 56(7), 635-651. doi:<http://dx.doi.org/10.1071/CH02254>

- Lindberg, D., de la Fuente Revenga, M., & Widersten, M. (2010). Deep eutectic solvents (DESs) are viable cosolvents for enzyme-catalyzed epoxide hydrolysis. *Journal of Biotechnology*, *147*(3–4), 169-171. doi:<http://dx.doi.org/10.1016/j.jbiotec.2010.04.011>
- Liu, P. (2005). Modifications of carbon nanotubes with polymers. *European Polymer Journal*, *41*(11), 2693-2703. doi:<http://dx.doi.org/10.1016/j.eurpolymj.2005.05.017>
- Liu, X., Wei, W., Zeng, X., Tang, B., Liu, X., & Xiang, H. (2009). Copper Adsorption Kinetics onto *Pseudomonas aeruginosa* Immobilized Multiwalled Carbon Nanotubes in an Aqueous Solution. *Analytical Letters*, *42*(2), 425-439. doi:10.1080/00032710802518262
- Liu, Y., Yan, J., Yuan, D., Li, Q., & Wu, X. (2013). The study of lead removal from aqueous solution using an electrochemical method with a stainless steel net electrode coated with single wall carbon nanotubes. *Chemical Engineering Journal*, *218*(0), 81-88. doi:<http://dx.doi.org/10.1016/j.cej.2012.12.020>
- Long, R. Q., & Yang, R. T. (2001). Carbon nanotubes as superior sorbent for dioxin removal. *Journal of the American Chemical Society*, *123*(9), 2058-2059.
- López-Salas, N., Jardim, E. O., Silvestre-Albero, A., Gutiérrez, M. C., Ferrer, M. L., Rodríguez-Reinoso, F., . . . del Monte, F. (2014). Use of Eutectic Mixtures for Preparation of Monolithic Carbons with CO₂-Adsorption and Gas-Separation Capabilities. *Langmuir*, *30*(41), 12220-12228. doi:10.1021/la5034146
- Lu, C., & Chiu, H. (2006). Adsorption of zinc(II) from water with purified carbon nanotubes. *Chemical Engineering Science*, *61*(4), 1138-1145. doi:<http://dx.doi.org/10.1016/j.ces.2005.08.007>
- Lu, C., Chung, Y.-L., & Chang, K.-F. (2005). Adsorption of trihalomethanes from water with carbon nanotubes. *Water Research*, *39*(6), 1183-1189. doi:<http://dx.doi.org/10.1016/j.watres.2004.12.033>
- Lu, J., Li, X.-T., Ma, E.-Q., Mo, L.-P., & Zhang, Z.-H. (2014). Superparamagnetic CuFeO₂ Nanoparticles in Deep Eutectic Solvent: an Efficient and Recyclable Catalytic System for the Synthesis of Imidazo[1,2-a]pyridines. *ChemCatChem*, *6*(10), 2854-2859. doi:10.1002/cctc.201402415
- Lu, X., & Chen, Z. (2005). Curved Pi-conjugation, aromaticity, and the related chemistry of small fullerenes. *Chemical Reviews*, *105*(10), 3643-3696.
- Luo, C., Tian, Z., Yang, B., Zhang, L., & Yan, S. (2013). Manganese dioxide/iron oxide/acid oxidized multi-walled carbon nanotube magnetic nanocomposite for enhanced hexavalent chromium removal. *Chemical Engineering Journal*, *234*(0), 256-265. doi:<http://dx.doi.org/10.1016/j.cej.2013.08.084>
- Luo, J., Conrad, O., & Vankelecom, I. F. J. (2012). Physicochemical properties of phosphonium-based and ammonium-based protic ionic liquids. *Journal of Materials Chemistry*, *22*(38), 20574-20579. doi:10.1039/C2JM34359B

- Ma, P.-C., Siddiqui, N. A., Mäder, E., & Kim, J.-K. (2011). Correlation between electrokinetic potential, dispersibility, surface chemistry and energy of carbon nanotubes. *Composites Science and Technology*, *71*(14), 1644-1651. doi:<http://dx.doi.org/10.1016/j.compscitech.2011.07.014>
- Ma, P.-C., Siddiqui, N. A., Marom, G., & Kim, J.-K. (2010). Dispersion and functionalization of carbon nanotubes for polymer-based nanocomposites: A review. *Composites Part A: Applied Science and Manufacturing*, *41*(10), 1345-1367. doi:<http://dx.doi.org/10.1016/j.compositesa.2010.07.003>
- Ma, P. C., Kim, J.-K., & Tang, B. Z. (2006). Functionalization of carbon nanotubes using a silane coupling agent. *Carbon*, *44*(15), 3232-3238. doi:<http://dx.doi.org/10.1016/j.carbon.2006.06.032>
- Mak, M. S. H., Rao, P., & Lo, I. M. C. (2009). Effects of hardness and alkalinity on the removal of arsenic(V) from humic acid-deficient and humic acid-rich groundwater by zero-valent iron. *Water Research*, *43*(17), 4296-4304. doi:<http://dx.doi.org/10.1016/j.watres.2009.06.022>
- Mąka, H., Szychaj, T., & Kowalczyk, K. (2014). Imidazolium and deep eutectic ionic liquids as epoxy resin crosslinkers and graphite nanoplatelets dispersants. *Journal of Applied Polymer Science*, *131*(12), n/a-n/a. doi:10.1002/app.40401
- Mandal, B. K., & Suzuki, K. T. (2002). Arsenic round the world: a review. *Talanta*, *58*(1), 201-235. doi:[http://dx.doi.org/10.1016/S0039-9140\(02\)00268-0](http://dx.doi.org/10.1016/S0039-9140(02)00268-0)
- Mansoori, G. A., & Soelaiman, T. F. (2005). Nanotechnology—an introduction for the standards community. *J. ASTM Int.*, *2*, 1-21.
- Martha H. Keating, K. R. M., Rita Schoeny, Glenn E. Rice, O. Russell Bullock, Robert B. Ambrose, Jeff Swartout, John W. Nichols. (December 1997). *Mercury Study Report to Congress*. (EPA-452/R-97-005). Washington, D.C.: United States Environmental Protection Agency.
- Martínez, M. T., Callejas, M. A., Benito, A. M., Cochet, M., Seeger, T., Ansón, A., . . . Maser, W. K. (2003). Modifications of single-wall carbon nanotubes upon oxidative purification treatments. *Nanotechnology*, *14*(7), 691.
- Martinson, C. A., & Reddy, K. J. (2009). Adsorption of arsenic(III) and arsenic(V) by cupric oxide nanoparticles. *Journal of colloid and interface science*, *336*(2), 406-411. doi:<http://dx.doi.org/10.1016/j.jcis.2009.04.075>
- Martis, P., Dilimon, V. S., Delhalle, J., & Mekhalif, Z. (2010). Electro-generated nickel/carbon nanotube composites in ionic liquid. *Electrochimica Acta*, *55*(19), 5407-5410. doi:<http://dx.doi.org/10.1016/j.electacta.2010.04.065>
- Mercury Study Report to Congress*. (EPA-452/R-97-005). (December 1997). Washington, D.C.: United States Environmental Protection Agency.
- Mittal, G., Dhand, V., Rhee, K. Y., Park, S.-J., & Lee, W. R. (2015). A review on carbon nanotubes and graphene as fillers in reinforced polymer nanocomposites. *Journal of Industrial and Engineering Chemistry*, *21*, 11-25. doi:<http://dx.doi.org/10.1016/j.jiec.2014.03.022>

- Mobasherpour, I., Salahi, E., & Ebrahimi, M. (2012). Removal of divalent nickel cations from aqueous solution by multi-walled carbon nano tubes: equilibrium and kinetic processes. *Research on Chemical Intermediates*, 38(9), 2205-2222. doi:10.1007/s11164-012-0537-6
- Moghaddam, H. K., & Pakizeh, M. (2015). Experimental study on mercury ions removal from aqueous solution by MnO₂/CNTs nanocomposite adsorbent. *Journal of Industrial and Engineering Chemistry*, 21, 221-229. doi:<http://dx.doi.org/10.1016/j.jiec.2014.02.028>
- Mohan, D., Gupta, V. K., Srivastava, S. K., & Chander, S. (2001). Kinetics of mercury adsorption from wastewater using activated carbon derived from fertilizer waste. *Colloids and Surfaces A: Physicochemical and Engineering Aspects*, 177(2-3), 169-181. doi:[http://dx.doi.org/10.1016/S0927-7757\(00\)00669-5](http://dx.doi.org/10.1016/S0927-7757(00)00669-5)
- Mohmood, I., Lopes, C. B., Lopes, I., Ahmad, I., Duarte, A. C., & Pereira, E. (2013). Nanoscale materials and their use in water contaminants removal—a review. *Environmental Science and Pollution Research*, 20(3), 1239-1260. doi:10.1007/s11356-012-1415-x
- Mondal, D., Bhatt, J., Sharma, M., Chatterjee, S., & Prasad, K. (2014). A facile approach to prepare a dual functionalized DNA based material in a bio-deep eutectic solvent. *Chemical Communications*, 50(30), 3989-3992. doi:10.1039/C4CC00145A
- Mondal, D., Sharma, M., Wang, C.-H., Lin, Y.-C., Huang, H.-C., Saha, A., . . . Prasad, K. (2016). Deep eutectic solvent promoted one step sustainable conversion of fresh seaweed biomass to functionalized graphene as a potential electrocatalyst. *Green Chemistry*, 18(9), 2819-2826. doi:10.1039/C5GC03106K
- Mota-Morales, J. D., Gutierrez, M. C., Ferrer, M. L., Jimenez, R., Santiago, P., Sanchez, I. C., . . . Luna-Barcenas, G. (2013). Synthesis of macroporous poly(acrylic acid)-carbon nanotube composites by frontal polymerization in deep-eutectic solvents. *Journal of Materials Chemistry A*, 1(12), 3970-3976. doi:10.1039/C3TA01020A
- Mubarak, N. M., Alicia, R. F., Abdullah, E. C., Sahu, J. N., Haslija, A. B. A., & Tan, J. (2013). Statistical optimization and kinetic studies on removal of Zn²⁺ using functionalized carbon nanotubes and magnetic biochar. *Journal of Environmental Chemical Engineering*, 1(3), 486-495. doi:<http://dx.doi.org/10.1016/j.jece.2013.06.011>
- Mubarak, N. M., Sahu, J. N., Abdullah, E. C., & Jayakumar, N. S. Rapid adsorption of toxic Pb(II) ions from aqueous solution using multiwall carbon nanotubes synthesized by microwave chemical vapor deposition technique. *Journal of Environmental Sciences*. doi:<http://dx.doi.org/10.1016/j.jes.2015.12.025>
- Mubarak, N. M., Sahu, J. N., Abdullah, E. C., & Jayakumar, N. S. (2014). Removal of Heavy Metals from Wastewater Using Carbon Nanotubes. *Separation & Purification Reviews*, 43(4), 311-338. doi:10.1080/15422119.2013.821996
- Mubarak, N. M., Sahu, J. N., Abdullah, E. C., Jayakumar, N. S., & Ganesan, P. (2015). Novel microwave-assisted multiwall carbon nanotubes enhancing Cu (II)

adsorption capacity in water. *Journal of the Taiwan Institute of Chemical Engineers*, 53, 140-152. doi:<http://dx.doi.org/10.1016/j.jtice.2015.02.016>

Müller, B., Zumbuehl, A., Walter, M. A., Pfohl, T., Cattin, P. C., Huwlyer, J., & Hieber, S. E. (2015). Translational Medicine: Nanoscience and Nanotechnology to Improve Patient Care. *The Nano-Micro Interface: Bridging the Micro and Nano Worlds*.

Netzer, A., & Hughes, D. E. (1984). Adsorption of copper, lead and cobalt by activated carbon. *Water Research*, 18(8), 927-933. doi:[http://dx.doi.org/10.1016/0043-1354\(84\)90241-0](http://dx.doi.org/10.1016/0043-1354(84)90241-0)

Ng, J. C. (2005). Environmental Contamination of Arsenic and its Toxicological Impact on Humans. *Environmental Chemistry*, 2(3), 146-160. doi:<http://dx.doi.org/10.1071/EN05062>

Ngueta, G., Prévost, M., Deshommes, E., Abdous, B., Gauvin, D., & Levallois, P. (2014). Exposure of young children to household water lead in the Montreal area (Canada): The potential influence of winter-to-summer changes in water lead levels on children's blood lead concentration. *Environment International*, 73(0), 57-65. doi:<http://dx.doi.org/10.1016/j.envint.2014.07.005>

Ning, R. Y. (2002). Arsenic removal by reverse osmosis. *Desalination*, 143(3), 237-241. doi:10.1016/S0011-9164(02)00262-X

Niyogi, S., Hamon, M. A., Hu, H., Zhao, B., Bhowmik, P., Sen, R., . . . Haddon, R. C. (2002). Chemistry of Single-Walled Carbon Nanotubes. *Accounts of Chemical Research*, 35(12), 1105-1113. doi:10.1021/ar010155r

Nriagu, J. O. (1988). A silent epidemic of environmental metal poisoning? *Environmental Pollution*, 50(1-2), 139-161. doi:[http://dx.doi.org/10.1016/0269-7491\(88\)90189-3](http://dx.doi.org/10.1016/0269-7491(88)90189-3)

NSTC/NNI/NSET. (August 29, 2003). National nanotechnology initiative: Research and development supporting the next industrial revolution. Retrieved from www.nano.gov

Ogata, A., Komaba, S., Baddour-Hadjean, R., Pereira-Ramos, J. P., & Kumagai, N. (2008). Doping effects on structure and electrode performance of K-birnessite-type manganese dioxides for rechargeable lithium battery. *Electrochimica Acta*, 53(7), 3084-3093. doi:<http://dx.doi.org/10.1016/j.electacta.2007.11.038>

Oh, J.-H., & Lee, J.-S. (2014). Synthesis of Gold Microstructures with Surface Nanoroughness Using a Deep Eutectic Solvent for Catalytic and Diagnostic Applications. *Journal of Nanoscience and Nanotechnology*, 14(5), 3753-3757. doi:10.1166/jnn.2014.8658

Ohno, H., & Yoshizawa, M. (2002). Ion conductive characteristics of ionic liquids prepared by neutralization of alkylimidazoles. *Solid State Ionics*, 154-155(0), 303-309. doi:[http://dx.doi.org/10.1016/S0167-2738\(02\)00526-X](http://dx.doi.org/10.1016/S0167-2738(02)00526-X)

- Orumwense, F. F. O. (1996). Removal of lead from water by adsorption on a kaolinitic clay. *Journal of Chemical Technology & Biotechnology*, 65(4), 363-369. doi:10.1002/(SICI)1097-4660(199604)65:4<363::AID-JCTB435>3.0.CO;2-3
- Oseguera-Galindo, D. O., Machorro-Mejia, R., Bogdanchikova, N., & Mota-Morales, J. D. (2016). Silver nanoparticles synthesized by laser ablation confined in urea choline chloride deep-eutectic solvent. *Colloids and Interface Science Communications*, 12, 1-4. doi:<http://dx.doi.org/10.1016/j.colcom.2016.03.004>
- Pagliari, M., & Rossi, M. (2010). *The future of glycerol* (Vol. 8): Royal Society of Chemistry.
- Pan, S.-C., Lin, C.-C., & Tseng, D.-H. (2003). Reusing sewage sludge ash as adsorbent for copper removal from wastewater. *Resources, Conservation and Recycling*, 39(1), 79-90. doi:[http://dx.doi.org/10.1016/S0921-3449\(02\)00122-2](http://dx.doi.org/10.1016/S0921-3449(02)00122-2)
- Park, M. J., Lee, J. K., Lee, B. S., Lee, Y.-W., Choi, I. S., & Lee, S.-g. (2006). Covalent Modification of Multiwalled Carbon Nanotubes with Imidazolium-Based Ionic Liquids: Effect of Anions on Solubility. *Chemistry of Materials*, 18(6), 1546-1551. doi:10.1021/cm0511421
- Patel, H. A., Byun, J., & Yavuz, C. T. (2012). Arsenic removal by magnetic nanocrystalline barium hexaferrite. *Journal of Nanoparticle Research*, 14(7), 1-7. doi:10.1007/s11051-012-0881-x
- Payne, K. B., & Abdel-Fattah, T. M. (2005). Adsorption of Arsenate and Arsenite by Iron-Treated Activated Carbon and Zeolites: Effects of pH, Temperature, and Ionic Strength. *Journal of Environmental Science and Health, Part A*, 40(4), 723-749. doi:10.1081/ESE-200048254
- Peng, X., Li, Y., Luan, Z., Di, Z., Wang, H., Tian, B., & Jia, Z. (2003). Adsorption of 1,2-dichlorobenzene from water to carbon nanotubes. *Chemical Physics Letters*, 376(1-2), 154-158. doi:[http://dx.doi.org/10.1016/S0009-2614\(03\)00960-6](http://dx.doi.org/10.1016/S0009-2614(03)00960-6)
- Peng, X., Luan, Z., Di, Z., Zhang, Z., & Zhu, C. (2005). Carbon nanotubes-iron oxides magnetic composites as adsorbent for removal of Pb(II) and Cu(II) from water. *Carbon*, 43(4), 880-883. doi:<http://dx.doi.org/10.1016/j.carbon.2004.11.009>
- Phadtare, S. B., & Shankarling, G. S. (2010). Halogenation reactions in biodegradable solvent: Efficient bromination of substituted 1-aminoanthra-9,10-quinone in deep eutectic solvent (choline chloride : urea). *Green Chemistry*, 12(3), 458-462. doi:10.1039/B923589B
- Pillay, K., Cukrowska, E. M., & Coville, N. J. (2013). Improved uptake of mercury by sulphur-containing carbon nanotubes. *Microchemical Journal*, 108, 124-130. doi:<http://dx.doi.org/10.1016/j.microc.2012.10.014>
- Polo-Luque, M. L., Simonet, B. M., & Valcárcel, M. (2013). Functionalization and dispersion of carbon nanotubes in ionic liquids. *TrAC Trends in Analytical Chemistry*, 47, 99-110. doi:<http://dx.doi.org/10.1016/j.trac.2013.03.007>

- Popov, V. N. (2004). Carbon nanotubes: properties and application. *Materials Science and Engineering: R: Reports*, 43(3), 61-102.
doi:<http://dx.doi.org/10.1016/j.mser.2003.10.001>
- Pyrzynska, K., & Stafiej, A. (2012). Sorption Behavior of Cu(II), Pb(II), and Zn(II) onto Carbon Nanotubes. *Solvent Extraction and Ion Exchange*, 30(1), 41-53.
doi:10.1080/07366299.2011.581056
- Ramos, M. A. V., Yan, W., Li, X.-q., Koel, B. E., & Zhang, W.-x. (2009). Simultaneous Oxidation and Reduction of Arsenic by Zero-Valent Iron Nanoparticles: Understanding the Significance of the Core–Shell Structure. *The Journal of Physical Chemistry C*, 113(33), 14591-14594. doi:10.1021/jp9051837
- Ramsden, J. (2009). *Essentials of nanotechnology*: BookBoon.
- Rao, G. P., Lu, C., & Su, F. (2007). Sorption of divalent metal ions from aqueous solution by carbon nanotubes: A review. *Separation and Purification Technology*, 58(1), 224-231. doi:<http://dx.doi.org/10.1016/j.seppur.2006.12.006>
- Rao, M., Parwate, A. V., & Bhole, A. G. (2002). Removal of Cr⁶⁺ and Ni²⁺ from aqueous solution using bagasse and fly ash. *Waste Management*, 22(7), 821-830. doi:[http://dx.doi.org/10.1016/S0956-053X\(02\)00011-9](http://dx.doi.org/10.1016/S0956-053X(02)00011-9)
- Raven, K. P., Jain, A., & Loeppert, R. H. (1998). Arsenite and Arsenate Adsorption on Ferrihydrite: Kinetics, Equilibrium, and Adsorption Envelopes. *Environmental Science & Technology*, 32(3), 344-349. doi:10.1021/es970421p
- Renjith, A., Roy, A., & Lakshminarayanan, V. (2014). In situ fabrication of electrochemically grown mesoporous metallic thin films by anodic dissolution in deep eutectic solvents. *Journal of colloid and interface science*, 426, 270-279. doi:<http://dx.doi.org/10.1016/j.jcis.2014.04.015>
- Richter, M., Berndt, H., Eckelt, R., Schneider, M., & Fricke, R. (1999). Zeolite-mediated removal of NO_x by NH₃ from exhaust streams at low temperatures. *Catalysis Today*, 54(4), 531-545. doi:[http://dx.doi.org/10.1016/S0920-5861\(99\)00215-1](http://dx.doi.org/10.1016/S0920-5861(99)00215-1)
- Ru, & König, B. (2012). Low melting mixtures in organic synthesis - an alternative to ionic liquids? *Green Chemistry*, 14(11), 2969-2982. doi:10.1039/C2GC36005E
- Ru, C. Q. (2000). Effect of van der Waals forces on axial buckling of a double-walled carbon nanotube. *Journal of Applied Physics*, 87(10), 7227-7231. doi:<http://dx.doi.org/10.1063/1.372973>
- Ruthiraan, M., Mubarak, N. M., Thines, R. K., Abdullah, E. C., Sahu, J. N., Jayakumar, N. S., & Ganesan, P. (2015). Comparative kinetic study of functionalized carbon nanotubes and magnetic biochar for removal of Cd²⁺ ions from wastewater. *Korean Journal of Chemical Engineering*, 32(3), 446-457. doi:10.1007/s11814-014-0260-7
- Saito, R., Dresselhaus, G., & Dresselhaus, M. S. (1998). *Physical Properties of Carbon Nanotubes*: Imperial College Press.

- Salam, M. A. (2013). Coating carbon nanotubes with crystalline manganese dioxide nanoparticles and their application for lead ions removal from model and real water. *Colloids and Surfaces A: Physicochemical and Engineering Aspects*, 419(0), 69-79. doi:<http://dx.doi.org/10.1016/j.colsurfa.2012.11.064>
- Salam, M. A., Al-Zhrani, G., & Kosa, S. A. (2012). Simultaneous removal of copper(II), lead(II), zinc(II) and cadmium(II) from aqueous solutions by multi-walled carbon nanotubes. *Comptes Rendus Chimie*, 15(5), 398-408. doi:<http://dx.doi.org/10.1016/j.crci.2012.01.013>
- Saleh, T. A. (2015). Isotherm, kinetic, and thermodynamic studies on Hg(II) adsorption from aqueous solution by silica- multiwall carbon nanotubes. *Environmental Science and Pollution Research*, 22(21), 16721-16731. doi:10.1007/s11356-015-4866-z
- Sato, T., Masuda, G., & Takagi, K. (2004). Electrochemical properties of novel ionic liquids for electric double layer capacitor applications. *Electrochimica Acta*, 49(21), 3603-3611. doi:<http://dx.doi.org/10.1016/j.electacta.2004.03.030>
- Sekar, M., Sakthi, V., & Rengaraj, S. (2004). Kinetics and equilibrium adsorption study of lead(II) onto activated carbon prepared from coconut shell. *Journal of colloid and interface science*, 279(2), 307-313. doi:<http://dx.doi.org/10.1016/j.jcis.2004.06.042>
- Selvakumar, R., Arul Jothi, N., Jayavignesh, V., Karthikaiselvi, K., Antony, G. I., Sharmila, P. R., . . . Swaminathan, K. (2011). As(V) removal using carbonized yeast cells containing silver nanoparticles. *Water Research*, 45(2), 583-592. doi:<http://dx.doi.org/10.1016/j.watres.2010.09.034>
- Serrano, E., Rus, G., & García-Martínez, J. (2009). Nanotechnology for sustainable energy. *Renewable and Sustainable Energy Reviews*, 13(9), 2373-2384. doi:<http://dx.doi.org/10.1016/j.rser.2009.06.003>
- Shahbaz, K., Baroutian, S., Mjalli, F. S., Hashim, M. A., & AlNashef, I. M. (2012). Densities of ammonium and phosphonium based deep eutectic solvents: Prediction using artificial intelligence and group contribution techniques. *Thermochimica Acta*, 527, 59-66. doi:<http://dx.doi.org/10.1016/j.tca.2011.10.010>
- Shahbaz, K., Mjalli, F. S., Hashim, M. A., & AlNashef, I. M. (2011). Prediction of deep eutectic solvents densities at different temperatures. *Thermochimica Acta*, 515(1-2), 67-72. doi:<http://dx.doi.org/10.1016/j.tca.2010.12.022>
- Shahidi, S., Iranpour, S., Iranpour, P., Alavi, A. A., Mahyari, F. A., Tohidi, M., & Safavi, A. (2015). A new X-ray contrast agent based on highly stable gum arabic-gold nanoparticles synthesised in deep eutectic solvent. *Journal of Experimental Nanoscience*, 10(12), 911-924. doi:10.1080/17458080.2014.933493
- Shanthilal, J., & Bhattacharya, S. (2014). Nanoparticles and Nanotechnology in Food *Conventional and Advanced Food Processing Technologies* (pp. 567-594): John Wiley & Sons, Ltd.

- Shao, D., Chen, C., & Wang, X. (2012). Application of polyaniline and multiwalled carbon nanotube magnetic composites for removal of Pb(II). *Chemical Engineering Journal*, 185–186(0), 144-150.
doi:<http://dx.doi.org/10.1016/j.cej.2012.01.063>
- Sharma, V. K., & Sohn, M. (2009). Aquatic arsenic: Toxicity, speciation, transformations, and remediation. *Environment International*, 35(4), 743-759.
doi:<http://dx.doi.org/10.1016/j.envint.2009.01.005>
- Shawky, H. A., El-Aassar, A. H. M., & Abo-Zeid, D. E. (2012). Chitosan/carbon nanotube composite beads: Preparation, characterization, and cost evaluation for mercury removal from wastewater of some industrial cities in Egypt. *Journal of Applied Polymer Science*, 125(S1), E93-E101. doi:10.1002/app.35628
- Sheng, G., Li, Y., Yang, X., Ren, X., Yang, S., Hu, J., & Wang, X. (2012). Efficient removal of arsenate by versatile magnetic graphene oxide composites. *RSC Advances*, 2(32), 12400-12407. doi:10.1039/C2RA21623J
- Simate, G. S., Iyuke, S. E., Ndlovu, S., & Heydenrych, M. (2012). The heterogeneous coagulation and flocculation of brewery wastewater using carbon nanotubes. *Water Research*, 46(4), 1185-1197.
doi:<http://dx.doi.org/10.1016/j.watres.2011.12.023>
- Singh, B., Lobo, H., & Shankarling, G. (2011). Selective N-Alkylation of Aromatic Primary Amines Catalyzed by Bio-catalyst or Deep Eutectic Solvent. *Catalysis Letters*, 141(1), 178-182. doi:10.1007/s10562-010-0479-9
- Smarrito-Menozzi, C., Matthey-Doret, W., Devaud-Goumoens, S., & Viton, F. (2013). Glycerol, an Underestimated Flavor Precursor in the Maillard Reaction. *Journal of Agricultural and Food Chemistry*, 61(43), 10225-10230.
doi:10.1021/jf3050044
- Smedley, P. L., & Kinniburgh, D. G. (2001). United Nations Synthesis Report on Arsenic in Drinking-Water. *British Geological Survey*, 1-61.
- Smith, B. C. (1998). *Infrared spectral interpretation: a systematic approach*: CRC press.
- Smith, E. L., Abbott, A. P., & Ryder, K. S. (2014). Deep Eutectic Solvents (DESs) and Their Applications. *Chemical Reviews*, 114(21), 11060-11082.
doi:10.1021/cr300162p
- Sonawane, Y. A., Phadtare, S. B., Borse, B. N., Jagtap, A. R., & Shankarling, G. S. (2010). Synthesis of Diphenylamine-Based Novel Fluorescent Styryl Colorants by Knoevenagel Condensation Using a Conventional Method, Biocatalyst, and Deep Eutectic Solvent. *Organic Letters*, 12(7), 1456-1459.
doi:10.1021/ol902976u
- Sountharajah, D. P., Loganathan, P., Kandasamy, J., & Vigneswaran, S. (2015). Adsorptive removal of heavy metals from water using sodium titanate nanofibres loaded onto GAC in fixed-bed columns. *Journal of Hazardous Materials*, 287, 306-316. doi:<http://dx.doi.org/10.1016/j.jhazmat.2015.01.067>

- Srivastava, N. K., & Majumder, C. B. (2008). Novel biofiltration methods for the treatment of heavy metals from industrial wastewater. *Journal of Hazardous Materials*, 151(1), 1-8. doi:<http://dx.doi.org/10.1016/j.jhazmat.2007.09.101>
- Srivastava, S., & Goyal, P. (2010). *Novel biomaterials: decontamination of toxic metals from wastewater*: Springer Science & Business Media.
- Stafiej, A., & Pyrzynska, K. (2007). Adsorption of heavy metal ions with carbon nanotubes. *Separation and Purification Technology*, 58(1), 49-52. doi:<http://dx.doi.org/10.1016/j.seppur.2007.07.008>
- Stephenson, J. J., Sadana, A. K., Higginbotham, A. L., & Tour, J. M. (2006). Highly Functionalized and Soluble Multiwalled Carbon Nanotubes by Reductive Alkylation and Arylation: The Billups Reaction. *Chemistry of Materials*, 18(19), 4658-4661. doi:10.1021/cm060832h
- Stoyanov, E. S., Kim, K.-C., & Reed, C. A. (2006). An Infrared vNH Scale for Weakly Basic Anions. Implications for Single-Molecule Acidity and Superacidity. *Journal of the American Chemical Society*, 128(26), 8500-8508. doi:10.1021/ja060714v
- Stuart, B. (2005). *Infrared spectroscopy*: Wiley Online Library.
- Stuart, B. H. (2005a). Organic Molecules *Infrared Spectroscopy: Fundamentals and Applications* (pp. 71-93): John Wiley & Sons, Ltd.
- Stuart, B. H. (2005b). Spectral Analysis *Infrared Spectroscopy: Fundamentals and Applications* (pp. 45-70): John Wiley & Sons, Ltd.
- Sun, Y.-P., Fu, K., Lin, Y., & Huang, W. (2002). Functionalized Carbon Nanotubes: Properties and Applications. *Accounts of Chemical Research*, 35(12), 1096-1104. doi:10.1021/ar010160v
- Sun, Z., Nicolosi, V., Rickard, D., Bergin, S. D., Aherne, D., & Coleman, J. N. (2008). Quantitative Evaluation of Surfactant-stabilized Single-walled Carbon Nanotubes: Dispersion Quality and Its Correlation with Zeta Potential. *The Journal of Physical Chemistry C*, 112(29), 10692-10699. doi:10.1021/jp8021634
- Tan, X., Yin, Q., Yang, X., Chen, S., Xu, R., Huang, X., & Dong, Y. (2012). Hyperchromic Effect and Mechanism of Carboxylic Carbon Nanotubes in Determination of Lead by Spectrophotometry. *Integrated Ferroelectrics*, 137(1), 126-133. doi:10.1080/10584587.2012.687314
- Tao, H.-C., Zhang, H.-R., Li, J.-B., & Ding, W.-Y. (2015). Biomass based activated carbon obtained from sludge and sugarcane bagasse for removing lead ion from wastewater. *Bioresource Technology*, 192, 611-617. doi:<http://dx.doi.org/10.1016/j.biortech.2015.06.006>
- Tawabini, B., Al-Khalidi, S., Atieh, M., & Khaled, M. (2010). Removal of mercury from water by multi-walled carbon nanotubes. *Water Science and Technology*, 61(3), 591-598. doi:10.2166/wst.2010.897

- Tawabini, B. S., Al-Khaldi, S. F., Khaled, M. M., & Atieh, M. A. (2011). Removal of arsenic from water by iron oxide nanoparticles impregnated on carbon nanotubes. *Journal of Environmental Science and Health, Part A*, 46(3), 215-223. doi:10.1080/10934529.2011.535389
- Tchobanoglous, G., & Burton, F. L. (1991). Wastewater engineering. *MANAGEMENT*, 7, 1-4.
- Thostenson, E. T., Ren, Z., & Chou, T.-W. (2001). Advances in the science and technology of carbon nanotubes and their composites: a review. *Composites Science and Technology*, 61(13), 1899-1912. doi:[http://dx.doi.org/10.1016/S0266-3538\(01\)00094-X](http://dx.doi.org/10.1016/S0266-3538(01)00094-X)
- Tofighy, M. A., & Mohammadi, T. (2011). Adsorption of divalent heavy metal ions from water using carbon nanotube sheets. *Journal of Hazardous Materials*, 185(1), 140-147. doi:<http://dx.doi.org/10.1016/j.jhazmat.2010.09.008>
- Tohidi, M., Mahyari, F. A., & Safavi, A. (2015). A seed-less method for synthesis of ultra-thin gold nanosheets by using a deep eutectic solvent and gum arabic and their electrocatalytic application. *RSC Advances*, 5(41), 32744-32754. doi:10.1039/C4RA17053A
- Tong, S., Schirnding, Y. E. v., & Prapamontol, T. (2000). Environmental lead exposure: a public health problem of global dimensions. *Bulletin of the World Health Organization*, 78, 1068-1077.
- Tresintsi, S., Simeonidis, K., Estradé, S., Martinez-Boubeta, C., Vourlias, G., Pinakidou, F., . . . Mitrakas, M. (2013). Tetravalent Manganese Peroxyhyte: A Novel Nanoadsorbent Equally Selective for As(III) and As(V) Removal from Drinking Water. *Environmental Science & Technology*, 47(17), 9699-9705. doi:10.1021/es4009932
- Tuutijärvi, T., Lu, J., Sillanpää, M., & Chen, G. (2009). As(V) adsorption on maghemite nanoparticles. *Journal of Hazardous Materials*, 166(2-3), 1415-1420. doi:<http://dx.doi.org/10.1016/j.jhazmat.2008.12.069>
- Tuzen, M., Saygi, K. O., Usta, C., & Soylak, M. (2008). Pseudomonas aeruginosa immobilized multiwalled carbon nanotubes as biosorbent for heavy metal ions. *Bioresource Technology*, 99(6), 1563-1570. doi:<http://dx.doi.org/10.1016/j.biortech.2007.04.013>
- Usui, Y., Aoki, K., Narita, N., Murakami, N., Nakamura, I., Nakamura, K., . . . Saito, N. (2008). Carbon nanotubes with high bone-tissue compatibility and bone-formation acceleration effects. *Small*, 4(2), 240-246. doi:10.1002/sml.200700670
- Veličković, Z., Vuković, G. D., Marinković, A. D., Moldovan, M.-S., Perić-Grujić, A. A., Uskoković, P. S., & Ristić, M. Đ. (2012). Adsorption of arsenate on iron(III) oxide coated ethylenediamine functionalized multiwall carbon nanotubes. *Chemical Engineering Journal*, 181-182, 174-181. doi:<http://dx.doi.org/10.1016/j.cej.2011.11.052>

- Veličković, Z. S., Marinković, A. D., Bajić, Z. J., Marković, J. M., Perić-Grujić, A. A., Uskokovic, P. S., & Ristic, M. D. (2013). Oxidized and Ethylenediamine-Functionalized Multi-Walled Carbon Nanotubes for the Separation of Low Concentration Arsenate from Water. *Separation Science and Technology*, 48(13), 2047-2058. doi:10.1080/01496395.2013.790446
- Venkata Ramana, D. K., Kumar Reddy, D. H., Kumar, B. N., Seshaiyah, K., Chandra Rao, G. P., & Lu, C. (2012). Adsorption of Pb(II) from Aqueous Solutions by Chemically Modified Zeolite supported Carbon Nanotubes: Equilibrium, Kinetic, and Thermodynamic Studies. *Separation Science and Technology*, 48(3), 403-412. doi:10.1080/01496395.2012.690638
- Vuković, G., Marinković, A., Obradović, M., Radmilović, V., Čolić, M., Aleksić, R., & Uskoković, P. S. (2009). Synthesis, characterization and cytotoxicity of surface amino-functionalized water-dispersible multi-walled carbon nanotubes. *Applied Surface Science*, 255(18), 8067-8075. doi:<http://dx.doi.org/10.1016/j.apsusc.2009.05.016>
- Vuković, G. D., Marinković, A. D., Čolić, M., Ristić, M. Đ., Aleksić, R., Perić-Grujić, A. A., & Uskoković, P. S. (2010). Removal of cadmium from aqueous solutions by oxidized and ethylenediamine-functionalized multi-walled carbon nanotubes. *Chemical Engineering Journal*, 157(1), 238-248. doi:<http://dx.doi.org/10.1016/j.cej.2009.11.026>
- Vuković, G. D., Marinković, A. D., Škapin, S. D., Ristić, M. Đ., Aleksić, R., Perić-Grujić, A. A., & Uskoković, P. S. (2011). Removal of lead from water by amino modified multi-walled carbon nanotubes. *Chemical Engineering Journal*, 173(3), 855-865. doi:<http://dx.doi.org/10.1016/j.cej.2011.08.036>
- Wang, H., Yan, N., Li, Y., Zhou, X., Chen, J., Yu, B., . . . Chen, Q. (2012). Fe nanoparticle-functionalized multi-walled carbon nanotubes: one-pot synthesis and their applications in magnetic removal of heavy metal ions. *Journal of Materials Chemistry*, 22(18), 9230-9236. doi:10.1039/C2JM16584H
- Wang, H. J., Zhou, A. L., Peng, F., Yu, H., & Chen, L. F. (2007). Adsorption characteristic of acidified carbon nanotubes for heavy metal Pb(II) in aqueous solution. *Materials Science and Engineering: A*, 466(1-2), 201-206. doi:<http://dx.doi.org/10.1016/j.msea.2007.02.097>
- Wang, S.-G., Gong, W.-X., Liu, X.-W., Yao, Y.-W., Gao, B.-Y., & Yue, Q.-Y. (2007). Removal of lead(II) from aqueous solution by adsorption onto manganese oxide-coated carbon nanotubes. *Separation and Purification Technology*, 58(1), 17-23. doi:<http://dx.doi.org/10.1016/j.seppur.2007.07.006>
- Wei, L., Fan, Y.-J., Tian, N., Zhou, Z.-Y., Zhao, X.-Q., Mao, B.-W., & Sun, S.-G. (2012). Electrochemically Shape-Controlled Synthesis in Deep Eutectic Solvents—A New Route to Prepare Pt Nanocrystals Enclosed by High-Index Facets with High Catalytic Activity. *The Journal of Physical Chemistry C*, 116(2), 2040-2044. doi:10.1021/jp209743h
- Wei, L., Fan, Y.-J., Wang, H.-H., Tian, N., Zhou, Z.-Y., & Sun, S.-G. (2012). Electrochemically shape-controlled synthesis in deep eutectic solvents of Pt

nanoflowers with enhanced activity for ethanol oxidation. *Electrochimica Acta*, 76, 468-474. doi:<http://dx.doi.org/10.1016/j.electacta.2012.05.063>

- Wei, L., Zhou, Z.-Y., Chen, S.-P., Xu, C.-D., Su, D., Schuster, M. E., & Sun, S.-G. (2013). Electrochemically shape-controlled synthesis in deep eutectic solvents: triambic icosahedral platinum nanocrystals with high-index facets and their enhanced catalytic activity. *Chemical Communications*, 49(95), 11152-11154. doi:10.1039/C3CC46473C
- Weng, C.-H., & Huang, C. P. (2004). Adsorption characteristics of Zn(II) from dilute aqueous solution by fly ash. *Colloids and Surfaces A: Physicochemical and Engineering Aspects*, 247(1-3), 137-143. doi:<http://dx.doi.org/10.1016/j.colsurfa.2004.08.050>
- Xia, H., Wang, Y., Lin, J., & Lu, L. (2012). Hydrothermal synthesis of MnO₂/CNT nanocomposite with a CNT core/porous MnO₂ sheath hierarchy architecture for supercapacitors. *Nanoscale Research Letters*, 7(1), 1-10. doi:10.1186/1556-276x-7-33
- Xiong, Q. Q., Tu, J. P., Ge, X., Wang, X. L., & Gu, C. D. (2015). One-step synthesis of hematite nanospindles from choline chloride/urea deep eutectic solvent with highly powerful storage versus lithium. *Journal of Power Sources*, 274, 1-7. doi:<http://dx.doi.org/10.1016/j.jpowsour.2014.10.020>
- Xu, K., Wang, Y., Ding, X., Huang, Y., Li, N., & Wen, Q. (2016). Magnetic solid-phase extraction of protein with deep eutectic solvent immobilized magnetic graphene oxide nanoparticles. *Talanta*, 148, 153-162. doi:<http://dx.doi.org/10.1016/j.talanta.2015.10.079>
- Yadav, A., & Pandey, S. (2014). Densities and Viscosities of (Choline Chloride + Urea) Deep Eutectic Solvent and Its Aqueous Mixtures in the Temperature Range 293.15 K to 363.15 K. *Journal of Chemical & Engineering Data*, 59(7), 2221-2229. doi:10.1021/je5001796
- Yamabe, T. (1995). Recent development of carbon nanotube. *Synthetic Metals*, 70(1), 1511-1518. doi:[http://dx.doi.org/10.1016/0379-6779\(94\)02939-V](http://dx.doi.org/10.1016/0379-6779(94)02939-V)
- Yamauchi, H., & Yamamura, Y. (1983). Concentration and chemical species of arsenic in human tissue. *Bulletin of Environmental Contamination and Toxicology*, 31(3), 267-270. doi:10.1007/BF01608697
- Yang, D., Hou, M., Ning, H., Zhang, J., Ma, J., Yang, G., & Han, B. (2013). Efficient SO₂ absorption by renewable choline chloride-glycerol deep eutectic solvents. *Green Chemistry*, 15(8), 2261-2265. doi:10.1039/C3GC40815A
- Yang, J., Wei, W., Pi, S., Ma, F., Li, A., Wu, D., & Xing, J. (2015). Competitive adsorption of heavy metals by extracellular polymeric substances extracted from *Klebsiella* sp. J1. *Bioresource Technology*, 196, 533-539. doi:<http://dx.doi.org/10.1016/j.biortech.2015.08.011>
- Yang, S., Li, J., Shao, D., Hu, J., & Wang, X. (2009). Adsorption of Ni(II) on oxidized multi-walled carbon nanotubes: Effect of contact time, pH, foreign ions and

PAA. *Journal of Hazardous Materials*, 166(1), 109-116.
doi:<http://dx.doi.org/10.1016/j.jhazmat.2008.11.003>

- Yang, W., Ding, P., Zhou, L., Yu, J., Chen, X., & Jiao, F. (2013a). Preparation of diamine modified mesoporous silica on multi-walled carbon nanotubes for the adsorption of heavy metals in aqueous solution. *Applied Surface Science*, 282, 38-45. doi:<http://dx.doi.org/10.1016/j.apsusc.2013.05.028>
- Yang, W., Ding, P., Zhou, L., Yu, J., Chen, X., & Jiao, F. (2013b). Preparation of diamine modified mesoporous silica on multi-walled carbon nanotubes for the adsorption of heavy metals in aqueous solution. *Applied Surface Science*, 282(0), 38-45. doi:<http://dx.doi.org/10.1016/j.apsusc.2013.05.028>
- Yi, W., Lu, L., Dian-lin, Z., Pan, Z. W., & Xie, S. S. (1999). Linear specific heat of carbon nanotubes. *Physical Review B*, 59(14), R9015-R9018.
- Yim, W. L., & Liu, Z. F. (2004). A reexamination of the chemisorption and desorption of ozone on the exterior of a (5,5) single-walled carbon nanotube. *Chemical Physics Letters*, 398(4-6), 297-303.
doi:<http://dx.doi.org/10.1016/j.cplett.2004.09.082>
- You, Y., Gu, C., Wang, X., & Tu, J. (2012). Electrochemical Synthesis and Characterization of Ni-P Alloy Coatings from Eutectic-Based Ionic Liquid. *Journal of The Electrochemical Society*, 159(11), D642-D648.
doi:10.1149/2.012211jes
- Yu, F., Ma, J., & Wu, Y. (2011). Adsorption of toluene, ethylbenzene and m-xylene on multi-walled carbon nanotubes with different oxygen contents from aqueous solutions. *Journal of Hazardous Materials*, 192(3), 1370-1379.
- Yu, F., Wu, Y., Ma, J., & Zhang, C. (2013). Adsorption of lead on multi-walled carbon nanotubes with different outer diameters and oxygen contents: Kinetics, isotherms and thermodynamics. *Journal of Environmental Sciences*, 25(1), 195-203. doi:[http://dx.doi.org/10.1016/S1001-0742\(12\)60023-0](http://dx.doi.org/10.1016/S1001-0742(12)60023-0)
- Yu, R., Chen, L., Liu, Q., Lin, J., Tan, K.-L., Ng, S. C., . . . Hor, T. S. A. (1998). Platinum Deposition on Carbon Nanotubes via Chemical Modification. *Chemistry of Materials*, 10(3), 718-722. doi:10.1021/cm970364z
- Yue, D., Jia, Y., Yao, Y., Sun, J., & Jing, Y. (2012). Structure and electrochemical behavior of ionic liquid analogue based on choline chloride and urea. *Electrochimica Acta*, 65(0), 30-36.
doi:<http://dx.doi.org/10.1016/j.electacta.2012.01.003>
- Yusof, R., Abdulmalek, E., Sirat, K., & Rahman, M. (2014). Tetrabutylammonium Bromide (TBABr)-Based Deep Eutectic Solvents (DESS) and Their Physical Properties. *Molecules*, 19(6), 8011.
- Zang, L. (2011). *Energy Efficiency and Renewable Energy Through Nanotechnology*: Springer.
- Zhang, C., Sui, J., Li, J., Tang, Y., & Cai, W. (2012). Efficient removal of heavy metal ions by thiol-functionalized superparamagnetic carbon nanotubes. *Chemical*

Engineering Journal, 210(0), 45-52.
doi:<http://dx.doi.org/10.1016/j.cej.2012.08.062>

- Zhang, D., Shi, L., Fang, J., Li, X., & Dai, K. (2005). Preparation and modification of carbon nanotubes. *Materials Letters*, 59(29-30), 4044-4047.
doi:10.1016/j.matlet.2005.07.081
- Zhang, F.-S., Nriagu, J. O., & Itoh, H. (2005). Mercury removal from water using activated carbons derived from organic sewage sludge. *Water Research*, 39(2-3), 389-395. doi:<http://dx.doi.org/10.1016/j.watres.2004.09.027>
- Zhang, J. (2013). Preparation, characterization and application of thiosemicarbazide grafted multiwalled carbon nanotubes for solid-phase extraction of Cd(II), Cu(II) and Pb(II) in environmental samples. *Journal of Environmental Sciences*, 25(11), 2331-2337. doi:[http://dx.doi.org/10.1016/S1001-0742\(12\)60329-5](http://dx.doi.org/10.1016/S1001-0742(12)60329-5)
- Zhang, J., Wu, T., Chen, S., Feng, P., & Bu, X. (2009). Versatile Structure-Directing Roles of Deep-Eutectic Solvents and Their Implication in the Generation of Porosity and Open Metal Sites for Gas Storage. *Angewandte Chemie International Edition*, 48(19), 3486-3490. doi:10.1002/anie.200900134
- Zhang, M., Gao, B., Cao, X., & Yang, L. (2013). Synthesis of a multifunctional graphene-carbon nanotube aerogel and its strong adsorption of lead from aqueous solution. *RSC Advances*, 3(43), 21099-21105.
doi:10.1039/C3RA44340J
- Zhang, Q., De Oliveira Vigier, K., Royer, S., & Jerome, F. (2012). Deep eutectic solvents: syntheses, properties and applications. *Chemical Society Reviews*, 41(21), 7108-7146. doi:10.1039/C2CS35178A
- Zhang, Q., Zhang, S., & Deng, Y. (2011). Recent advances in ionic liquid catalysis. *Green Chemistry*, 13(10), 2619-2637. doi:10.1039/C1GC15334J
- Zhang, Q. B., Abbott, A. P., & Yang, C. (2015). Electrochemical fabrication of nanoporous copper films in choline chloride-urea deep eutectic solvent. *Physical Chemistry Chemical Physics*, 17(22), 14702-14709. doi:10.1039/C5CP01276G
- Zhao, H., Baker, G. A., & Holmes, S. (2011). Protease activation in glycerol-based deep eutectic solvents. *Journal of Molecular Catalysis B: Enzymatic*, 72(3-4), 163-167. doi:<http://dx.doi.org/10.1016/j.molcatb.2011.05.015>
- Zhao, X., Jia, Q., Song, N., Zhou, W., & Li, Y. (2010). Adsorption of Pb(II) from an Aqueous Solution by Titanium Dioxide/Carbon Nanotube Nanocomposites: Kinetics, Thermodynamics, and Isotherms†. *Journal of Chemical & Engineering Data*, 55(10), 4428-4433. doi:10.1021/je100586r
- Zheng, Y., Ye, L., Yan, L., & Gao, Y. (2014). The electrochemical behavior and determination of quercetin in choline chloride/urea deep eutectic solvent electrolyte based on abrasively immobilized multi-wall carbon nanotubes modified electrode. *Int. J. Electrochem. Sci*, 9, 238-248.
- Zhou, L., Ji, L., Ma, P.-C., Shao, Y., Zhang, H., Gao, W., & Li, Y. (2014). Development of carbon nanotubes/CoFe₂O₄ magnetic hybrid material for

removal of tetrabromobisphenol A and Pb(II). *Journal of Hazardous Materials*, 265(0), 104-114. doi:<http://dx.doi.org/10.1016/j.jhazmat.2013.11.058>

Zhu, H. T., Luo, J., Yang, H. X., Liang, J. K., Rao, G. H., Li, J. B., & Du, Z. M. (2008). Birnessite-type MnO₂ Nanowalls and Their Magnetic Properties. *The Journal of Physical Chemistry C*, 112(44), 17089-17094. doi:10.1021/jp804673n

Zhu, H. W., Xu, C. L., Wu, D. H., Wei, B. Q., Vajtai, R., & Ajayan, P. M. (2002). Direct Synthesis of Long Single-Walled Carbon Nanotube Strands. *Science*, 296(5569), 884-886. doi:10.1126/science.1066996

University of Malaya

LIST OF PUBLICATIONS AND PAPERS PRESENTED

Published papers

1. **AlOmar, M.K.**, Hayyan, M., Alsaadi, M.A., Akib, S., Hayyan, A., Hashim, M.A., 2016. *Glycerol-based deep eutectic solvents: Physical properties*. Journal of Molecular Liquids 215, 98-103. **ISI-Cited publication.**
2. **AlOmar, M.K.**, Alsaadi, M.A., Hayyan, M., Akib, S., Hashim, M.A, 2016, *Functionalization of CNTs surface with Phosphonium based deep eutectic solvents for arsenic removal from water*. Applied Surface Science 389, 216-226. **ISI-Cited publication.**
3. **AlOmar, M.K.**, Alsaadi, M.A., Hayyan, M., Akib, S., Ibraheem R.K., Hashim, M.A, 2016 *Lead removal from water by Choline chloride based deep eutectic solvents functionalized Carbon nanotubes*, Journal of Molecular Liquids 222, 883-894. **ISI-Cited publication.**
4. **AlOmar, M.K.**, Alsaadi, M.A., Hayyan, M., Akib, S., Hashim, M.A, 2016, *Allyl triphenyl phosphonium bromide based DES-functionalized carbon nanotubes for the removal of mercury from water*. Chemosphere, 167, 44-52. doi:http://dx.doi.org/10.1016/j.chemosphere.2016.09.133, **ISI-Cited publication.**
5. **AlOmar, M. K.**, Alsaadi, M. A., Jassam, T. M., Akib, S., & Ali Hashim, M. (2017). *Novel deep eutectic solvent-functionalized carbon nanotubes adsorbent for mercury removal from water*. Journal of colloid and interface science, 497, 413-421. doi:http://doi.org/10.1016/j.jcis.2017.03.014. **ISI-Cited publication.**
6. **AlOmar, M.K.**, Alsaadi, M.A., Aljumaily M. M, Akib, S., Hashim, M.A, 2016, *N,N-diethylethanolammonium chloride based DES-functionalized carbon nanotubes for arsenic removal from aqueous solution*. Desalination and Water Treatment, Accepted manuscript. **ISI-Cited publication.**

Submitted papers (under review)

7. **AlOmar, M.K.**, Hayyan, M., Alsaadi, M.A., Akib, S., Hashim, M.A, 2016, *Study of physical properties of novel Benzyl trimethyl ammonium chloride-based deep eutectic solvents*. PHYSICS AND CHEMISTRY OF LIQUIDS, under review. **ISI-Cited publication.**
8. **AlOmar, M.K.**, Alsaadi, M.A., Akib, S., Hashim, M.A, 2016, *Chromium adsorption on Benzyl trimethyl ammonium chloride based DES-functionalized carbon nanotubes*. JOURNAL OF HAZARDOUS MATERIALS, Submitted. **ISI-Cited publication.**
9. **AlOmar, M.K.**, Alsaadi, M.A., Akib, S., Hashim, M.A, 2016, *Heavy metals adsorption by Carbon Nanotubes (recent development): A review*. Environmental Science-Water Research & Technology, Under review. **ISI-Cited publication.**

Conference papers (presenter)

1. **Mohammed Khalid Alomar**, Mohammed Abdulhakim AlSaadi, Maan Hayyan, Shatirah Mohamed Akib, Mohd Ali Hashim, (2014) [*Densities of Phosphonium and Ammonium Based Deep Eutectic Solvents*]. Design for Scientific Renaissance DSR. Non Scopus-non ISI
2. **Mohammed Khalid Alomar**, Mohammed Abdulhakim AlSaadi, Maan Hayyan, Shatirah Mohamed Akib, Mohd Ali Hashim, (2015) [*Stable Molar Ratios of Novel Deep Eutectic Solvents and Their Physical Properties*]. Design for Scientific Renaissance DSR. Non Scopus-non ISI
3. **Mohammed Khalid Alomar**, Mohammed Abdulhakim AlSaadi, Wan Hamidon Wan Badruzaman (2015) [*Sensitivity Analysis of Profile Steel Sheeting Dry Board (PSSDB) Floor System Using Finite Element Method*]. Design for Scientific Renaissance DSR. Non Scopus-non ISI

University of Malaysia

